Institut für Pharmazeutische Biotechnologie der Universität Ulm

Molecular aspects of RNA-recognition by the neuronal mRNA transport factor Staufen 2

Dissertation zur Erlangung des Doktorgrades

Dr. rer. nat.

der Fakultät für Naturwissenschaften

der Universität Ulm

vorgelegt von

Simone Heber aus Laupheim

2018

Fakultät für Naturwissenschaften
Universität Ulm

Dekan: Prof. Dr. Peter Dürre

Betreuer: Prof. Dr. Dierk Niessing
Zweitgutachter: Prof. Dr. Nils Johnsson

Tag der mündlichen Prüfung: 19.06.2018

Zusammenfassung

Staufen ist ein Doppelstrang-RNA-Bindeprotein, das ursprünglich als RNA-Transportfaktor und Keimzellenmarker in *Drosophila* entdeckt wurde. Das Säugetier-Homolog Staufen 2 (Stau2) wird spezifisch in Neuronen exprimiert, in denen es sich in RNA-Partikeln anhäuft und sich entlang von Mikrotubuli von den Zellkörpern zu Dendriten bewegt. Stau2 ist ein wichtiger Kernfaktor des neuronalen RNA-Transports und wurde mit synaptischer Plastizität, Gedächtnis und Lernen in Verbindung gebracht. Stau2 knockdown in Ratten führt zu einer reduzierten Anzahl dendritisches Dornen und beeinträchtigt die Langzeit-Depression von Synapsen. Alle Stau Proteine besitzen vier bis fünf Doppelstrang-RNA-Bindedomänen (RBDs). Für alle Stau Proteine wird angenommen, dass RBD3 und RBD4 die einzigen aktiven RBDs sind, während RBDs 1, 2 und 5 oft als pseudo-RBDs bezeichnet werden, in denen zwar die Faltung, aber nicht RNA-Bindeaktivität einer RBD konserviert ist. Bisher ist die mechanistische Grundlage der Funktion von Stau2 in der Zelle nicht gut verstanden. Der translationale Repressor Pumilio 2 (Pum2) wirkt in denselben Signalwegen wie Stau2. Beide Proteine bilden gemeinsame Ribonukleoproteine (mRNPs). Die 3' untranslatierte Region (UTR) der Stau2 Target-*RNA Regulator of G-protein signaling 4* (*Rgs4*) enthält zwei vorhergesagte 'Staufen-Recognized Structures' (SRSs) und zwei vorhergesagte Pum2 Bindestellen in unmittelbarer Nähe, was auf einen funktionellen Komplex aus Stau2, Pum2 und *Rgs4* hindeutet.

In dieser Arbeit konnte bestätigt werden, dass Stau2 und Pum2 beide direkt an die *Rgs4* 3'UTR binden. Ein funktioneller Komplex aus Stau2 und Pum2 mit *Rgs4*, der die gemeinsamen biologischen Funktionen der Proteine vermitteln könnte, konnte jedoch nicht bestätigt werden.

Diese Arbeit zeigt, dass in Stau2 auch die beiden nicht-kanonischen RBDs 1 und 2 RNA-Bindeaktivität besitzen. Diese Aktivität wurde durch biochemische und biophysikalische Methoden charakterisiert und eine wichtige Rolle der beiden Domänen für die RNA-Erkennung gezeigt. Obwohl RBD3 und 4 alleine mit hoher Affinität an RNA binden, sind RBD1 und 2 nötig, um stabile Komplexe mit RNA zu bilden. Diese Eigenschaft könnte sehr wichtig für die biologische Target-Erkennung und den RNA-Transport über größere Distanzen sein.

Abstract

Staufen (Stau) is a double-stranded RNA-binding protein (dsRBP) originally identified as an mRNA transport factor and germ-cell marker in *Drosophila*. The mammalian homolog Staufen 2 (Stau2) is specifically expressed in neurons, where it clusters in RNA granules and moves along microtubules from cell bodies to dendrites. Stau2 is an important core factor for neuronal mRNA transport and has been implicated in synaptic plasticity, memory and learning. Stau2 knockdown in rats results in reduced numbers of mature dendritic spines and impairs long-term depression of synapses. All Stau proteins contain four to five dsRNA-binding domains (RBDs). For all Stau proteins RBD3 and RBD4 are thought to be the only active RNA-binding domains, whereas RBDs 1, 2 and 5 are considered to be pseusoRBDs, which retained the fold but no activity for RNA binding. To date, the mechanistic basis of Stau2 function in the cell is not well understood. The translational repressor Pumilio 2 (Pum2) acts in the same pathways as Stau2 by forming joint messenger ribonucleoproteins (mRNPs). The 3' untranslated region (UTR) of the Stau2 target mRNA *Regulator of G-protein signaling 4* (*Rgs4)* comprises two predicted Staufen-recognized structures (SRSs) and two Pum2 binding sites in close proximity, suggesting a functional complex of Stau2, Pum2 and *Rgs4*.

In this work, it could be confirmed that Stau2 and Pum2 both bind to the *Rgs4* 3'UTR. However, a functional complex of Stau2 and Pum2 with *Rgs4* that could mediate their role in common biological processes could not be confirmed.

This work shows that in Stau2 also the non-canonical RBDs 1 and 2 exhibit RNA-binding activity. Their RNA-binding activity was characterized by biochemical and biophysical methods and an important role for both domains in RNA-recognition is demonstrated. Although RBDs 3 and 4 alone achieve high affinity binding, RBDs 1 and 2 are required to form stable complexes with RNA. This feature might be of great importance for biological target recognition and the transport of RNAs over longer distances.

Table of Contents

1. INTRODUCTION 10
1.1 RNA LOCALIZATION AND LOCAL TRANSLATION IN REGULATION OF GENE EXPRESSION 10
1.2 RNA LOCALIZATION IN NEURONS AND SYNAPTIC PLASTICITY 12
1.3 THE MAMMALIAN DSRNA-BINDING PROTEIN STAU2 15
1.3.1 Functions of the brain-specific Stau2 16
1.3.2 Staufen-mediated mRNA decay 17
1.3.3 Structure of mammalian Stau 19
1.3.4 RNA recognition by dsRNA-binding domains 20
1.3.5 Staufen-recognized structures (SRSs) 23
1.4 THE MAMMALIAN RNA-BINDING PROTEIN PUMILIO 2 24
1.4.1 Functions of Puf proteins 24
1.4.2 Pum2 in the nervous system 26
1.4.3 Structure of Pum2 and RNA recognition by the Pum-HD 27
1.5 A COMMON FUNCTION FOR STAUFEN AND PUMILIO 29
1.6 REGULATOR OF G-PROTEIN SIGNALING 4 (RGS4) IN THE NERVOUS SYSTEM 30
1.7 SPECIFIC AIMS OF THIS WORK 33
1.7.1 Characterization of Stau2-binding to a natural target RNA and identification of its specific binding sites 33
1.7.2 Characterization of the trimeric complex between Stau2, Pum2 and Rgs4 mRNA 33

2 MATERIALS AND METHODS 35
2.1 CHEMICALS AND CONSUMABLES 35
2.2 MEDIA, SUPPLEMENTS AND ANTIBIOTICS 35
2.3 GENERAL BUFFERS AND SOLUTIONS 38
2.4 ENZYMES 39
2.5 ORGANISMS AND STRAINS 39
2.6 PLASMIDS AND PRIMERS 40
2.7 RNA 52
2.8 MOLECULAR BIOLOGY 59
2.8.1 Transformation of chemically competent E. coli cells 59
2.8.2 Amplification of plasmid DNA 59
2.8.3 Agarose gel electrophoresis 60
2.8.4 Molecular cloning 60
2.8.5 Small scale RNA in vitro transcriptions 62
2.8.6 Large scale RNA in vitro transcriptions 62
2.8.7 PAGE purification of RNA 63
2.9 PROTEIN EXPRESSION AND PURIFICATION 63
2.9.1 Protein expression 63
2.9.2 Protein purification 65
2.10 CHEMICAL AND BIOPHYSICAL METHODS 67
2.10.1 Determination of DNA and RNA concentration 67
2.10.2 Determination of protein concentration 67
2.10.3 Polyacrylamide Gel Electrophoresis (PAGE) 68
2.10.4 Radioactive labeling of RNA 68
2.10.5 Electrophoretic mobility shift assay (EMSA) 69
2.10.6 TAR(+)/TAR(-) annealing assay 69
2.10.7 Biotinylation of RNA 70
2.10.8 Surface Plasmon Resonance (SPR) 70
2.10.9 In vitro Pull-Down assay 71

2.10.10 Static light scattering (SLS) ... *71*
2.10.11 Dynamic light scattering (DLS) ... *72*
2.10.12 Circular Dichroism (CD) spectroscopy ... *72*
2.10.13 Isothermal titration calorimetry (ITC) ... *72*
2.10.14 UV-Crosslinking ... *72*
2.11 BIOINFORMATICS ... 72
2.12 STRUCTURAL BIOLOGY ... 73
2.12.1 X-ray crystallography ... *73*
2.12.2 Nuclear Magnetic Resonance (NMR) ... *75*

3 RESULTS ... 76
3.1 PROTEIN PURIFICATION ... 76
3.1.1 Purification of Stau2 proteins ... *76*
3.1.2 Purification of Pum2 proteins ... *84*
3.1.3 Co-expression and purification of Stau2 and Pum2 full-length proteins ... *85*
3.2 STAU2 BINDING TO *RGS4* RNA ... 86
3.2.1 Stau2 binds unspecifically to Rgs4 3'UTR and to SRS motifs ... *86*
3.2.2 Stau2 RBD3-4 binds SRS RNA ... *88*
3.2.3 RBD1-2 binds SRS RNA with comparable affinity as RBD3-4 ... *90*
3.2.4 Elongation of SRS2 RNA improves binding by Stau2 tandem-domains ... *91*
3.2.5 Minimal length requirement of dsRNA ... *92*
3.3 PUM2 BINDING TO THE *RGS4* 3'UTR ... 94
3.3.1. Pum2 binds to Rgs4 3'UTR via non-canonical sequences ... *94*
3.3.1 The disordered N-terminal part of Pum2 contributes to Rgs4 binding ... *95*
3.3.2 Pum2 binds to SRS3 RNA ... *96*
3.4 TRIMERIC COMPLEX FORMATION BY STAU2, PUM2 AND *RGS4* RNA ... 97
3.4.1 No trimeric complex of Stau2, Pum2 and RNA can be observed in EMSAs ... *97*
3.4.2 UV radiation crosslinks only Pum2 to Rgs4 RNA, not Stau2 ... *98*
3.4.3 Stau2 cannot pull down Pum2 in in vitro pull-down assays ... *100*
3.4.4 No interaction of Stau2 and Pum2 can be observed by SPR ... *101*
3.4.5 Stau2 and Pum2 aggregate in ITC experiments ... *103*
3.5 CRYSTALLOGRAPHY OF STAU2-RNA AND PUM2-RNA COMPLEXES ... 103
3.5.1 Crystallography of Stau2-RNA complexes ... *103*
3.5.2 Crystallography of Pum2-RNA complexes ... *110*
3.6 CHARACTERIZATION OF THE STAU2 RBD1-2-RNA COMPLEX ... 111
3.6.1 RNA-binding activity and domain boundaries of single domains RBD1 and RBD2 111
3.6.2 Stau2 RBDs 1 and 2 are structured, independent domains ... *113*
3.6.3 Both Stau2 domains RBD1 and RBD2 bind RNA with different dynamics ... *114*
3.6.4 Stau2 tandem-domains bind RNA with fast kinetics ... *116*
3.6.5 Identification and characterization of Stau2 RBD1-2 RNA-binding mutants 122
3.6.6 Stochiometry and oligomeric state of the Stau2 RBD1-2-RNA complex ... *137*
3.7 STAU2 FUNCTIONS AS AN RNA CHAPERONE ... 143
3.7.1 Cloning of Stau2 RBD1-2 double-mutants for functional in vivo studies ... *145*

4 DISCUSSION ... 147
4.1 CHARACTERIZATION OF THE INTERACTION BETWEEN STAU2 AND *RGS4* ... 147
4.1.1 Assessment of Stau2-binding to Rgs4 3'UTR and to predicted SRS RNAs ... *147*
4.1.2 Stau2 tandem-domains act together for full functionality ... *149*
4.1.3 Crystallization and structure determination of the Stau2 RBD1-2-RNA complex ... *151*
4.1.4 Mutational analysis of Stau2 RBD1-2 RNA-binding ... *153*
4.1.5 A possible RNA-chaperone function of Stau2 ... *154*
4.1.6 Oligomerization of Stau2-RNA complexes ... *154*

4.1.7 Functional relevance of the RBD1-2 RNA binding activity *155*
4.2 TRIMERIC INTERACTION BETWEEN STAU2, PUM2 AND *RGS4* 156
4.2.1 Pum2 binds Rgs4 3'UTR via a non-canonical mechanism *156*
4.2.2 No evidence of trimeric Stau2-Pum2-Rgs4 complex formation *158*

5 ACKNOWLEDGEMENTS **159**

6 APPENDIX **160**
6.1 LIST OF ABBREVIATIONS 160
6.2 LIST OF FIGURES 162
6.3 SUPPLEMENTARY FIGURES 165

7 REFERENCES **168**

1. Introduction

1.1 RNA localization and local translation in regulation of gene expression

The regulation of gene expression by posttranscriptional or translational control is a common cellular strategy involved in a wide range of biological processes, for example migration, establishment and maintenance of polarity and cell fate specification. The great advantage of controlling gene expression on the translational level is that it allows for faster responses to external or internal signals than transcription. Furthermore, it allows for the regulated amplification of the information from a single RNA molecule into up to hundreds of proteins. Translational control can occur temporally or spatially, or in a combination of both. Spatial control requires mRNA localization to subcellular compartments before translation, allowing for an asymmetric distribution of mRNAs in steep gradients. This can be achieved by three different mechanisms. First, mRNA can simply diffuse through the cytoplasm and, once it reaches its destination, be anchored. Second, localization can be achieved by asymmetric degradation of mRNA, leaving transcripts only in certain compartments of the cell. Third, mRNA can be actively transported in a directional fashion. In this case, mRNA localization is initiated by recognition of *cis*-acting regions termed zip-code or localization elements (LEs) in the mRNA by dedicated RNA-binding proteins (RBPs), forming so-called messenger ribonucleoproteins (mRNPs). Assembly of such mRNPs begins often already co-transcriptionally in the nucleus. LEs often but not exclusively reside in the 3'UTRs of mRNAs and are very heterogeneous. They can range in size from few nt to ~1 kb in length and contain secondary structures such as stem-loops. One transcript can contain several LEs that may either be redundant or involved in distinct localization steps. Once exported into the cytoplasm, these mRNPs are remodeled into motor-protein containing complexes, which are subsequently actively transported along the cytoskeleton, usually in a translationally repressed state (Jansen and Niessing, 2012, Singer-Kruger and Jansen, 2014, Marchand et al., 2012). Such mRNPs regulate cellular protein production in a spatiotemporal way, e.g. by asymmetric stabilization or

decay of mRNAs and translational control. Thus, RBPs have a strong impact on protein levels in different subregions of cells (Moore, 2005).

Few well-studied examples that significantly contributed to the general understanding of mRNPs are described below. For instance in budding yeast, *ASH1*-mRNA is actively transported from the mother to the daughter cell by a motor-dependent translocation complex (Heym et al., 2013, Edelmann et al., 2015). *ASH1* encodes for a transcriptional repressor that inhibits mating-type switching in the daughter cell and thus ensures different cell fates. During mitosis, the *ASH1*-mRNA is co-transcriptionally recognized by the RBP She2p via its four *cis*-acting elements E1, E2A, E2B and E3 (Olivier et al., 2005). Nuclear joining of Loc1p stabilizes this complex. Even though Loc1 is a strictly nuclear protein, cytosplasmic *ASH1* transport depends on this interaction. Upon nuclear export, Loc1p is replaced by the cytoplasmic RBP She3p (Niedner et al., 2013), which then results in a synergistic and specific complex of She2p and She3p with *ASH1*. The complex is tethered via She3p to the type V myosin Myo4p (Bohl et al., 2000, Long et al., 2000, Takizawa and Vale, 2000) and transported along actin filaments to the bud tip, where it is anchored and translationally activated (Takizawa et al., 1997, Chartrand et al., 2002).

Other well-studied examples come from *Drosophila* oogenesis (Bastock and St Johnston, 2008, Kugler and Lasko, 2009). Notably, >70 % of transcribed RNAs are asymmetrically localized in early *Drosophila* embryos (Lecuyer et al., 2007) (Jambor et al., 2015). Here, mRNA localization is a fundamental requirement for body axis formation (Lasko, 2012, Bashirullah et al., 1998, Riechmann and Ephrussi, 2001). Maternal RNAs such as *bicoid* (Cha et al., 2001), *gurken* (MacDougall et al., 2003) (Jaramillo et al., 2008) and *oskar* (*osk*) (Ephrussi et al., 1991) (Kim-Ha et al., 1991) are first transported from the nurse cells to the oocyte and subsequently localized to distinct domains in the oocyte. *osk* mRNA is localized to the posterior pole of the oocyte and exclusivley translated upon arrival. It encodes the posterior determinant Oskar, which induces abdomen and germline formation in the embryo (Lasko, 2012). *Osk* transport from the nurse cells to the oocyte is directed by the well-described oocyte entry signal LE, which recruits the Egalitarian-Bicaudal-dynein transport machinery (Jambor et al., 2014, Navarro et al., 2004, Dienstbier et al., 2009). In the oocyte, localization to

the posterior domain is mediated by the kinesin-1 motor. This requires splicing (Hachet and Ephrussi, 2004) of the first intron of *osk* which results in the formation of a new LE, the spliced oskar localization element (SOLE), and the deposition of the exon-junction complec (EJC) on the mRNA. Formation of the EJC/SOLE is crucial for kinesin-1-dependent *osk* transport to the posterior pole (Ghosh et al., 2012). During transport, *osk* is packaged in large particles containing multiple *osk* molecules for efficient transport and making them inaccessible for the translation machinery (Jambor et al., 2011), thus repressing translation during transport. These particles contain the polypyrimidine tract-binding protein, which mediates their formation by binding to multiple sites in the *osk* 3'UTR, and the translational repressor Bruno, which binds to several Bruno response elements in the *osk* 3'UTR (Kim-Ha et al., 1995, Nakamura et al., 2004, Chekulaeva et al., 2006). Large *osk* particles furthermore contain the double-stranded RNA-binding protein (dsRBP) Staufen (Stau). *Drosophila melanogaster* (dm) Stau is required for posterior localization of *osk*. Mutations in dmStau cause accumulation of *osk* mRNA at the anterior pole (Ephrussi et al., 1991, St Johnston et al., 1991). *staufen null* mutant embryos fail to form abdominal patterns.

A fundamental problem in understanding the molecular principles underlying mRNA localization and localized translation in mammals is the high complexity of these mRNP assemblies. This makes it difficult to link general cellular observations of gene regulation with the molecular interactions required for mRNP function.

1.2 RNA localization in neurons and synaptic plasticity

Neurons are highly polarized cells with a cell body, an extended axon and a differentiated dendritic tree. mRNAs are transcribed exclusively in the nucleus, however, protein synthesis is required also at remote cellular compartments, meaning that mRNAs must travel long distances from the soma before being translated. mRNA localization occurs in mRNPs and plays important roles from neurogenesis to the mature nervous system (Holt and Schuman, 2013). For example in immature neurites, local translation of mRNAs in axonal growth cones critically contributes to axon guidance and the ability of axons to respond to environmental cues (Lin and Holt, 2007).

In the mature nervous system, neuronal mRNA localization to pre- and postsynaptic areas followed by local translation has been implicated in memory and learning (Doyle and Kiebler, 2011, Sutton and Schuman, 2006, Kiebler and DesGroseillers, 2000). Long-term memory formation requires synaptic plasticity, meaning the ability of neurons to alter the efficacy of individual synapses in an experience-dependent manner. Synaptic plasticity is achieved by balanced long-term potentiation (LTP) and long-term depression (LTD) of individual synapses. Both processes require local protein sythesis in dendrites and thus synaptic mRNA localization, as it provides the synapse with the possibility of spatially and temporally restricted gene expression, altering only function and morphology of its own microenvironment independently of the cell soma. Such dendritically expressed genes produce proteins with synaptic functions, for example the Ca^{2+}/calmodulin kinase II (CaMKIIα), the cytoskeletal protein Arc or microtubule-associated protein 2 (MAP2), and α-amino-3-hydroxy-5-methyl-4-isoxazolepropionic acid (AMPA) or *N*-methyl-D-aspartic acid (NMDA) receptors (Doyle and Kiebler, 2011) (Buxbaum et al., 2015). Two types of mRNPs have been implicated in synaptic plasticity: mRNA particles and mRNA granules, which differ by the absence or presence of ribosomes, respectively. Although neuronal granules contain ribosomal subunits and translation initiation factors, the contained mRNAs are translationally silent (Anderson and Kedersha, 2006).

One current model of dendritic mRNA transport is summarized in the so-called 'sushi belt model' (Doyle and Kiebler, 2011) depicted in Figure 1. In this model, pre-mRNPs are made in the neuron's nucleus. While RNA is transcribed and processed, certain RBPs are deposited on it, for example the EJC. These pre-mRNPs are exported into the cytoplasm where they undergo remodeling for instance by recruiting adaptor and motor proteins. Furthermore, certain RBPs may be exchanged at this step. These mature mRNPs are constantly and bidirectionally transported in dendrites along the microtubule cytoskeleton, passing synapses regularly. Only when a synapse is activated and undergoes synaptic tagging, meaning it obtains a local signal that marks it for remodeling, it can recruit and capture mRNPs. This may occur by recruitment of dynamic microtubules into the dendritic spine, however, the exact nature of synaptic tags remains unclear and may vary in different regions of the brain. Possible

mechanisms are posttranslational modifications or conformational changes of existing proteins. After delivery to the activated synapse, mRNA is released from the mRNP and locally translated. This local protein synthesis allows for remodeling of the synapse, for example for LTP or LTD.

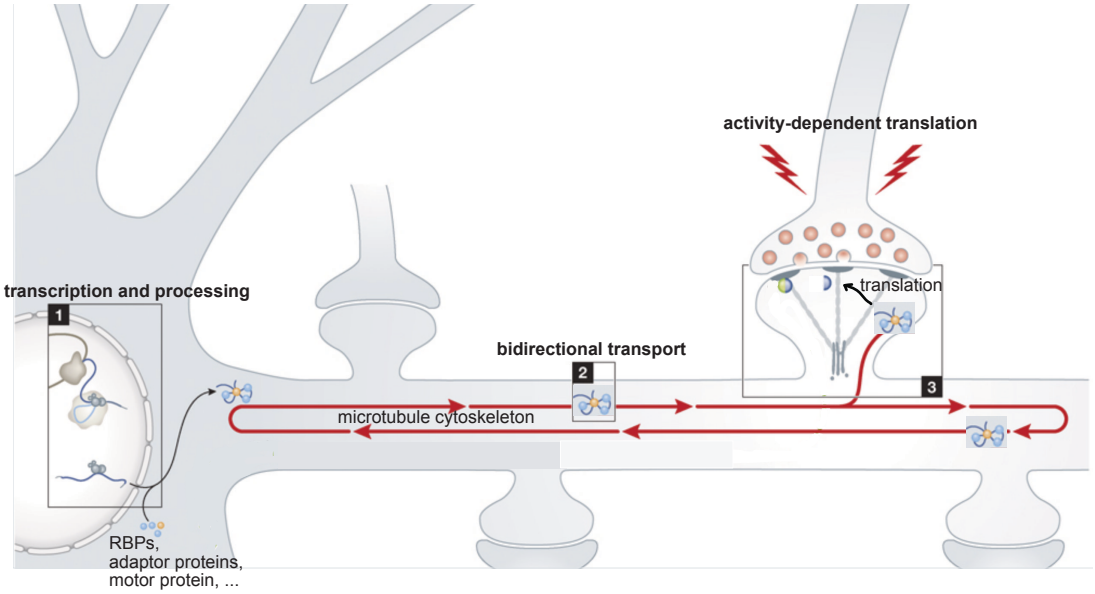

Figure 1: The sushi belt model. Adapted with permission by John Wiley and Sons from (Doyle and Kiebler, 2011). 1) RNA is transcribed, processed and loaded with initial RBPs to form a pre-mRNP in the nucelus. The pre-mRNP is exported to the cytoplasm and remodeled to form a mature mRNP, e.g. loaded with further RBPs, adaptor and motor proteins. 2) mRNPs are transported bidirectionally through the dendrite by motor proteins on the microtubule cytoskeleton and patrols synapses. 3) When a synapse undergoes synaptic tagging due to activation, it recruits mRNPs by recruiting dynamic microtubules into the dendritic spine and capturing the mRNP. mRNA is released from the mRNP and locally translated, providing protein for synapse remodeling.

Very recently, evidence was found that mRNA can also be transported to synapses intercellularly from neighbouring neurons in virus-like capsids formed by the neuronal protein Arc and that this mRNA can undergo activity-dependent translation (Pastuzyn et al., 2018), pointing at an additional mechanism to provide mRNA for synaptic plasticity.

Among the best-studied examples for neuronal mRNA transport is *β-actin* localization by zipcode binding protein 1 (ZBP1). ZBP1 binds the LE of *β-actin* in the axonal growth cones of developing neurons and regulates its local translation there (Lin and Holt, 2007). In mature neurons the *β-actin*-ZBP1 complex trafficks to dendritic spines upon synaptic activation. ZBP1 represses *β-actin* translation during transport and, once at its destination, is released from the complex upon phosphorylation by Src, allowing local β-actin expression (Huttelmaier et al.,

2005, Doyle and Kiebler, 2011). The LE of *β-actin* is a 54 nt bipartite motif in which the properly spaced sequences C/A-CA-C/U and CGGAC are recognized by the ZBP1 hnRNP K homology (KH) domains KH3 and KH4, respectively (Patel et al., 2012).

Another important neuronal mRNP is Fragile X Mental Retardation Protein (FMRP). FMRP regulates transport of several localized transcripts such as CaMKIIα in dendrites. It was reported to directly associate with kinesin heavy chain, suggesting that it links transported mRNAs to motor proteins (Dictenberg et al., 2008). Furthermore, FMRP acts as a translational regulator at the synapse upon activation of metabotropic Glutamate receptors (mGluRs). This is controlled by FMRP phosphorylation and miRNA interaction (Muddashetty et al., 2011). Thus, as does ZBP1, FMRP acts as a transport factor and translational regulator of dendritic transcripts and its malfunction causes altered dendritic spine morphology, loss of translation-dependent synaptic plasticity and impaired synaptic function, resulting in neurological disorders as fragile X syndrome (Doyle and Kiebler, 2011, Santoro et al., 2012, Bagni and Oostra, 2013).

1.3 The mammalian dsRNA-binding protein Stau2

The dsRBP Stau was originally identified as an mRNA transport factor and germ-cell marker in *Drosophila* (St Johnston et al., 1991). The two mammalian Stau homologs, Stau1 and Stau2 have been implicated in RNA transport, stability and decay, translation regulation and anchoring (Dugre-Brisson et al., 2005, Kim et al., 2005, Micklem et al., 2000, Tang et al., 2001, Zimyanin et al., 2008). In neurons, Stau has been implicated in asymmetric cell divisions during neurogenesis (Vessey et al., 2012, Kusek et al., 2012), memory formation in the mature nervous system (Lebeau et al., 2011), and is associated with RNA granules involved in neurodegenerative disorders (Tosar et al., 2012). The two paralogs Stau1 and Stau2 were reported to bind distinct, yet overlapping, sets of target mRNAs (Furic et al., 2008), indicating distinct but possibly complementary functions.

1.3.1 Functions of the brain-specific Stau2

Whereas Stau1 is ubiquitously expressed, the expression of Stau2 is specific for brain and heart (Duchaine et al., 2002, Monshausen et al., 2004, Tang et al., 2001) and is a well-confirmed factor in mRNA localization.

In rat hippocampal neurons, both Stau1 and Stau2 localize in large RNA-containing particles (Kiebler et al., 1999), but Stau1 and Stau2 mRNPs contain distinct sets of target mRNAs. Both sets of target RNAs, however, are predominantly involved in cell metabolism, transport and localization, transcription, alternative splicing, metal-ion binding, regulation of cell processes and catalytic activity (Furic et al., 2008), indicating overlapping or complementary functions of Stau1 and Stau2. Both Stau paralogs move along microtubules from cell bodies to dendrites (Kiebler et al., 1999) but do not co-localize in dendrites, further indicating their location in distinct mRNPs (Duchaine et al., 2002). Knockdown of Stau1 inhibits the transport of reporter-RNA into distal dendrites (Kanai et al, 2004). Overexpression of Stau2 increases the amount of reporter-RNA localized to dendrites (Kanai et al., 2004, Tang et al., 2001). Stau is thus commonly used as a stable marker for tracking of neuronal transport mRNPs.

When Stau1 (Lebeau et al., 2008) or Stau2 (Goetze et al., 2006) are downregulated in neurons by RNA interference (RNAi), these neurons show morphological changes, marked by the reduction of dendritic spine density, and reduced synaptic transmission. Whereas Stau1 is required for synaptic LTP (Lebeau et al., 2008), Stau2 affects mGluR-dependent LTD (Lebeau et al., 2011), indicating that the two proteins have specific functions in separate physiological processes and clearly demonstrating that Stau proteins critically contribute to synaptic plasticity.

Recently, phenotypic changes in a conditional Stau2 knockdown rat model have been reported. These animals had reduced dendritic spine density, enhanced LTP and impaired LTD as well as altered spatial working memory and associative memory (Berger et al., 2017).

During neurogenesis, Stau2 is required for asymmetric mRNA distribution of cell fate markers in asymmetric neural stem cell divisions (Kusek et al., 2012, Vessey et al., 2012). Its knockdown leads to premature differentiation and

overexpression to the formation of abnormal periventricular masses (Kusek et al., 2012, Vessey et al., 2012), demonstrating its importance for progenitor cell maintenance and differentiation during normal development.

Several protein components of Stau2 mRNPs have been reported, for instance Y box binding protein 1 and Polyadenylate-binding protein 1, both of which are known as translational modulators that can repress or activate translation as well as stabilize mRNA (Maher-Laporte et al., 2010). Furthermore, Heat shock cognate 71 kDa protein (Hsc70) was found in Stau2 mRNPs, a chaperone that can stabilize RNA by binding tu AU-rich stretches and modulate the folding of RNA (Maher-Laporte et al., 2010). Hsc70 might also be involved in nuclear shuttling of Stau2 mRNPs and their release from motor proteins (Maher-Laporte et al., 2010). In neuronal progenitor cells, Stau2 mRNPs were reported to contain the translational repressor Pumilio 2 (Pum2) and the DEAD-box helicase (DDX) 1 (Vessey et al., 2012). An interactome study used immunoprecipitation (IP) to identify a set of 65 proteins in Stau2 mRNPs (Fritzsche et al., 2013). Examples are the nuclear cap-binding protein 80 and the poly(A) binding protein nuclear 1, both of which are displaced from RNA upon translation. Furthermore, the translational repressors Pum2, FMRP, Pur-α, DDX6 and RNA-binding protein 14 were found in Stau2 mRNPs. Taken together, this indicates that mRNAs in Stau2 mRNPs are translationally silent. Also, the members of the RNA-induced silencing complex Mov10, Ago2 and protein activator of the dsRNA-activated protein kinase were identified in Stau2 mRNPs.

Despite the importance of the brain-specific Stau2, its molecular action is little understood.

1.3.2 Staufen-mediated mRNA decay

Aside from spatial and temporal control, gene regulation can also be controlled posttranscriptionally by mRNA decay. A number of cytoplasmic mRNA decay mechanisms perform quality control of transcripts to circumvent abberant gene expression from incorrectly processed mRNAs, for example nonsense-mediated mRNA decay (NMD), nonstop mRNA decay or no-go decay. Additionally, *cis*-acting elements in mRNAs, often located in their 3'UTRs, serve normal gene regulation by determining the cytoplasmic half-life of mRNA to maintain cellular homeostasis, for example AU-rich element (ARE)-mediated decay (von Roretz

and Gallouzi, 2008), NMD (Nasif et al., 2018), miRNA-mediated decay (Iwakawa and Tomari, 2015) or Staufen-mediated decay (SMD) (Park and Maquat, 2013).

SMD is a translation-dependent decay mechanism that requires the interaction of up-frameshift protein (UPF) 1 with RNA-bound Stau1. UPF1 is an RNA helicase that is essential also for NMD (Gupta and Li, 2018). During SMD, Stau1 directly recruits UPF1 to mRNA 3'-UTRs. It triggers mRNA decay when translation terminates sufficiently upstream of the site of its Stau1-dependent recruitment (Park and Maquat, 2013).

This way, Stau1 was shown to decrease the half-lifes of a number of RNAs by binding to their 3'UTRs (Kim et al., 2005, Kim et al., 2007). Binding occurs at so called Staufen-binding sites (SBSs) (Kim et al., 2005) downstream of the translation termination site that can be formed either intramolecularly or intermolecularly. The only well-characterized SBS formed by one RNA is the one of *ADP ribosylation factor* (*ARF*) 1, a 19 bp-stem formed by nt 75-93 and 194-212 of its 3'UTR with a 100 nt apex (Kim et al., 2007, Park and Maquat, 2013). Such structures could, however, not be identified in other known SMD targets. Another subset of SMD targets includes an Alu element (named after the *Arthrobacter luteus* restriction enzyme AluI, which cleaves the element into two pieces) in their 3'UTRs. Alu elements are short interspersed elements that make up 11 % of primate genomes (Deininger, 2011). More than 300 long non-coding RNAs (lncRNAs) comprise one or more of them (Park and Maquat, 2013). Such lncRNAs can serve as so-called ½ sbsRNAs, which base pair with Alu elements in the 3'UTRs of SMD target mRNA. These intermolecular duplexes can be bound and stabilized by Stau1, triggering SMD (Gong and Maquat, 2011, Park and Maquat, 2013).

Recent reports show conflicting results on whether Stau2 mediates SMD. In HeLa cells, both paralogs were reported to mediate SMD to approximately the same extents (Park et al., 2013, Park and Maquat, 2013). This is in conflict with a previous study, which showed that tethering Stau2 to the 3'UTR of a reporter mRNA does not influence its protein levels in HeLa cells (Miki et al., 2011). The authors conclude that Stau2 is unlikely to mediate SMD in HeLa cells. However, both studies find that Stau2 directly interacts with UPF1.

SMD requires dimerization or possibly multimerization of Stau1 (Gleghorn et al.,

2013). Also heterodimerization with Stau2 was reported to trigger SMD (Park et al., 2013).

During human epidermal differentiation, Stau1 together with the terminal differentiation-induced non-coding RNA (TINCR), was shown to stabilize mRNAs in an UPF1-independent manner ensuring high mRNA abundance of key differentiation genes (Kretz et al., 2013). Stau2 was also reported to stabilize mRNA independently of UPF1 in 293F cells and to enhance translation in a UPF1-dependent manner (Miki et al., 2011), arguing for a cell-type dependent function of Stau on gene regulation. Furthermore, in primary cortical neurons, the majority of target RNAs are downregulated upon Stau2 knockdown but a subset of RNAs is upregulated (Heraud-Farlow et al., 2013), indicating that regulation is also transcript-specific.

1.3.3 Structure of mammalian Stau

Stau1 and Stau2 share about 50 % overall sequence identity and have at least two and four protein isoforms by alternative splicing, respectively (for an overview, see Figure 2 A) (Wickham et al., 1999, Monshausen et al., 2004, Miki et al., 2005, Gleghorn et al., 2013). All Stau proteins contain four to five dsRNA-binding domains (RBDs) and a tubulin-binding domain (TBD) located between RBD4 and RBD5. In human Stau, RBD3 and RBD4 are thought to mainly, if not solely, bind RNA (Wickham et al., 1999, Gleghorn et al., 2013, Duchaine et al., 2002), whereas RBDs 1, 2 and 5 are often referred to as pseudo-RBDs, which retained only the fold but not activity of true RBDs (Gleghorn et al., 2013). The longest isoform of Stau2, Stau2^{62}, is most similar to the well-known *Drosophila* Stau, possessing all five RBDs. Stau2^{62} shuttles between nucleus and cytoplasm and has thus been proposed to transport RNAs from the nucleus to distal dendrites (Macchi et al., 2004, Miki et al., 2005, Doyle and Kiebler, 2011). In the shorter isoforms, RBD1 is either truncated or missing. Stau1 isoforms neither comprise RBD1. RBD5 of Stau2 is truncated as compared to Stau1, comprising only its N- and C-terminal sequences. In Stau1, a so-called Staufen swapping motif (SSM) was identified. The SSM is located N-terminal of RBD5 and mediates protein dimerization together with RBD5 (Gleghorn et al., 2013). Although Stau2 was reported to form homodimers and heterodimers with Stau1 in cells (Park et al., 2013), a physical interaction has not yet been confirmed.

To date, high-resolution structures are available only for single RBDs without RNA bound or in complex with a non-physiological RNA Figure 2 B). The known Stau RBD structures adopt the expected canonical α-β-β-β-α RBD fold (see section 1.3.4).

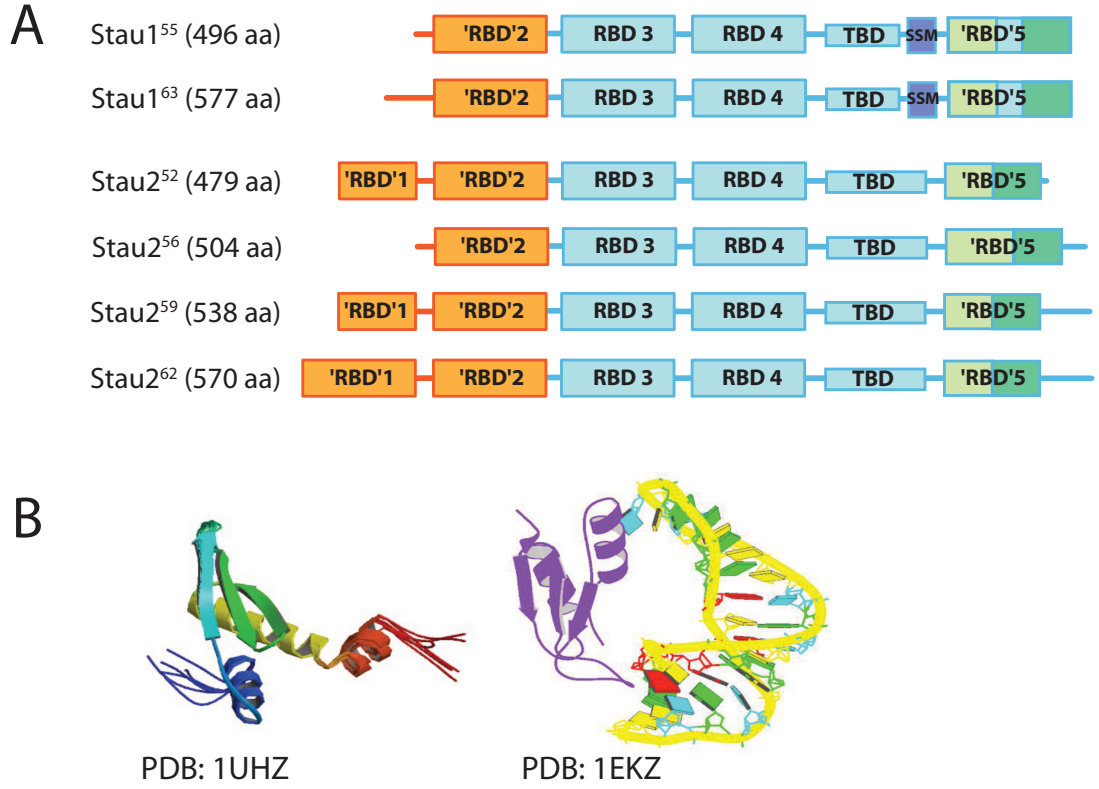

Figure 2: Mammalian Stau proteins. A) Scheme of domain architectures of mammalian Stau proteins. By alternative splicing, there are at least two isoforms of Stau1 and four isoforms of Stau2. RBD=dsRNA-binding domain, SSM=Staufen swapping motif, TBD=Tubulin-binding domain. **B)** Solution NMR structures of Staufen RBDs. PDB 1UHZ (left): RBD4 from mouse Stau2 (Gu et al., 2004). PDB 1EKZ (right): RBD3 from *Drosophila* Staufen bound to RNA (Ramos et al., 2000). Both structures show the canonical α-β-β-β-α fold of RBDs.

1.3.4 RNA recognition by dsRNA-binding domains

The double-stranded RNA-binding domain is a conserved protein motif that marks the protein family of dsRBPs. dsRBPs occur in a wide range of proteins across many species that are involved in many different biological processes, including RNA interference pathways, RNA processing and RNA transport. The dsRBD motif was first identified based on sequence similarity between *Drosophila* Staufen, human TRBP and its *Xenopus laevis* homolog Xlrbpa (St Johnston et al., 1992). The domain is, next to the RNA recognition motif (RRM) and zinc finger domains, among the most abundant RNA-binding domains. It is roughly 65-70 amino acids (aa) in size and comprises a typical αββββα-fold in

which the two helices on one side pack against an antiparallel β-sheet on the other side (Masliah et al., 2013). The consensus sequence of the dsRBD is shown in Figure 3 A. The most conserved part is the C-terminal third of the domain. The dsRBD can mediate protein-RNA but also protein-protein interactions. Notably, dsRBDs that differ from the consensus sequence in the N-terminal two thirds were termed type B or type II dsRBDs and are thought to be involved in protein-protein interactions while having only low affinity to RNA (Masliah et al., 2013, Wang et al., 2015) (Gleghorn and Maquat, 2014).

Canonical RNA recognition by a dsRBD is structure- but not sequence-dependent, as it binds to the phosphate backbone of an A-form RNA helix (Masliah et al., 2013, Lunde et al., 2007). A number of structural studies showed that binding occurs via three conserved regions, located in helix α_1, loop 2 (connecting β_1 and β_2) and helix α_2. The domain spans a minor-major-minor groove of A-form dsRNA. α_1 contains a conserved glutamate residue that binds to the minor groove of dsRNA. On α_2, there is a conserved KKxxK motif, which interacts with dsRNA across the adjacent major groove. Loop 2 contains a conserved histidine in a GPxH motif which hydrogen bonds with the subsequent minor groove (Masliah et al., 2013, Wang et al., 2015). These three regions recognize the dsRNA by probing its shape. The KKxxK motif in region 3 probes the width of the major groove (10 Å in A-form RNA as opposed to 17 Å in B-form DNA (Saenger, 1984)) by interaction with the non-bridging oxygens of the phosphodiester backbone. The regions in α_1 and loop 2 sense by direct or water-mediated hydrogen-bonding the 2'-OH groups present in dsRNA, which line up in the wide minor grooves of A-form RNA (15 Å as opposed to 11 Å in B-form DNA (Saenger, 1984)) and are not present in DNA. As observed in several dsRBD structures, for instance of dmStau dsRBD3 bound to a stem-loop RNA (PDB 1EKZ, Figure 2 B) (Ramos et al., 2000), region 1 in α_1 can also recognize apical loops by contacting the sugars and bases of the loop and the base pair immediately adjacent to it. α_1 contacts the minor groove of the loop with most of its side chains occupying the same positions as in dsRNA minor groove recognition. Another almost absolutely conserved residue plays an important indirect role for RNA-binding. The phenylalanine at the beginning of β_2 orients

key positively charged residues optimally for RNA-binding (Masliah et al., 2013). The canonical dsRBD-RNA interaction is illustrated in Figure 3 B.

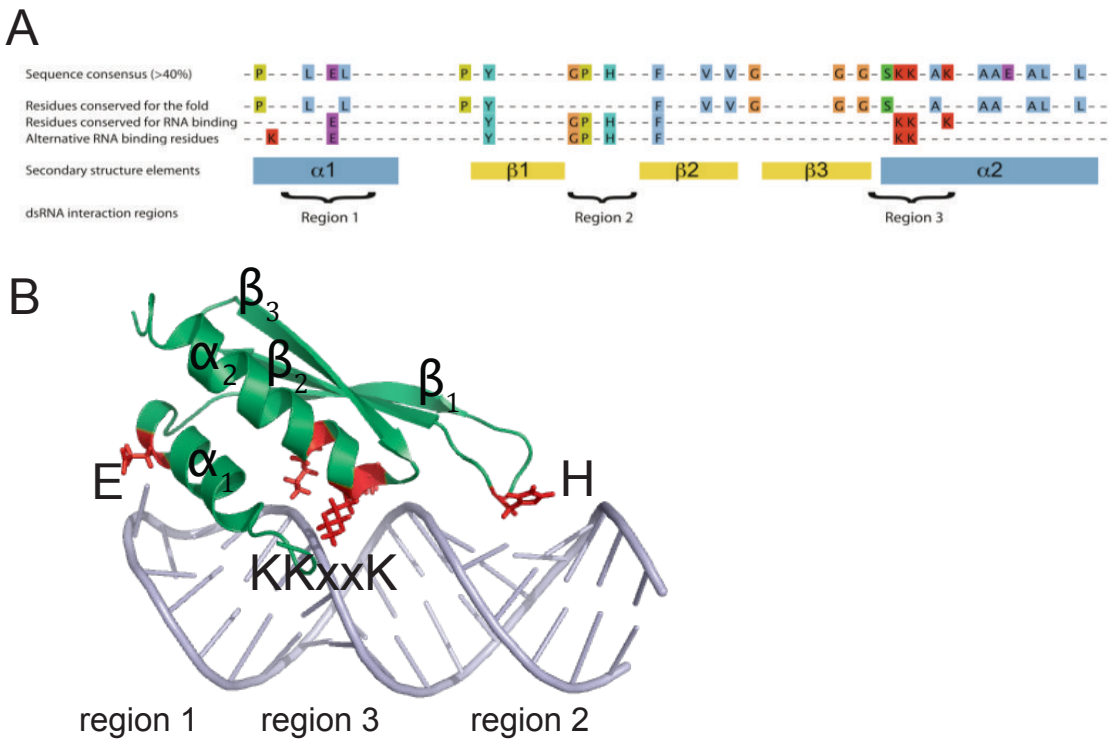

Figure 3: The double-stranded RNA-binding domain. A) Consensus sequence and secondary structure of the dsRNA-binding domain. Adapted with permission by Springer Nature from (Masliah et al., 2013). **B)** Canonical binding mode of a dsRBD at the example of ADAR2 dsRBD1 (PDB 2LC3).

Overall, the structures of dsRBDs are well conserved, but some variations have been reported, for instance the loop 2 connecting β_1 and β_2 which usually has six aa can contain insertions. In *S. pombe* Dicer1, shortening of this loop abolishes RNA-binding (Barraud et al., 2011). Residues in an extended loop 2 can also mediate protein binding as shown for *A. thaliana* HEN1, in which this loop interacts with the protein's catalytic domain, possibly orienting it properly towards the dsRNA substrate (Huang et al., 2009, Masliah et al., 2013). Furthermore, few dsRBDs have been reported to read out the sequence of the dsRNA minor groove to add some specificity to the canonical shape recognition, for instance the dsRBDs of ADAR2 harbor a methionine in α_1 that extends into the minor groove and contacts an adenine in a physiologic target RNA. A guanine in this position would induce a sterical clash, thus excluding dsRNA with a guanine as targets (Stefl et al., 2010).

Despite the fact that dsRBPs often contain multiple dsRBDs, little is known about their interplay. The number of dsRBDs in a protein does not correlate with overall binding affinity (Wang et al., 2015). In the two available solution structures of tandem-dsRBDs (from PKR and ADAR2), the linkers between the domains are flexible, leading to independent domains (Nanduri et al., 1998, Stefl et al., 2006). The crystal structure of the tandem-dsRBDs from DiGeorge syndrome chromosomal region 8 (DGCR8) is the only known example in which two C-terminally extended dsRBDs interact extensively (Sohn et al., 2007). It remains unclear if and how multiple dsRBDs interact with each other and work together to modulate RNA-binding with regards to specificity and affinity.

Whereas dsRBDs bind dsRNA quite unspecifically *in vitro*, they function on specific targets *in vivo*. For instance in *Drosophila*, dmStau recognizes *osk* mRNA very specifically at its 3'UTR. It remains puzzling how this specificity is achieved and further investigation of the interplay of these domains in dsRBPs that contain multiple dsRBDs are likely to improve our current understanding of their function.

1.3.5 Staufen-recognized structures (SRSs)

Cell-based assays in several cell-types helped to identify certain sets of target RNAs for different Stau proteins (Furic et al., 2008, Kusek et al., 2012, Maher-Laporte et al., 2010, Heraud-Farlow et al., 2013). Generally, Stau target RNAs tend to have very long 3'UTRs (Laver et al., 2013). Yet, how these targets are specifically recognized and what distinguishes Stau targets from non-targets is not clear. Few short and well-defined RNA-binding regions for mammalian Stau have been characterized to date. One known target of SMD is *ARF1*. Its SBS is a 19 bp stem with an apex of 100 nucleotides located in the 3'-UTR (see section 1.3.2).

A genome-wide, microarray-based analysis of dmStau bound RNAs identified three types of secondary structures that are highly enriched in these RNAs and proposed them as Staufen-recognized structures (Laver et al., 2013). SRSs are dsRNA stems of 19 or 12 bp in length with the latter often contained in the longer one. An SRS is generally described by [M, N, U] in which M denotes the number of bases in the contiguous segment, N is the minimum number of paired bases in this contiguous segment and U is the maximum number of unpaired

bases in the stem. A type I SRS is a [19,15,0] containing a [12,10,0] ([19,15,0]&[12,10,0]), a type II SRS is [19,15,4]&[12,10,2] and type III is a [12,10,2] (Laver et al., 2013). These structures fit previously discovered Stau binding sites, for instance in *Drosophila bicoid* or in human *ARF1*. An enrichment of type III SRSs was also reported in neuronal Stau2-target RNAs identified by microarray-based experiments (Heraud-Farlow et al., 2013).

1.4 The mammalian RNA-binding protein Pumilio 2

Pum 1 and Pum2 are the mammalian members of the highly conserved PUF (Pumilio and FBF) family of RNA-binding proteins (Wang et al., 2018). PUF proteins are posttranscriptional regulators that influence stability and translation of mRNAs (Quenault et al., 2011, Wickens et al., 2002, Wharton and Aggarwal, 2006). The protein family is characterized by the presence of a Pumilio-homology domain (Pum-HD) (Wang et al., 2001). Pum1 and Pum2 are co-expressed in diverse tissues (Spassov and Jurecic, 2003) and associated mRNAs strongly overlap, indicating partially redundant functions (Morris et al., 2008, Galgano et al., 2008).

1.4.1 Functions of Puf proteins

The cellular functions of PUF proteins are diverse. They have been implicated in stem-cell maintenance and renewal, differentiation, developmental patterning, neuronal functioning and memory, organelle biogenesis and cell cycle (Wickens et al., 2002, Quenault et al., 2011, Wang et al., 2018). The canonical function of PUF proteins is translational repression of their target mRNAs by direct recruitment of the Ccr4-Pop2-NOT complex via its Pop2 subunit, an mRNA deadenylase that shortens poly(A)-tails, thus decreasing mRNA half-life (Goldstrohm et al., 2006, Goldstrohm et al., 2007, Lee et al., 2010, Hook et al., 2007).

Additionally, several other repression mechanisms of PUF proteins have been reported. *Xenopus* Pum2, for example, binds to the mRNA 5'cap to inhibit binding of the translation initiation factor eIF4E, thereby preventing translation initiation (Cao et al., 2010). In yeast, the non-canonical Puf6p binds the

translation initiation factor eIF5B/Fun12 to inhibit translation of *ASH1* during transport (Deng et al., 2008).

Drosophila Pum was first discovered for its role in embryonic development, where it is required for abdominal segmentation through translational control of *hunchback* (Lehmann and Nusslein-Volhard, 1987). Together with Nanos, Pum represses hunchback expression at the posterior pole (Sonoda and Wharton, 1999). While Nanos activates Pum, Pum can also repress translation independently through three repression domains within its N-terminal two-thirds (Weidmann and Goldstrohm, 2012). This repressive function seems to be conserved in mammalian Pum1 and Pum2 as indicated by sequence alignments and tethering assays (Weidmann and Goldstrohm, 2012).

Furthermore, several examples have been reported in which PUFs act as translational activators, for instance during development by supporting cytoplasmic polyadenylation. In *Xenopus* oocytes, Pum stabilizes the binding of cytoplasmic polyadenylation element-binding protein (CPEB) to the cytoplasmic polyadenylation element by cooperative binding to a Pum-binding element in the same mRNA, thereby contributing to translational activation by CPEB (Pique et al., 2008). Also the *C. elegans* PUF FBF is thought to recruit and stimulate the cytoplasmic polyadenylase GLD-2/GLD-3 to its target mRNA (Suh et al., 2009). FBF has also been proposed to activate the translation of *egl-4* in olfactory sensory neurons during odor adaptation by direct binding to its 3'UTR (Kaye et al., 2009).

To date, it remains unclear whether all PUFs can act as both repressors and activators and whether they can have both functions on the same mRNAs or repress some targets while activating others (Quenault et al., 2011).

Some PUFs, such as Puf6p from yeast, are also involved in mRNA localization (Gu et al., 2004, Vessey et al., 2006). During budding, Puf6p directly binds to the *ASH1* 3'UTR and inhibits its translation during transport to the bud tip (see chapter 1.1). Upon arrival at the bud tip, Puf6p is phosphorylated and repression is relieved. Asymmetric *ASH1* localization depends on translational repression and is defective in *puf6* mutants (Deng et al., 2008, Gu et al., 2004). Puf3p is

involved in mitochondrial localization of mRNAs encoding mitochondrial proteins (Gerber et al., 2004, Saint-Georges et al., 2008).

For most target mRNAs, their regulation is mediated by direct binding of the PUF protein to specific sites in the 3'UTR. Canonical binding of mRNAs by PUFs occurs via conserved UGUR elements in their 3'UTRs. The minimal binding sequence is typically 8-10 bases in length (Lebeau et al., 2011).

1.4.2 Pum2 in the nervous system

Drosophila Pum controls neuron function and memory formation (Dubnau et al., 2003, Mee et al., 2004, Menon et al., 2004, Schweers et al., 2002). *pum* mutant phenotypes uncovered several functions in the nervous system. Pum controls dendrite morphogenesis (Ye et al., 2004) and regulates synaptic growth by repression of the translation factor eIF4E and the glutamate receptor subunit GluRIIA (Menon et al., 2004, Menon et al., 2009). Additionally, Pum inhibits neuronal excitability by repression of the voltage-gated sodium channel *paralytic* (Muraro et al., 2008). Pum deficient larvae thus suffer from hyperexcitability in motor neurons at the neuromuscular junction (Schweers et al., 2002). Loss of Pum leads to phenotypes with impaired long-term memory (Dubnau et al., 2003). Thus, Pum plays an important role in the fly's nervous system.

Mammalian Pum2 is expressed in hippocampal neurons where it plays a role in activity-independent morphogenesis of dendrites, dendritic spines and excitatory synapses by regulating the number of excitatory synapses along the dendritic shaft (Vessey et al., 2010). Similar to *Drosophila* Pum, Pum2 likely translationally controls eIF4E and the voltage-gated sodium channel Scn1a (Vessey et al., 2010). Pum2 has also been implicated in miRNA regulated activity-dependent dendritogenesis. Specifically, dendritic miR-134 promotes dendritic outgrowth by inhibiting translation of Pum2 mRNA (Fiore et al., 2009). During embryonic neurogenesis, a complex involving Pum2 and the protein 4E-T selectively represses cell fate specifying mRNAs in radial glial precursors to ensure daughter cell differentiation in diverse neuron subtypes (Zahr et al., 2018).

Pum2 is also involved in mRNA localization in neurons. It localizes in mRNPs in the somatodendritic compartment in microtubule-associated puncta (Vessey et al., 2006) similar to other RBPs involved in mRNA transport.

Only very recently, a role of Pum2 in the development and maintenance of epilepsy has been reported. Pum2 knockdown mice develop spontaneous epileptic seizures with an onset at the age of 5 months (Follwaczny et al., 2017). In this mouse model, the expression of the inhibitory GABA receptor *Gabra2* and several voltage-gated sodium channels is misregulated, indicating that the epileptic phenotype is mediated by altered neuronal inhibition.

1.4.3 Structure of Pum2 and RNA recognition by the Pum-HD

The characteristic feature of all PUF proteins is the presence of a Pum-HD domain, also sometimes referred to as Puf repeat domain. Pum-HDs are often located near the C-terminus of the protein and can mediate protein-RNA as well as protein-protein interactions (Miller and Olivas, 2011). Regions outside the Pum-HD are poorly conserved between PUFs. Mammalian Pum2 comprises a C-terminal Pum-HD domain and is otherwise unstructured. Several known crystal structures showed that the canonical Pum-HD RNA-binding domain adopts an arc-like shape comprising eight α-helical Puf repeats of ~36 aa each with flanking half-repeats at the N- and C-termini. Each repeat folds into three helices, which stack with the helices of the neighboring repeats, so that both the concave and the convexe surface of the arc comprise layers of helices. The crystal structure of the Pum-HD domain from the canonical human Pum2 is shown in Figure 4 A. RNA-binding by a Pum-HD occurs at the positively charged concave surface at which every Puf repeat interacts with one single nucleotide of the single-stranded consensus motif. Whereas the amino acid at position 13 of each repeat base-stacks with two successive RNA bases, aa 12 and aa 16 make base-specific contacts via hydrogen bonds or van der Waals interactions, thus determining the sequence specifity of the PUF protein. Consensus sequences recognized by PUFs from different organisms are very similar. The conserved UGU is recognized by Puf repeats 8-6. Flanking sequences of this central UGUR element mediate differences in specificities of different PUF proteins. The minimal Pumilio-response element (PRE) of both human Pum1 and Pum2 is UGUANAUA. Cognate RNA recognition by human Pum2 is shown in Figure 4 B.

There is, however, evidence that Pufs can recognize non-cognate RNA sequences. A crystal structure of Pum1 bound to a 9 nt target RNA showed that Pum1 could recognize the RNA by simply flipping out the extra base and non-canonical bases were accommodated by alternative hydrogen bonds with the Puf repeats (Gupta et al., 2008). Such flipping out of bases was also observed for Puf proteins that naturally recognize 9 or 10 base consensus sequences, for instance *C. elegans* FBF. In this protein, the fifth, nonconserved base of its target sequence is flipped out and adopts a less curved surface shape for proper spacing to the recognized bases (Wang et al., 2009). Changing their curvature and flipping out of bases is thought to allow Pufs to recognize different target sequences and possibly also to specifically recruit different protein co-factors for different regulatory functions.

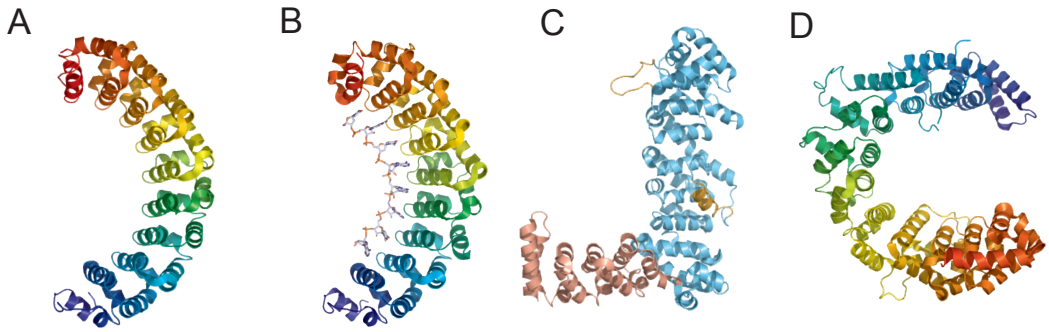

Figure 4: Crystal structures of Puf RNA-binding domains. A) Pum-HD of human Pum2 (PDB 3GVT). **B)** Pum-HD of human Pum2 in complex with RNA (PDB 3Q0Q). The structures of Pum2 show the canonical Pum-HD domain with its eight α-helical repeats of 36 aa, stacking together to produce layers of helices with an arc-like shape. The concave surface contacts RNA, while the convex surface often mediates protein-protein interactions. **C)** Puf repeats of the non-canonical human Puf-A (PDB 4WZR). Puf-A comprises eleven Puf repeats arranged in two subdomains, which are arranged perpendicularly to each other. Three repeats have insertions and diverge from the canonical Puf repeat. **D)** Structure of Nop9 Puf repeats (PDB 5SVD). Nop9 adopts a 'C'-shaped fold formed by eleven Puf repeats.

In addition to the canonical PUFs like Pum2, other classes of PUF proteins have been identified: the Puf-A and the Nop9 classes (Kuo et al., 2009). A Puf-A repeat domain has eleven Puf repeats that adopt an L-shape (Figure 4 C) (Qiu et al., 2014). Its two Puf repeat subdomains are oriented to each other perpendicularly. The C-terminal subdomain with eight repeats resembles the curved form of a canonical Pum-HD, yet three of its repeats diverge structurally from the canonical Puf repeat. The N-terminal subdomain comprises three additional Puf repeats. Puf-A proteins can bind ssRNA, dsRNA as well as ssDNA and dsDNA without sequence specificity. Yeast Puf6p is an ortholog of human

Puf-A protein. Puf-A proteins have been implicated in mRNA localization and pre-rRNA processing (Qiu et al., 2014).

The Nop9 class adopts a 'C'-shaped fold formed by eleven Puf repeats with variable helix and loop lengths (Figure 4 D). Nop9 is a conserved ribosome biogenesis factor that specifically binds 20S pre-rRNA at a fragment that has both ss and ds regions and plays an essential role in ribosome biogenesis (Zhang et al., 2016).

Many organisms throughout the metazoans are known to express several PUF proteins, for instance *C. elegans* has nine PUFs. However, only six out of the eleven Puf repeats identified by the crystal structure of Puf-6 could be predicted, pointing at the possibility that the number of Puf repeat proteins is still underestimated and that other folds and specificities are yet to be identified.

1.5 A common function for Staufen and Pumilio

Pumilio and Staufen have been implicated in similar cellular processes. Both proteins are involved in *Drosophila* long-term memory formation (Dubnau et al., 2003), indicating a functional link and perhaps a direct connection of both pathways. Additionally, it was shown that mammalian Stau2 and Pum2 form apically localized, mRNA-containing co-complexes in neuronal progenitors (Vessey et al., 2012). Knockdown of Stau2 results in premature differentiation of murine radial glial cells into neurons and mislocalization of target RNAs, indicating that Stau2 is important for stem cell self-renewal and differentiation. Pum2 knockdown phenocopies these effects (Vessey et al., 2012), suggesting that Stau2 and Pum2 act in the same pathway by forming joint mRNPs. It is thought that this specific mRNP complex binds, localizes and represses mRNAs promoting neurogenesis to prevent differentiation and maintain precursor cells. An obvious possibility is that this function is mediated via Stau2 and Pum2 binding and subsequent regulation of target mRNAs. One interesting candidate mRNA is the Stau2-regulated *Regulator of G-protein signaling 4 (Rgs4)* mRNA. *Rgs4* is regulated by Stau2 via its 3'UTR as shown by luciferase reporter assays (Heraud-Farlow et al., 2013), which is roughly 2200 nt long and contains two predicted type III SRSs (Heraud-Farlow et al., 2013). Stau2 knockdown in primary neurons leads to a significant reduction of *Rgs4* mRNA (Heraud-Farlow

et al., 2013). Also in brains of Stau2-deficient rats, which have impaired spatial short term and spatial working memory, *Rgs4* levels are reduced (Berger et al., 2017).

A sequence analysis revealed two putative Pum2 PREs in the vicinity of these SRSs, suggesting again a functional complex of both proteins with their target RNA. Furthermore, *Rgs4* 3'UTR contains two Pum2 PRE consensus sequences in proximity to these SRSs. A fold prediction of the region of *Rgs4* 3'UTR that contains all these predicted binding sites is shown in Figure 5. This RNA region will be termed *Rgs4* binding region (BR) in the following.

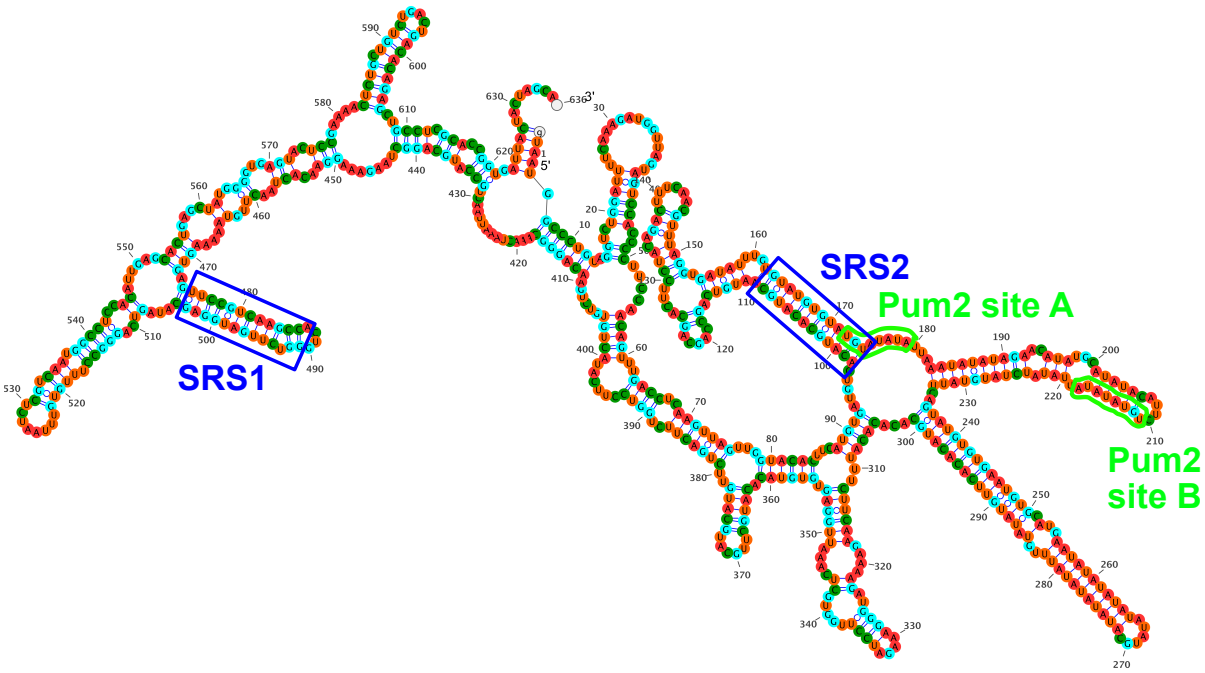

Figure 5: Predicted secondary structure of the *Rgs4* BR. Predicted binding sites for Stau2 and Pum2 are marked in blue or green, respectively.

1.6 Regulator of G-protein signaling 4 (RGS4) in the nervous system

The Regulator of G-protein signaling (RGS) proteins belongs to a family of important negative regulators of G-protein coupled receptor (GPCR) and G-protein signaling. GPCRs bind heterotrimeric G-proteins consisting of a GDP-bound α subunit and a βγ-heterodimer. Their activation causes an exchange of GDP to GTP and leads to the release of Gα-GTP and Gβγ subunits, which both stimulate downstream effectors of the GPCR signaling pathway (Hollinger and Hepler, 2002, Willars, 2006, Gerber et al., 2016). RGS tightly control GPCRs and G-protein signaling by activating the intrinsic GTPase activity of Gα subunits,

which restores inactive Gα-GDP that in turn reassociates with Gβγ, thus terminating downstream signaling. This GTPase-activating activity is a hallmark feature of RGS proteins and is mediated by the functionally conserved RGS homology domain (Gerber et al., 2016) (Roman and Traynor, 2011).

GPCRs control a variety of neurophysiological processes such as pre- and postsynaptic neurotransmission and synaptic plasticity. Gα-proteins can be divided in several families with different functions. The Gαi family inhibits adenylate cyclase as downstream target. Gαq proteins activate phospholipase C thus releasing intracellular Ca^{2+} stores. Also Gβγ subunits can interact with various downstream effectors such as potassium channels, calcium channels, phospholipase C or mitogen-activated protein (MAP) kinase (Roman and Traynor, 2011). Various metabotropic GPCRs regulate presynaptic neurotransmitter release, for example by Gβγ-mediated inhibition of voltage-gated calcium channels. While Gβγ inhibits neurotransmitter release, inhibition of Gβγ by RGS proteins facilitates transmitter release. On postsynaptic membranes, GPCRs modulate neurotransmission by ligand-gated ion channels such as glutamate and γ-butyric acid (GABA) receptors. Here, Gβγ directly binds to G-protein coupled inwardly rectifying potassium (GIRK) channels. GIRK channel activation causes hyperpolarization and depotentiation. GIRK channel activity is modulated by many RGS proteins (Gerber et al., 2016, Willars, 2006).

RGS4 is a roughly 24 kDa protein comprising one RGS domain that is expressed throughout the brain. Its roles in synaptic plasticity and signaling were characterized in the hippocampus, striatum, hypothalamus and prefrontal cortex (Gerber et al., 2016).

In the CA1-region of the hippocampus, RGS4 has been shown to inhibit signaling through group I mGluRs thereby downregulating synaptic excitability (Saugstad et al., 1998).

Expression levels of RGS4 in the striatum have been linked to Parkinson's disease (PD) in which decreased striatal dopamine levels lead to increased acetylcholine release, which causes the motor symptoms of PD (Barbeau, 1962). Dopamine depletion upregulates RGS4 expression in cholinergic interneurons. RGS4 blocks the inhibition of $Ca_V2.2$ channels by M4 muscarinic acetylcholine autoreceptor signaling, thus increasing acetylcholine release into the synapse,

thereby intensifying motor symptoms (Ding et al., 2006). Furthermore, RGS4 modulates synaptic plasticity in the striatum by regulating dopaminergic control of endocannabinoid-dependent LTD. This form of LTD requires activation of group I mGluRs (mGluR1 and mGluR5) and is positively regulated by Gαi-coupled D_2 dopamine receptors. RGS4 can inhibit both receptors thus blocking LTD. In a mouse model of PD, the release of LTD inhibition by RGS4 was reported to lead to fewer behavioral deficits, making RGS4 an interesting therapeutic target in PD (Lerner and Kreitzer, 2012). However, a more recent study could not confirm these results but found that inhibition of RGS4 had no protective effects in a PD mouse model (Ashrafi et al., 2017), showing that further research is needed to understand the role of RGS4 in PD.

RGS4 has been implicated as a risk factor for psychiatric diseases like schizophrenia (Schwarz, 2018). For instance, in the dorsolateral prefrontal cortex, polymorphisms and decreased expression of RGS4 are linked to schizophrenia. In the prefrontal cortex, excitatory glutamatergic signaling is modulated by type 2 α-adrenergic receptors and type B GABA receptors, both of which are localized in close proximity in the dendritic spine and coupled to Gαi. Despite both receptors mediate downregulation of cAMP via Gαi, they modulate different downstream targets. This independent control of the two pathways requires RGS4, which is thought to prevent crosstalk between the different signaling pathways (Lur and Higley, 2015).

In parvocellular neuroendocrine cells of the hypothalamus, RGS4 acts as an inhibitor of synaptic plasticity by inhibiting mGluR5 signaling. Glucocorticoid release, however, can suppress RGS4 expression via the activation of glucocorticoid receptors, thereby increasing mGluR5 signaling and allowing for LTD, thus decreasing excitability during prolonged glucocorticoid release (Gerber et al., 2016).

1.7 Specific aims of this work

1.7.1 Characterization of Stau2-binding to a natural target RNA and identification of its specific binding sites

Despite the importance of Stau proteins, their molecular actions are little understood. Cell-based assays in several cell-types identified certain sets of target RNAs (Furic et al., 2008, Kusek et al., 2012). However, how these targets are specifically recognized is not clear. The only known co-structure of a Stau dsRBD with RNA is the *dm*Stau RBD3 with a non-physiological stem-loop RNA (Ramos et al., 2000), which can naturally not reveal any target specificity. Furthermore, no studies on the interplay between the four to five dsRBDs of Stau proteins are available.

A genome-wide analysis of *dm*Stau targets suggested certain secondary structure elements as SRSs (Laver et al., 2013). Immunoprecipitation- and microarray-based experiments identified neuronal target RNAs of the brain-specific Stau2, validated *Rgs4* mRNA as a Stau2-regulated target and identified two SRS stem loops in the *Rgs4* 3'UTR (Heraud-Farlow et al., 2013). This finding opens up the possibility to directly assess Stau2 binding to this natural target mRNA, using biochemical and structural approaches. One aim of this work was to perform a molecular characterization of Stau2-binding to *Rgs4* 3'UTR and its SRSs, identify its specific binding sites and understand how target specificity is achieved.

1.7.2 Characterization of the trimeric complex between Stau2, Pum2 and *Rgs4* mRNA

A fundamental problem in understanding the molecular principles underlying mRNA localization and local translation in the nervous system is the high complexity of neuronal mRNP assemblies. In Stau2 mRNPs, >50 proteins were identified by immunoprecipitation (Fritzsche et al., 2013). To better understand the function of Stau2-containing mRNPs, it is thus not only important to identify their cargo mRNAs but also their protein content as well as the interactions between these molecules.

Pum2 has been implicated in similar processes as Stau2 (see chapter 1.5). The 3'UTR of the Stau2 target mRNA *Rgs4* comprises two SRSs and two putative Pum2-binding sites in close vicinity, suggesting a functional and physical

complex of both proteins with their target RNA and indicating an either direct or RNA-dependent interaction of Stau2 and Pum2.

One aim of this work was thus to characterize the trimeric complex between Stau2, Pum2 and *Rgs4* mRNA. One intriguing possibility is that the combinatorial action of Stau2 with additional factors such as Pum2 is required to increase the specificity of RNA-binding. Defining the characteristics of a Stau2-Pum2-RNA complex is thus likely to significantly improve our understanding of the function of Stau2-containing mRNPs.

2 Materials and Methods

2.1 Chemicals and consumables

Unless stated otherwise, chemicals used in this study were generally supplied by Sigma Aldrich (Taufkirchen, Germany), Roth (Karlsruhe, Germany) or AppliChem (Darmstadt, Germany). Ingredients for bacterial growth media were supplied by Becton Dickinson (Heidelberg, Germany). Insect cell media were purchased from Thermo Scientific (Bonn, Germany). Culture flasks and plates were supplied by Greiner Bio-One (Frickenhausen, Germany) or Thermo Scientific (Bonn, Germany).

Molecular biology enzymes such as polymerases or restriction enzymes, their corresponding buffers, nucleotides, and molecular weight markers were supplied by New England Biolabs (Frankfurt, Germany), Agilent Technologies (Waldbronn, Germany) or GE Healthcare (München, Germany).

Resins, devices and columns for liquid chromatography were purchased from GE Healthcare (München, Germany).

Commercially available crystallization screens from Hampton Research (Aliso Viejo, USA) and Qiagen (Hilden, Germany) were used.

2.2 Media, supplements and antibiotics

Table 1: Media

Name	Composition	Application
LB (Luria Bertani)	10 g/L BD Bacto™ tryptone, 5 g/L BD Bacto™ yeast extract, 5 g/L NaCl, pH 7.0 with NaOH,	*E. coli* growth and protein expression medium
LB agar plates	10 g/L BD Bacto™ tryptone, 5 g/L BD Bacto™ yeast extract, 5 g/L NaCl, pH 7.0 with NaOH, 5 g/L agar	*E. coli* growth medium

Name	Composition	Application
SOC	20 g/L BD BactoTM tryptone, 5 g/L BD BactoTM yeast extract, 20 mM glucose, 20 mM$MgSO_4$, 10 mM NaCl, 10 mM $MgCl_2$, 2.5 mM KCl, pH 7.0 with NaOH	Transformation of *E. coli*
SOB	20 g/L BD Bacto™ tryptone, 5g/L BD Bacto™ yeast extract, 10 mM NaCl, 2.5 mM KCl, pH 7.0 with NaOH	Preparation of chemically competent of *E. coli*
ZYM 5052 auto-induction media	10 g/L BD Bacto™ tryptone, 5 g/L BD Bacto™ yeast extract	*E. coli* autoinduction protein expression medium
SelenoMet™ Medium Base (Molecular Dimensions)	21.6 g in 1 L ddH2O	*E. coli* protein expression medium for selenomethionine-labeling
^{15}N- (^{13}C-) labeled M9 mineral medium	33.7 mM Na_2HPO_4 22.0 mM KH_2PO_4 8.55 mM NaCl 9.35 mM $^{15}NH_4Cl$ 0.2 % (^{13}C)-glucose 1 mM $MgSO_4$ 0.3 mM $CaCl_2$ 1 µg biotin 1 µg thiamin 1x trace elements	*E. coli* protein expression medium for ^{15}N- (^{13}C-) labeling
SF-900™ III SFM (Thermo Scientific)	As supplied by manufacturer	*Sf*21 insect cell culture medium
HyClone SFX-Insect MP™ Cell Culture Medium (Thermo Scientific)	42.32 g/L HyClone(R) SFX-Insect MP™, 0.35 g/L Na bicarbonate, 1.5 mL/L glycerol, pH 6.1-6.4 with NaOH	High Five insect cell culture medium

Table 2: Supplements

Name	Composition	Application
50x 5052 sugar mix	25 % (v/v) glycerol, 2.5 % (w/v) glucose, 10% (w/v) lactose	*E. coli* autoinduction protein expression
25x M salt mix	1.25 M Na_2HPO_4, 1.25 M KH_2PO_4, 2.5 M NH_4Cl, 0.25 M Na_2SO_4	*E. coli* autoinduction protein expression
SelenoMet™ Nutrient Mix (Molecular Dimensions)	5.1 g in 50 ml ddH2O	*E. coli* expression of selenomethionine-labeled proteins
1000 x trace metal mix	40 mM HCl, 50 mM $FeCl_3$, 20 mM $CaCl_2$, 10 mM $MnCl_2$, 10 mM $ZnCl_2$, 2 mM $CoCl_2$, 2 mM $CuCl_2$, 2 mM Na_2MoO_4, 2 mM H_3BO_3	*E. coli* autoinduction or isotope-labeled protein expression
20 % glucose	20 %(v/v) glucose	*E. coli* media
20x ^{15}N-labelled M9 salt solution	150.4 g/L Na_2HPO_4-$2H_2O$ 60 g/L KH_2PO_4 10 g/L NaCl 10 g/L $^{15}NH_4Cl$	isotope-labeled protein expression

Table 3: Antibiotics

Name	Stock concentration	Application
Ampicillin 1000x	100 mg/mL	*E. coli* selection
Carbenicillin 1000x	100 mg/mL	*E. coli* selection
Chloramphenicol 1000x	34 mg/mL in absolute ethanol	*E. coli* selection
Kanamycin 1000x	50 mg/mL	*E. coli* selection
Tetracyclin 1000x	10 mg/mL	*E. coli* DH10Bac selection
Gentamicin 1000x	7 mg/mL	*E. coli* DH10Bac selection
Gentamicin 5000x	50 mg/mL	Insect cell culture
IPTG	1 M	Induction of protein expression, *E. coli* DH10Bac selection
X-Gal 1000x	100 mg/mL in DMSO	*E. coli* DH10Bac selection plates

2.3 General buffers and solutions

Table 4: General buffers and solutions

Name	Composition	Application
4x SDS-loading dye	110 mM Tris/Cl pH 6.8, 40 % (v/v) glycerol, 40 mM DTT, 4 % (w/v) SDS, 0.25 % (w/v) bromophenol blue	SDS-PAGE
4x separating gel buffer	3 M Tris/Cl pH 8.5, 0.4 % (w/v) SDS	SDS-PAGE
4x stacking gel buffer	0.5 M Tris/Cl pH 6.8, 0.4 % (w/v) SDS	SDS-PAGE
6x DNA loading dye	30 % (w/v) glycerol, 0.25 % (w/v) bromophenol blue 0.025 % (w/v) xylene cyanol	DNA agarose gel electrophoresis
2x denaturing RNA-loading dye	95 % (v/v) formamide, 5 mM EDTA, 0.025 % (w/v) bromophenol blue, 0.025 % (w/v) xylene cyanol, 0.025 % (w/v) SDS	Denaturing RNA PAGE
4x native RNA loading dye	40 % (v/v) glycerol	Native RNA PAGE
50x TAE	2 M Tris base, 50 mM EDTA pH 8.3	DNA agarose gel electrophoresis
10x TBE	765 mM Tris base, 890 mM boric acid, 32 mM EDTA	RNA PAGE and agarose gel electrophoresis
10x TGS	0.5 M Tris, 1.9 M glycine, 1 % (w/v) SDS	SDS-PAGE
Fixing solution	30 % (v/v) acetic acid, 10 % (v/v) methanol	EMSA
TAR stop solution	20 % glycerol 20 mM EDTA 2 % SDS 0.25 % bromophenol blue 0.4 mg/mL yeast tRNA pH 8	Annealing assays
Crush'n'Soak buffer	0.5 M ammonium acetate 0.1 mM EDTA 0.1 % SDS	PAGE purification of DNA/RNA
10 x TRX	400 mM Tris/HCl pH_{RT} 8.0 10 mM spermidine 1 % Triton X-100 50 mM DTT	

2.4 Enzymes

Table 5: Enzymes (additional to molecular biology enzymes)

Name	Source
PreScission protease (His_6-GST-HRV 3C protease)	Generally prepared in the Niessing lab according to protocol from Arie Gerloof (Protein Expression and Purification facility, HMGU)
T7 RNA polymerase	Generally prepared in the Niessing lab according to protocol from Arie Gerloof (Protein Expression and Purification facility, HMGU)
Proteinase K	Purchased from Ambion

2.5 Organisms and Strains

Table 6: Bacteria

Strain	Genotype	Source
E. coli DH5α	*fhuA2 lac(del)U169 phoA glnV44 Φ80' lacZ(del)M15 gyrA96 recA1 relA1 endA1 thi-1 hsdR17*	Invitrogen
E. coli Stellar	F- *endA1 supE44 thi-1 recA1 relA1 gyrA96 phoA* Φ80*d lacZΔ M15, Δ(lacZYA-argF) U169, Δ(mrr*-hsdRMS-*mcr*BC) *ΔmcrA λ*-	Clontech
E. coli Rosetta	F- *ompT hsdS*B(r_B- m_B-) *gal dcm* (DE3) pRARE (Cam^R)	Novagen
E. coli DH10Bac	F-*mcr*A Δ(*mrr*-hsdRMS-*mcr*BC) Φ80*lac*ZΔM15 Δ*lac*X74 *rec*A1 *end*A1 *ara*D139 Δ(*ara*,*leu*)7697 *gal*U *gal*K λ- *rps*L *nup*G/bMON14272/pMON7124	Invitrogen
E. coli B834 (DE3)	F- *ompT hsdS*B(r_B - m_B-) *gal dcm met* (DE3)	Novagen

Table 7: Insect cells

Strain	Genotype	Source
Sf21	*Spodoptera frugiperda* (*Sf*) ovarian cell line	Invitrogen
High Five	Derived from the *Trichopulsia ni* cell line	Invitrogen

2.6 Plasmids and primers

Table 8: Plasmids

Short name	Full name/description	Source/Cloning strategy
pGEX-Stau2 FL	pGEX-6P-mStau2 FL	Niessing lab
pMALC-Pum2 FL	pMAL™-c5X –mPum2 FL	Cloned by Foong-Yee Ang, Kiebler lab (LMU München)
pOPINM-Pum2 ΔHD	pOPINM-Pum2 ΔHD (aa1-641)	Cloned by Foong-Yee Ang, Kiebler lab (LMU München)
pRgs4	pExpress1 - Rgs4 ((B) ... IMAGp998E0615376Q)	Courtesy of Kiebler lab (LMU München)
pRgs4 3'UTR Pum2 B mutant	psiCheck2-Rgs4 3'UTR (full length) Pum2 bindingsite B mut	Courtesy of Kiebler lab (LMU München)
pRgs4 3'UTR Pum2 A mutant	psiCheck2-Rgs4 3'UTR (full length) Pum2 bindingsite A mut	Courtesy of Kiebler lab (LMU München)
pRgs4 3'UTR Pum2 A+B mutant	psiCheck2-Rgs4 3'UTR (full length) Pum2 bindingsite A and B mut	Courtesy of Kiebler lab (LMU München)
pRgs4 3'UTR ΔSRS2	pEGFP-C2-Rgs4 3'UTR SRS2 deletion 3'UTR	Courtesy of Kiebler lab (LMU München)
pRgs4 3'UTR ΔSRS1	pEGFP-C2-Rgs4 3'UTR SRS1 deletion	Courtesy of Kiebler lab (LMU München)
pRgs4 3'UTR ΔSRS1 ΔSRS2	pEGFP-C2-Rgs4 3'UTR SRS1 and SRS2 deletion 3'UTR	Courtesy of Kiebler lab (LMU München)
RH99	pBSM-HIV TAR 57	Niessing lab
pBlueScript-KS	pBlueScript-KS	Courtesy of Ephrussi lab (EMBL Heidelberg)
pET-dmStaufen	pET3a-Staufen cDNAE10	Courtesy of Ephrussi lab (EMBL Heidelberg)
pUASp-attB	pUASp2-attB	Courtesy of Ephrussi lab (EMBL Heidelberg)
pHsp83	pHsp83-4xIN-3GFP	Courtesy of Ephrussi lab (EMBL Heidelberg)
prsEGFP2		Courtesy of Ephrussi lab (EMBL Heidelberg)
Plasmids created in this study		
SH17	pCR-II-Blunt-TOPO-Rgs4 BR	Blunt end TOPO cloning
SH22	pOPINS3C-Stau2 FL (Staufen homolog 2 isoform 3 [Mus Musculus], NCBI Reference Sequence: NP_079579.2)	InFusion cloning, primers Stau2 FW and Stau2 RV

Short name	Full name/description	Source/Cloning strategy
SH23	pOPINS3C-Stau2 RBD3-4 (mStau2 200-373)	InFusion cloning, primers RBD3 FW and RBD4 RV
SH24	pOPINM-Pum2 Pum HD (Pum2 aa642-963)	InFusion cloning, primers Pum2 HD aa642 FW and Pum2 HD 963 RV
SH25	pOPINS3C-Stau2 RBD2-4 (mStau2 141-373)	InFusion cloning, primers RBD2 FW and RBD4 RV
SH26	pOPINS3CStau2 RBD3-5 (mStau2 200-470)	InFusion cloning, primers RBD3 FW and Stau2 RV
SH27	pOPINS3C-Stau2 RBD4 (mStau2 272-373)	InFusion cloning, primers RBD4 FW and RBD4 RV
SH28	pOPINS3C-Stau2 RBD4-5 (mStau2 272-470)	InFusion cloning, primers RBD4 FW and Stau2 RV
SH29	pOPINS3C-Stau2 RBD1-4 (mStau2 1-373)	InFusion cloning, primers Stau2 FW and RBD4 RV
SH30	pFastBacDual-Stau2 FL (Staufen homolog 2 isoform 3 [Mus Musculus], NCBI Reference Sequence: NP_079579.2)	InFusion cloning, primers His-SUMO FW and Stau2 RV-pFBD
SH31	pOPINS3C-Stau2 RBD1-2 (mStau2 1-208)	InFusion cloning, primers Stau2 FW and RBD2 RV
SH32	pOPINM-Pum2	InFusion cloning,
SH34	pOPINS3C-Stau2 RBD1 (mStau2 1-139)	InFusion cloning, primers Stau2 FW and RBD1 RV
SH36	pOPINF-Stau2 RBD1 (mStau2 1-139)	InFusion cloning, primers Stau2 FW and RBD1 RV
SH37	pOPINS3C-Stau2 RBD2 (mStau2 141-208)	InFusion cloning, primers RBD2 FW and RBD2 RV
SH38	pOPINS3C-Stau2 RBD1-2 C11S C140S (mStau2 1-208 C11S C140S)	InFusion cloning, 4-point PCR with primers Stau2 FW+ Stau2 C11S antisense, Stau2 C11S sense+ Stau2 C140S antisense, Stau2 C140S sense+RBD2 RV

Short name	Full name/description	Source/Cloning strategy
SH39	pOPINS3C- Stau2 RBD2 (as in SwissModel Homology Model) (mStau2 94-180)	InFusion cloning, primers RBD2 SM FW and RBD2 SM RV
SH40	pOPINS3C-Stau2 RBD1 (as in SwissModel Homology Model) (mStau2 1-74)	InFusion cloning, primers Stau2 FW and RBD1 SM RV
SH41	pOPINS3C-Stau2 RBD1-2 E15A (mStau2 1-208 E15A)	InFusion cloning, 3-point PCR with primers Stau2 FW+Stau2 E15A antisense, Stau2 E15A sense+RBD2 RV
SH42	pOPINS3C-Stau2 RBD1-2 K59A K60A (mStau2 1-208 K59A K60A)	InFusion cloning, 3-point PCR with primers Stau2 FW+Stau2 K59A K60A antisense, Stau2 K59A K60A sense+RBD2 RV
SH43	pOPINS3C-Stau2 RBD1-2 Δ119-135 (mStau2 1-208 Δ119-135)	InFusion cloning, 3-point PCR with primers Stau2 FW+Stau2 Δ119-135 antisense, Stau2 Δ119-135 sense +RBD2 RV
SH44	pOPINS3C-Stau2 RBD1-6xHis (mStau2 (1-74) - 6xHis)	InFusion cloning, PCR1 with Stau2 FW and RBD1+6xHis RV, PCR2 on product of PCR1 with Stau2 FW and pOPIN-6xHis RV
SH45	pOPINS3C-Stau2 RBD2 long (mStau2 94-208)	InFusion cloning, primers RBD2 SM FW and RBD2 RV
SH46	pOPINJ-Stau2 RBD1-6xHis (mStau2 (1-74) - 6xHis)	InFusion cloning, PCR1 with Stau2 FW and RBD1+6xHis RV, PCR2 on product of PCR1 with Stau2 FW and pOPIN-6xHis RV
SH47	pOPINS3C-Stau2 RBD1 linker (mStau2 1-93)	InFusion cloning, primers Stau2 FW and RBD1-linker RV
SH48	pOPINS3C-Stau2 linker-RBD2 (mStau2 75-208)	InFusion cloning, primers linker-RBD2 FW and RBD2 RV

Short name	Full name/description	Source/Cloning strategy
SH49	pOPINS3C-Stau2 RBD1-2 H36A (mStau2 1-208 H36A)	InFusion cloning, 3-point PCR with primers Stau2 FW+Stau2 H36A antisense, Stau2 H36A sense+RBD2 RV
SH50	pOPINS3C-Stau2 RBD1-2 F40A (mStau2 1-208 F40A)	InFusion cloning, 3-point PCR with primers Stau2 FW+Stau2 F40A antisense, Stau2 F40A sense+RBD2 RV
SH51	pOPINS3C-Stau2 RBD1-2 K59A (mStau2 1-208 K59A)	InFusion cloning, 3-point PCR with primers Stau2 FW+Stau2 K59A antisense, Stau2 K59A sense+RBD2 RV
SH52	pOPINS3C-Stau2 RBD1-2 K60A (mStau2 1-208 K60A)	InFusion cloning, 3-point PCR with primers Stau2 FW+Stau2 K60A antisense, Stau2 K60A sense+RBD2 RV
SH53	pBlueScript-KS-rsEGFP2-Stau2 FL	InFusion cloning, restriction enzymes BamHI and XbaI, 3-point PCR with primers pBSKS-rsEGFP2 FW + rsEGFP+3C RV, 3C+Stau2 FW+ pBSKS-Stau2 RV
SH54	pBlueScript-KS-rsEGFP2-dmStaufen FL	InFusion cloning, restriction enzymes BamHI and XbaI, 3-point PCR with primers pBSKS-rsEGFP2 FW + rsEGFP+3C RV and 3C+dmStaufen FW + pBSKS-dmStaufen RV
SH55	pOPINS3C-Stau2 RBD1-2 E99A (mStau2 1-208 E99A)	InFusion cloning, 3-point PCR with primers Stau2 FW+Stau2 E99A antisense, Stau2 E99A sense+RBD2 RV
SH56	pOPINS3C-Stau2 RBD1-2 F157A (mStau2 1-208 F157A)	InFusion cloning, 3-point PCR with primers Stau2 FW+Stau2 F1570A antisense, Stau2 F157A sense+RBD2 RV

Short name	Full name/description	Source/Cloning strategy
SH57	pOPINS3C-Stau2 RBD1-2 Q165A (mStau2 1-208 Q165A)	InFusion cloning, 3-point PCR with primers Stau2 FW+Stau2 Q165A antisense, Stau2 Q165A sense+RBD2 RV
SH58	pOPINS3C-Stau2 RBD1-2 H169A (mStau2 1-208 H169A)	InFusion cloning, 3-point PCR with primers Stau2 FW+Stau2 H169A antisense, Stau2 H169A sense+RBD2 RV
SH59	pUASp attb-rsEGFP2-Stau2	Infusion cloning with primers pUASp-rsEGFP2 FW and pUASp-Stau2 RV, template SH53
SH60	pOPINS3C-Stau2 RBD1-2 K106A (mStau2 1-208 K106A)	InFusion cloning, 3-point PCR with primers Stau2 FW+Stau2 K106A antisense, Stau2 K106A sense+RBD2 RV
SH61	pHsp83p attb-rsEGFP2-Stau2	InFusion cloning, 3-point PCR with primers Hsp83prom ex FW + Hsp83p modify RV and pHsp83p-rsEGFP2 FW + pHsp83p-Stau2 RV
SH63	pUASp attb-rsEGFP2-dmStaufen	
SH64	pOPINS3C-Stau2 RBD1-2 F40A H169A (mStau2 1-208 F40A H169A)	InFusion cloning, 3-point PCR with primers Stau2 FW+Stau2 F40A antisense, Stau2 F40A sense+RBD2 RV on SH58 as template
SH65	pOPINS3C-Stau2 RBD1-2 F40A H169A (mStau2 1-208 F40A F157A)	InFusion cloning, 3-point PCR with primers Stau2 FW+Stau2 F40A antisense, Stau2 F40A sense+RBD2 RV on SH56 as template
SH66	pBlueScript-KS-rsEGFP2-Stau2 F40A	Site-directed mutagenesis (QuikChange II kit) with Stau2 F40A sense and Stau2 F40A antisense

Short name	Full name/description	Source/Cloning strategy
SH67	pBlueScript-KS-rsEGFP2-Stau2 F40A F157A	Site-directed mutagenesis (QuikChange II kit) on SH66 with Stau2 F157A sense and Stau2 F157A antisense
SH68	pBlueScript-KS-rsEGFP2-Stau2 F40A H169A	Site-directed mutagenesis (QuikChange II kit) on SH66 with Stau2 H169A sense and Stau2 H169A antisense
SH69	pOPINS3C-Stau2 RBD1-4 F40A H169A	InFusion cloning with primers Stau2 FW and RBD4 RV on template SH68
SH70	pOPINS3C-Stau2 RBD1-4 F40A F157A	InFusion cloning with primers Stau2 FW and RBD4 RV on template SH67
SH71	pUASp attB-rsEGFP2-Stau2 F40A F157A	Infusion cloning with primers pUASp-rsEGFP2 FW and pUASp-Stau2 RV, template SH67
SH72	pUASp attB-rsEGFP2-Stau2 F40A H169A	Infusion cloning with primers pUASp-rsEGFP2 FW and pUASp-Stau2 RV, template SH68
SH73	pBlueScript-KS-rsEGFP2-dmStaufen F343A F533A	InFusion cloning, restriction enzymes BamHI and XbaI, 4-point PCR with primers pBSKS-rsEGFP2 FW + F343A antisense, F343A sense + F533A antisense and F533A sense + pBS-KS-Staufen RV
SH74	pBlueScript-KS-rsEGFP2-dmStaufen F343A H545A	InFusion cloning, restriction enzymes BamHI and XbaI, 4-point PCR with primers pBSKS-rsEGFP2 FW + F343A antisense, F343A sense + H545A antisense and H545A sense + pBS-KS-Staufen RV

Short name	Full name/description	Source/Cloning strategy
SH75	pUASp attB-rsEGFP2-Staufen F343A F533A	Infusion cloning with primers pUASp-rsEGFP2 FW and pUASp-Staufen RV, template SH73
SH76	pUASp attB-rsEGFP2-Staufen F343A H545A	Infusion cloning with primers pUASp-rsEGFP2 FW and pUASp-Staufen RV, template SH74

Table 9: Cloning primers

Primer name	Primer description	Sequence 5'→ 3'
Stau2 FW	pOPIN- Stau2 FW +PPsite	AAGTTCTGTTTCAGGGCCCGATGGCAAACCCCAAAGAGA
RBD2 FW	pOPIN- Stau2 RBD2 FW +PPsite	AAGTTCTGTTTCAGGGCCCGATGCCCAAGATCTTTTATGTTCAGT
RBD2 SM FW	pOPIN- Stau2 RBD2 as in SwissModel FW +PPsite	AAGTTCTGTTTCAGGGCCCGATAACTCCAACTGTGGAACTG
Linker-RBD2 FW	pOPIN- Stau2 RBD2 long FW +PPsite	AAGTTCTGTTTCAGGGCCCGCTTCCCAAACCAGTTCAGAAAC
RBD3 FW	pOPIN- Stau2 RBD3 FW +PPsite	AAGTTCTGTTTCAGGGCCCGATAAGCTTAGTGTTTGAGATTGCGC
RBD4 FW	pOPIN- Stau2 RBD4 FW +PPsite	AAGTTCTGTTTCAGGGCCCGCTTAAAAAACTCCCACCTCTTCC
RBD1 RV	Stau2 RBD1 RV-pOPIN	CTGGTCTAGAAAGCTTCTACAATGATACCTCTGATTGTACATGC
RBD1 SM RV	Stau2 RBD1 as in SwissModel RV-pOPIN	CTGGTCTAGAAAGCTTCTCGTAGATTCAGTCAAAGCTTTGT
RBD1-linker RV	Stau2 RBD1-linker RV-pOPIN	CTGGTCTAGAAAGCTTCTCTAACTACCTGGGTTATTATTGACATTAC
RBD2 RV	Stau2 RBD2 RV-pOPIN	CTGGTCTAGAAAGCTTCTATTCAGATTTATTTGCATCTTTATCGTC
RBD2 SM RV	Stau2 RBD2 as in SwissModel RV-pOPIN	CTGGTCTAGAAAGCTTCTCTGTAGGGCTTGAAGCG
RBD3 RV	Stau2 RBD3 RV-pOPIN	CTGGTCTAGAAAGCTTCTACCTGTAAGACAGTGGT
RBD4 RV	Stau2 RBD4 RV-pOPIN	CTGGTCTAGAAAGCTTCTAAAGCTGTAACAGCATTGCTT
Stau2 RV	Stau2 FL RV-pOPIN	CTGGTCTAGAAAGCTTCTAGATGGCCGACTTTGAT
His-SUMO FW	pFastBacDual-His-SUMO FW	CATCGGGCGCGGATCCATGGCACACCATCACCAC
Stau2 RV-pFBD	Stau2 FL RV-pFastBacDual	ACTTCTCGACAAGCTTCTAGATGGCCGACTTTGAT
pOPIN-6xHis RV	pOPIN-6xHis RV	CTGGTCTAGAAAGCTTCTAgtgatggtggtgatggtg

Primer name	Primer description	Sequence 5'→ 3'
RBD1-6xHis RV	RBD1-6xHis RV	gtgatggtggtgatggtgCGTAGATTCGT CAAACGCTT
pBSKS-rsEGFP2 FW	pBSKS-rsEGFP2 FW	gcggtggcggccgctctagaatggtgagcaag ggcga
rsEGFP+3C RV	rsEGFP+3C RV	cgggccctgaaacagaacttccagcttgtaca gctcgtccatgc
3C+Stau2 FW	3C+Stau2 FW	ctggaagttctgtttcagggcccgATGGCA AACCCCAAAGAGAA
3C+dmStaufen FW	3C+dmStaufen FW	ctggaagttctgtttcagggcccgATGCAGC ACAACGTTCATGC
pBSKS-Stau2 RV	pBSKS-Stau2 RV	tcctgcagcccgggggatccCTAGATGGC CGACTTTGATTTCT
pBSKS-dmStaufen RV	pBSKS-dmStaufen RV	tcctgcagcccgggggatccTTTCATGGC ATTGTTGAGCCC
pUASp-rsEGFP2 FW	pUASp-rsEGFP2 FW	AGGCCACTAGTGGATCTGGATCCat ggtgagcaagggcga
pUASp-Stau2 RV	pUASp-Stau2 RV	TTAACGTTCGAGGTCGACTCTAGA CTAGATGGCCGACTTTGATT
pUASp-Staufen RV	pUASp-Staufen RV	TTAACGTTCGAGGTCGACTCTAGA ctaTTTCATGGCATTGTTGAGCC
pUASp-Hsp83p FW	pUASp-Hsp83p FW	TCTCTCTCTCTTTCTCGAGTTAAC GGGGAACTTGAAGAAGTG
pUASp-Hsp83p RV	pUASp-Hsp83p RV	CTAGTGGCCTATGCGGCCGCTTGG TGGAAATTCGTCTAAGTGGT
pHsp83p-rsEGFP2 FW	pHsp83p-rsEGFP2 FW	ATAGGCCACTAGTGGATCTGGATC Catggtgagcaagggcga
pHsp83p-Staufen RV	pHsp83p-Staufen RV	TGTTATCAAGCTCCTCGActaTTTC ATGGCATTGTT
pHsp83p-Stau2 RV	pHsp83p-Stau2 RV	GTTATCAAGCTCCTCGACTAGATG GCCGACTTTG
pHsp83p modify RV	pHsp83p-Stau2/Staufen RV	catGGATCCAGATCCACTAGTGGCC TATGCGG
pHsp83p RV	pHsp83p-Stau2/Staufen RV	GTTATCAAGCTCCTCGA
pFBD-HisMBP FW	pFastBac Dual-His-MBP-Pum2 FW XhoI	CATCTCCCGGTACCGTTACAGCAT CCCATTTGGTG
pFBD-Pum2 RV	Pum2 RV-pFastBac Dual SphI	CACCCGGGATCTCGAATGGCACAC CATCACCAC
Pum HD aa642 FW	pOPIN+PPsite-mPum2 642 FW	AAGTTCTGTTTCAGGGCCCGAACC TTCAGCTCAGAGACT
Pum HD aa963 RV	mPum2 963 RV-pOPIN	CTGGTCTAGAAAGCTTTACAACTT GGCCAGTATATG

Table 10: Mutagenesis primers

Primer name	Primer description	Sequence 5'→ 3'
Stau2 C11S antisense	t31a_antisense	gctaactcatttaccagactcactggagttttctctttg
Stau2 C11S sense	t31a	caaagagaaaactccagtgagtctggtaaatgagtt agc
Stau2 C140S antisense	t418a_antisense	tgggcattgggctatgatacctctgattgtacatgc
Stau2 C140S sense	t418a	gcatgtacaatcagaggtatcatagcccaatgccca
Stau2 E15A antisense	a44c_antisense	ggaaacgggctaacgcatttaccagacacactgga g
Stau2 E15A sense	a44c	ctccagtgtgtctggtaaatgcgttagcccgtttcc
Stau2 H36A antisense	c106g_a107c antisense	caccgaaaacatcttcgaagcagcaggcccgctttc attc
Stau2 H36A sense	c106g_a107c_	gaatgaaagcgggcctgctgcttcgaagatgttttcg gtg
Stau2 F40A antisense	t118g_t119c_ antisense	agactcagctgcaccgaagccatcttcgaatgagca gg
Stau2 F40A sense	t118g_t119c	cctgctcattcgaagatggcttcggtgcagctgagtc t
Stau2 K59A antisense	a175g_a176c_ antisense	ttgttgggccttcgctatactgctcccttcggattccc
Stau2 K59A sense	a175g_a176c	gggaatccgaagggagcagtatagcgaaggcccaa caa
Stau2 K60A antisense	a178g_a179c_ant isense	caacagcttgttgggccgcctttatactgctcccttcg g
Stau2 K60A sense	a178g_a179c_	ccgaagggagcagtataaaggcggcccaacaagct gttg
Stau2 K59A K60A antisense	a175g_a176c_a1 78g_a179c_antis ense	cagcttgttgggccgccgctatactgctcccttcggat tcccatgt
Stau2 K59A K60A sense	a175g_a176c_a1 78g_a179c	acatgggaatccgaagggagcagtatagcggcggc ccaacaagctg
Stau2 Δ119-135 antisense		ggcaatgatacctctgtggatctagtggcctg
Stau2 Δ119-135 sense		caggccactagatccacagaggtatcattgcc
Stau2 E99A antisense	a296c_antisense	tagcgagcccattcagtgccacagttggagttata
Stau2 E99A sense	a296c_sense	tataactccaactgtggcactgaatgggctcgcta
Stau2 K106A antisense	a316g_a317c antisense	ggcaggctctccccttgccatagcgagcccattc
Stau2 K106A sense	a316g_a317c	gaatgggctcgctatggcaaggggagagcctgcc
Stau2 F157A sense	t469g_t470c	gttcagttaactgtaggaaataatgaagcctttggtg aagggaagactc
Stau2 F157A antisense	t469g_t470c antisense	gagtcttcccttcaccaaaggcttcattatttcctaca gttaactgaac

Primer name	Primer description	Sequence 5'→ 3'
Stau2 Q165A antisense	c493g_a494c antisense	tgtgtctggcagctgctcgagtcttcccttcacc
Stau2 Q165A sense	c493g_a494c	ggtgaagggaagactcgagcagctgccagacaca
Stau2 H169A antisense	c505g_a506c antisense	ctttcatcgcagcattggctctggcagcttgtcgag
Stau2 H169A sense	c505g_a506c	ctcgacaagctgccagagccaatgctgcgatgaaa g
dmStau F343A sense	t1027g_t1028c	tgcccactgcaagaccgccacggtgacactgatg
dmStau F343A antisense	t1027g_t1028c antisense	catcagtgtcaccgtggcggtcttgcagtgggca
dmStau F533A sense	t1597g_t1598c	gtgggcaagcagaaggctgtgggcatcggacg
dmStau F533A antisense	t1597g_t1598c antisense	cgtccgatgcccacagccttctgcttgcccac
dmStau H545A antisense	c1633g_a1634c	ccgcagcgtcagctttcgcttgctgcagtgtgcg
dmStau H545A sense	c1633g_a1634c antisense	cgcacactgcagcaagcgaaagctgacgctgcgg

Table 11: Template primers for RNA *in vitro* transcription

Primer name	Primer description	Sequence 5'→ 3'
3'UTR FW	T7prom+*Rgs4* 3'UTR FW	AATTTAATACGACTCACTATAGGttctc acacagaggcagagaacc
3'UTR RV	*Rgs4* 3'UTR nt2129 RV	aggcctataaagcacatggcagaaacagacat
BR FW	T7prom+*Rgs4* 3'UTR 257FW	AATTTAATACGACTCACTATAGGtaat ggccctgtaggtctgg
BR RV	*Rgs4* 3'UTR 870 RV	acgtgagcaaccaaccac
T7 FW	T7prom FW	AATTTAATACGACTCACTATAGG
SRS1 RV	SRS1-T7prom RV	GCTCCATCAAGACCCAGTGGCTTGAC GGAACCCTATAGTGAGTCGTATTAAA TT
SRS2 RV	SRS2-T7prom RV	ACATACACATACACAAATTGCATGTG CATGTCCCTATAGT GAGTCGTATTAAATT
SRS3 RV	SRS3-T7prom RV	Catgtgtgaacatatacaaatatatatatgcata tatatatatattcatgcacattcacacataCCTA TAGTGAGTCGTATTAAATT
SRS2+5 RV	SRS2+5-T7prom RV	ATATACATACACATACACAAATTGCA TGTGCATGTCCTATAGTGAGTCGTAT TAAATT
dsSRS2+5 RV	dsSRS2+5-T7prom RV	TATATACATACACATACACAAATTGC ATGTGCATGTATATACCTATAGTGAG TCGTATTAAATT

Primer name	Primer description	Sequence 5'→ 3'
11bpSRS2+5 RV	11bpSRS2+5- T7prom RV	TATATACATACACATACAAATCATGTGCATGTCCTATAGTGAGTCGTATTAAATT
9bpSRS2+5 RV	9bpSRS2+5-T7prom RV	TATATACATACACACAAATTGTGCATGTCCTATAGTGAGTCGTATTAAATT
8ntSRS2+5 RV	8ntSRS2+5-T7prom RV	TATATACATACACaaaGTGCATGTCCTATAGTGAGTCGTATTAAATT
7bpSRS2+5 RV	7bpSRS2+5-T7prom RV	TATATACATACACAAATTGCATGTCCTATAGTGAGTCGTATTAAATT
6bpSRS2+5 RV	6bpSRS2+5-T7prom RV	TATATACATACCAAATGCATGTCCTATAGTGAGTCGTATTAAATT
5bpSRS2+5 RV	5bpSRS2+5-T7prom RV	TATATACATATaaaGCATGTCCTATAGTGAGTCGTATTAAATT
ssPum2 RV	ssPum2-T7prom RV	ATATACATACACATACACCTATAGTGAGTCGTATTAAATT
SRS2+5/GAAA RV	SRS2+5nt/GAAA scaffold RV	GCATAGACTTTCATCCTTAGCTATATACATACACATACACAAATTGCATGTGCATGTCCTATAGTGAGTCGTATTAAATT
SRS2+3/GAAA RV	SRS2+3nt/GAAA scaffold RV	GCATAGACTTTCATCCTTAGCTATACATACACATACACAAATTGCATGTGCATGTCCTATAGTGAGTCGTATTAAATT
SRS2+7/GAAA RV	SRS2+7nt/GAAA scaffold RV	GCATAGACTTTCATCCTTAGCAATATATACATACACATACACAAATTGCATGTGCATGTCCTATAGTGAGTCGTATTAAATT
SRS2+5/GAAAins RV	SRS2+5nt/GAAAins RV	TATATACATACACATACACGCATAGACTTTCATCCTTAGCTTGCATGTGCATGTCCTATAGTGAGTCGTATTAAATT
SRS2tet+5/GAAAins RV	SRS2tetraloop+5nt/GAAA scaffold RV	GCATAGACTTTCATCCTTAGCTATATACATACACATACAAAATTGCATGTGCATGTCCTATAGTGAGTCGTATTAAATT
SRS2+3/GAAAins RV	SRS2+3nt/GAAAins RV	TATACATACACATACACGCATAGACTTTCATCCTTAGCTTGCATGTGCATGTCCTATAGTGAGTCGTATTAAATT
SRS2+6/GAAAins RV	SRS2+6nt/GAAAins RV	ATATATACATACACATACACGCATAGACTTTCATCCTTAGCTTGCATGTGCATGTCCTATAGTGAGTCGTATTAAATT
SRS2+5/longGAAAins RV	SRS2+5/long GAAA scaffold insertion RV	TATATACATACACATACACGCATAGCACTTTCATGCCTTAGCTTGCATGTGCATGTCCTATAGTGAGTCGTATTAAATT
T7prom+minRNA FW	T7prom+minRNA	AATTTAATACGACTCACTATAGGatgtgatgtcacatgcacatg
minRNA part1	minRNA 5' FW	atgtgatgtcacatgcacatgcaatttgtgtatgtgtatgtatatattaaatatatagaacatatgcat

Primer name	Primer description	Sequence 5'→ 3'
minRNA part2	minRNA 3' RV	tacatagatataatatatacagaatgtatatgca tatgttctatatatttaatatataca

Table 12: DNA oligos for anneling assays

Primer name	Primer description	Sequence 5'→ 3'
TAR (+)	HIV-1 TAR sense derived 56 nt sequence	GGTCTCTCTTGTTAGACCA GGTCGAGCCCGGGAGCTCT CTGGCTAGCAAGGAACCC
TAR (-)	HIV-1 TAR antisense derived 56 nt sequence	GGGTTCCTTGCTAGCCAGA GAGCTCCCGGGCTCGACCT GGTCTAACAAGAGAGACC

2.7 RNA

Table 13: RNA sequences

Short name	Full name/ description (numbering relative to start of 3'UTR)	Sequence 5'→ 3'	Production
Rgs4 3'UTR	*Rgs4* 3'UTR FL Rattus norvegicus regulator of G-protein signaling 4 (Rgs4), mRNA NCBI Reference Sequence: NM_017214.1 (3'UTR: nt 728-2919 of mRNA)	gUUCUCACACA GAGGCAGAGA ACCGAAAUGC CAAGACUCUA UGCUCUGGAA AACCUGAGGC CAAAUAUUGA UCUGUAUUAA GCAUCAAUGC UUUCUCCACA UUGUAGCCUA GUAUCCAUGC UGCCUGCCGU GUGUGAGUCA CUUCCAUGUA AAACUAGACU UAGCUGUGGU GUGGGGGUUU UCAUUGGGGU AAGACCCAAC UUGUUUUCAA UUUUCCCAAG UUUCCUUAAA GGGUGUCAGG UGAGCAAGUC UCCAAAUAAU GGCCCUGUAG GUCUGGAUUU UCAAAGAUGG UUAGUAGUCC ACCCCUUCCA ACAGUUUGAC CUCAAGUUAG UUGGUACACU UCAUGUGAUG UCACAUGCAC AUGCAAUGUC AGCCAGCAGC ACUUCCUACA GACUUUCAAC GUUUAGGUGA UAUUUGUGUA UGUGUAUGUA UAUAUUAAAU AUAUAGAACA UAUGCAUAUA CAUUCUGUAU AUAUUAUAUC UAUGUAUUCA GUAUGUGUGA AUGUGCAUGA AUAUAUAUAU AUAUGCAUAU AUAUAUUUGU AUAUGUUCAC ACAUGCACAC ACAUUUCUUC AAGAAAAGAU GGGAAAGAUC CUUGGUGCUC AAAUUGGAGU GUGUACACAU GCUUGCAUGC AUGUUCUGAC UUCUGGUCCU UCAUACUGUG UCUGAACAGG GCAAACUAAA UUAACUGCCA UGCAGGCUAA GAAAGGAACA CUAACUUGUA AAAAGUGAGU UCCGUCAAGC CACUGGGUCU UGAUGGAGCA UAGUCAGGGC CUUUGUGUUU AAUCUCGUCA AUGGCCUCCA CAUUGAGCAC UGAGCUAUGG GGUGAGUACU CCGAAAACUC UGCUGUCUGA CUGACACAGA GCUGCCUCGC ACCGGUGAUU ACUACUAGCA CUUUUAAGUC CCUAUGCUGU UGGCCAUCCC UCCUUUGCCU GGGUGCUCAG GGCAUGCUGA CUAGCAGCUG GGUUGGUCUG GAGAUGGAUG UUUGAGAGGA AUGAAGGAAU GCGGUCCAGG CCUUGUUGCC UAGCCCUACA AAUGACUACU GCUUAGGUGA GGGCAGAAGA CCCCGAGGUU AUCUUAAUUC UUUCCUCUCU UGAUAAGGUG CUCUCCUAUU CCUACCCCCA AAGAACGUCA CCUGUCAGAU GAGCCUCUUU ACUUCCCCGU GGUUGGUUGC UCACGUUAGG AACCAUGGCC ACCUGCAAGU CAUUCUAAGC UACCCGCUUA CAUUUUUCAA AAGCAUCACC AGGGGGAAAG GUUAUGCUGU CCCAGGAGGA AGUAAGCUCU UAUGAGCUGU AAACCCCUUU UUGGUUUUCU GCUUUGAGGU AAGAGCUUGU UCAUCCCAUC CCAAACACCA AAGUUAGCAG AGACCAACGG AAGGAGAGAG GAAAGAAAAA AAAAAAGAAA GAGAAGAGAA AAGAGGAGGA CGGGAUAUCA GUUGGUAGGA CUACUGUUUG GAGCUUUUUA AGGCACGUGA AAUACUUGAA AAUUUCUCAU UUGUGUUAUU UAUGUUGUUU UGUACAAUGU UUUUAUUACU GUAUUGUUUU AUAAAUGGAG GUACAGGAUA UUACCCGAAU UAUUAAUGAA UGCCCAAGAA GUAAUUUUCU UCUCAUUCCU CUAAAAGUCC UGCCUUUGAG AGCGCACACA GACUCGUGCA UACUGCAGGC ACAGCUCCAG UUUAAAUUCC AUGCAUGAGC ACCAUUGUGG CUGCAAAGUG AAGACACUCA UAGUGUGAAU CCAAGUCUCA CCAUUAUUGA AGAAGUCAGU UUUCUAACAG UACUGUUGUC UCUCUUGACA GUCUUGCGUA UAAUAUCCCC AGAGCUCCCC CAUCAGUGGU CCUAACUCCU UUUUGUAAUA CACAAGUCCA	*In vitro* transcription (Ambion MegaScript), primer: 3'UTR FW, 3'UTR RV

Short name	Full name/ description (numbering relative to start of 3'UTR)	Sequence 5'→ 3'	Production
		CAGUCGUGUC UGUAUAACUC UCCGGUCUUG CCCUAAUAUU AUCAUGACUU UGAGAUUGUA CCUGUACUCC CAGACUGCUG UCUCACAAAU AGGUCUGGGA AAAGUCAUUC UGAAUGAGAA GUAAAUUAUUUUAUGUAAUA CAUCUUGAGU GUGUCUUCAG UUGUAUUUGC CAUCGCUCUU UGGUCUGGCG AGCCUGCCUG CUGCUGGCCC CUGCAAAGGA CGCUCCUUCC AGAUGCAUGU CUGUUUCUGC CAUGUGCUUU AUAGGCCUCA GCGCUGAUGC UUCCAAUGAA ACACAUAGAU CUGAAUGAUA ACAGGAAAUA AAUGCUUCCUAC	
BR	*Rgs4* 3'UTR (257-890)	gUAAUGGCCCU GUAGGUCUGG AUUUUCAAAG AUGGUUAGUA GUCCACCCCU UCCAACAGUU UGACCUCAAG UUAGUUGGUA CACUUCAUGU GAUGUCACAU GCACAUGCAA UGUCAGCCAG CAGCACUUCC UACAGACUUU CAACGUUUAG GUGAUAUUUG UGUAUGUGUA UGUAUAUAUU AAAUAUAUAG AACAUAUGCA UAUACAUUCU GUAUAUAUUA UAUCUAUGUA UUCAGUAUGU GUGAAUGUGC AUGAAUAUAU AUAUAUAUGC AUAUAUAUAU UUGUAUAUGU UCACACAUGC ACACACAUUU CUUCAAGAAA AGAUGGGAAA GAUCCUUGGU GCUCAAAUUG GAGUGUGUAC ACAUGCUUGC AUGCAUGUUC UGACUUCUGG UCCUUCAUAC UGUGUCUGAA CAGGGCAAAC UAAAUUAACU GCCAUGCAGG CUAAGAAAGG AACACUAACU UGUAAAAAGU GAGUUCCGUC AAGCCACUGG GUCUUGAUGG AGCAUAGUCA GGGCCUUUGU GUUUAAUCUC GUCAAUGGCC UCCACAUUGA GCACUGAGCU AUGGGGUGAG UACUCCGAAA ACUCUGCUGU CUGACUGACA CAGAGCUGCC UCGCACCGGU GAUUACUACU AGCA	*In vitro* transcription (Ambion MegaScript), primer: BR FW, BR RV
BR mutant Pum2 B site	*Rgs4* 3'UTR (257-890) G467C T468C	GUAAUGGCCC UGUAGGUCUG GAUUUUCAAA GAUGGUUAGU AGUCCACCCC UUCCAACAGU UUGACCUCAA GUUAGUUGGU ACACUUCAUG UGAUGUCACA UGCACAUGCA AUGUCAGCCA GCAGCACUUC CUACAGACUU UCAACGUUUA GGUGAUAUUU GUGUAUGUGU AUGUAUAUAU UAAAUAUAUA GAACAUAUGC AUAUACAUUC UCCAUAUAUU AUAUCUAUGU AUUCAGUAUG UGUGAAUGUG CAUGAAUAUA UAUAUAUAUG CAUAUAUAUA UUUGUAUAUG UUCACACAUG CACACACAUU UCUUCAAGAA AAGAUGGGAA AGAUCCUUGG UGCUCAAAUU GGAGUGUGUA CACAUGCUUG CAUGCAUGUU CUGACUUCUG GUCCUUCAUA CUGUGUCUGA ACAGGGCAAA CUAAAUUAAC UGCCAUGCAG GCUAAGAAAG GAACACUAAC UUGUAAAAAG UGAGUUCCGU CAAGCCACUG GGUCUUGAUG GAGCAUAGUC AGGGCCUUUG UGUUUAAUCU CGUCAAUGGC CUCCACAUUG AGCACUGAGC UAUGGGGUGA GUACUCCGAA AACUCUGCUG UCUGACUGAC ACAGAGCUGC CUCGCACCGG UGAUUACUAC UAGCACU	*In vitro* transcription (Ambion MegaScript), primer: BR FW, BR RV
BR mutant Pum2 A site	*Rgs4* 3'UTR (257-890) G428C T429C	gUAAUGGCCCU GUAGGUCUGG AUUUUCAAAG AUGGUUAGUA GUCCACCCCU UCCAACAGUU UGACCUCAAG UUAGUUGGUA CACUUCAUGU GAUGUCACAU GCACAUGCAA UGUCAGCCAG CAGCACUUCC UACAGACUUU CAACGUUUAG GUGAUAUUUG UGUAUGUGUA UCCAUAUAUU AAAUAUAUAG AACAUAUGCA UAUACAUUCU GUAUAUAUUA UAUCUAUGUA UUCAGUAUGU GUGAAUGUGC AUGAAUAUAU AUAUAUAUGC AUAUAUAUAU UUGUAUAUGU UCACACAUGC	*In vitro* transcription (Ambion MegaScript), primer: BR FW, BR RV

Short name	Full name/ description (numbering relative to start of 3'UTR)	Sequence 5'→ 3'	Production
		ACACACAUUU CUUCAAGAAA AGAUGGGAAA GAUCCUUGGU GCUCAAAUUG GAGUGUGUAC ACAUGCUUGC AUGCAUGUUC UGACUUCUGG UCCUUCAUAC UGUGUCUGAA CAGGGCAAAC UAAAUUAACU GCCAUGCAGG CUAAGAAAGG AACACUAACU UGUAAAAAGU GAGUUCCGUC AAGCCACUGG GUCUUGAUGG AGCAUAGUCA GGGCCUUUGU GUUUAAUCUC GUCAAUGGCC UCCACAUUGA GCACUGAGCU AUGGGGUGAG UACUCCGAAA ACUCUGCUGU CUGACUGACA CAGAGCUGCC UCGCACCGGU GAUUACUACU AGCACU	
BR mutant Pum2 A site and B site	*Rgs4* 3'UTR (257-890) G428C T429C G467C T468C	gUAAUGGCCCU GUAGGUCUGG AUUUUCAAAG AUGGUUAGUA GUCCACCCCU UCCAACAGUU UGACCUCAAG UUAGUUGGUA CACUUCAUGU GAUGUCACAU GCACAUGCAA UGUCAGCCAG CAGCACUUCC UACAGACUUU CAACGUUUAG GUGAUAUUUG UGUAUGUGUA UCCAUAUAUU AAAUAUAUAG AACAUAUGCA UAUACAUUCU CCAUAUAUUA UAUCUAUGUA UUCAGUAUGU GUGAAUGUGC AUGAAUAUAU AUAUAUAUGC AUAUAUAUAU UUGUAUAUGU UCACACAUGC ACACACAUUU CUUCAAGAAA AGAUGGGAAA GAUCCUUGGU GCUCAAAUUG GAGUGUGUAC ACAUGCUUGC AUGCAUGUUC UGACUUCUGG UCCUUCAUAC UGUGUCUGAA CAGGGCAAAC UAAAUUAACU GCCAUGCAGG CUAAGAAAGG AACACUAACU UGUAAAAAGU GAGUUCCGUC AAGCCACUGG GUCUUGAUGG AGCAUAGUCA GGGCCUUUGU GUUUAAUCUC GUCAAUGGCC UCCACAUUGA GCACUGAGCU AUGGGGUGAG UACUCCGAAA ACUCUGCUGU CUGACUGACA CAGAGCUGCC UCGCACCGGU GAUUACUACU AGCACU	*In vitro* transcription (Ambion MegaScript), primer: BR FW, BR RV
BR ΔSRS2	*Rgs4* 3'UTR (257-890) Δ(354-366)(417-429)	gUAAUGGCCCU GUAGGUCUGG AUUUUCAAAG AUGGUUAGUA GUCCACCCCU UCCAACAGUU UGACCUCAAG UUAGUUGGUA CACUUCAUGU GAUGUCAUGU CAGCCAGCAG CACUUCCUAC AGACUUUCAA CGUUUAGGUG AUAUUUGAUA UAUUAAAUAU AUAGAACAUA UGCAUAUACA UUCUGUAUAU AUUAUAUCUA UGUAUUCAGU AUGUGUGAAU GUGCAUGAAU AUAUAUAUAU AUGCAUAUAU AUAUUUGUAU AUGUUCACAC AUGCACACAC AUUUCUUCAA GAAAAGAUGG GAAAGAUCCU UGGUGCUCAA AUUGGAGUGU GUACACAUGC UUGCAUGCAU GUUCUGACUU CUGGUCCUUC AUACUGUGUC UGAACAGGGC AAACUAAAUU AACUGCCAUG CAGGCUAAGA AAGGAACACU AACUUGUAAA AAGUGAGUUC CGUCAAGCCA CUGGGUCUUG AUGGAGCAUA GUCAGGGCCU UUGUGUUUAA UCUCGUCAAU GGCCUCCACA UUGAGCACUG AGCUAUGGGG UGAGUACUCC GAAAACUCUG CUGUCUGACU GACACAGAGC UGCCUCGCAC CGGUGAUUAC UACUAGCACU	*In vitro* transcription (Ambion MegaScript), primer: BR FW, BR RV
BR ΔSRS1	*Rgs4* 3'UTR (257-890)Δ(729-759)	gUAAUGGCCCU GUAGGUCUGG AUUUUCAAAG AUGGUUAGUA GUCCACCCCU UCCAACAGUU UGACCUCAAG UUAGUUGGUA CACUUCAUGU GAUGUCACAU GCACAUGCAA UGUCAGCCAG CAGCACUUCC UACAGACUUU CAACGUUUAG GUGAUAUUUG UGUAUGUGUA UGUAUAUAUU AAAUAUAUAG AACAUAUGCA UAUACAUUCU GUAUAUAUUA UAUCUAUGUA UUCAGUAUGU GUGAAUGUGC AUGAAUAUAU AUAUAUAUGC AUAUAUAUAU UUGUAUAUGU UCACACAUGC ACACACAUUU CUUCAAGAAA AGAUGGGAAA	*In vitro* transcription (Ambion MegaScript), primer: BR FW, BR RV

Short name	Full name/ description (numbering relative to start of 3'UTR)	Sequence 5'→ 3'	Production
		GAUCCUUGGU GCUCAAAUUG GAGUGUGUAC ACAUGCUUGC AUGCAUGUUC UGACUUCUGG UCCUUCAUAC UGUGUCUGAA CAGGGCAAAC UAAAUUAACU GCCAUGCAGG CUAAGAAAGG AACACUAACU UGUAAAAAGU GAAUAGUCAG GGCCUUUGUG UUUAAUCUCG UCAAUGGCCU CCACAUUGAG CACUGAGCUA UGGGGUGAGU ACUCCGAAAA CUCUGCUGUC UGACUGACAC AGAGCUGCCU CGCACCGGUG AUUACUACUA GCACU	
BR ΔSRS1 ΔSRS2	*Rgs4* 3'UTR (257-890)Δ(354-366)(417-429)(729-759)	UAAUGGCCCU GUAGGUCUGG AUUUUCAAAG AUGGUUAGUA GUCCACCCCU UCCAACAGUU UGACCUCAAG UUAGUUGGUA CACUUCAUGU GAUGUCAUGU CAGCCAGCAG CACUUCCUAC AGACUUUCAA CGUUUAGGUG AUAUUUGAUA UAUUAAAUAU AUAGAACAUA UGCAUAUACA UUCUGUAUAU AUUAUAUCUA UGUAUUCAGU AUGUGUGAAU GUGCAUGAAU AUAUAUAUAU AUGCAUAUAU AUAUUUGUAU AUGUUCACAC AUGCACACAC AUUUCUUCAA GAAAAGAUGG GAAAGAUCCU UGGUGCUCAA AUUGGAGUGU GUACACAUGC UUGCAUGCAU GUUCUGACUU CUGGUCCUUC AUACUGUGUC UGAACAGGGC AAACUAAAUU AACUGCCAUG CAGGCUAAGA AAGGAACACU AACUUGUAAA AAGUGAAUAG UCAGGGCCUU UGUGUUUAAU CUCGUCAAUG GCCUCCACAU UGAGCACUGA GCUAUGGGGU GAGUACUCCG AAAACUCUGC UGUCUGACUG ACACAGAGCU GCCUCGCACC GGUGAUUACU ACUAGCACU	*In vitro* transcription (Ambion MegaScript), primer: BR FW, BR RV
SRS1	*Rgs4* 3'UTR (729-759)	GUUCCGUCAA GCCACUGGGU CUUGAUGGAG C	*In vitro* transcription (Ambion MegaShortScript), Chemical synthesis (IBA)
SRS2	*Rgs4* 3'UTR (354-429)-Δ(367-416)AUUUG	ACAUGCACAU GCAAUUUGUG UAUGUGUAUG U	*In vitro* transcription (Ambion MegaShortScript), Chemical synthesis (Dharmacon & IBA)
SRS3	*Rgs4* 3'UTR (492-555)	gUAUGUGUGAA UGUGCAUGAA UAUAUAUAUA UAUGCAUAUA UAUAUUUGUA UAUGUUCACA CAUG	*In vitro* transcription (Ambion MegaShortScript)
SRS2+4	*Rgs4* 3'UTR (354-433)-Δ(367-416)AUUUG	gACAUGCACAU GCAAUUUGUG UAUGUGUAUG UAUAU	*In vitro* transcription (Ambion MegaShortScript), primers: T7prom, SRS2+4 RV

Short name	Full name/ description (numbering relative to start of 3'UTR)	Sequence 5'→ 3'	Production
minRNA	*Rgs4* 3'UTR (343-486)-Δ(367-416)AUUUG	gAUGUGAUGUC ACAUGCACAU GCAAUUUGUG UAUGUGUAUG UAUAUAUUAA AUAUAUAGAA CAUAUGCAUA UACAUUCUGU AUAUAUUAUA UCUAUGUA	*In vitro* transcription (Ambion MegaShortScript) primers: T7prom+minRNA, minRNA part1, min RNA part2
SRS2+5	*Rgs4* 3'UTR (354-434)-Δ(367-416)AUUUG	gACAUGCACAU GCAAUUUGUG UAUGUGUAUG UAUAUA	*In vitro* transcription, primers: T7prom, SRS2+5 RV
dsSRS2+5	*Rgs4* 3'UTR (349-434)-Δ(367-416)AUUUG	gUAUAUACAUGCACAU GCAAUUUGUG UAUGUGUAUG UAUAUA	*In vitro* transcription, primers: T7prom, dsSRS2+5 RV
12bpSRS2+5	*Rgs4* 3'UTR (354-434)-Δ(368-417)AUUUG	gACAUGCACAU GCAUUUGG UAUGUGUAUG UAUAUA	*In vitro* transcription (Ambion MegaShortScript), primers: T7prom, 12bpSRS2+5 RV
11bpSRS2+5	*Rgs4* 3'UTR (354-434)-Δ(369-418)AUUUG	gACAUGCACAU GAUUUG UAUGUGUAUG UAUAUA	*In vitro* transcription (Ambion MegaShortScript), primers: T7prom, 11bpSRS2+5 RV
10bpSRS2+5	*Rgs4* 3'UTR (354-434)-Δ(370-418)AUUUG	gACAUGCACAU AUUUG AUGUGUAUG UAUAUA	*In vitro* transcription (Ambion MegaShortScript), primers: T7prom, 10bpSRS2+5 RV
9bpSRS2+5	*Rgs4* 3'UTR (354-434)-Δ(371-419)AUUUG	gACAUGCACA AUUUG UGUGUAUGU AUAUA	*In vitro* transcription (Ambion MegaShortScript), primers: T7prom, 9bpSRS2+5 RV

Short name	Full name/ description (numbering relative to start of 3'UTR)	Sequence 5'→ 3'	Production
8ntSRS2 +5	*Rgs4* 3'UTR (354-434)-Δ(372-420)UUU	gACAUGCAC UUU GUGUAUGU AUAUA	*In vitro* transcription (Ambion MegaShortScript), primers: T7prom, 8ntSRS2+5 RV
7bpSRS 2+5	*Rgs4* 3'UTR (354-434)-Δ(373-421)AUUUG	gACAUGCA AUUUG UGUAUG UAUAUA	*In vitro* transcription (Ambion MegaShortScript), primers: T7prom, 7bpSRS2+5 RV
6bpSRS 2+5	*Rgs4* 3'UTR (354-434)-Δ(374-422)AUUUG	gACAUGC AUUUG GUAUG UAUAUA	*In vitro* transcription (Ambion MegaShortScript), primers: T7prom, 6bpSRS2+5 RV
5bpSRS 2+5	*Rgs4* 3'UTR (354-434)-Δ(375-423)AUUUG	gACAUGCUUUAUAUGUAUAUA	*In vitro* transcription (Ambion MegaShortScript), primers: T7prom, 5bpSRS2+5 RV
SRS2+5/ GAAA	SRS2+5 nt - GAAA scaffold	gACAUGCACAU GCAAUUUGUG UAUGUGUAUG UAUAUAgcuaaggaugaaagucua ugc	*In vitro* transcription, primers: T7prom, SRS2+5/GAAA RV
SRS2tet +5/GAA A	SRS2tetraloop+ 5 nt - GAAA scaffold	gACAUGCACAUGCAAUUUUGU AUGUGUAUGUAUAUAGCUAA GGAUGAAAGUCUAUGC	*In vitro* transcription, primers: T7prom, SRS2+5tet/GAAA RV
SRS2+7/ GAAA	SRS2+7 nt - GAAA scaffold	gACAUGCACAUGCAAUUUUGU AUGUGUAUGUAUAUAUUGCU AAGGAUGAAAGUCUAUGC	*In vitro* transcription, primers: T7prom, SRS2+7/GAAA RV
SRS2+3/ GAAA	SRS2+3 nt - GAAA scaffold	gACAUGCACAUGCAAUUUUGU AUGUGUAUGUAUAGCUAAGGA UGAAAGUCUAUGC	*In vitro* transcription, primers: T7prom, SRS2+3/GAAA RV

Short name	**Full name/ description (numbering relative to start of 3'UTR)**	**Sequence 5'→ 3'**	**Production**
SRS2+5/ GAAAins	SRS2+5 nt with GAAA scaffold insertion	gACAUGCACAUGCAAgcuaaggaugaaagucuaugc GUGUAUGUGUAUGUAUAUA	*In vitro* transcription, primers: T7prom, SRS2+5/GAAAins RV
SRS2+3/ GAAAins	SRS2+3 nt with GAAA scaffold insertion	gACAUGCACAUGCAAgcuaaggaugaaagucuaugc GUGUAUGUGUAUGUAUA	*In vitro* transcription, primers: T7prom, SRS2+3/GAAAins RV
SRS2+5/ longGAAAins	SRS2+5 nt with long GAAA scaffold insertion	gACAUGCACAUGCAAgcuaaggCaugaaaguGcuaugc GUGUAUGUGUAUGUAUAUA	*In vitro* transcription, primers: T7prom, SRS2+5/longGAAAins RV
SRS2+6/ GAAAins	SRS2+6 nt with GAAA scaffold insertion	gACAUGCACAUGCAAgcuaaggaugaaagucuaugc GUGUAUGUGUAUGUAUAUAU	*In vitro* transcription, primers: T7prom, SRS2+6/GAAAins RV
SRS3+6	*Rgs4* 3'UTR (492-561)	gUAUGUGUGAAUGUGCAUGAAUAUAUAUAUAUGCAUAUAUAUAUUUGUAUAUGUUCACACAUGCACACA	
TAR-57	HIV TAR-57 nt	GGUCUCUCUGGUUAGACCAGAUCUGAGCCUGGGAGCUCUCUGGCUAACUAGGGAACC	*In vitro* transcription, primer: T7prom, template: linearized RH99

2.8 Molecular biology

Generally, equipment and solutions used for molecular biology were sterilized by autoclaving before use.

For work with RNA, RNAse-free equipment, reagents and water were used. RNAse-free water was prepared by dethylpyrocarbonate (DEPC)-treatment. 0.05 % (v/v) DEPC were mixed into ddH_2O and subsequently incubated o/n at 37 °C. DEPC was afterwards inactivated by autoclaving.

Surfaces were decontaminated with RNAse Away (Fisher Scientific) before handling of RNA.

2.8.1 Transformation of chemically competent *E. coli* cells

Chemically competent *E. coli* were prepared as described by Inoue et al 1990 (Inoue et al., 1990). For transformation of chemically competent *E. coli*, 100-300 ng plasmid in 1–2 µL were added to 100 µL cells on ice and incubated for approximately 30 min. Cells were heat-shocked at 42 °C for 45 s and then immediately put on ice for 2–5 min. After addition of 400 µL LB or SOC medium, cells were incubated for at least 45 min at 37 °C. 100–200 µL cell suspension were plated on LB plates supplemented with selection antibiotics and incubated o/n at 37 °C.

E. coli DH10Bac were incubated for 48 h at 37 °C and two consecutive steps of blue-white screening were performed (see section 2.9.1.1).

2.8.2 Amplification of plasmid DNA

For plasmid DNA amplification, a single *E. coli* colony containing the desired plasmid was used to inoculate 5 mL LB medium supplemented with selection antibiotics. After incubation on a shaker at 150 rpm and 37 °C, cells were harvested by centrifugation and plasmid DNA was extracted using the NucleoSpin Plasmid kit (Macherey-Nagel) according to the manufacturer's instructions. Plasmid DNA was stored at -20 °C.

For the preparation of large Bacmid DNA for insect cell expression, cells were lysed using the ingredients of the kit, but plasmid DNA was precipitated with 800 µL ice-cold isopropanol for 10 min on ice. The Bacmid was pelleted by centrifugation at 11,000 g in 30 min and subsequently washed with 500 µL of ice-cold 70 % ethanol. The pellet was air-dried and subsequently dissolved in

elution buffer from the NucleoSpin Plasmid kit (Macherey-Nagel). Bacmid DNA was stored at 4 °C.

2.8.3 Agarose gel electrophoresis

DNA separation by agarose gel electrophoresis was performed on 0.8-1.5 % agarose (Biozym) in 1x TAE supplemented with 1:10,000 GelRed (Biotium) for fluorescence detection at a constant voltage of 110 V. 1x TAE was used as running buffer.

DNA samples were loaded in 1x DNA loading dye. As size markers, 2-10 µL of GeneRuler 1 kb (Thermo Scientific) or GeneRuler 100 bp (Thermo Scientific) were used, depending on the size of the DNA of interest.

RNA separation was performed accordingly but in 1x TBE agarose gels without GelRed and 1x TBE as running buffer. Depending on the application, RNA samples were loaded in 1x native RNA loading dye or 1x denaturing loading dye. Gels were stained after electrophoresis in 1x TBE supplemented with 1:10,000 GelRed (Biotium) for 2 min, then rinsed with 1x TBE to remove excess stain.

Fluorescence was visualized with a Fusion SL imaging system (Vilber Lourmat) by UV at 254 nm.

2.8.4 Molecular cloning

Specific DNA sequenes of interest were amplified by polymerase chain reaction (PCR) from template plasmids using salt-free In-Fusion cloning (Clontech)-pimers purchased at Eurofins MWG Biotech (Ebersberg). Plasmids were linearized by restriction digest with suitable restriction enzymes. PCR inserts and linear plasmids were purified by agarose gel electrophoresis and the NucleoSpin Gel and PCR Clean-Up kit (Macherey Nagel). Cloning was performed with the In-Fusion HD Cloning kit (Clontech) according to the manufacterer's protocol. 1-2 µL of each In-Fusion cloning reaction were used to transform *E.coli* DH5α or Stellar.

In the case of pFastBacDual-Stau2-Pum2, the two inserts were subsequently inserted using In-Fusion cloning. First, pFastBacDual was linearized with BamHI and HindIII for insertion of a HisSUMO-Stau2 FL sequence after the P_{PH} promotor. The resulting plasmid was linearized with Sph I and Xho I for insertion of a HisMBP-Pum2 FL sequence after the P_{p10} promotor.

Point mutations or deletions were introduced by 3-point PCR with overlap-extension (Ho et al., 1989) or with the QuikChange II Site-directed mutagenesis kit (Agilent technologies) according to the manufacturer's instructions.

Cloning of the *Rgs4* BR sequence in pCR-II-Blunt-TOPO was performed with the Zero Blunt TOPO PCR cloning kit (Invitrogen) according to the manufacturer's instructions.

For *in vivo* experiments in *D. melanogaster*, rsEGFP2-fusions of Stau2 and the fly homolog dmStau were cloned into pBlueScript-KS as a template for mutagenesis by 3-point PCR (Ho et al., 1989) with Phusion polymerase (Thermo Scientific) according to the manufacturer's protocol. As first step, the primers pBSKS-rsEGFP2 FW and rsEGFP+3C RV were used to create an rsEGFP2 sequence with a pBlueScript-KS 5' overhang for In-Fusion cloning and a PreScission protease cleavage site as 3' overhang, and the primers 3C+Stau2 FW and pBSKS-Stau2 RV or 3C+dmStaufen FW and pBSKS-dmStaufen RV to create a Stau2 or dmStau sequence, respectively, with a PreScission cleavage site 5' overhang and a pBlueScript-KS 3' overhang for InFusion cloning. The PCR products from these reactions served as templates for a third PCR with the primers pBSKS-rsEGFP2 FW and pBSKS-Stau2 RV or pBSKS-dmStaufen RV to create rsEGFP2-Stau2/dmStau sequences with 5' and 3' overhangs for InFusion (Clontech) cloning into BamHI/XbaI-linearized pBlueScript-KS according to the manufacturer's protocol.

The resulting plasmids served as templates for PCRs with pUASp-rsEGFP2 FW and pUASp-Stau2 RV or pUASp-Staufen RV to amplify rsEGFP2-Stau2/dmStaufen sequences with 5' and 3' overhangs for InFusion cloning into BamHI/XbaI-linearized pUASp-attB.

Furthermore, they served as templates for PCR amplification of rsEGFP2-Stau2/dmStau sequences with 5' and 3' overhangs for fusion to the Hsp83 promotor with the primers pHsp83p-rsEGFP2 FW and pHsp83p-Stau2 RV or pHsp83p-Staufen RV. Together with an Hsp83 promotor sequence created with pUASp-Hsp83p FW and pUASp-Hsp83p RV, the resulting sequences were used as a template for a third PCR with the primers pUASp-Hsp83p FW and pHsp83p modify RV to create a sequence with 5' and 3' overhangs for In-Fusion cloning

into XhoI-linearized pUASp-attB, resulting in a plasmid in which the inducible UAS promotor is exchanged for the constitutive Hsp83 promotor.
For details on primers and specific cloning strategies, see Table 8 and Table 9.

2.8.5 Small scale RNA *in vitro* transcriptions

RNAs for EMSAs were produced by small scale *in vitro* transcriptions with the MegaShortScript or MegaScript T7 Transcription kit (Ambion), depending on the RNA size, according to the manufacturer's protocol. For long RNAs (>100 nt) DNA templates were either produced by PCR or, in the case of *Rgs4* BR, by linearization of the template plasmid pCR-II-Blunt-TOPO-*Rgs4* BR. Template DNA was agarose gel-purified before use. For short RNAs, HPLC-purified primers (Eurofins) were used as templates. In order to produce partially double-stranded template DNA, FW and RV primers were annealed after unfolding at 60 °C for 5 min by slow cooling to RT. For details on template DNA used, see Table 11.
In case of minRNA, template DNA was produced by PCR. For this, two overlapping primers, minRNA part1 and minRNA part2, creating the full minDNA sequence were amplified using MyFi Mix (Bioline) according to the manufacturer's protocol. The resulting PCR product was gel-purified and then again PCR-amplified using OneTaq HotStart polymerase (New England Biolabs), with T7prom+minRNA as FW primer and minRNA part2 as RV primer to create a T7 promotor-containing template DNA. This final PCR product was again gel-purified.
After *in vitro* transcription, remaining DNA was DNAse I digested, RNA was purified by phenol/cloroform extraction and precipitated with ice-cold absolute ethanol for >15 min. RNA was redissolved in RNAse-free water and its quality was assessed by native and denaturing PAGE.

2.8.6 Large scale RNA *in vitro* transcriptions

RNAs needed in large amounts for crystallography or nuclear magnetic resonance (NMR) experiments were produced by large scale *in vitro* transcription. As template, 4 µM HPLC-purified FW primer and 3.4 µM HPLC-purified RV primer (for primer details, see Table 11) were annealed after unfolding at 60 °C for 5 min by slow cooling to RT in 34 mM $MgCl_2$ in a total volume of 594 µL. This DNA template mixture was used for a 5 mL *in vitro* transcription reaction containing, next to the template, 4 mM of each NTP, a

template-specifically optimized concentration $MgCl_2$, 80 mg/mL PEG8000 and 0.5 mg/mL T7 RNA polymerase in 1x TRX buffer (40 mM Tris/HCl pH_{RT} 8.0, 1 mM spermidine, 0.1 % Triton X-100, 5 mM DTT). The reaction was incubated for 2 h at 37 °C. The reaction was stopped by removal of precipitants by centrifugation at 48,384 g in 5 min and subsequent RNA precipitation with 0.1 V 3 M NaOAc and 3 V absolute ethanol at -20 °C o/n.

The optimal $MgCl_2$ concentration for each RNA was determined beforehand by $MgCl_2$ screening in 50 µL reactions containing 4–60 mM $MgCl_2$. Quality and quantity of RNA in each $MgCl_2$ concentration were examined by 8 % 1x-urea-PAGE.

2.8.7 PAGE purification of RNA

RNA was pelleted by centrifugation at 48,384 g, 4°C, in 30 min, air-dried and subsequently dissolved in 1x denaturing RNA loading dye. The RNA was purified by 8 % 1x TBE-8 M urea PAGE in an Owl sequencing chamber (Thermo Fisher Scientific) in 1x TBE running buffer at constant 300 V for 17-20 h. RNA bands were visualized by UV shadowing and the desired band was excised from the gel and extracted by electroelution in a Whatman Elutrap electroelution system (GE Healthcare) at constant 200 V in 1x TBE for 8 h. Eluted RNA was collected in 1 h intervals. Eluted RNA was dialyzed against 5 M NaCl at 4 °C o/n and subsequently twice against RNAse-free water at 4 °C o/n before drying in a Concentrator Plus SpeedVac (Eppendorf).

2.9 Protein expression and purification

2.9.1 Protein expression

2.9.1.1 Full-length Stau2 protein

Stau2 FL was expressed as HisSUMO-tagged fusion protein in High Five insect cells. After cloning in pFastBacDual, recombinant baculovirus was produced with the Bac-to-Bac Expression System (Invitrogen) as described by the manufacterer's protocol. The plasmid was amplified in *E. coli* DH5α for transformation of *E. coli* DH10Bac for recombination to Bacmid DNA. Transformed DH10Bac cells were grown at 37 °C on DH10Bac agar plates supplemented with 40 µg/mL IPTG and 100 µg/mL X-Gal to allow for blue/white screening. Isolation of Bacmid was performed from 5 mL LB cultures

(supplemented with antibiotics) of positive, white colonies, as described in section 2.8.2.

Bacmid DNA was used to transfect Sf21 insect cells with FuGeneHD (Roche). Sf21 cells were incubated in 6-well plates (2 mL, 0.4 x 10^6 cells/mL per well) for four days at 27.5 °C with 3 µL FuGeneHD + 2 µg Bacmid preincubated for 45 min in 300 µL HyClone SF medium. The supernatant of this P0 culture was used for infection of 10 mL Sf21 cells at 1.4 x 10^6 cells/mL in shaking culture. Cells were harvested by centrifugation after 4 days of incubation at 27.5 °C and the supernatant (P1) was used for infection of 500 mL Sf21 cells at 0.4 x 10^6 cells/mL. Cells were again harvested by centrifugation after 4 days at 27.5 °C and the virus-containing supernatant (P2) was sterile-filtered and stored at 4 °C. For protein expression, 20 mL virus-stock P2 was used for infection of 500 mL Hi5 insect cells at 1 x 10^6 cells/mL in shaking culture. After expression at 27.5 °C for 3 days, cells were harvested by centrifugation at 2,000 g in 10 min at 4 °C.

2.9.1.2 Truncated Stau2 RBD protein constructs

Other Stau2 proteins were expressed after cloning into the expression vectors pOPINS3C or pOPINJ as fusion proteins with HisSUMO- or HisGST-tag, respectively, in *E. coli* Rosetta cells using autoinduction in ZY-medium with selection antibiotics if not stated otherwise. Cells were grown for approximately 6 h at 37 °C, then temperature was decreased to 18 °C for protein expression for 16-18 h. Cells were harvested by centrifugation.

2.9.1.3 Pum2 proteins

Pum2 proteins were expressed after cloning into the expression vectors pOPINM or pOPINJ as HisMBP- or HisGST-fusion proteins, respectively, in *E. coli* Rosetta cells using autoinduction in ZY-medium with selection antibiotics if not stated otherwise. Cells were grown for approximately 6 h at 37 °C, then temperature was decreased to 18 °C for protein expression for 16-18 h. Cells were harvested by centrifugation.

2.9.1.4 Co-expression of full-length Stau2 and Pum2 proteins

Stau2 FL and Pum2 FL were co-expressed as HisSUMO- and HisMBP-tagged fusion proteins, respectively, in High Five insect cells. After cloning in pFastBacDual, recombinant baculovirus was produced with the Bac-to-Bac

Expression System (Invitrogen) and protein was expressed as described above for Stau2 FL (see section 2.9.1.1).

2.9.1.5 Selenomethionine-labeled proteins

For expression of selenomethionine (SeMet)-labeled proteins, the methionine auxotrophic *E. coli* B834 (DE3) strain was used. SelenoMet™ Medium (Molecular Dimensions) was prepared according to the manufacturer's instructions and supplemented with 100 mg/L SeMet.

100 mL precultures were grown o/n at 3°C, 150 rpm and used to inoculate 3 L pre-warmed SelenoMet™ Medium. Cultures were grown at 37 °C, 150 rpm to OD_{600nm}=0.6. Protein expression was induced with 0.25 mM IPTG and cultures were cooled for protein expression o/n to 18 °C.

2.9.1.6 Isotope-labeled proteins for NMR

^{15}N- or ^{15}N,^{13}C-labeled proteins for NMR experiments were expressed in ^{15}N-M9 mineral medium (1x ^{15}N-labeled M9 salt solution, 0.2 % (^{13}C-) glucose, 1 mM $MgSO_4$, 0.3 mM $CaCl_2$, 1 µg/L biotin, 1 µg/L thiamin, 1x trace metals) supplemented with antibiotics. 100 ml precultures were grown o/n at 37 °C, 150 rpm and used to inoculate 1 L pre-warmed M9 mineral medium. Cultures were grown at 37 °C, 150 rpm to OD_{600nm} = 0.6. Protein expression was induced with 0.25 mM IPTG and cultures were cooled for protein expression o/n to 18 °C.

2.9.2 Protein purification

2.9.2.1 Full-length Stau2 protein

High Five cell pellets containing His-SUMO-tagged Stau2 FL were lysed by sonication in lysis buffer (1x PBS, 880 mM NaCl, 400 mM arginine, 2 mM DTT, 10 mM imidazole). The lysate was cleared by centrifugation and the soluble protein fraction was purified by Ni-IMAC on HisTrap FF (GE). Bound protein was eluted with 200 mM imidazole after extensive washing with 15 CV lysis buffer. The protein was dialyzed in low salt buffer (40 mM Bis-Tris pH 7, 150 mM NaCl, 50 mM arginine, 2 mM DTT) o/n before further purification on a HiTrap Heparin HP column (GE) and size exclusion chromatography (SEC) on Superdex200 Increase (GE).

2.9.2.2 Truncated Stau2 RBD proteins

E. coli Rosetta cell pellets containing HisSUMO-tagged fusion proteins were lysed by sonication in lysis buffer (1x PBS, 880 mM NaCl, 400 mM arginine, 2 mM DTT, 10 mM imidazole). The lysate was cleared by centrifugation and the soluble protein fraction was purified by Ni-IMAC on HisTrap FF (GE). Bound protein was eluted with 200 mM imidazole after extensive washing with 15 CV lysis buffer. For fusion-tag removal, the protein was digested o/n with PreScission protease upon dialysis in low salt buffer (40 mM Bis-Tris pH 7, 150 mM NaCl, 50 mM arginine, 2 mM DTT). The protein was purified with a second, subtractive Ni-IMAC, affinity chromatography on a HiTrap Heparin HP column (GE) and size exclusion chromatography (SEC) on Superdex 75 (GE) unless stated otherwise. Size exclusion chromatography was performed in minimal buffer (40 mM Bis-Tris pH 7, 150 mM NaCl, 2 mM DTT) or the buffer required for downstream applications.

SEC of Stau2 RBD3-5 was performed on Superose 12 (GE).

RBD1-His was cloned into pOPINJ as a HisGST-fusion protein to allow for separation from the cleaved fusion tag. The second, subtractive purification step was performed on a GSTrap FF (GE) column. Because RBD1-only constructs did not bind to HiTrap Heparin, this purification step was skipped for all RBD1 constructs. Apart from that, purification was performed as described above.

2.9.2.3 Full-length Pum2 and N-terminal proteins

E. coli Rosetta cell pellets containing HisMBP-tagged fusion proteins were lysed by sonication in lysis buffer (1x PBS, 880 mM NaCl, 400 mM arginine, 2 mM DTT, 10 mM imidazole). The lysate was cleared by centrifugation and the soluble protein fraction was purified by Ni-IMAC on HisTrap FF (GE). Bound protein was eluted with 200 mM imidazole after extensive washing with 15 CV lysis buffer. After o/n dialysis in low salt buffer (40 mM Bis-Tris pH 7, 150 mM NaCl, 50 mM arginine, 2 mM DTT), the protein was further purified by anion exchange in negative mode on a HiTrap Q FF column to remove nucleic acid contaminations and SEC on Superdex 200 Increase (GE).

In case Pum2 FL was needed without His-tag, it was expressed as MBP-fusion protein from a pMALC vector kindly provided by Foong-Yee Ang (group of Prof.

Dr. Michael Kiebler, Department for Cell Biology, LMU München) and in the first step affinity-purified on amylose resin.

2.9.2.4 Pum2 homology domain (HD) proteins

Cell lysis and Ni-IMAC were performed as described above for full-length protein. For removal of the fusion tag, the protein was digested o/n with PreScission protease upon dialysis in low salt buffer (40 mM Bis-Tris pH 7, 150 mM NaCl, 50 mM arginine, 2 mM DTT). The protein was further purified with a second, subtractive Ni-IMAC, negative mode anion exchange chromatography on a HiTrap Q FF column (GE) and SEC on Superdex 75 (GE).
In case the protein was needed with HisMBP-fusion tag, PreScission protease and the subtractive Ni-IMAC were skipped.

2.10 Chemical and biophysical methods

2.10.1 Determination of DNA and RNA concentration

Concentration of DNA and RNA was determined by UV-spectroscopy with a Nanodrop ND-1000 UV/Vis- Spectrophotometer (Peqlab) by measuring absorption of UV light at 260 nm ($A_{260\ nm}$). Concentrations were calculated assuming an $A_{260\ nm}$ of 1.0 to relate to 50 ng/µL dsDNA or 40 ng/µL RNA.
To detect protein impurities, the sample absorption at 280 nm ($A_{280\ nm}$) was determined. Purity of nucleic acids was acceptable if $A_{260\ nm}/A_{280\ nm}$ was between 1.8-2.0.

2.10.2 Determination of protein concentration

Concentration of protein was determined by UV-spectroscopy with a Nanodrop ND-1000 UV/Vis- Spectrophotometer (Peqlab) by measuring absorption of UV light at 280 nm ($A_{280\ nm}$). Concentrations were calculated according to the Lambert-Beer law $A = \varepsilon \cdot c \cdot d$, wherein A = absorbance, ε = molar extinction coefficient [$M^{-1}cm^{-1}$], c = protein concentration [M] and d = cell length [cm]. Protein specific extinction coefficients were calculated beforehand using the ProtParam tool of the ExPASy server (Gasteiger et al., 2003).
Additionally, $A_{260\ nm}$ was measured to detect nucleic acid impurities. Proteins were considered nucleic acid-free if $A_{260\ nm}/A_{280\ nm}$ was between 0.5-0.6.
The concentration of proteins which do not absorb UV was determined with a DirectDetect system (EMD Millipore).

2.10.3 Polyacrylamide Gel Electrophoresis (PAGE)

Protein separation by Sodium dodecyl sulfate-polyacrylamide gel Electrophoresis (SDS-PAGE) was performed as described by Laemmli (Laemmli, 1970). Depending on the protein size, 1.5 mm thick 10-19 % polyacrylamide separating gels covered with 5 % stacking gels were used. Before loading, protein samples were supplemented with 1x SDS-loading dye and denatured at 98 °C for 5 min. Electrophoresis was performed in 1x TGS at constant voltage of 200-220 V. Separated proteins were visualized by Coomassie staining with PageBlue Protein Staining Solution (Thermo Scientific) according to the manufacterer's instructions.

Denaturing PAGE separation of RNA was performed on 8–10 % polyacrylamide gels containing 1x TBE and 8 M urea. Before loading, RNA samples were supplemented with 1x denaturing loading dye and denatured at 98 °C for 2 min. Electrophoresis was performed at constant 110 V in 1x TBE.

Native PAGE separation of RNA was performed in 4-12 % polyacrylamide 1x TBE gels. Before loading, RNA samples were supplemented with 1x native loading dye. Electrophoresis was performed at constant 110 V in 1x TBE.

RNA gels were stained after electrophoresis in 1x TBE supplemented with 1:10,000 GelRed (Biotium) for 2 min, then rinsed with 1x TBE to remove excess stain. Fluorescence was visualized with a Fusion SL imaging system (Vilber Lourmat) by UV at 254 nm.

2.10.4 Radioactive labeling of RNA and DNA

RNAs for electrophoretic mobility shift assays (EMSA) were labeled radioactively for sensitive detection. *In vitro* transcribed RNA was 5' dephosphorylated in 20 µL reactions containing 10 pmol RNA, 1x Tango Buffer with BSA (Thermo Fisher), 2 U FastAP thermosensitive alkaline phosphatase (Thermo Fisher) and 20 U of the RNAse inhibitor SUPERaseIn (Thermo Fisher). After incubation at 37 °C for 30 min, the dephosphorylated RNA was phenol/chloroform extracted and precipitated with 0.1 V 3 M NaOAc, 3 V absolute ethanol and subsequent chilling at -20 °C for ≥ 15 min.

For radioactive labeling, 10 pmol dephosphorylated RNA or chemically synthesized RNA were 5'-phosphorylated with ^{32}P from γ-^{32}P ATP (Hartmann Analytic) in a 20 µL reaction with T4 polynucleotide kinase (New England

Biolabs) in 1x buffer A. The labeling reaction was incubated at 37 °C for 30 min and subsequently stopped at 72 °C for 10 min.

Remaining free nucleotides were removed by purification on a NucAway™ Spin column (Ambion) according to the manufacturer's instructions. Eluted radiolabeled RNA was diluted to a final concentration of 100 nM in RNAse-free H_2O and stored at -20 °C.

DNA for annealing assays was labeled accordingly but purified by urea-PAGE. RNA was resolved on an 8 % urea-Midi Gel, detected with radiograph films, excised from the gel and eluted in 300 µL Crush'n'Soak buffer o/n. Subsequently, RNA was precipitated with 3 V 100 % EtOH, redissolved in 100 µL RNAse-free H_2O to a final concentration of 100 nM and stored at -20 °C.

2.10.5 Electrophoretic mobility shift assay (EMSA)

For EMSAs with short RNAs (<100 nt), protein at the indicated final concentration was mixed with 5 nM radiolabeled RNA in RNAse-free protein buffer supplemented with 4 % glycerol and 30 µg/mL yeast tRNA as competitor in a final volume of 20 µL. In order to allow protein-RNA complexes to form, the mixtures were incubated for > 20 min at RT.

Separation of protein-RNA complexes was performed by native PAGE on 6 % polyacrylamide 1x TBE gels in 40 min at constant 110 V in 1x TBE running buffer. Subsequently, the gels were fixed in 30 % (v/v) methanol, 10 % (v/v) acetic acid for 10 min before drying in a vacuum gel drier (BioRad). Visualization of radioactivity occurred after exposure of radiograph films (Kodak) in a Protec Optimax developer (Hohmann) or by PhosphorImaging with a Fujifilm FLA-3000.

In the case of long, unlabeled RNA (>100 nt), 10-100 nM RNA were used and separation of protein-RNA complexes was performed by 1-1.5 % agarose gel electrophoresis. Visualization of RNA occurred by GelRed (Biotium) staining. Fluorescence was visualized with a Fusion SL imaging system (Vilber Lourmat) by UV at 254 nm.

2.10.6 TAR(+)/TAR(-) annealing assay

TAR(+)/TAR(-) annealing assays were performed as essentially described before (Guichard et al., 2011). Cold TAR(+) DNA and hot (radiolabeled) TAR (-) DNA were incubated at 5 nM each in 20 µL Stau2-minimal buffer in presence of

increasing concentrations of protein and incubated for 5 min at 37 °C. The negative control did not contain protein and the positive control was incubated at 72 °C for 5 min and subsequently snap-cooled on ice. The reaction was stopped by addition of 1 µL Proteinase K (18 mg/mL), followed by incubation at RT for 5 min and subsequent addition of 5 µL TAR stop solution. Samples were resolved by 8 % native 1x TBE-PAGE at 4 °C. Subsequently, the gels were fixed in 30 % (v/v) methanol, 10 % (v/v) acetic acid for 10 min before drying in a vacuum gel-drier (BioRad). ssDNA and dsDNA were subsequently visualized by PhosphorImaging with a Fujifilm FLA-3000.

2.10.7 Biotinylation of RNA

Ligand RNA for binding studies by Surface Plasmon Resonance (SPR) was biotinylated to allow immobilization on a streptavidin-coated surface. For biotinylation, the Pierce™ RNA 3' End Biotinylation Kit (Thermo Fisher Scientific) was used according to the manufacterer's protocol. 50 pmol RNA were used per 30 µL reaction. After extraction and precipitation, the RNA was redissolved in 100 µL RNAse-free water.

2.10.8 Surface Plasmon Resonance (SPR)

SPR experiments were performed with a BIACORE 3000 system (GE Healthcare). To assess protein-RNA interactions, biotinylated RNA in a volume of 60 µL was streptavidin-captured on an SA-Chip (GE Healthcare) surface at a flowrate of 10 µL/min after three consecutive 1 min conditioning injections of 50 mM NaOH, 1 M NaCl.

Kinetic analysis of protein-RNA interactions was performed at a flow rate of 30 µL/min in HBS-EP buffer (10 mM HEPES pH 7.4, 150 mM NaCl, 3 mM EDTA, 0.005 % surfactant P20). Analyte protein in HBS-EP buffer at the indicated concentrations was injected for 4 min to allow for association, subsequent dissociation was allowed for 15 min in HBS-EP buffer. To remove any residual bound protein, two 1 min regeneration injections with 1 M NaCl were performed. Data were analyzed in the BIAevaluation software (GE Healthcare). After double-referrencing of obtained binding curves against the signal in a ligand-free reference channel and a buffer run, average values for the analyte response at equilibrium were calculated. Steady state binding curves were obtained by plotting the response at equilibrium against protein concentration and curve

fitting with the Origin Pro 9.0 (OriginLab) software using the two-site binding or Hill1 fits available in the software. All experiments were performed at least in triplicates and the results of these n≥3 experiments averaged. Kinetic fits, if applicable, were performed with the BIAevaluation software (GE Healthcare) using the bivalent analyte model available in the software.

To assess protein-protein interactions, the ligand protein was covalently amine-coupled to a CM5-Chip (GE Healthcare) surface according to the manufacterer's instructions. For this purpose, ligand protein was diluted in 10 mM Na acetate pH 4.5 just before coupling. The immobilization wizard of the Biacore Control software (GE Healthcare) was used to aim for a desired immobilization level.

Kinetic analysis of protein-protein interactions was performed at a flowrate of 30 µL/min in HBS-EP buffer. Analyte protein in HBS-EP buffer at the indicated concentrations was injected for 3 min to allow for association. Subsequent dissociation was allowed for 10 min in HBS-EP buffer. To remove any residual bound protein, two 1 min regeneration injections with 1 M NaCl were performed.

2.10.9 *In vitro* Pull-Down assay

5 µM HisSUMO-Stau2 FL and 5 µM MBP-Pum2 were mixed in a total volume of 100 µL in the presence or absence of 1 µM *Rgs4* BR RNA in low salt buffer supplemented with 10 mM imidazole. Samples were centrifuged for 10 min and the supernatants were incubated for 40 min at 4 °C on an overhead shaker with 120 µL equilibrated Ni sepharose beads. These binding reactions were washed three times with 533 µL low salt buffer + 10 mM imidazole and once with 50 µL low salt buffer + 10 mM imidazole and subsequently eluted with 50 µL elution buffer (250 mM imidazole/low salt buffer) in 20 min on the overhead shaker at 4 °C. 10 % of the input, 20 % of the last wash step and 34 % of the elution were analyzed by SDS-PAGE with Coomassie blue staining. RNA was analyzed on a 1.5 % agarose gel with GelRed DNA stain.

2.10.10 Static light scattering (SLS)

Static light scattering (SLS) experiments were performed with a 270 Dual Detector and a VE3580 RI Detector (Malvern) after SEC on a 10/300 or 5/150 Superdex200 Increase column (GE Healthcare) at 7 °C and flow rates of 0.4-0.5 mL/min. System calibration was performed with BSA. Data were analyzed

with the OmniSEC 5.02 software (Malvern). Details on sample concentrations, complex formation and SEC will be given in the results section.

2.10.11 Dynamic light scattering (DLS)

Dynamic light scattering (DLS) was measured with a DynaPro NanoStar (Wyatt) system using a Quartz Cuvette. Unless stated otherwise, ten aquisitions of 5 s were collected per sample. Evaluation was performed with the DYNAMICS software (Wyatt).

2.10.12 Circular Dichroism (CD) spectroscopy

CD spectra were collected with a Jasco J-715 spectropolarimeter from 260 nm to 190 nm in continuous scanning mode with a scanning speed of 50 nm/min at a bandwidth of 1 nm. Five scans were collected per measurement and response time was 8 s. The measurements were performed at 20 °C. Spectra were analyzed with SpectraManager (Jasco).

2.10.13 Isothermal titration calorimetry (ITC)

ITC experiments to identify protein-protein interactions were performed with a MicroCal iTC200 (Malvern Instruments, Malvern, UK). Before each experiment, the samples were thoroughly centrifuged to remove aggregates. The syringe was filled with a solution of the first protein at > 200 µM and was titrated into the sample cell, which was filled with a ten fold less concentrated solution of the second protein. The data was analyzed using the MicroCal Origin program.

2.10.14 UV-Crosslinking

5 nM radiolabeled minRNA, 100 µg/mL tRNA, and the indicated protein concentrations were mixed in low salt buffer (40 mM Bis-Tris pH 7, 150 mM NaCl, 50 mM arginine, 2 mM DTT) in a total volume of 20 µL. After 20 min incubation at RT the samples were subjected to 2.25 J UV radiation over 15 min on ice. The distance between the samples and the UV lamp was ~8 cm. After adding SDS-loading dye, samples were incubated for 5 min at 90 °C and separated on 10 % SDS-PAGE. Gels were fixed, dried, and analyzed with radiograph films.

2.11 Bioinformatics

DNA and protein sequences were obtained from the National Center for Biotechnology Information (NCBI) databases.

Physico-chemical properties of proteins such as molecular weight and extinction coefficient were computed using the ProtParam tool of the ExPASy server (Gasteiger et al., 2003).

PSIPRED v3.3 (Jones, 1999) and DISOPRED3 (Buchan et al., 2013) were used to predict secondary structures of proteins, the SWISS-MODEL workspace (Biasini et al., 2014) (Kiefer et al., 2009, Arnold et al., 2006, Guex and Peitsch, 1997) and Phyre2 (Kelley et al., 2015) were used for homology modeling.

RNA secondary structure predictions were made with the RNA folding form of the Mfold webserver (Zuker, 2003) and visualized with the Java applet VARNA (version 3.9, http://www.varna.lri.fr). DNA or RNA extinction coefficients were calculated as the sum of the individual nucleotides extinction coefficients assuming

A = 15.4 mM^{-1} cm^{-1},

C = 7.4 mM^{-1} cm^{-1},

G = 11.8 mM^{-1} cm^{-1},

T = 9.6 mM^{-1} cm^{-1},

U = 9.9 mM^{-1} cm^{-1}.

Multiple sequence alignments were made with Clustal Omega (Sievers et al., 2011) or MAFFT (Multiple Alignment using Fast Fourier Transform) (Katoh and Standley, 2013) on the EMBL-EBI bioinformatics webserver (McWilliam et al., 2013) (Li et al., 2015) and visualized in JalView (Waterhouse et al., 2009).

2.12 Structural Biology

2.12.1 X-ray crystallography

2.12.1.1 Preparation of protein-RNA complexes for crystallography

For preparation of protein-RNA complexes suitable for crystallization, protein was purified as decribed above (see section 2.9.2) to >95 % purity. RNA was refolded before use by denaturing at 85 °C for 2 min and slow cooling to RT and subsequently supplemented with 1x protein buffer. Protein and RNA were mixed at the indicated molar ratios and concentrations and incubated at RT for >20 min to allow for complex formation. Before crystallization, eventual contaminating

aggregates/precipitates were separated by centrifugation at 16,100 g at 4 °C for >15 min.

2.12.1.2 Pre-Crystallization Test

In order to estimate appropriate sample concentrations for crystallization, the Pre-Crystallization Test (Hampton Research) was performed according to the manufacterer's instructions and sample concentration adjusted accordingly.

2.12.1.3 Initial screening of crystallization conditions

For identification of suitable crystallization conditions, a range of initial screens (JCSG+, Nucleix, PACT, Natrix 1+2, Classics I and Classics II) was set up using a Mosquito (TTP LabTech) crystallization robot. 100 nL sample were mixed with 100 nL reservoir solution on 96-well MRC Crystallization Plates™ (Molecular Dimensions) in a sitting-drop approach over 80 µL reservoir solution.

The screens were incubated at 20 °C or 4 °C and regularly inspected visually for crystal growth by light microscopy.

2.12.1.4 Crystal optimization

Crystallization conditions which produced initial hits were optimized in optimization screens. Parameters of the condition (e.g. salt concentration, precipitant concentration, pH) were systematically varied in manually set up 24-well plates. Solutions used for crystal optimization were sterile-filtered before use. 500-1000 µL reservoir solution were used. Sitting drop and hanging drop techniques were tested and total dropsizes between 2–3 µL. Details will be given in the results section.

2.12.1.5 Crystal freezing

Crystals were harvested with cryogenic loops and flash-frozen in liquid nitrogen. In case the crystallization condition did not contain a cryoprotectant in sufficient concentration, the crystals were first quickly transferred to a cryoprotectant drop. Details on cryoprotection will be given in the results section. Crystals were stored in liquid nitrogen until measurement.

2.12.1.6 X-ray data collection and processing

X-ray data were collected at 100 K at the European Synchrotron Radiation Facility (ESRF, Grenoble, France) or Swiss Light Source (SLS, Villigen, Switzerland). Unless stated otherwise, native data were collected at an X-ray

wavelength of 1 Å. Details will be given in the results section. Data were indexed and integrated using XDS and scaled via XSCALE. Structure factor amplitudes were obtained with Truncate (CCP4 package, (Winn et al., 2011)).

2.12.1.7 Structure determination of SRS2 RNA

Native datasets were collected at the Swiss Light Source (SLS) synchrotron, beamline PXIII. Anomalous data for phasing were collected at the European Synchrotron radiation Facility (ESRF) at beam line ID 23-2 at wavelength 1.25439 Å. Data were indexed and integrated using XDS and scaled via XSCALE. Structure factor amplitudes were obtained with Truncate (CCP4 package, (Winn et al., 2011)). The structure was solved by MAD phasing with Barium from the mother liquor, using the AutoRickshaw web server (Panjikar et al., 2005). The structure was completed by iterative manual building in COOT and refinement with RefMac5 (CCP4 package). All crystallographic software was used from the SBGRID software bundle5. Images of the crystal structure were prepared with PyMol (Version 1.7; Schrodinger; http://www.pymol.org/).

2.12.2 Nuclear Magnetic Resonance (NMR)

NMR measurements were performed by Jan-Niklas-Tants (Group of Prof. Dr. Michael Sattler, Center for Integrated Protein Science Munich at the chair of Biomolecular NMR Spectroscopy, Department of Chemistry, TUM, Munich, Germany).

All samples were dialyzed to 150 mM NaCl, 20 mM sodium phosphate buffer pH 7.0, 5mM DTT prior to analysis and 5% D_2O was added. Measurements were performed at 298K on Bruker AVIII 600 or AVIII 900 NMR spectrometers with cryogenic (TCI) triple resonance gradient probes. Data were processed with Topspin 3.0 and analyzed with Sparky 3 (Kneller, 2000). RNA assignment of imino groups was based on $^{1}H,^{1}H$-NOESY spectra; an initial protein backbone assignment was made with HNCACB spectra. Titration experiments with the individual Stau2 RBDs 1 and 2 as well as the tandem-domain RBD1-2 were performed at approximately 50 µM protein concentration. After snap-cooling, the RNA ligand was added in ratios of 0.5, 1.0, 2.0 and 3.0 to the protein and full saturation was achieved.

3 Results

3.1 Protein purification

3.1.1 Purification of Stau2 proteins

Expression vectors for Stau2 proteins were cloned as described in section 2.8.4. All constructs for the expression of truncated Stau2 protein yielded soluble protein that could be stably expressed and purified from *E. coli* as described in section 2.9. Only full-length Stau2 was insoluble and degraded when purified from *E. coli*. This problem was overcome by expression in High Five insect cells as described in section 2.9.1.1.

To optimize yield and purity of the recombinant proteins, several fusion-tags were tested. Generally, expression and purification worked well for His-SUMO- or His-MBP-tagged fusion proteins by Ni-IMAC capture followed by fusion-tag-cleavage and removal with a subsequent second, subtractive Ni-IMAC, affinity chromatography on a Heparin column and a final size exclusion chromatography. Cleavage of the fusion-tag did not affect stability and solubility of the truncated Stau2 RBD domain constructs, yet Stau2 full-length heavily degraded without the tag and was thus purified with fusion-tag.

Several Stau2 RBD1 protein fragments were tested to identify a stable C-terminus. A degrading RBD1 construct could be stabilized with a C-terminal His-tag and was thus purified with a HisGST fusion-tag to allow tag-removal with a GST-affinity column. Stau2 RBD1 proteins did not bind to Heparin, so the Heparin affinity purification step was skipped here. Also, several RBD2 proteins were tested to identify a well-behaved protein. The annotated short RBD2 (aa 94-180) protein eluted from the size exclusion column with a much smaller retention volume than all other proteins, indicating that the protein was much larger in solution and thus was not properly folded or aggregated. The protein's behavior could be improved by elongation of the C-terminus. The long RBD2 (aa 94-208) was well-behaved and eluted with the expected retention volume.

An overview of used purification procedures for each protein is given in Table 14. All proteins were isolated to >90 % purity after the final size exclusion chromatography purification step as shown in Figure 6 and Figure 7.

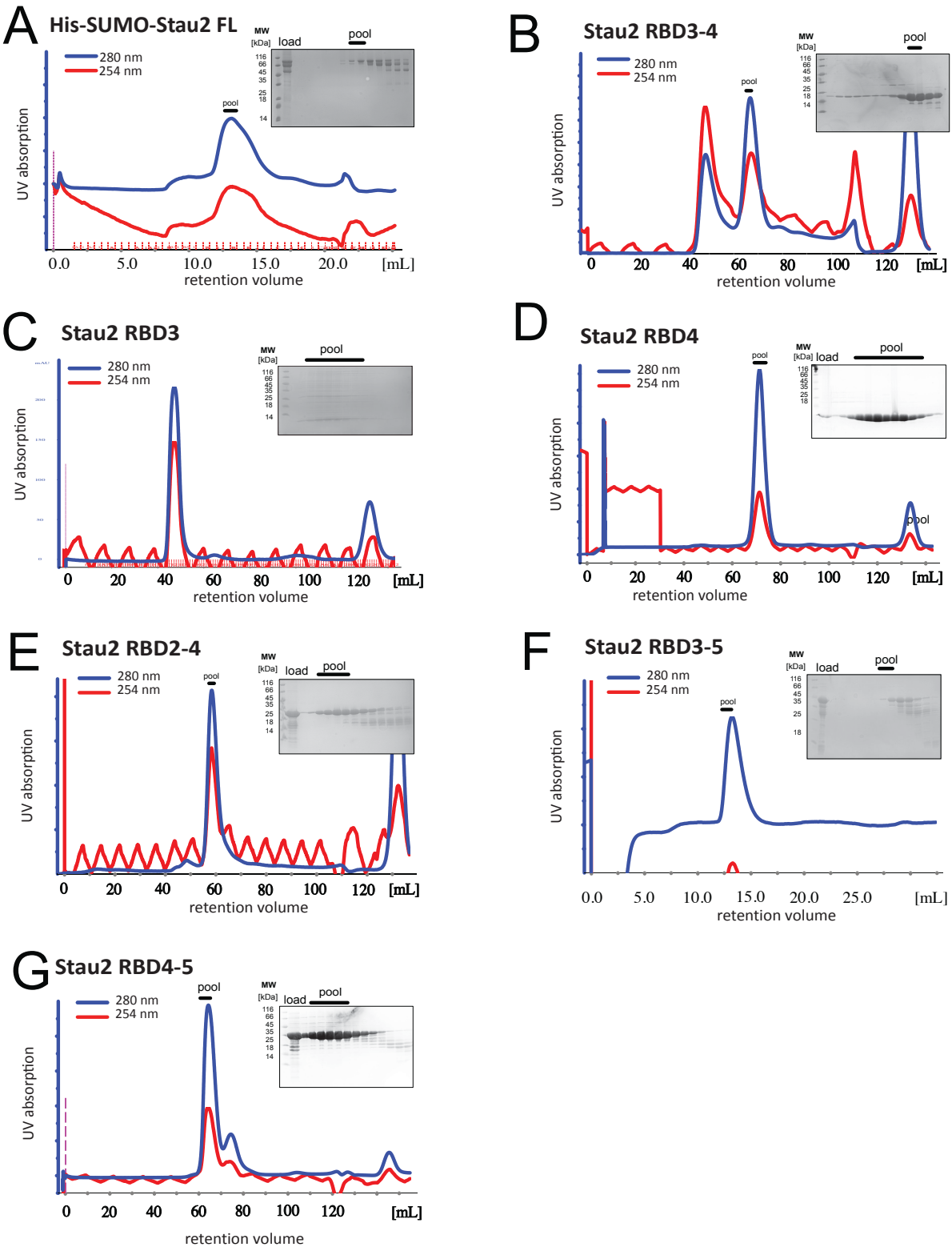

Figure 6: Result of Stau2 protein purifications. Shown are chromatograms at 280 nm (protein absorption) and 254 nm (nucleic acid absorption, the regular waves represent detector noise) of the final size exclusion chromatography step and analysis of the elution fractions by SDS-PAGE. All proteins could be purified to >90 % purity.

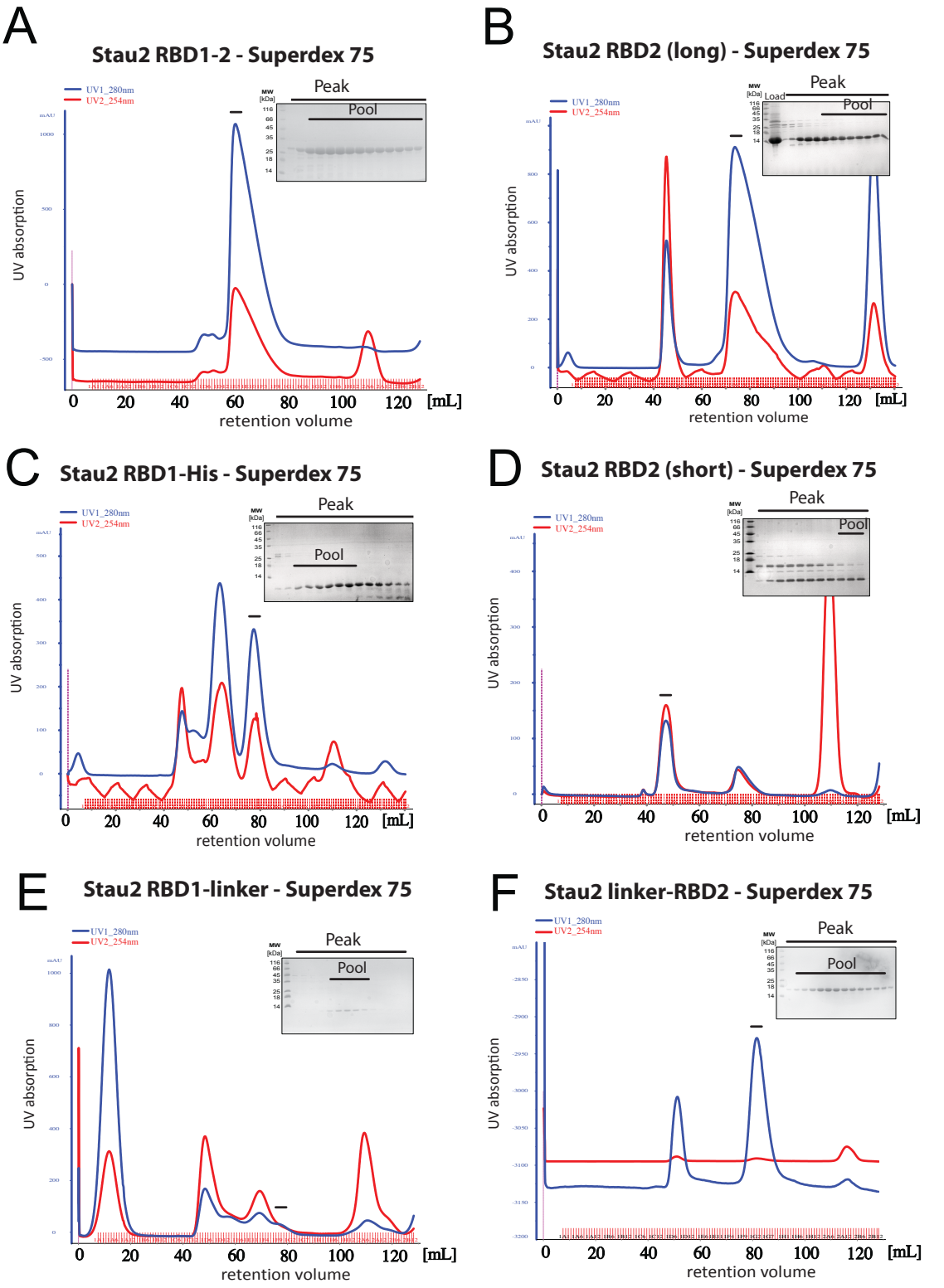

Figure 7: Result of Stau2 RBD1-2 protein purifications. Shown are chromatograms of the final size exclusion chromatography step and analysis of the elution fractions by SDS-PAGE. All proteins could be purified to >90 % purity. The short RBD2 construct (D) eluted with a much smaller retention volume than the other proteins, indicating aggregation or unfolding of the protein.

Table 14: Results of Stau2 protein purifications

Name	Protein	Expression vector	Purification
HisSUMO-Stau2 FL	Staufen homolog 2 isoform 3 [Mus Musculus], NCBI Reference Sequence: NP_079579.2	pOPINS3C-Stau2FL, pFastBacDual-HisSUMO-Stau2FL	Affinity capture on HisTrap, affinity purification on HiTrap Heparin, SEC on Superdex75 GL
RBD3-4	mStau2 (aa 200-373)	pOPINS3C-Stau2RBD3-4	Affinity capture on HisTrap, 3C cleavage, subtractive HisTrap, affinity purification on HiTrap Heparin, SEC on Superdex75 GL
RBD3	mStau2 (aa 200-272)	pOPINS3C-Stau2RBD3	Affinity capture on HisTrap, 3C cleavage, subtractive HisTrap, affinity purification on HiTrap Heparin, SEC on Superdex75 GL
RBD4	mStau2 (aa 272-373)	pOPINS3C-Stau2RBD4	Affinity capture on HisTrap, 3C cleavage, subtractive HisTrap, affinity purification on HiTrap Heparin, SEC on Superdex75 GL

Name	Protein	Expression vector	Purification
RBD2-4	mStau2 (aa 141-373)	pOPINS3C-Stau2RBD2-4	Affinity capture on HisTrap, 3C cleavage, subtractive HisTrap, affinity purification on HiTrap Heparin, SEC on Superdex75 GL
RBD3-5	mStau2 (aa 200-470)	pOPINS3C-Stau2RBD3-5	Affinity capture on HisTrap, 3C cleavage, subtractive HisTrap, affinity purification on HiTrap Heparin, SEC on Superose12 GL
RBD4-5	mStau2 (aa 272-470)	pOPINS3C-Stau2RBD4-5	Affinity capture on HisTrap, 3C cleavage, subtractive HisTrap, affinity purification on HiTrap Heparin, SEC on Superdex75 GL
RBD1-2	mStau2 (aa 1-208)	pOPINS3C-Stau2RBD1-2	Affinity capture on HisTrap, 3C cleavage, subtractive HisTrap, affinity purification on HiTrap Heparin, SEC on Superdex75 GL

Name	Protein	Expression vector	Purification
RBD1-2 E15A	mStau2 (aa 1-208) E15A	pOPINS3C-Stau2RBD1-2 E15A	Affinity capture on HisTrap, 3C cleavage, subtractive HisTrap, affinity purification on HiTrap Heparin, SEC on Superdex75 GL
RBD1-2 H36A	mStau2 (aa 1-208) H36A	pOPINS3C-Stau2RBD1+2 H36A	Affinity capture on HisTrap, 3C cleavage, subtractive HisTrap, affinity purification on HiTrap Heparin, SEC on Superdex75 GL
RBD1-2 F40A	mStau2 (aa 1-208) F40A	pOPINS3C-Stau2RBD1+2 F40A	Affinity capture on HisTrap, 3C cleavage, subtractive HisTrap, affinity purification on HiTrap Heparin, SEC on Superdex75 GL
RBD1-2 K59A	mStau2 (aa 1-208) K59A	pOPINS3C-Stau2RBD1+2 K59A	Affinity capture on HisTrap, 3C cleavage, subtractive HisTrap, affinity purification on HiTrap Heparin, SEC on Superdex75 GL

Name	Protein	Expression vector	Purification
RBD1-2 K60A	mStau2 (aa 1-208) K60A	pOPINS3C-Stau2RBD1+2 K60A	Affinity capture on HisTrap, 3C cleavage, subtractive HisTrap, affinity purification on HiTrap Heparin, SEC on Superdex75 GL
RBD1-2 K59A K60A	mStau2 (aa 1-208) K59A K60A	pOPINS3C-Stau2RBD1+2 K59A K60A	Affinity capture on HisTrap, 3C cleavage, subtractive HisTrap, affinity purification on HiTrap Heparin, SEC on Superdex75 GL
RBD1	mStau2 (aa 1-139)	pOPINS3C-Stau2RBD1	Not expressed
RBD1 (SwissModel)	mStau2 (aa 1-74)	pOPINS3C-Stau2RBD1 SM	Affinity capture on HisTrap, 3C cleavage, subtractive HisTrap, affinity purification on HiTrap Heparin, SEC on Superdex75 GL
RBD1-His	mStau2 (aa 1-74)-6xHis	pOPINJ-Stau2RBD1-His	Affinity capture on HisTrap, 3C cleavage, subtractive GSTrap, SEC on Superdex75 GL

Name	Protein	Expression vector	Purification
RBD1-linker	mStau2 (aa 1-93)	pOPINS3C-Stau2RBD1-linker	Affinity capture on HisTrap, 3C cleavage, subtractive HisTrap, SEC on Superdex75 GL
RBD2 (short)	mStau2 (aa 94-180)	pOPINS3C-Stau2RBD2 SM	Affinity capture on HisTrap, 3C cleavage, subtractive HisTrap, affinity purification on HiTrap Heparin, SEC on Superdex75 GL
RBD2long	mStau2 (aa 94-208)	pOPINS3C-Stau2RBD2long	Affinity capture on HisTrap, 3C cleavage, subtractive HisTrap, affinity purification on HiTrap Heparin, SEC on Superdex75 GL
Linker-RBD2	mStau2 (aa 75-208)	pOPINS3C-Stau2 linker-RBD2	Affinity capture on HisTrap, 3C cleavage, subtractive HisTrap, affinity purification on HiTrap Heparin, SEC on Superdex75 GL

Name	Protein	Expression vector	Purification
RBD2 Δ119-135	mStau2 (aa 75-208) Δ119-135	pOPINS3C-Stau2 RBD2 Δ119-135	Affinity capture on HisTrap, 3C cleavage, subtractive HisTrap, affinity purification on HiTrap Heparin, SEC on Superdex75 GL
RBD1-3	mStau2 (aa 1-272)	pOPINS3C-Stau2RBD1-3	Not expressed
RBD1-4	mStau2 (aa 1-373)	pOPINS3C-Stau2RBD1-4	Affinity capture on HisTrap, 3C cleavage, subtractive HisTrap, affinity purification on HiTrap Heparin, SEC on Superdex75 GL

3.1.2 Purification of Pum2 proteins

Expression vectors for Pum2 proteins were cloned as described in section 2.8.4. Expression and purification was performed as described in sections 2.9.1.3, 2.9.2.3 and 2.9.2.4.

To optimize yield and purity of the recombinant proteins, several fusion-tags were tested. Generally, expression and purification worked well for HisMBP-tagged fusion proteins by capture on amylose resin followed by, in case of Pum2 HD, fusion-tag-cleavage and removal with a subsequent subtractive Ni-IMAC, a negative mode anion exchange chromatography on a HiTrap Q column to remove nucleic acids and a final size exclusion chromatography. Cleavage of the fusion-tag did not affect stability and solubility of the Pum2 HD. Only the full-length Pum2 and Pum2 ΔHD heavily degraded without the tag and were thus purified with HisMBP-fusion-tag. All proteins could be purified to >90 % purity as shown in Figure 8. Since full-length Pum2 and Pum2 ΔHD degraded over time, the final SEC step was always performed immediately prior to the following experiments.

In case Pum2 FL was needed without His-tag (for pull-down experiments), it was expressed as MBP-fusion protein from a pMALC vector kindly provided by Foong-Yee Ang (group of Prof. Dr. Michael Kiebler, Department for Cell Biology, LMU München) and in the first step affinity-purified on amylose resin.

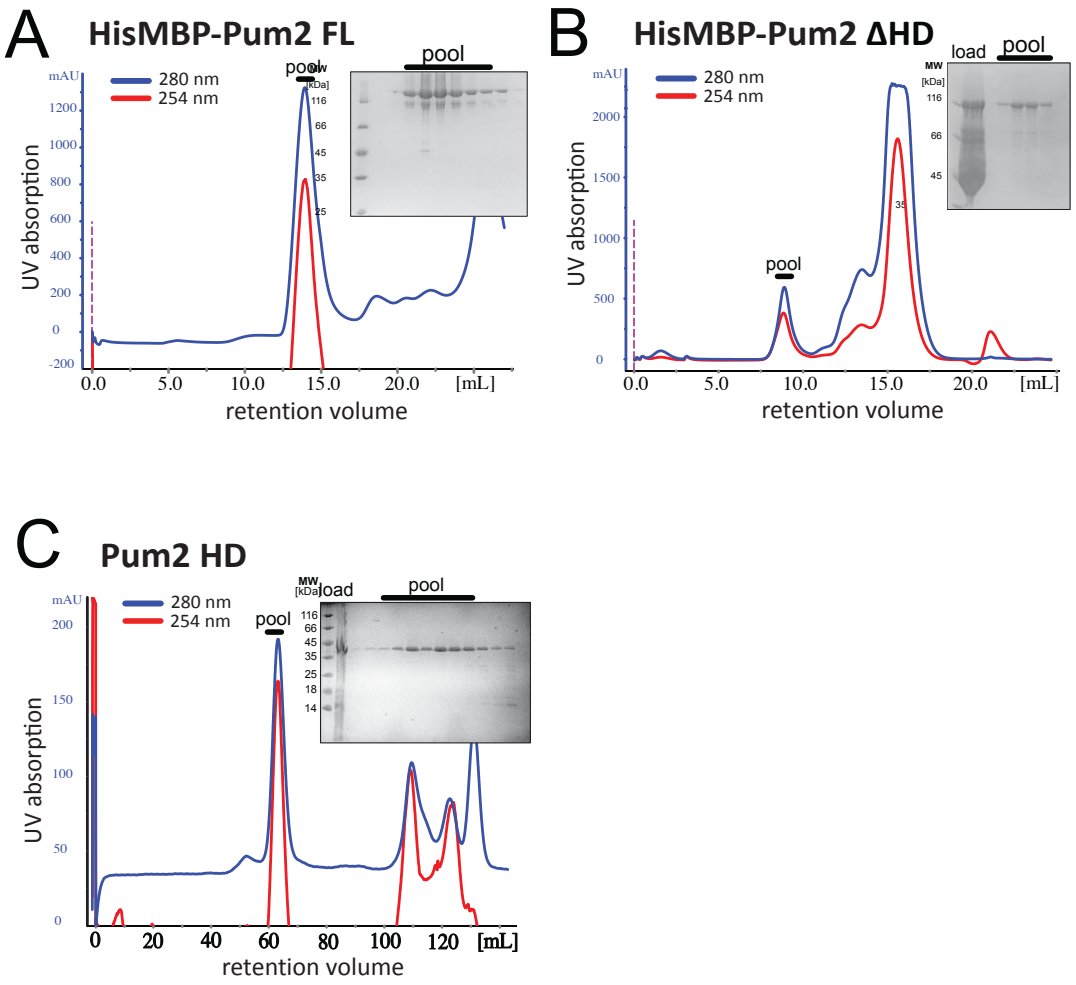

Figure 8: Result of Pum2 protein purifications. Shown are chromatograms of the final size exclusion chromatography step and analysis of the elution fractions by SDS-PAGE. All proteins could be purified to >90 % purity.

3.1.3 Co-expression and purification of Stau2 and Pum2 full-length proteins

Both full-length Stau2 and Pum2 proteins were poorly expressed and degrading rather fast when recombinantly produced in *E.coli*. Both proteins precipitated heavily in low salt buffer and fast degradation occured during the purification procedure. In case both proteins would interact, co-expression could stabilize them by providing a natural binding partner. Co-expression in High Five insect cells was performed from a pFastBacDual plasmid with HisSUMO-Stau2 under the control of the P_{PH} promtor and HisMBP-Pum2 under the control of the P_{p10}

promotor. To stabilize the proteins during purification, both proteins were co-captured by Ni-IMAC in high salt buffer. This did, however, not prevent precipitation of the proteins upon buffer exchange in low salt buffer required for downstream applications. Neither were yield, solubility or degradation improved by the co-expression.

3.2 Stau2 binding to *Rgs4* RNA

3.2.1 Stau2 binds unspecifically to *Rgs4* 3'UTR and to SRS motifs

To test whether Stau2 binds to *Rgs4* 3'UTR *in vitro*, EMSA experiments with recombinant Stau2 and *in vitro* transcribed *Rgs4* 3'UTR or a truncated *Rgs4* 3'UTR sequence containing all predicted Stau2 and Pum2 binding sites (termed *Rgs4* binding region, BR in the following) were performed as described in section 2.10.5. Additionally, *beta-actin* RNA was tested as a non-target control of similar length. Stau2 bound to all three RNAs with a dissociation contstant K_D in the low nanomolar concentration range as shown in Figure 9 A, indicating that Stau2-binding to *Rgs4* is non-specific. Also, no specific Stau2-*Rgs4* complex could be observed. Instead a continuous upwards shift with increasing concentrations was seen, indicating that the interactions are non-specific. To test whether Stau2 recognizes the predicted SRS motifs in *Rgs4* 3'UTR, SRS deletion mutants of *Rgs4* 3'UTR were tested. As shown in Figure 9 B, Stau2 bound to all deletion mutants with similar affinity to the wt *Rgs4* 3'UTR, indicating that Stau2 does not require SRSs to bind RNA *in vitro*.

Next, binding of Stau2 to the isolated SRS motifs was tested by EMSA. Because deletion of the published SRSs 1 and 2 (Heraud-Farlow et al., 2013) did not show a significant decrease in binding by Stau2, a third, longer RNA stem-loop and potential cryptic SRS from the *Rgs4* 3'UTR was additionally tested. This stem-loop is termed SRS3 in the following. SRS3 is an imperfect stem-loop with 26 paired bases interrupted by two bulges. In contrast to the less stable SRS1 and SRS2, its folding in the context of the *Rgs4* 3'UTR is predicted by RNA fold programs to be energetically favorable. Stau2 bound to SRSs 1 and 2 with K_Ds in the micromolar concentration range but to SRS3 in the range of a few hundred nanomolar, as shown in Figure 9 C. Furthermore, elongation of SRS2 by 5 single-stranded nucleotides on the 3' end (SRS2+5 nt) somewhat improved the affinity

to Stau2 to a few hundred nanomolar, similar to SRS3 (Figure 9 C). Taken together, this indicates that recognition of SRS motifs is unspecific.

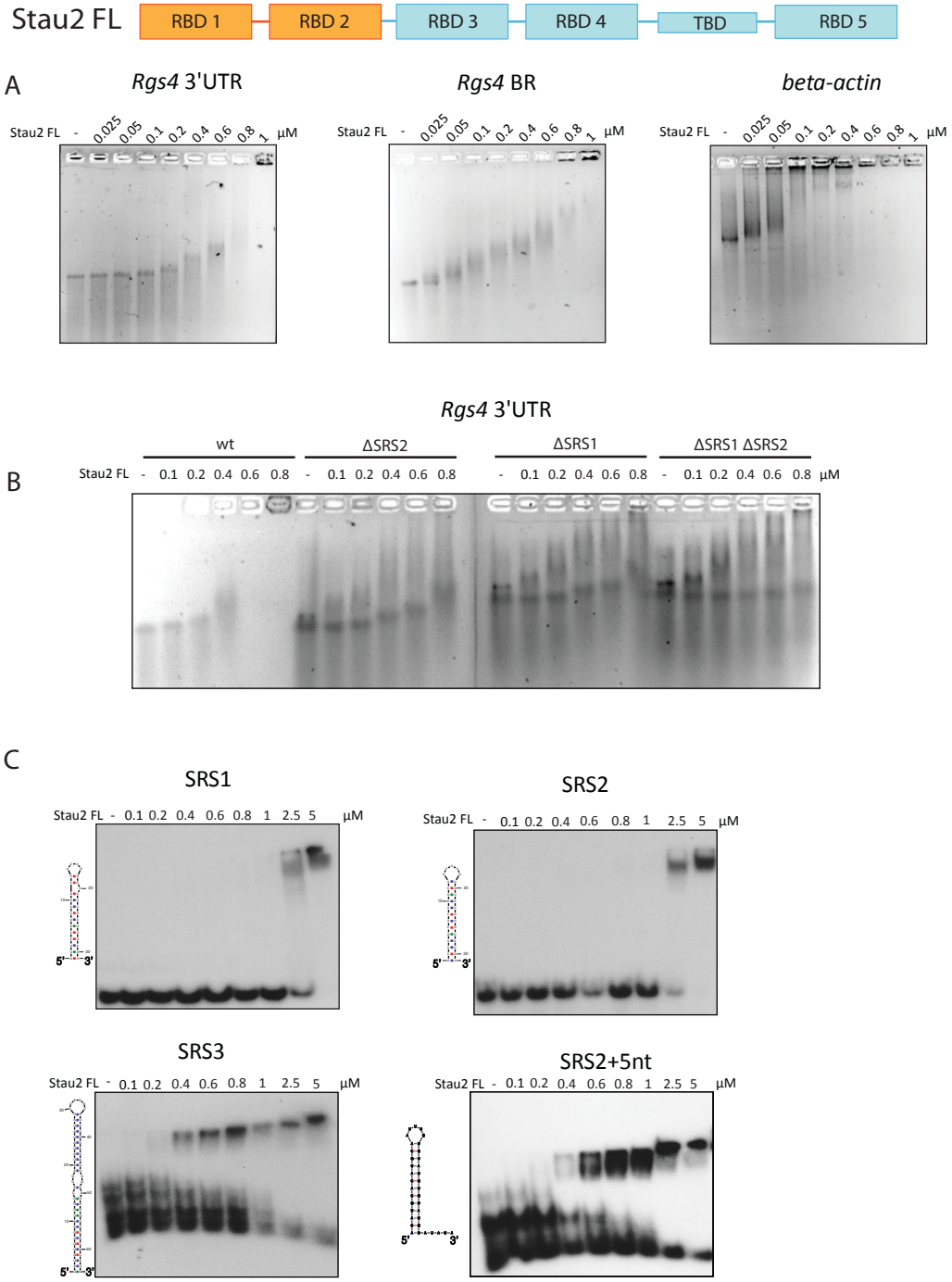

Figure 9: EMSAs with recombinant Stau2 and *Rgs4* 3'UTR sequences. A) Full-length *Rgs4* 3'UTR compared to the *Rgs4* BR sequence and a non-target RNA (beta-actin) of similar length. Complexes were resolved by agarose gel electrophoresis. **B)** SRS deletion mutants of *Rgs4* 3'UTR. Stau2 binds to all tested RNAs with nanomolar affinities. Complexes were resolved by agarose gel electrophoresis. **C)** EMSAs with recombinant Stau2 and isolated *Rgs4* SRS motifs. Stau2 binds to SRS1 and SRS2 RNAs with micromolar affinities and to SRS3 with an affinity in the range of a few hundred nanomolar. Extension of SRS2 with 5 single-stranded nucleotides at the 3'end improves affinity to a similar level as for SRS3. Complexes were resolved by native PAGE.

3.2.2 Stau2 RBD3-4 binds SRS RNA

After showing that Stau2 binds *in vitro* to *Rgs4* 3'UTR, it should be tested whether RNA-binding is indeed mediated by the RBDs 3 and 4. EMSAs with recombinant Stau2 RBD3-4 and *Rgs4* BR were performed on the wild-type (wt) sequence and SRS deletion mutants. As shown in Figure 10 A, Stau2 RBD3-4 indeed binds to all *Rgs4* BR sequences with affinities similar to the full-length protein (Figure 9 A), confirming again that SRSs are not required for Stau2 binding *in vitro*.

Next, binding of Stau2 RBD3-4 to isolated SRS motifs was tested. Like the full-length protein, Stau2 RBD3-4 bind SRSs 1 and 2 with micromolar affinities but bound SRS3 with lower affinity than the full-length protein with an apparent K_D of approximately 1 μM (Figure 10 B). Additionally, binding to non-target dsRNAs of similar lengths (E3 28 nt stem-loop as compared to SRSs 1 and 2, TAR-57 nt as compared to SRS3) was tested. Stau2 RBD3-4 bound to non-target RNAs of similar length with the same affinities as to SRSs (Figure 10 C), indicating again that binding to SRSs is non-specific.

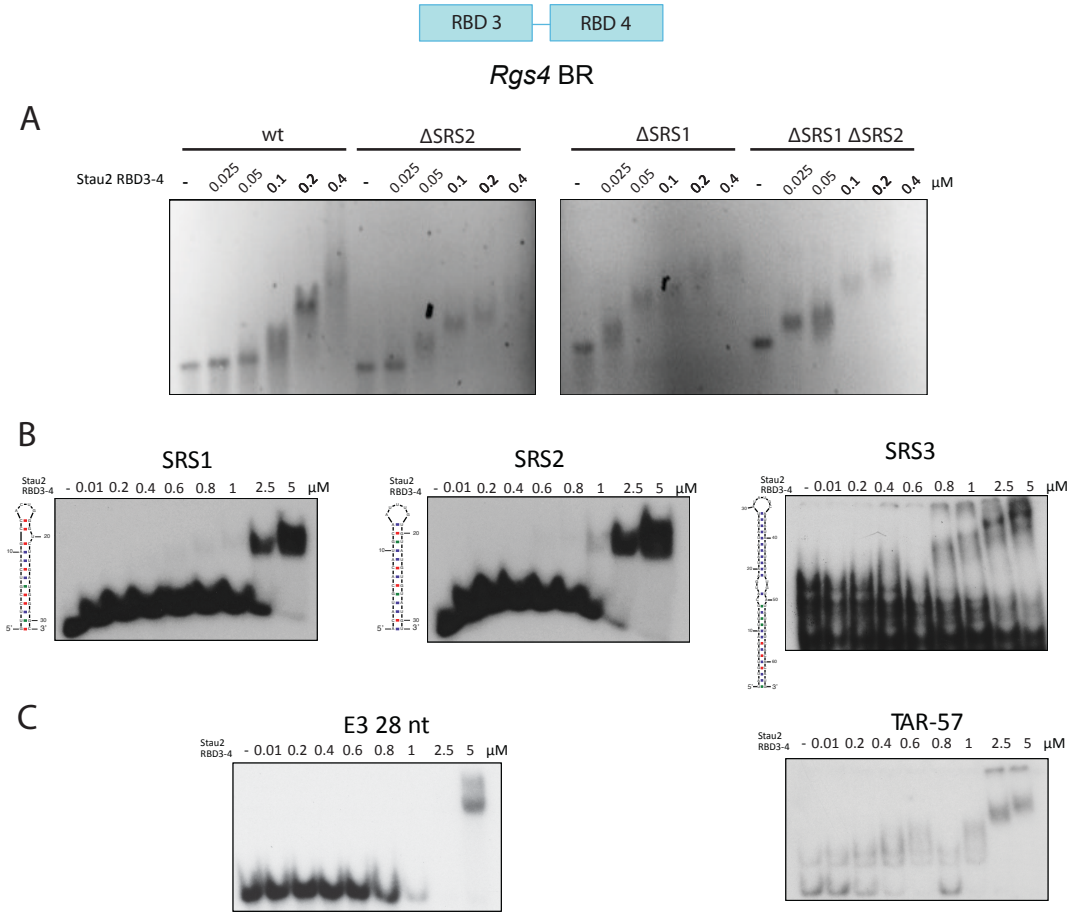

Figure 10: EMSAs with recombinant Stau2 RBD3-4. A) Comparison between *Rgs4* BR wt and SRS deletion mutants. Stau2 binds to all tested RNAs with K_Ds in the nanomolar range. Complexes were resolved by agarose gel electrophoresis. **B)** Stau2 RBD3-4 binding to isolated *Rgs4* SRS motifs or **C)** non-target RNAs of similar length. Stau2 binds to SRS1 and 2 and non-target E3 28 nt stem-loop RNAs with micromolar affinities and to SRS3 and non-target TAR-57 RNA with an apparent K_D of ~1 µM.. Complexes were resolved by native PAGE.

Next, it was tested whether both RBDs 3 and 4 bind RNA with comparable affinities. In EMSAs with the individual RBDs binding to SRS RNA in the micromolar concentration range was observed only for RBD4 but not for RBD3 (Figure 11 A), indicating that mainly RBD4 has RNA-binding activity. The affinity of RBD4 was comparable to the one of the RBD3-4 tandem domain.

Furthermore, it was tested whether addition of RBDs N- or C-terminally to the RBD3-4 tandem-domain would improve RNA binding. Neither addition of the physiological RBD5 sequence at the C-terminus nor addition of RBD2 on the N-terminus of the tandem-domain dramatically improved binding to SRS2 RNA (Figure 11 B).

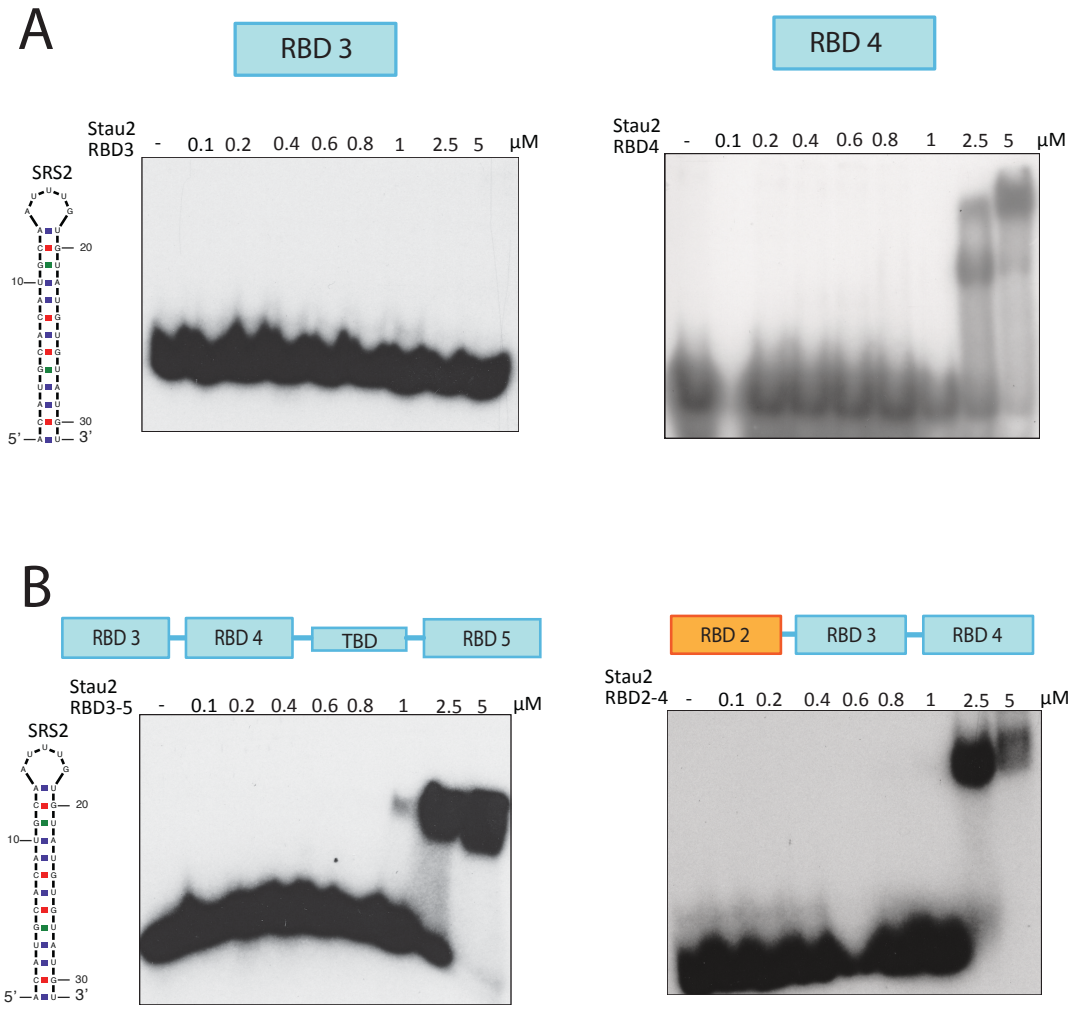

Figure 11: EMSAs with A) individual Stau2 RBDs 3 and 4 and *Rgs4* SRS2 RNA or B) extended RBD3-4 constructs comprising either an additional N-terminal or C-terminal RBD. RBD4 binds to SRS2 at micromolar concentrations. No binding was observed for RBD3. Neither addition of the C-terminal RBD5 nor addition of N-terminal RBD2 improved binding to SRS2 RNA compared to RBD3-4. Complexes were resolved by native PAGE.

3.2.3 RBD1-2 binds SRS RNA with comparable affinity as RBD3-4

To investigate whether Stau2 RBDs 3-4 are indeed solely responsible for RNA-binding, a protein construct comprising only RBDs 1-2 was tested in EMSAs. As shown in Figure 12, RBD 1-2 binds SRS2 stem-loop RNA with an affinity comparable to RBD3-4, indicating that, in contrast to a previous report (Duchaine et al., 2002), RBD1-2 are not inactive pseudo-RBDs but contribute to RNA recognition by Stau2.

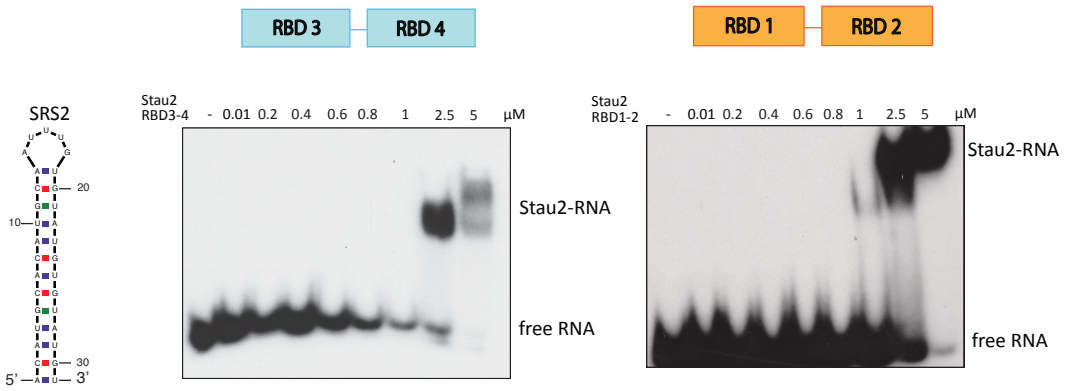

Figure 12: EMSAs with Stau2 tandem-domains RBD3-4 and RBD1-2 with SRS2 RNA. RBD1-2 binds SRS2 with similar, micromolar affinity as RBD3-4. Complexes were resolved by native PAGE.

3.2.4 Elongation of SRS2 RNA improves binding by Stau2 tandem-domains

Because of the improved binding of Stau2 FL to longer RNA stem-loops, it was tested by EMSAs whether elongation of SRS2 would also improve binding of Stau2 tandem-domains RBD3-4 and RBD1-2. Indeed, elongation of the SRS2 stem by 5 basepairs (Figure 13 B) improved binding by RBD3-4 and RBD1-2. This RNA is termed dsSRS2+5 in the following. In case of RBD1-2, RNA-binding was improved approximately 2-fold from an apparent K_D of 5 µM to 2.5 µM. For RBD3-4 the effect was even stronger, increasing the affinity from the micromolar concentration range to the nanomolar concentration range.

Furthermore, to test whether the loop region of the RNA was required for recognition by Stau2 tandem-domains, the elongated SRS2-stem was also tested without loop (SRS2+5Δloop). This elongated stem was bound by both tandem-domains RBD3-4 and RBD1-2 with similar affinities as the original SRS2 stem-loop (Figure 13 C), indicating that the loop region is not essential for recognition. Affinity is rather determined by the total length of RNA.

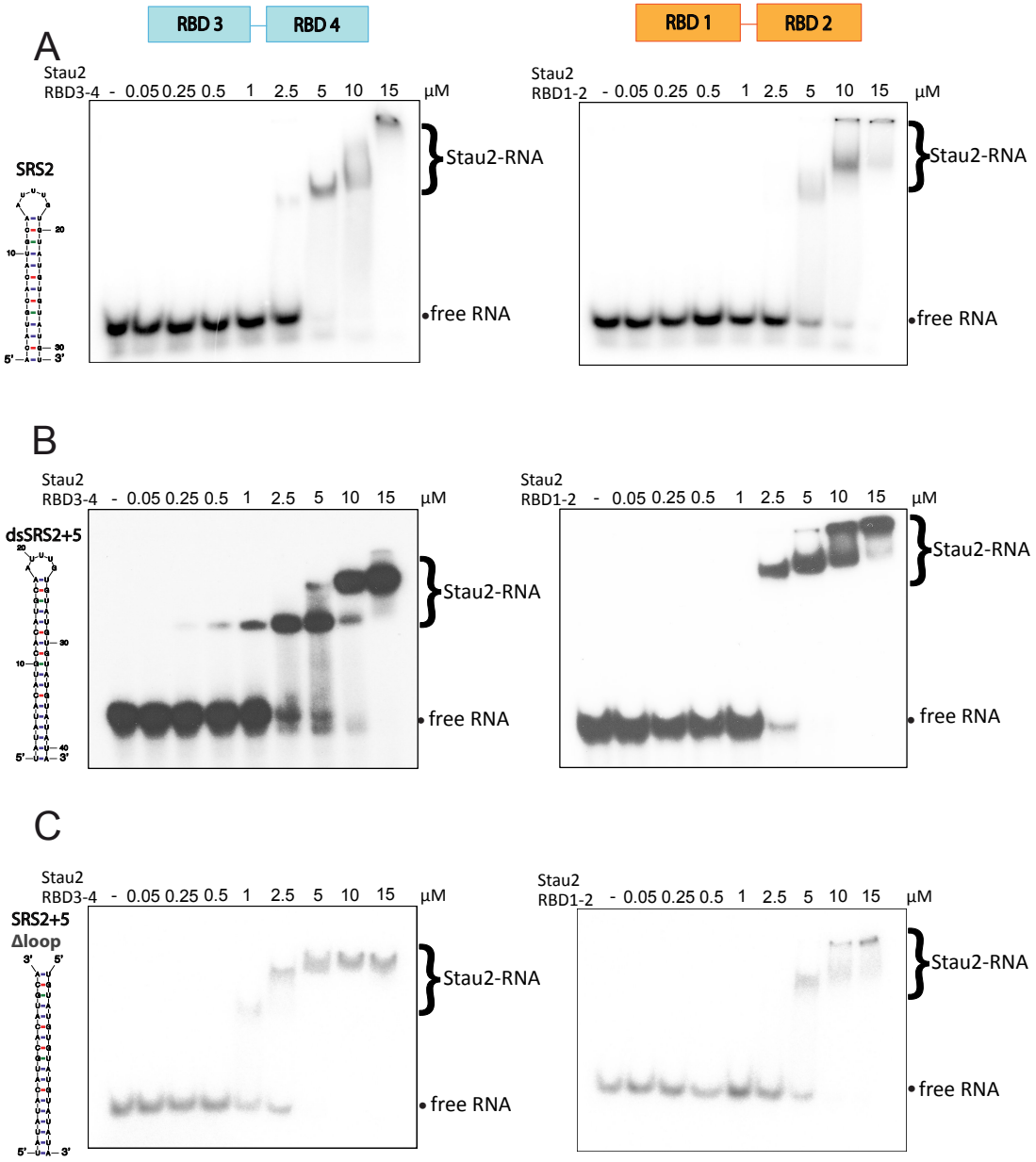

Figure 13: EMSAs with Stau2 tandem-domains RBD3-4 and RBD1-2 and modified SRS2 RNAs. A) *Rgs4* SRS2 RNA compared to **B)** an SRS2 RNA elongated by five basepairs or **C)** the elongated stem of SRS2 RNA without the loop region. Binding by both tandem-domains to the elongated stem-loop is improved, the stem RNA is bound with similar affinity as SRS2, indicating that total length of the RNA determines binding rather than its specific structure. Complexes were resolved by native PAGE.

3.2.5 Minimal length requirement of dsRNA

After showing that the affinity of Stau2 to RNA improves with the length of dsRNA, it should be tested whether a minimal length of an RNA stem-loop for recognition by the Stau2 tandem-domains could be identified. In order to avoid indirect effects from shortening the overall sequence, reduction in stem length was compensated for by the addition of bases as ssRNA at the 3' ends of the stem to maintain a total length of 12 nt. Both tandem-domains RBD3-4 and RBD1-2

bound to RNA stem-loops with 11, 9 and 7 paired bases with similar affinities with K_Ds in the micromolar concentration range (Figure 14 A-C). Only when the stem was decreased to 6 bp, binding was almost completely abolished and no protein-RNA complex could be detected (Figure 14 D), showing that 7 bp is the minimal length of the double-stranded stem required for recognition by Stau2 tandem-domains.

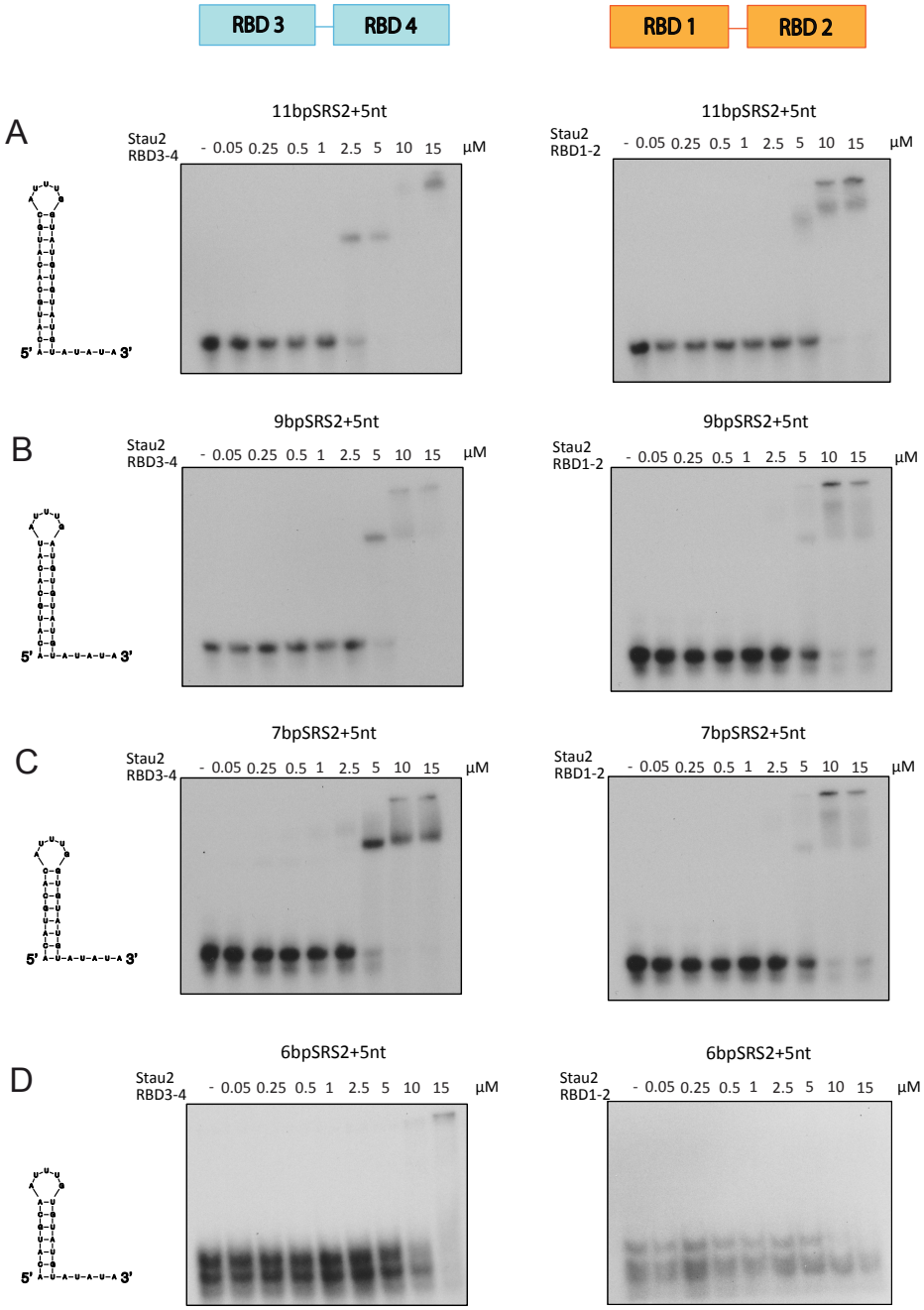

Figure 14: EMSAs with Stau2 tandem-domains and shortened SRS2 RNAs. dsRNA stem-loops with **A)** 11bp, **B)** 9 bp and **C)** 7 bp are bound by both RBD3-4 (left) and RBD1-2 (right) with similar affinities in the micromolar concentration range. **D)** For a stem-loop with only 6 bp, binding is almost completely abolished. No protein-RNA complex is observed. Complexes were resolved by native PAGE.

3.3 Pum2 binding to the *Rgs4* 3'UTR

3.3.1. Pum2 binds to *Rgs4* 3'UTR via non-canonical sequences

To test whether Pum2 indeed binds to *Rgs4* 3'UTR *in vitro*, EMSAs with recombinant Pum2 and *in vitro* transcribed *Rgs4* BR were performed as described in section 2.10.5. To examine whether binding indeed occurs to the canonical Pum consensus sequences in the RNA, binding was also tested to *Rgs4* BR sequences in which Pum2 sites A, B or A and B (see Figure 5) were deleted. Full-length Pum2 bound *Rgs4* BR wt and ΔPum2 site A with similar affinities. Unfortunately, the large complex of the 643 nt *Rgs4* BR and the large MBP-tagged Pum2 FL protein (~150 kDa) aggregated in the loading pockets of the agarose gel, making exact evaluation of affinities impossible. However, assessing the decreasing amounts of free RNA (arrowheads in Figure 15 A) allowed for an estimation of the affinities. The apparent K_Ds were in the range of 100-200 nM. Pum2 also bound to *Rgs4* BR ΔPum2 site B and ΔPum2 site A+B with roughly two-fold decreased affinities (Figure 15 A).

To test whether *Rgs4*-binding by Pum2 is mediated by the conserved Pum homology domain (HD), the experiment was also performed with recombinant Pum2 HD. Pum2 HD bound to wt *Rgs4* BR and ΔPum2 site A with similar affinities as compared to full-length Pum2. *Rgs4* BR ΔPum2 site B and ΔPum2 site A+B were bound with decreased affinities (Figure 15 B). However, the gel shift of the large *Rgs4* BR RNA caused by the small Pum2 HD is rather small, making exact K_Ds difficult to estimate. To allow for definite conclusions, the experiment requires optimization.

Taken together, these findings indicated that *Rgs4* binding by Pum2 is not dependent on the Pum2 PRE consensus sequences and that *Rgs4* recognition might occur via non-canonical sequences.

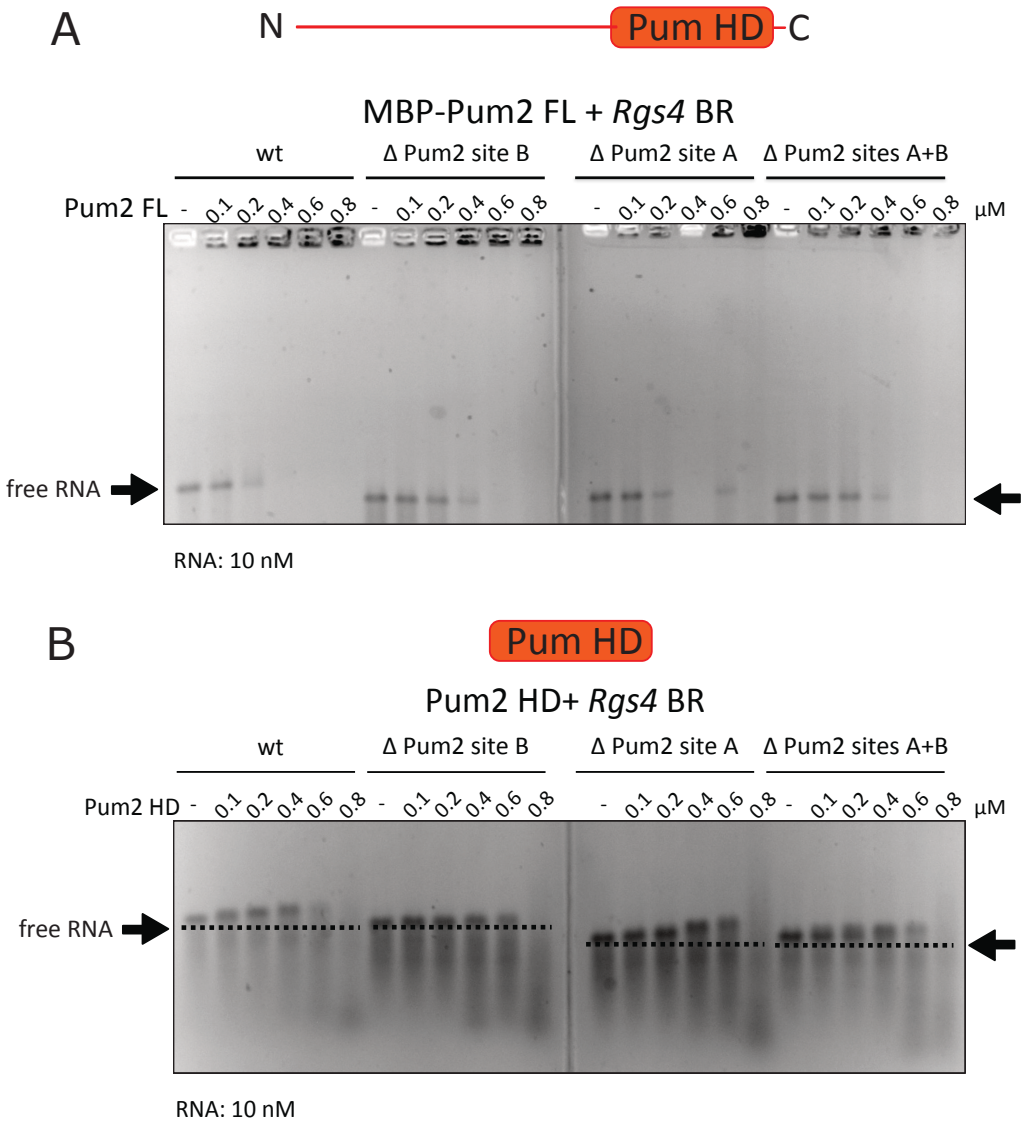

Figure 15: EMSAs with recombinant Pum2 proteins and *in vitro* transcribed *Rgs4* BR. A) Full-length Pum2 binds to wt *Rgs4* BR but also all mutants in which Pum consensus sequences A, B or A and B were deleted. *Rgs4* BR wt and ΔPum2 site A bind with similar K_D of 100-200 nM. ΔPum2 site B and ΔPum2 site A and B bind with approximately 2-fold decreased affinities. Complexes were resolved by agarose gel electrophoresis. **B**) Pum2 HD also binds to wt *Rgs4* BR and ΔPum2 site A with similar K_D of 100-200 nM. ΔPum2 site B and ΔPum2 site A and B bind with decreased affinities. Running height of free RNA is marked by the dashed line. Complexes were resolved by agarose gel electrophoresis.

3.3.1 The disordered N-terminal part of Pum2 contributes to *Rgs4* binding

Because *Rgs4* BRs with mutated Pum2-binding sites were still bound by Pum2 with reasonable affinity, an additional, non-canonical RNA-binding mechanism was suspected that is independent of Pum2 consensus sequences. The disordered N-terminal part of Pum2, termed Pum2 ΔHD, was thus tested for binding activity by EMSAs.

Whereas for full-length Pum2 and Pum2 HD binding was observed already at concentrations of 50 to 100 nM, Pum2 ΔHD bound RNA at concentration of

400 nM or higher (Figure 16). With Pum2 FL, all RNA was bound at 400 nM and stuck in the gel pockets. With Pum2 HD, all RNA is already clearly shifted at 50 nM. Pum2 ΔHD shifts only a fraction of the RNA to the gel pockets, even at the highest tested concentration of 1.6 µM (Figure 16 A and B). Thus, Pum2 ΔHD by itself possesses weak RNA-binding activity but likely contributes to RNA-binding in the full-length protein context. Due to the observed aggregation in the gel pockets, a quantification or even estimation of K_Ds is not possible.

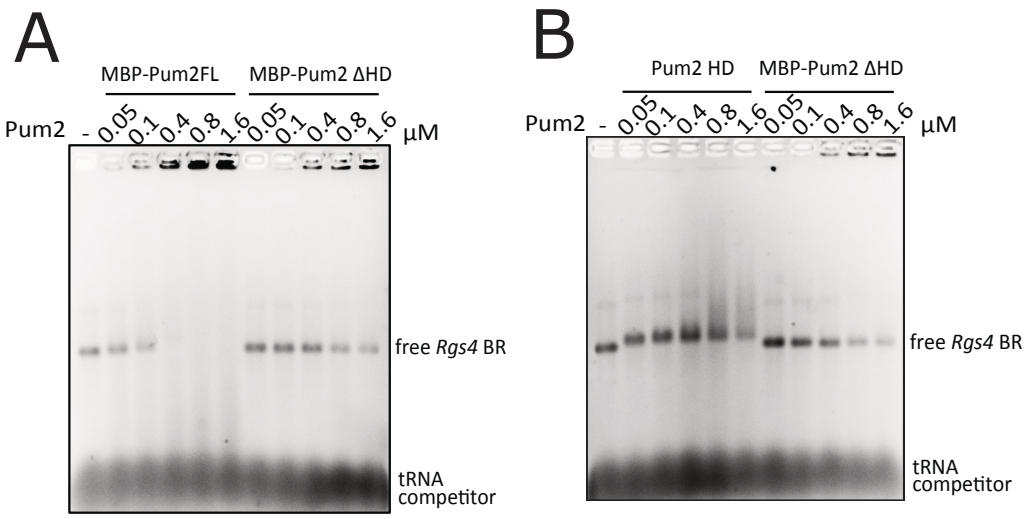

Figure 16: EMSAs with Pum2 protein constructs and *Rgs4* BR RNA. A) Binding of Pum2 ΔHD compared to Pum2 FL. Pum2 FL binds *Rgs4* BR with an apparent KD of 0.1-0.4 µM. Pum2 ΔHD binds *Rgs4* BR weakly at concentrations above 0.4 µM. **B)** Binding of Pum2 ΔHD compared to Pum2 HD. Pum2 HD shifts *Rgs4* BR already at 0.05 µM. Pum2 ΔHD again binds *Rgs4* BR weakly at concentrations above 0.4 µM.

3.3.2 Pum2 binds to SRS3 RNA

In an attempt to identify a short, physiological but non-canonical Pum2 target RNA suitable for structural analyses by X-ray crystallography, Pum2-binding to *Rgs4* SRS3 RNA was tested by EMSA. SRS3 contains an imperfect Pum2 consensus sequence in which the 8th nucleotide is G instead of A (UGUAUAU**G** instead of UGUANAU**A**). As shown in Figure 17, full-length Pum2 binds to SRS3 at nanomolar concentrations. Notably, SRS3 is a stem-loop RNA with two bulges, whose imperfect Pum2 PRE consensus is located partially in the double-stranded region, limiting its accessibility for ssRNA-binding proteins like Pum2. SRS3 is thus an interesting target RNA for co-crystallization with Pum2.

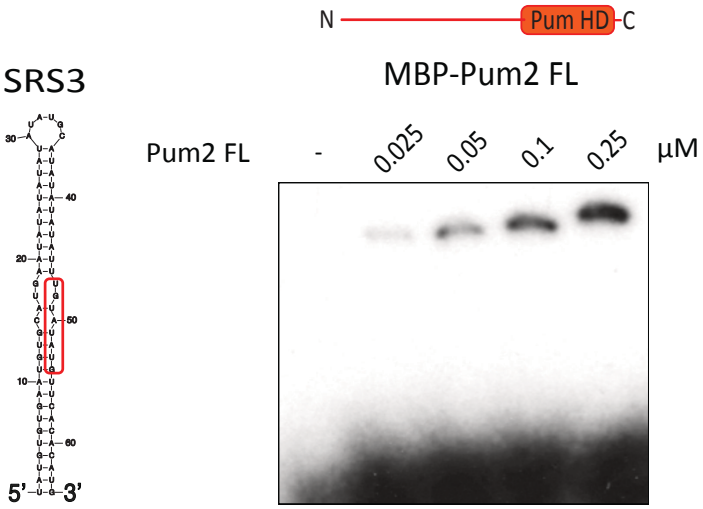

Figure 17: EMSA with Pum2 FL and *Rgs4* SRS3 RNA. A scheme of SRS3 is shown on the left in which the imperfect Pum2 consensus sequence in SRS3 is marked in red. Pum2 binds to SRS3 at nanomolar concentrations. Complexes were resolved by native PAGE.

3.4 Trimeric complex formation by Stau2, Pum2 and *Rgs4* RNA

One of the main aims of this work was to examine whether the two neuronal RBPs Stau2 and Pum2, which have been reported to act in the same pathways (see chapter 1.5), form a trimeric complex with *Rgs4* mRNA and if so, whether they directly interact with each other. Such a co-complex could allow for a joint mRNA regulation by both proteins. Several biochemical and biophysical methods were applied to tackle this question and the results are given below.

3.4.1 No trimeric complex of Stau2, Pum2 and RNA can be observed in EMSAs

First, EMSAs with *Rgs4* BR RNA were performed in which one of the proteins was provided at a constant concentration whereas the second protein was titrated as indicated. Attempts to perform this experiment with the full-length proteins lead to aggregation of the samples. Thus, the RNA-binding domains Stau2 RBD3-4 and Pum2 HD were used instead. When Stau2 RBD3-4 was titrated to *Rgs4* BR, binding occurred starting already at 50 nM Stau2 RBD3-4 (Figure 18 A). When Pum2 HD was added in addition, binding was not improved, suggesting that no trimeric complex is formed.

When Pum2 HD was titrated to *Rgs4* BR in presence of constant amounts of Stau2 RBD3-4, binding was apparently decreased as compared to absence of Stau2, possibly due to competition for binding to the RNA or possibly by

formation of a protein-protein complex that interfered with RNA-binding. Again, no indication for cooperative binding was observed (Figure 18 B).

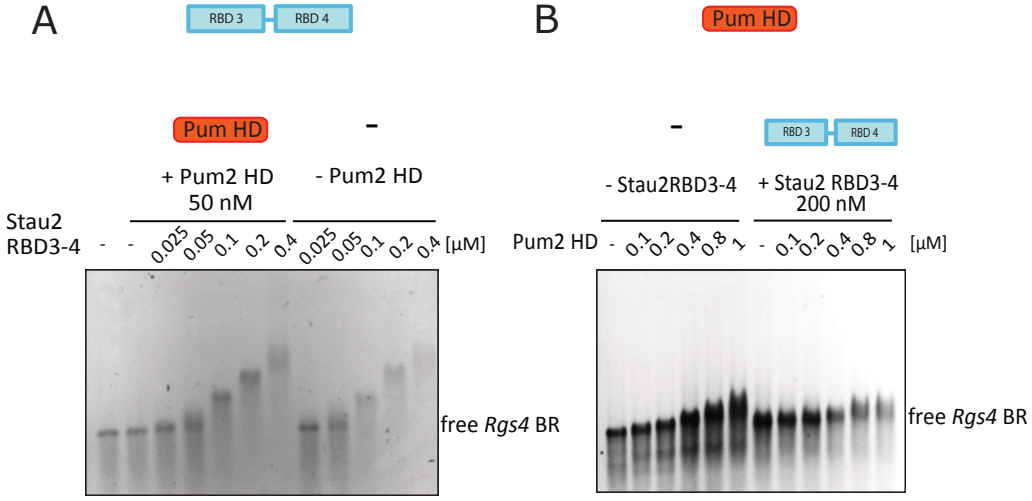

Figure 18: EMSAs with Stau2 RBD3-4, Pum2 HD and *Rgs4* BR. A) Stau2 RBD3-4 was titrated to *Rgs4* BR in prescence or absence of Pum2 HD but binds in both cases with equal affinities. No trimeric complex is observed. **B)** Pum2 HD is titrated to *Rgs4* BR in absence or presence of Stau2 RBD3-4. Binding is apparently decreased in presence of Stau2 RBD3-4. Complexes were resolved by agarose gel electrophoresis.

A trimeric complex between Stau2, Pum2 and *Rgs4* could not be observed in EMSAs, indicating that Pum2 HD and Stau2 RBD3-4 to not interact or bind simultaneously to *Rgs4* RNA. However, the full-length proteins could not be used in these experiments, leaving the possibility that other parts of the proteins are required for their interaction.

3.4.2 UV radiation crosslinks only Pum2 to *Rgs4* RNA, not Stau2

Because in EMSAs, only stable complexes can be detected, UV crosslinking of a trimeric Stau2-Pum2-*Rgs4* complex was attempted to capture any transient interactions. For this purpose, a minimal RNA construct (minRNA, 98 nt) small enough for PAGE analysis comprising SRS2 and Pum2 sites A and B from *Rgs4* 3'UTR was designed. For details on minRNA production, see section 2.8.5. Binding of both proteins to minRNA was verified by EMSA (see Figure 19).

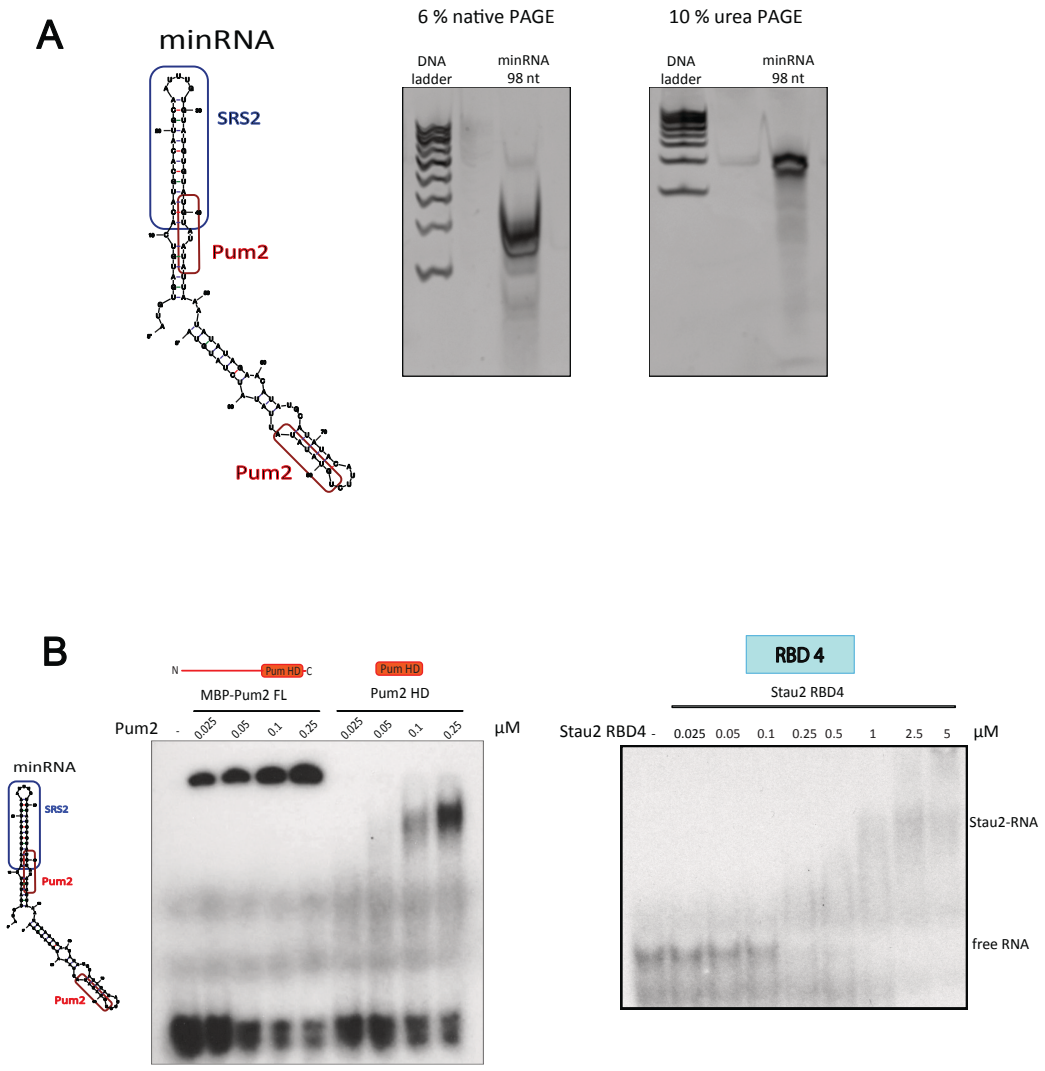

Figure 19: Control experiments with minRNA. A) Scheme and PAGE quality control of minRNA. **B)** EMSAs with minRNA and Pum2 FL and Pum2 HD (left) and Stau2 RBD4. Both Pum2 and Stau2 bind minRNA.

UV crosslinking was performed as described in section 2.10.14. However, no crosslinks of Stau2 to minRNA could be observed (Figure 20). This lack of crosslinking activity despite clear RNA binding in EMSAs is possibly due to the low crosslinking efficiency of dsRBPs to dsRNA strands, in which reactive sites are poorly accessible and hydrogen-bonded bases may crosslink with each other, competing with RNA-protein crosslinks. Only crosslinks of Pum2 to minRNA could be observed (Figure 20). To test whether crosslinking efficiency of Pum2 would change in presence of Stau2 and thus could offer an indirect indication for their interaction, for instance by improving RNA-binding or causing a sterical

change in the proteins conformation that is beneficial for crosslinking efficiency, Pum2 was titrated to minRNA in absence or presence of Stau2 at different concentrations. As shown in Figure 20, no systematic changes in crosslinking efficiency were observed upon Stau2 addition. Taken together, UV crosslinking experiments did not yield any indication for an interaction between Stau2 and Pum2 or a trimeric interaction of the two with *Rgs4*. However, since Stau2 itself could not be crosslinked, this method is only suitable for indirect detection of Stau2 interactions.

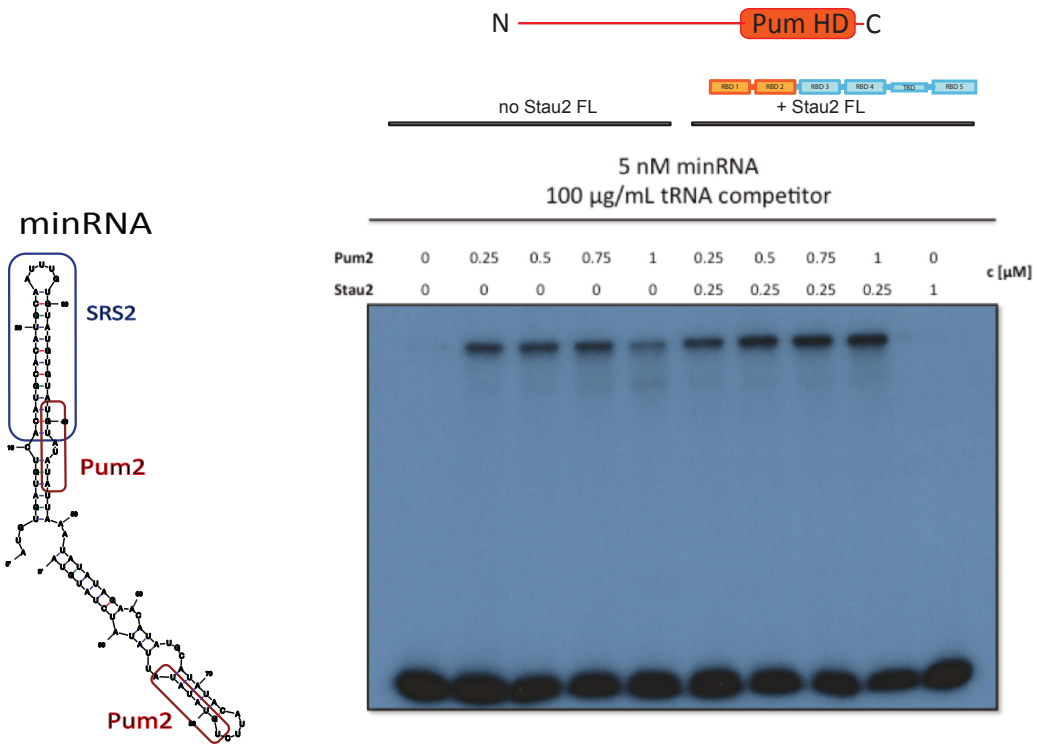

Figure 20: UV-crosslinking experiment with HisMBP-Pum2 FL and HisSUMO-Stau2 FL. Pum2 was titrated to minRNA in absence or presence of Stau2 at different concentrations. Crosslinking efficiency of Pum2 does not change in presence of Stau2. Complexes were resolved by PAGE.

3.4.3 Stau2 cannot pull down Pum2 in *in vitro* pull-down assays

Next, *in vitro* pull-down assays with purified full-length Stau2 and Pum2 were performed in absence or presence of *Rgs4* BR RNA as described in section 2.10.9. His-SUMO-tagged full-length Stau2 was captured in Ni sepharose beats as bait whereas MBP-Pum2 FL was used as prey. As shown in Figure 21, Stau2 was not able to pull down Pum2 neither in absence (Figure 21 A) nor presence (Figure 21 B) of *Rgs4* BR RNA. A very faint Pum2 band is visible not only in the Stau2

pull-down, but also in the Pum2 negative control in which Pum2 was incubated with Ni sepharose beads without Stau2, pointing at a weak unspecific interaction with the beads. In the presence of Pum2, Stau2 could not pull down *Rgs4* BR anymore, indicating that *Rgs4* BR was preferably bound by Pum2 in this setting and washed off in complex with Pum2.

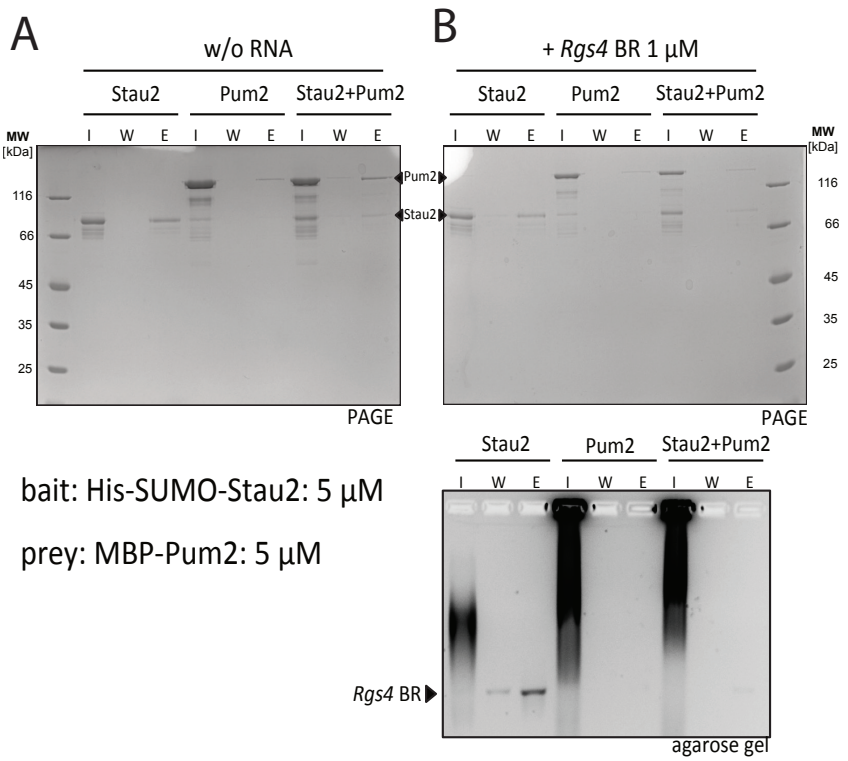

Figure 21: *In vitro* pull-down assay with recombinant Stau2 and Pum2. 5 µM His-SUMO-Stau2 FL were captured on Ni sepharose beads as bait to pull down 5 µM MBP-Pum2 FL prey in **A)** absence of RNA or **B)** presence of 1 µM *Rgs4* BR RNA. In both cases, Stau2 was not able to pull down Pum2.

Taken together, this indicated once more that Stau2 and Pum2 do not directly interact. Furthermore, both proteins seem to compete for *Rgs4* RNA-binding rather than bind *Rgs4* RNA simultaneously, possibly due to steric hindrance. The interaction between the two proteins could, however, be of transient nature and thus not stable enough to be detected in pull-down experiments.

3.4.4 No interaction of Stau2 and Pum2 can be observed by SPR

To test whether a transient interaction between Stau2 and Pum2 occurred that was not detectable by EMSA or pull-down, surface plasmon resonance (SPR) experiments were performed with the two recombinant proteins. For this purpose, HisSUMO-Stau2 FL was diluted in 10 mM Na acetate pH 4.5 and covalently amine-coupled to a CM5-sensorchip surface channel. As reference, a

HisSUMO-coupled channel was used. Different amounts of ligands with responses of up to ~1300 RU were tested. When a concentration series of HisMBP-Pum2 FL was injected at continuous flow (30 µL/min), no response over reference levels and thus no interaction could be observed (Figure 22 A).

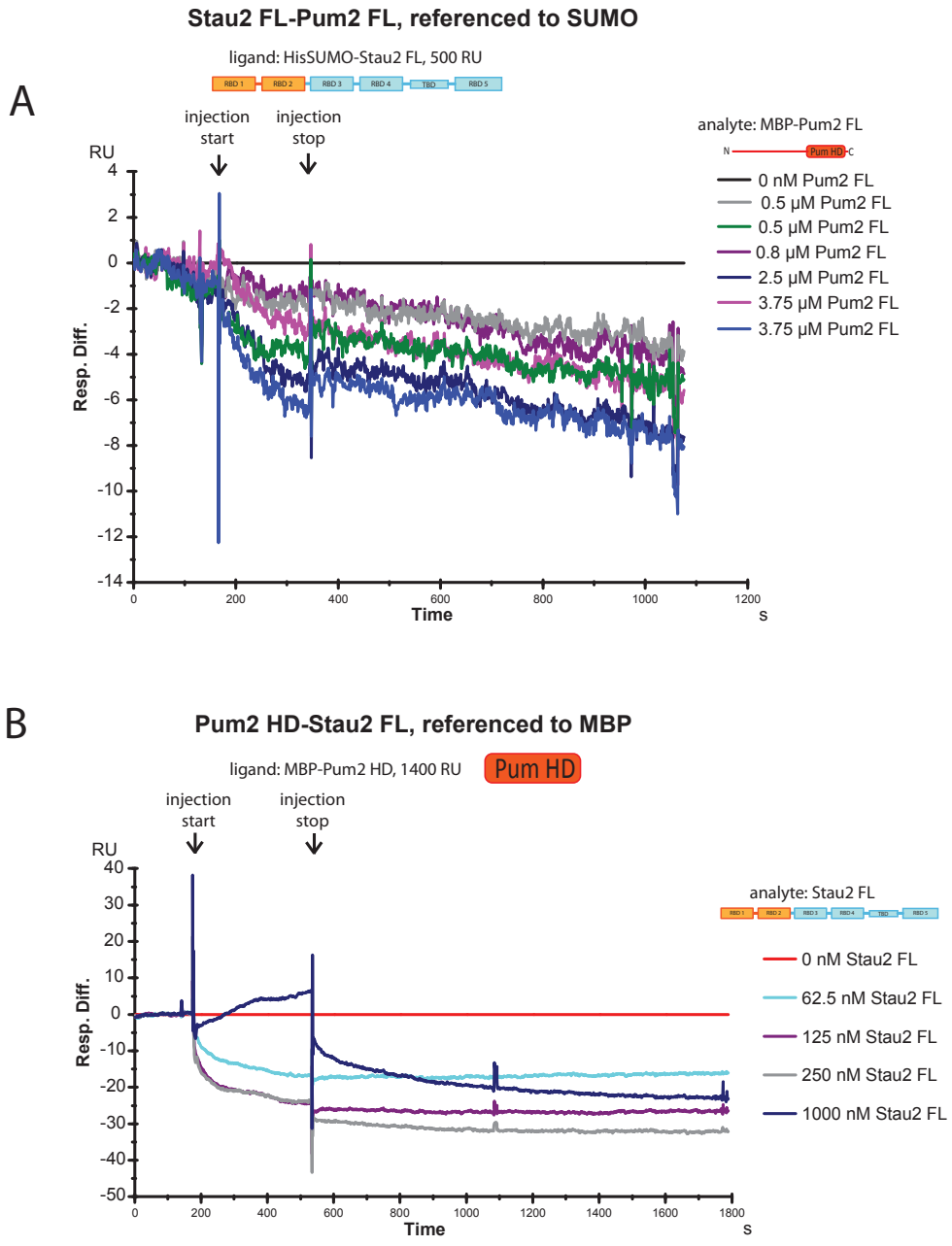

Figure 22: SPR sensorgrams of a kinetic analysis of Stau2 FL and Pum2 FL binding. A) 500 RU HisSUMO-Stau2 FL (ligand) were coupled to a CM5 sensor chip surface. A concentration series of HisMBP-Pum2 FL (analyte) from 0-3.75 µM was injected. The sensorgrams are referenced to a HisSUMO-coupled channel. No response over reference levels can be observed upon analyte injection. **B)** 1400 RU MBP-Pum2 HD (ligand) were coupled to a CM5 sensor chip surface. A concentration series of HisSUMO-Stau2 FL (analyte) from 0-1000 nM was injected. The sensorgrams are referenced to a MBP-coupled channel. No response over reference levels can be observed upon analyte injection.

Because reaction conditions for amine-coupling are rather harsh and Stau2 FL partially precipitated at the low pH required, it is possible that the protein was denatured and thus could not interact with Pum2. To circumvent this problem, Pum2 should be used as ligand and coupled to the sensorchip surface. However, Pum2 FL also precipitated at low pH. Instead the more soluble Pum2 HD (with HisMBP fusion-tag to further improve solubility) was coupled to CM5 and a MBP-coupled channel used as reference. When a concentration series of Stau2 was injected, no interaction was observed, indicating that Stau2 does not interact with Pum2 HD (Figure 22 B). It cannot be excluded that an interaction between the two proteins requires other parts of the protein, however. Taken together, no evidence for a direct interaction of Stau2 and Pum2 was found by SPR.

3.4.5 Stau2 and Pum2 aggregate in ITC experiments

Since SPR did not show an interaction of Stau2 and Pum2 possibly because the proteins suffered damage from the harsh conditions required for covalent coupling, isothermal titration calorimetry (ITC) experiments were performed instead. Because the full-length proteins could not be concentrated to sufficient concentrations for ITC (>100 µM in the needle), Stau2 RBD2-4 and Pum2 HD were used. Titration of Stau2 RBD2-4 to Pum2 HD as well as titration of Pum2 HD to Stau2 RBD2-4 was attempted. However, in both cases the protein solution in the cell aggregated upon titration and thus no meaningful results could be obtained by this method.

3.5 Crystallography of Stau2-RNA and Pum2-RNA complexes

3.5.1 Crystallography of Stau2-RNA complexes

To gain insight into the molecular mechanisms of recognition of a physiological target RNA by Stau2, crystallization trials for structure determination by X-ray crystallography were performed with several Stau2 protein constructs and SRS RNAs. No crystals were obtained with SRS1 or SRS3 RNA in complex with Stau2. Trials which yielded crystals are described below.

3.5.1.1 Structure of the Rgs4 SRS2 RNA

Crystallization screens with complexes of *Rgs4* SRS2 and the Stau2 RBD 3-4 or RBD4 proteins yielded crystals in 80 mM NaCl or 80 mM KCl, 20 mM $BaCl_2$,

40 mM Na cacodylate pH 6.5, 40 % MPD, 12 mM spermine after 4 days at RT. Crystals could be reproduced in sitting drops at 34-46 % MPD. These crystals diffracted to 1.7 Å resolution. Native datasets were collected at the Swiss Light Source (SLS) synchrotron, beamline PXIII. Anomalous data for phasing were collected at the European Synchrotron Radiation Facility (ESRF) beamline ID23-2. The structure was solved by MAD phasing with Barium. Procedures of data collection and processing as well as refinement are given in sections 2.12.1.6 and 2.12.1.7. Crystallographic details on data collection and refinement are given in Table 15.

Table 15: Data collection and refinement statistics

	SRS2 RNA
Data collection	
Space group	C 1 2 1
Cell dimensions	
a, b, c (Å)	114.020 32.390 46.370
α, β, γ (°)	90.00 103.47 90.00
Resolution (Å)	55.44 - 1.73
I/σ(I)	17.92 (1.88)
$CC_{1/2}$	99.9 (75.7)
Completeness (%) (in resolution range)	96.8 (39.82 - 1.73)
Redundancy	5.1 (5.4)
Refinement	
Resolution (Å)	39.82 - 1.73
No. of reflections	16965
R_{work}/R_{free}	18.5/23.7
R_{free} test set	819 reflections (4.83 %)
No. of atoms	1421
RNA	1290
Ba ion	13
Mg ion	1
Water	116
Wilson *B* factor ($Å^2$)	30.6
Average B, all atoms ($Å^2$)	45.0
Anisotropy	0.048
F_o,F_c correlation	0.97
R.m.s. deviations	
Bond lengths (Å)	0.007
Bond angles (°)	0.910

The crystals contained, however, only the SRS2 RNA stem-loop. One asymmetric unit contained two SRS2 molecules contacting each other at their loop regions. Both molecules adopt the typical RNA A-form characterized by a wide and shallow minor groove and a deep and narrow major groove and form the expected stem-loop structure. Both molecules (chain A and chain B) are shown in Figure 23 A. Whereas electron density in the stem-region of both molecules is very well defined, the density map in the loop region is poor, indicating flexibility of the RNA in this region (Figure 23 B).

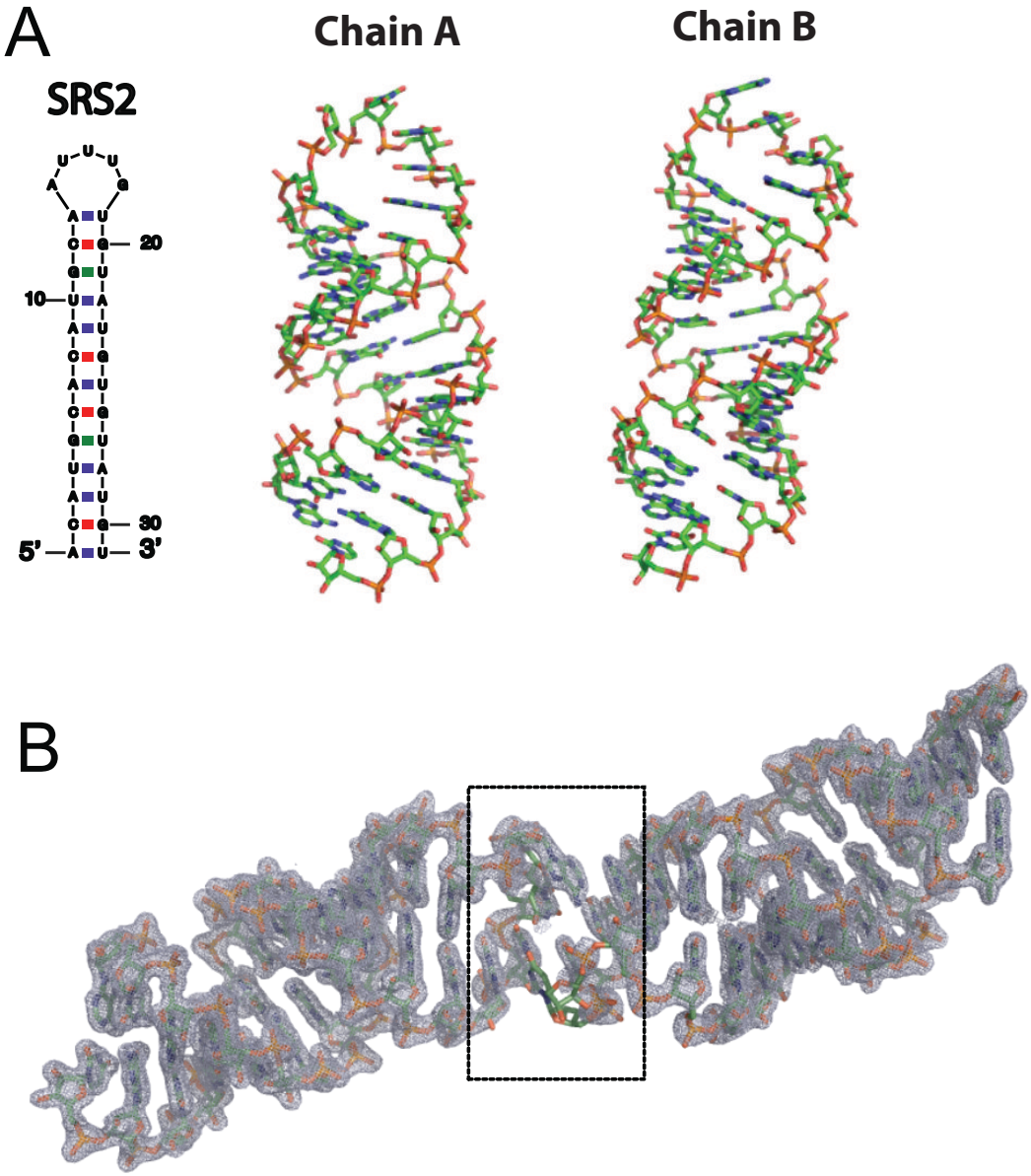

Figure 23: Crystal structure of the isolated *Rgs4* SRS2 RNA stem-loop. A) Schematic drawing of SRS2 RNA and the two molecules chain A and chain B contained in the ASU. Both molecules adopt the typical RNA A-form and form the expected stem-loop. Bot chains differ slightly in their loop-regions, which appear to be disordered. **B)** ASU with electron density map. Whereas the map in the stem region of the RNA is very well defined, it is rather poor around the two loops (indicated by dashed box), indicating disorder of the molecule.

3.5.1.2 Optimisation of the Rgs4 SRS2 RNA for co-crystallization with Stau2

Since SRS2 RNA crystallized only alone instead of in complex with Stau2, the RNA was optimized for further crystallization trials. As described above (section 3.2.4), elongation of SRS2 RNA at the 3' end improved Stau2-binding and thus possibly also co-crystallization. An SRS2+5 nt RNA did, however, not yield any crystals, so the RNA was extended with a GAAA scaffold (Murphy and Cech, 1994) to enhance crystallization. This GAAA tetraloop/11 nt receptor stem serves as a core for crystal contacts, thus facilitating crystal packing. This scaffold has succesfully been used to aid crystallization of RNA in several studies (Coonrod et al., 2012, Ferre-D'Amare et al., 1998 {Reiter, 2010 #488)}.

Addition of the scaffold at the 3' end and insertion into the loop region of SRS2+5 nt was tested. Only the insertion RNA shown in Figure 24 A, termed SRS2+5/GAAAinsertion, yielded crystals in co-crystallization trials with Stau2 RBD1-2 protein.

3.5.1.3 Crystallization of the Stau2 RBD1-2-SRS2+5/GAAAinsert RNA complex

Co-crystallization trials with Stau2 RBD1-2 and SRS2+5/GAAAinsert RNA at 2:1 ratio yielded initial crystals in 0.05 M Na cacodylate pH 6.0, 2.5 mM spermidine, 10 mM $MgCl_2$, 2.5 M NaCl after 1 day (Figure 24 B). The crystals could be reproduced by sitting-drop vapor-diffusion and optimized at pH 6 to 6.5 and NaCl concentrations of 2.2 to 2.5 M. For freezing, the crystals were cryoprotected in 20- 30 % glycerol or ethylene glycol. Data from reproduced crystals were collected to 3.0 Å resolution at the ESRF, beamline ID 23-2. Data quality, however, was rather poor. Data processing indicated crystals with the space group $P2_12_12_1$. Molecular Replacement (MR) solutions could be obtained with MolRep (CCP4 package, (Winn et al., 2011)), using the SRS2 RNA structure and a RBD model derived from a published RBD structure (PDB 1UHZ) as phasing models. However, none of the obtained solutions could be refined. Analysis of the unit cell volume indicated that a complex ratio of 3:1 for Stau2 RBD1-2:RNA was possible.

Thus, crystals were further optimized by variation of the protein:RNA mixing ratio. Indeed, crystals obtained in the same condition at 3:1 ratio diffracted to 2 Å. Data were collected at ESRF (beamline ID 23-2). The apparent space group was either $P4_12_12$ or $P4_32_12$. Both matched the data with very good statistics.

Data analysis with an L-Test (Padilla and Yeates, 2003), however, showed perfect pseudomerohedral twinning (twin fraction 0.47). The L-test uses the parameter L that describes intensity statistics by examining local differences between pairs of reflections. In contrast to other intensity statistic calculations, L is insensitive to pseudo-centering and can thus still detect twinning in its presence.

The true space group must thus have lower symmetry. In case of hemihedral twinning, again $P2_12_12_1$ or $P4_1$ and $P4_3$ were possible. However, also twinning with more than two twin domains was possible. Additionally, the data show pseudo-centering along the c-axis, which changes intensity statistics and further complicates data processing. The real space group could thus not be determined. MR trials in $P2_12_12_1$ or $P4_1$ and $P4_3$ but also P1 yielded only poor solutions, which could not be refined and produced electron density maps that could not be interpreted as biological macromolecules.

Another approach of optimization of the Stau2 RBD1-2-SRS2+5/GAAAinsert crystals attempted to slightly change the crystal lattice and thus abolish twinning (Figure 24 C). An additive screen was performed and yielded crystals with optimzed morphology with $BaCl_2$, $MgCl_2$ and NDSB-195. Different approaches of seeding of microcrystals were tried and streak-seeding produced crystals of similar morphology. The protein:RNA ratio was further varied and crystals were also obtained at a 4:1 ratio. A cysteine-to-alanine mutant of Stau2 RBD1-2 was cloned and purified and produced similar crystals. Hanging drop crystallization was attempted but produced smaller, needle-shaped crystals. Crystal cross-linking trials by direct addition of formaldehyde or glutaraldehyde dissolved the crystals. However, crystals crosslinked more mildly by vapor diffusion with 25 % glutaraldehyde remained intact. All crystals that were obtained by any of these methods failed to diffract or produced again twinned data. Mercury derivatization with $HgBr_2$ or Hg acetate was tested but derivative protein failed to crystallize.

In an attempt to obtain experimental phase information, crystals were soaked with $BaCl_2$. Also, Stau2 RBD1-2 protein was SeMet-labeled. SeMet-Stau2 RBD1-2 produced crystals similar to the original ones. Neither soaked nor SeMet crystals diffracted with reasonable quality.

Additionally, slight modifications of the RNA molecule were tested to improve crystal quality (Figure 24 D). Elongation or shortening of the single-stranded 3' end yielded RNAs (SRS2+3/GAAAinsert or SRS2+6/GAAAinsert, respectively) that failed to produce crystals. An RNA in which the GAAA scaffold stem was elongated by 1 bp (SRS2+5longGAAAinsert) produced crystals, which were again twinned.

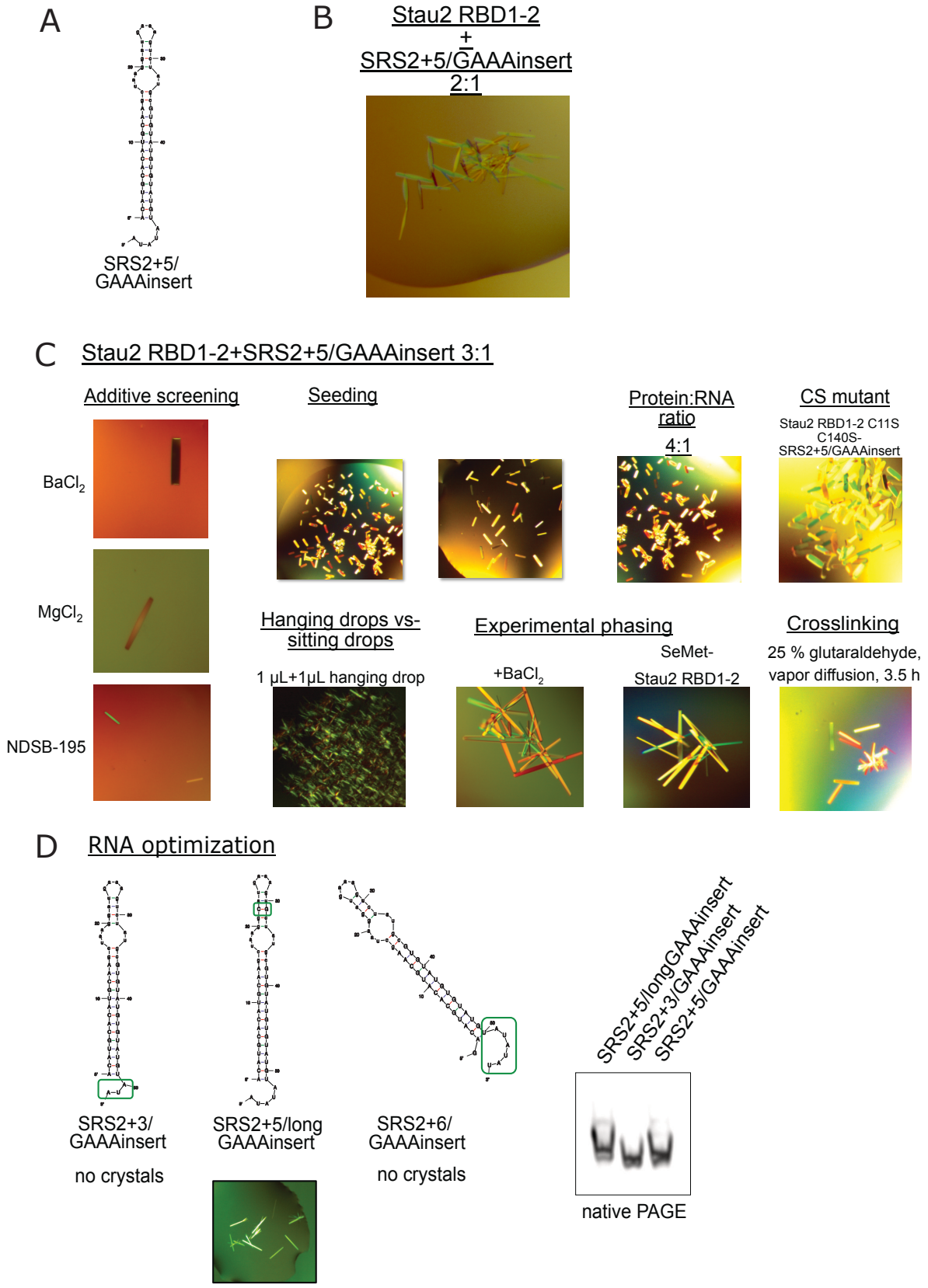

Figure 24: Stau2 RBD1-2-RNA complex crystal optimization. A) Scheme of the RNA used for complex crystallization. SRS2 was extended with five ss nucleotides at the 3'end and a GAAA scaffold was inserted in the loop to enhance crystallization. **B)** Initial crystals of the Stau2 RBD1-2 SRS2+5/GAAAinsert RNA. **C)** Examples of crystals obtained during optimization. **D)** Modifications of the SRS2+5/GAAAinsert tested for crystal optimization (left) and quality control of the produced RNAs by native PAGE (right), showing high quality of the used samples.

3.5.2 Crystallography of Pum2-RNA complexes

As described above (see section 3.3.2), Pum2 bound SRS3 RNA, which does not contain a complete Pum2 PRE and furthermore forms an imperfect stem-loop limiting accessibility for the ssRNA-binding Pum2. To gain insight into the molecular mechanism of this non-canonical binding, crystallization of a Pum2-SRS3 complex for structure determination by X-ray crystallography was attempted.

Co-crystallization screens with Pum2 HD and SRS3 RNA at 1:1 ratio at ~3.5 mg/mL yielded tiny (~10-20 µm x 5 µm x 5 µm) initial crystals in 2 M ammonium sulfate, 0.1 M sodium acetate pH 4.6 after 4 days at RT (Figure 25). These crystals could be reproduced and were screened for X-ray diffraction. The crystals showed very little diffraction, possible owed to their small size. First optimization trials failed to improve crystal morphology. For structure determination, further crystal optimization is thus required.

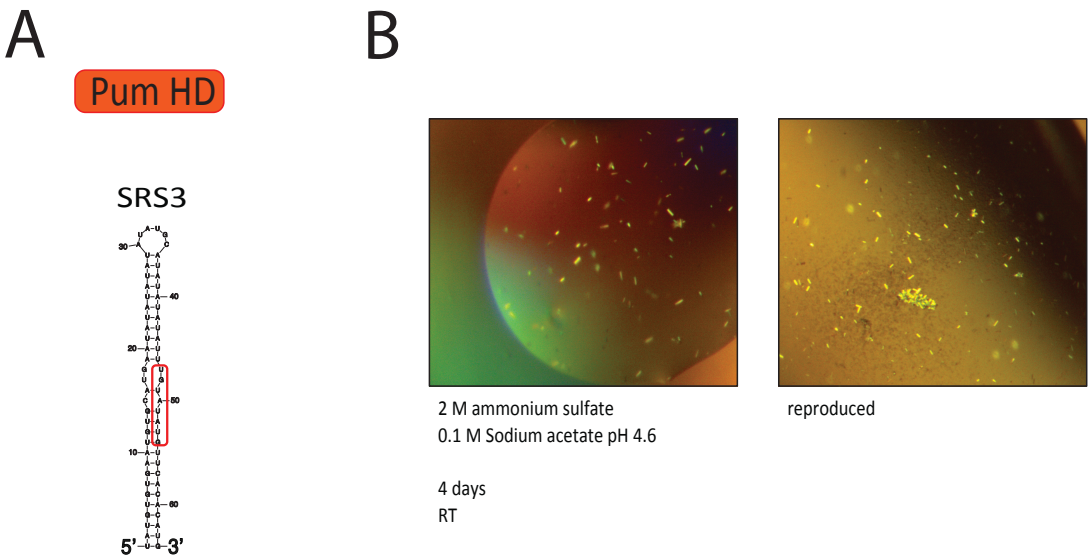

Figure 25: Crystallization of Pum2 HD in complex with SRS3 RNA. A) Schemes of the crystallized molecules Pum2 HD and SRS3 RNA. **B)** Initial (left) and reproduced (right) crystals of Pum2 HD-SRS3.

3.6 Characterization of the Stau2 RBD1-2-RNA complex

After the discovery that Stau2 RBDs 1 and 2 possess, as opposed to previous reports, RNA-binding activity by a possibly non-canonical mechanism, this activity should be further characterized. Understanding the molecular mechanisms of RNA-binding by RBD1-2 could help to gain insight into their role in specific RNA recognition by Stau2.

3.6.1 RNA-binding activity and domain boundaries of single domains RBD1 and RBD2

To examine whether both RBDs 1 and 2 have RNA-binding activity, both domains were purified and tested in EMSAs separately. RBD1 as annotated (aa 1-74) was not expressed and was thus C-terminally fused to a His_6-tag to allow purification. As shown in Figure 26 A, this RBD1-His fragment did not show any binding activity to dsSRS2+5 RNA. Also, RBD2 as annotated in the NCBI Protein database (aa 94-180) degraded during purification and needed to be elongated at the C-terminus to improve stability. The longer RBD2 (aa 94-208) bound dsSRS2+5 with about 10-fold lower affinity than the tandem-domain RBD1-2 (Figure 26 A). To test whether the linker sequence between the two domains contributed to RNA-binding, both proteins were expressed with the linker (RBD1-linker and linker-RBD2) and tested in EMSAs. RBD1-linker showed some weak binding-activity to dsSRS2+5 at 20-30 µM whereas linker-RBD2 bound dsSRS2+5 with slightly improved affinity as compared to RBD2 (Figure 26 B). This indicated that the linker contributes to RNA-binding. To test whether mixing the two separate domains could restore the activity of the tandem-domain RBD1-2, EMSAs with both proteins were performed. While one of the domains containing the linker was titrated, the respective other domain was added at a constant concentration of 10 µM. As shown in Figure 26 C, both titrated RBDs bound dsSRS2+5 similar in presence or absence of the other domain. Mixing the separate domains could not restore the activity of tandem RBD1-2, indicating that both domains act cooperatively in the tandem-domain and their close spatial proximity is required for their activity.

Furthermore, the poor expression or degradation of the annotated RBDs 1 and 2 and the improvement of their behavior and activity by additional sequences indicate that these domains are non-canonical but active RBDs.

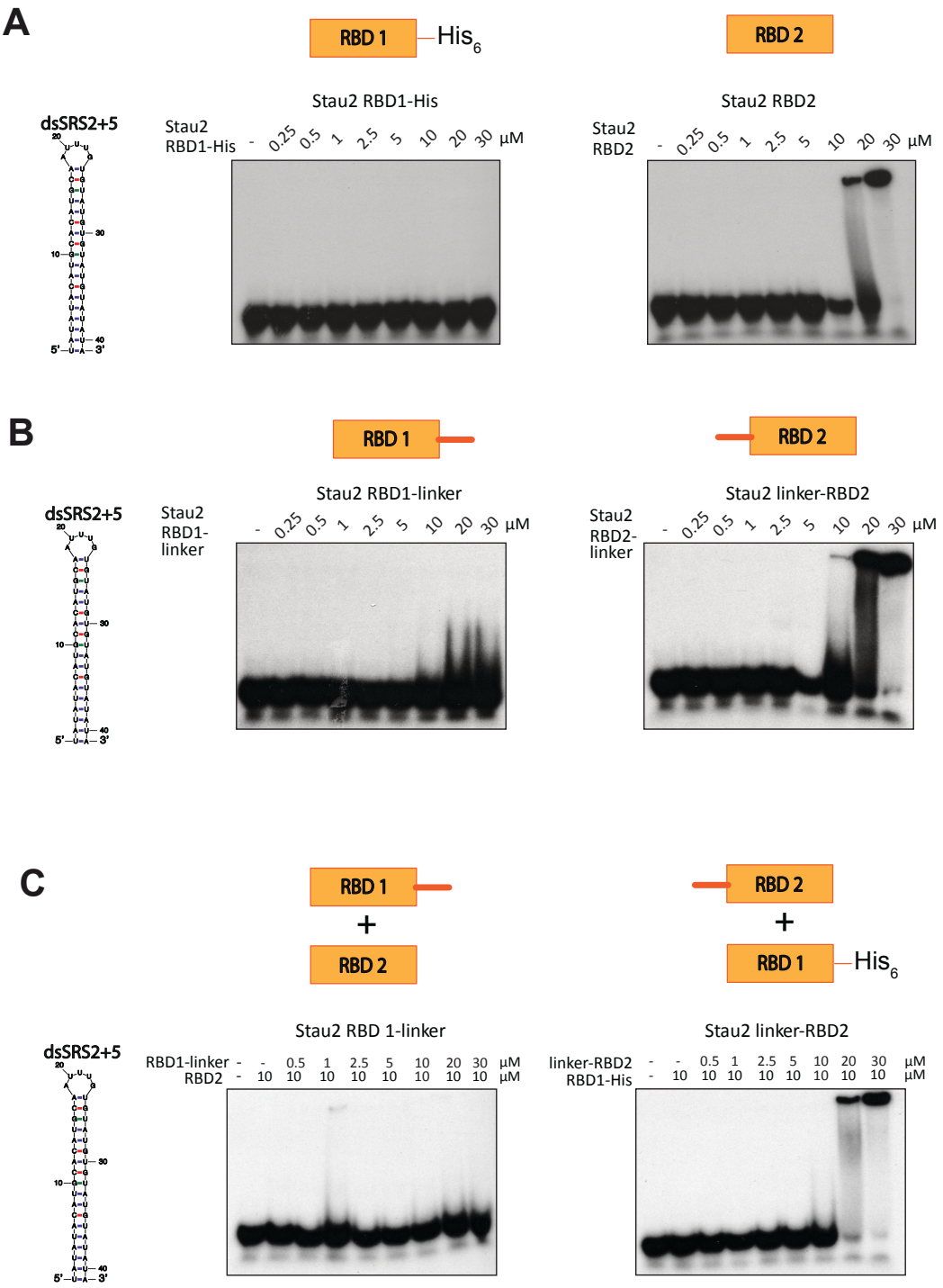

Figure 26: EMSAs with the individual domains RBD1 and 2. A) Binding of RBD1 (left) and RBD2 (right) to dsSRS2+5. **B)** Binding of RBD1-linker (left) and linker-RBD2 (right) to dsSRS2+5. **C)** Binding of RBD1-linker (left) and linker-RBD2 (right) to dsSRS2+5 in presence of the respective other domain at 10 µM.

3.6.2 Stau2 RBDs 1 and 2 are structured, independent domains

Because the crystal structure of the Stau2 RBD1-2-RNA complex could not be solved, NMR experiments were performed to obtain structural information on the complex. For this purpose, different isotope-labeled proteins were produced as described in section 2.9.1.6. NMR experiments were performed by Jan-Niklas Tants (Group of Prof. Dr. Michael Sattler, Chair of Biomolecular NMR Spectroscopy, TUM, Munich, Germany). For details, see section 2.12.2.

First, $^{1}H,^{15}N$-HSQC fingerprint spectra of the tandem domain RBD1-2 and the two individual RBDs 1 and 2 were collected. For both domains, linker-containing fragments were used in all following experiments because of their improved RNA-binding affinities observed in EMSAs (see section 3.6.1). In this and the following chapters, these linker-containing constructs will now be referred to as RBD1 and RBD2.

The $^{1}H,^{15}N$-HSQC spectra prove that both domains are mainly structured. The spectra of the individual domains nicely overlap with those from the tandem domain construct (Figure 27), suggesting that RBD1 and RBD2 are independent domains in solution in their free form. Their structural integrity is not affected by the presence of the other domain. Strong signals in the center of all three proteins' spectra indicate a high degree of flexibility, probably due to unstructured regions.

For RBD1 more signals than expected were observed in a 2D correlation spectrum, pointing at multiple conformations or oligomerization. Indeed, a partial assignment suggested the presence of several states likely due to the high abundance of prolines (10.5 %).

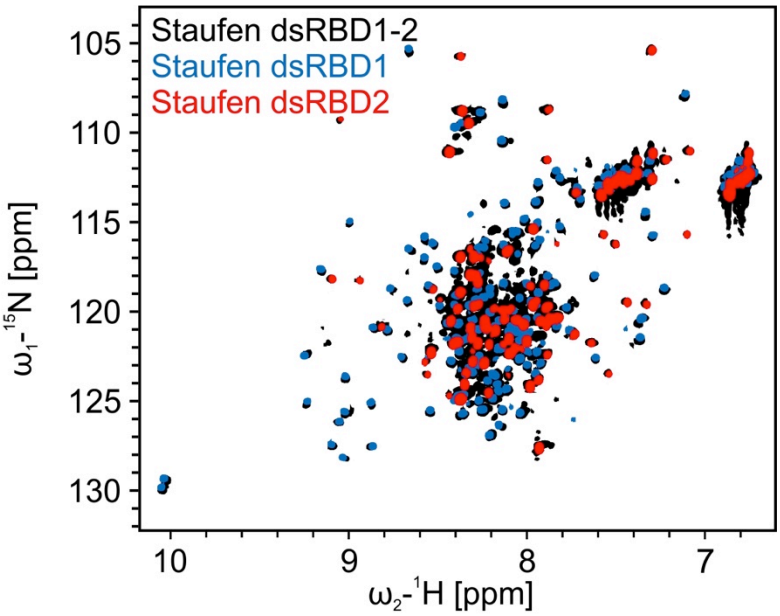

Figure 27: Overlay of the $^{1}H,^{15}N$-HSQC spectra of the tandem-domain RBD1-2 and the individual RBDs 1 and 2. The spectra of RBDs 1 and 2 overlap and add up to the spectrum of the tandem-domain, indicating that RBDs 1 and 2 are separate, partly disordered domains.

3.6.3 Both Stau2 domains RBD1 and RBD2 bind RNA with different dynamics

First, NMR titration experiments were performed in which dsSRS2+5 RNA was titrated to ^{15}N-labeled Stau2 RBD1-2 protein. The dsSRS2+5 RNA was used because of its improved affinity compared to SRS2 (Figure 13). Protein HSQC spectra and RNA 1D imino spectra were collected as described in section 2.12.2.

Upon addition of the RNA to the tandem-domain, shifts of individual signals were observed (Figure 28 A). Additionally, several signals experienced severe line broadening.

Severe line broadening of RNA signals is oberserved in the imino traces at excess of protein (Figure 28 B). Strong line broadening of imino signals can point at dynamic binding comprising sliding as it was shown for other dsRBDs before (Tants et al., 2017). Alternatively, frequent association and dissociation is possible.

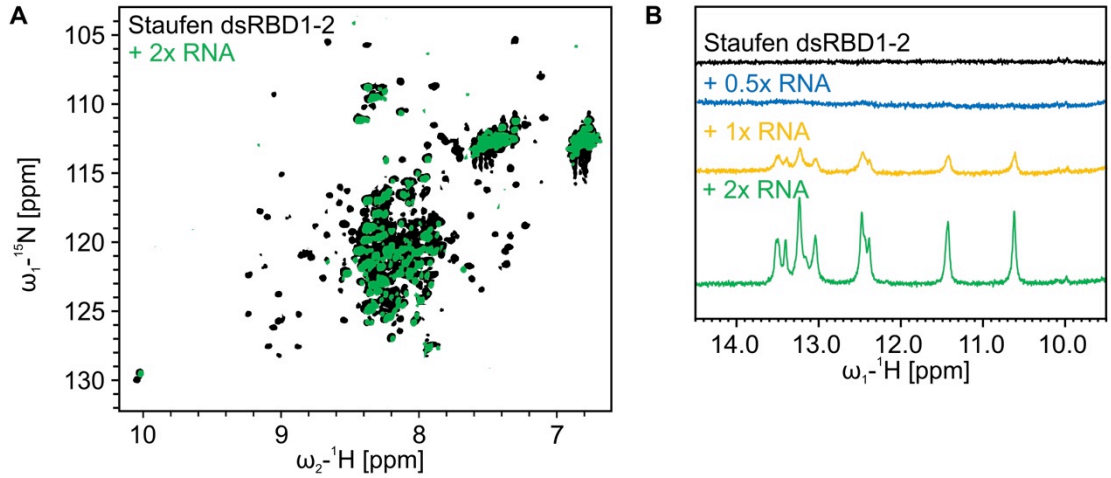

Figure 28: NMR titration experiments of Stau2 RBD1-2 with dsSRS2+5 RNA. A) Overlay of $^{1}H,^{15}N$-HSQC spectra of RBD1-2 in absence and presence of 2x excess dsSRS2+5 RNA. Resonance shifts and line broadening of several signals are observed. **B)** Comparison of 1D imino traces of dsSRS2+5 RNA at different stoichiometric ratios with RBD1-2. Strong line broadening of imino signals is observed in presence of protein.

Upon titration of the dsSRS2+5 RNA to both the individual ^{15}N-labeled domains RBD1 and RBD2, shifts of individual signals were observed for both domains and several signals experienced severe line broadening (Figure 29 A and C). Residues affected by RNA binding in the single RBDs are similar to those in the tandem-domain experiment suggesting both domains bind the RNA independently. Interestingly, the RNA is affected differently by the two domains. A comparison of the 1D imino traces reveals line broadening at substoichiometric concentrations for RBD2 binding (Figure 29 D), similar to the tandem-domain. In contrast, for RBD1 sharp imino signals are observed (Figure 29 B) at a protein:RNA ratio of 1:0.5, pointing at differences in the binding mechanisms of the two domains.

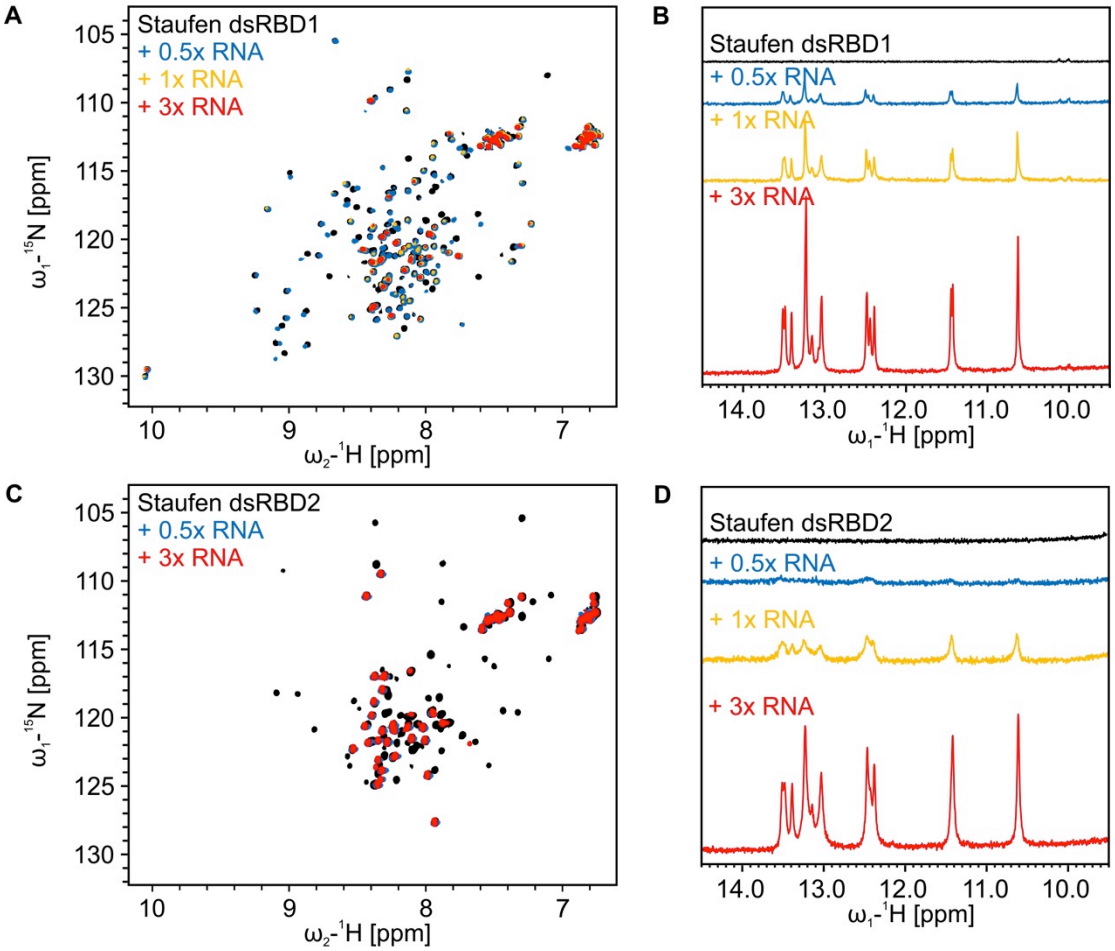

Figure 29: NMR titration experiments of Stau2 RBD1 (A and B) and RBD2 (C and D) with dsSRS2+5 RNA. A) and **C)** Overlay of ^{1}H, ^{15}N-HSQC spectra of RBD1 (A) or RBD2 (C) in absence and presence of dsSRS2+5 RNA. Resonance shifts and line broadening of several signals are observed for both domains. **B)** and **D)** Comparison of 1D imino traces of dsSRS2+5 RNA at different stoichiometric ratios with RBD1 (B) or RBD2 (D). Strong line broadening of imino signals is observed in presence of RBD2 but not RBD1, pointing at differences in binding.

3.6.4 Stau2 tandem-domains bind RNA with fast kinetics

To allow for investigation of not only stable Stau2-RNA complexes but also binding kinetics, SPR experiments were performed with the Stau2 tandem-domains RBD1-2 and, for comparison, RBD3-4 as well as a protein fragment comprising all four domains RBD1-4. As ligands, dsSRS2+5 RNA or, for cross-validation, SRS3 RNA were biotinylated and coupled to a streptavidin sensorchip surface. Subsequently, a concentration series of Stau2 protein as analyte was injected onto the sensorchip at a continuous flow rate. For details, see section 2.10.8.

For the tandem-domains RBD3-4 and RBD1-2, fast binding to both RNAs was observed immediately after injection start as marked by the fast increase of

response units and steady-state is reached already at the lowest tested concentration of 10 nM (Figure 30 and Figure 31), indicating a fast on-rate of the binding reaction. However, also dissociation is fast as the response units drop rapidly when washing with buffer, indicating a fast off-rate. Because the kinetics of the binding reactions are so fast, they cannot properly be described by a kinetic fit. The steady-state affinity, however, can well be described by a two-site binding fit with a K_D1 in the concentration range of 9-18 nM for RBD3-4 and 25-130 nM for RBD1-2 and a K_D2 in the micromolar range (Figure 30 A and B and Figure 31 A and B). K_D2 could not be exactly determined because at concentrations > 1 µM, the obtained binding curves were not analyzable, probably due to oligomerization or aggregation of Stau2 protein on the sensorchip surfaces. This is consistent with the previous observation that both RBDs 1 and 2 possess RNA-binding activity with different mechanisms and indicates that RBD3 and 4 might act similarly. The observed kinetics are consistent with transient binding, which explains why the high affinities observed by SPR could not be seen in EMSAs, which only allows for the detection of stable complexes.

Interestingly, when the experiments were repeated with Stau2 RBD1-4, the binding kinetics changed dramatically with both RNAs. Binding occurred much slower after injection start and hardly any binding was observed at the lowest tested concentration (10 nM). After injection stop and onset of buffer wash, fast complex dissociation was not observed, indicating that the formed complex was stable. Both on- and off-rate of the binding reactions are strongly decreased and steady-state affinities can no longer be described by a two-site binding fit, probably due to even higher order binding with its four RBDs. However, Hill-fits with K_Ds of a few hundred nanomolar and Hill coefficients n > 1, indicating positive cooperativity of binding, describe steady-state binding of RBD1-4 to both RNAs well (Figure 30 C and Figure 31 C).

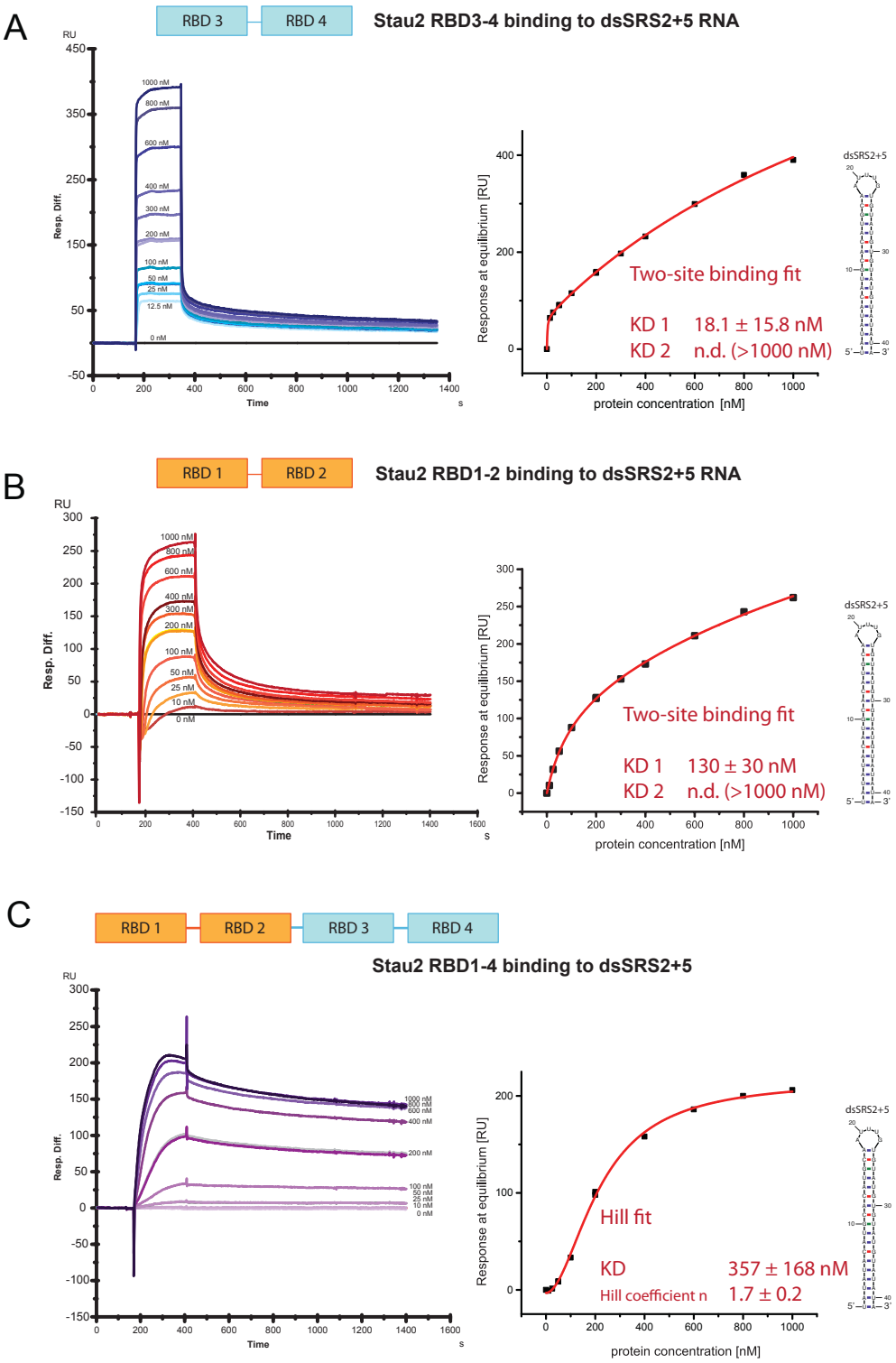

Figure 30: SPR sensorgrams (left) and steady-state binding curves (right) of Stau2 protein binding to SRS2+5 RNA. A) Stau2 RBD3-4, and **B)** Stau2 RBD1-2 binding to dsSRS2+5 RNA. The tandem-domains RBD3-4 and RBD1-2 bind transiently with fast kinetics. The steady state binding curves do not saturate up to 1 µM protein concentration but can be described by a two-site binding fit with K_D1 of 18 or 130 nM, respectively. **C)** Stau2 RBD1-4 binding to dsSRS2+5 RNA. Binding of RBD1-4 is stable with slower kinetics. The steady state binding curve saturates at approximately 1 µM and is described by a Hill fit with an apparent overall K_D of 357 nM and a Hill coefficient n=1.7, indicating positive comoperative binding.

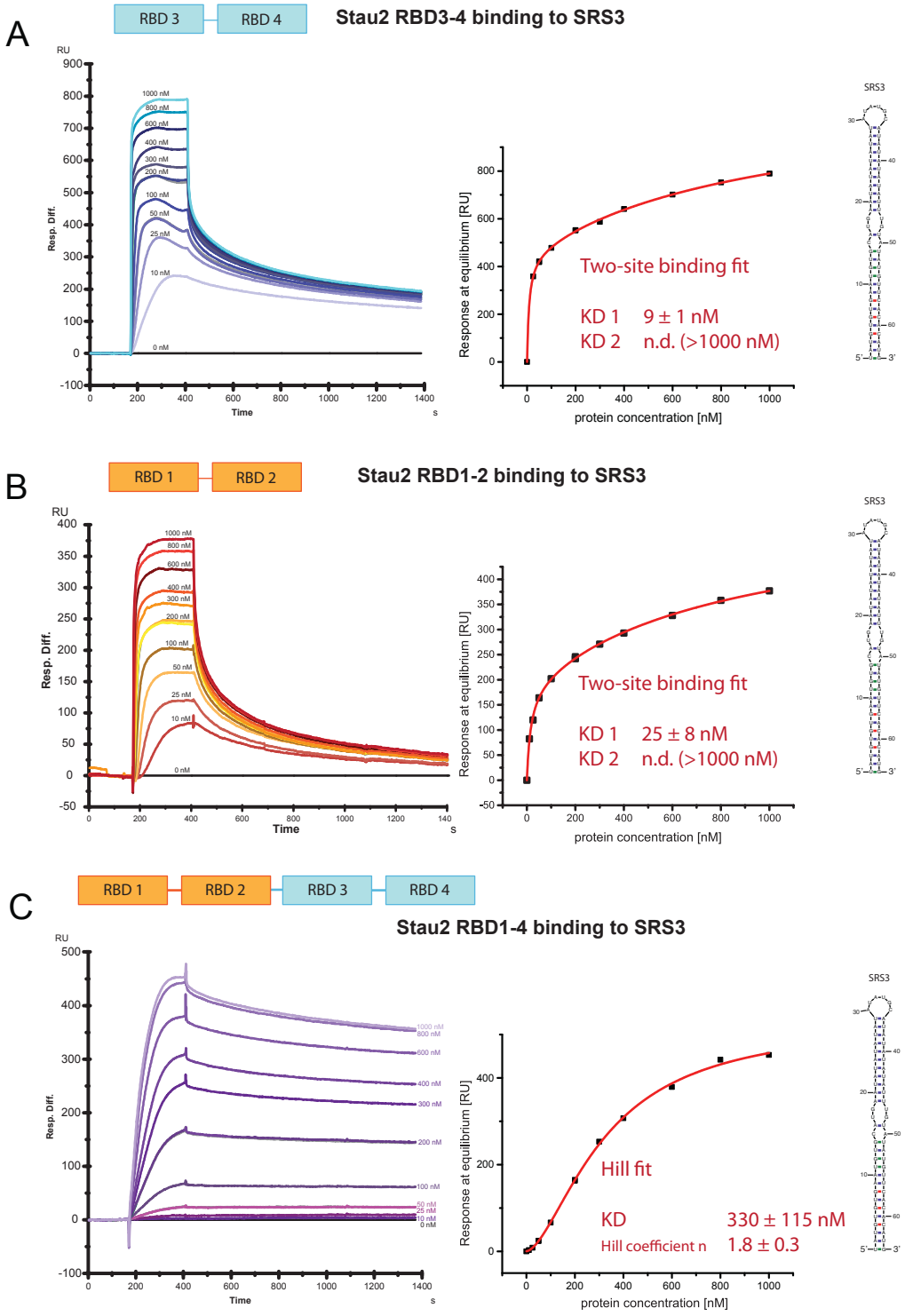

Figure 31: SPR sensorgrams (left) and steady-state binding curves (right) of Stau2 protein binding to SRS3 RNA. A) Stau2 RBD3-4, and **B)** Stau2 RBD1-2 binding to SRS3 RNA. The tandem-domains RBD3-4 and RBD1-2 bind transiently with fast kinetics. The steady state binding curves do not saturate up to 1 µM protein concentration but can be described by a two-site binding fit with K_D1 of 9 or 25 nM, respectively. **C)** Stau2 RBD1-4 binding to dsSRS2+5 RNA. Binding of RBD1-4 is stable with slower kinetics. The steady state binding curve saturates at approximately 1 µM and is described by a Hill fit with an apparent overall K_D of 330 nM and a Hill coefficient n=1.8, indicating positive comoperative binding.

.

To identify the contributions of the individual domains RBD1 and RBD2 to RNA-binding, SPR experiments were also performed with the single domain constructs. For RBD1, binding could neither be observed to dsSRS2+5 RNA nor to the SRS3 RNA at concentrations ≤ 1 µM (Figure 32, left). This was unexpected since binding of RBD1 was clearly observed in NMR experiments. However, these NMR experiments were performed at much higher protein concentrations (>50 µM). Furthermore, the lack of RNA binding for RBD1 alone indicates that within the tandem-domain, RBD1 and RBD2 act cooperatively. For RBD2, binding was observed with fast kinetics similar to the tandem-domain and steady-state affinity can be described with a Hill-fit (Figure 32, right). The observed K_Ds for RBD2 are in the high nanomolar range (650 ± 247 nM for dsSRS2+5 and 829 ± 29 nM for SRS3) and Hill coefficients are close to 1, indicating non-cooperative binding.

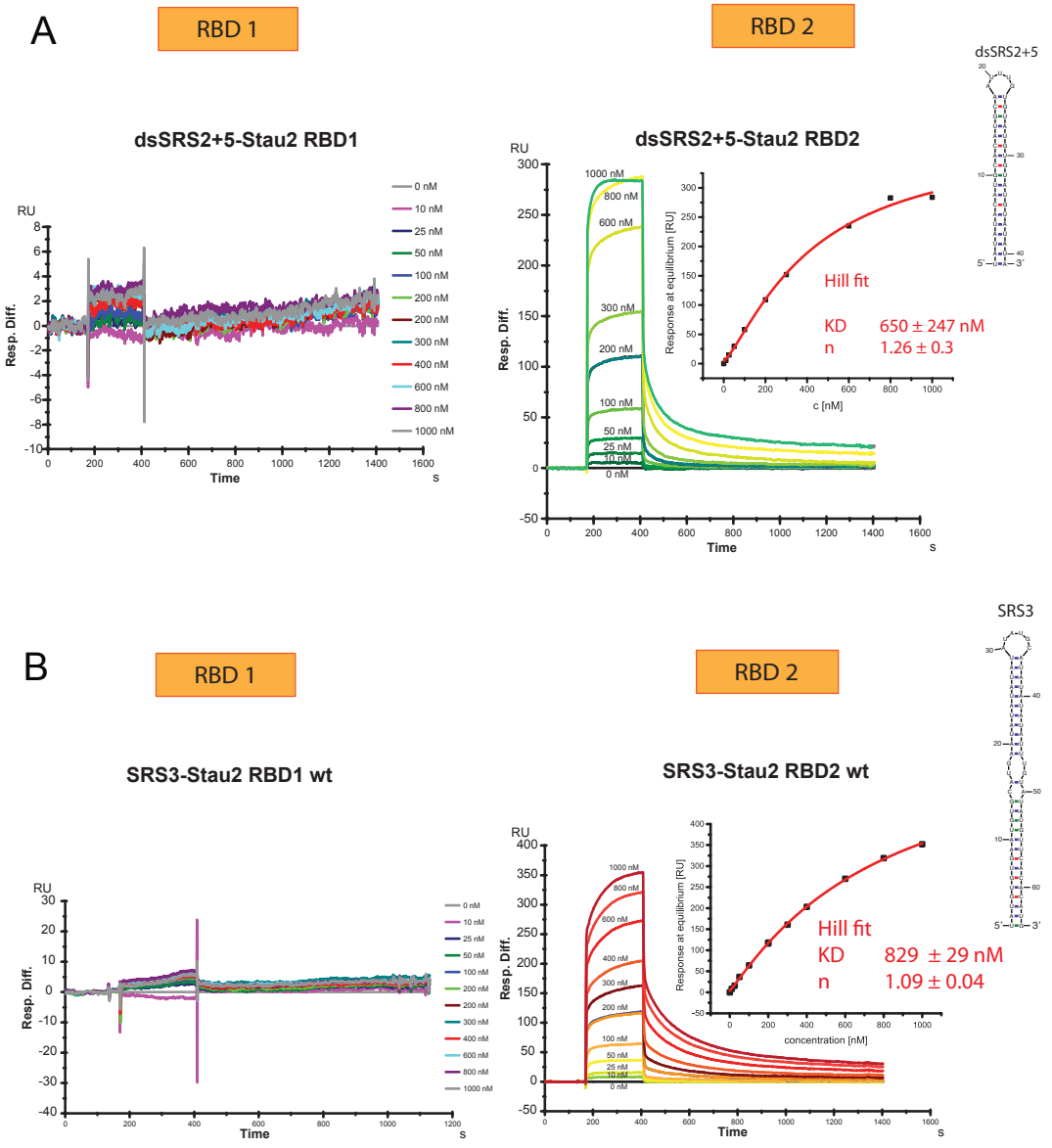

Figure 32: SPR sensorgrams and steady-state binding curves (for RBD2) of Stau2 RBD1 and Stau2 RBD2 binding to A) dsSRS2+5 or B) SRS3. Whereas no binding is observed for RBD1, RBD2 binds both RNAs, dsSRS2+5 and SRS3, with fast kinetics in a non-cooperative fashion with K_Ds of 650 nM or 829 nM, respectively. Steady-state binding curves are described by a Hill fit.

The results of the SPR experiments with wild-type (wt) Stau2 proteins are summarized in Table 16: Stau2-binding to dsSRS2+5 RNA and Table 17: Stau2-binding to SRS3 RNA.

Table 16: Stau2-binding to dsSRS2+5 RNA

Stau2 wt	binding	kinetics	K_D1 [nM]	K_D2 [nM]	Hill coefficient
RBD3-4	two-site	transient	18 ± 16	n.d. (>1000)	-
RBD1-2	two-site	transient	130 ± 30	n.d. (>1000)	-
RBD1-4	Hill	stable	-	330 ± 148	1.6 ± 0.2
RBD2	Hill	transient	-	650 ± 247	1.3 ± 0.3
RBD1	no binding	no binding	-	-	-

Table 17: Stau2-binding to SRS3 RNA

Stau2 wt	binding	kinetics	K_D1 [nM]	K_D2 [nM]	Hill coefficient
RBD3-4	two-site	transient	9 ± 1	n.d. (>1000)	-
RBD1-2	Two-site	transient	25 ± 8	n.d. (>1000)	-
RBD1-4	Hill	stable	-	287 ± 127	1.7 ± 0.4
RBD2	Hill	transient	-	828 ± 29	1.1 ± 0.04
RBD1	no binding	-	-	-	-

3.6.5 Identification and characterization of Stau2 RBD1-2 RNA-binding mutants

3.6.5.1 Mutant design

For verification of the observed binding mechanisms *in vitro* and to allow for functional *in vivo* studies of the RNA-binding activity of Stau2 RBD1-2, RNA-binding mutants of the RBDs 1 and 2 were created.

For RBD1, mutants were designed based on the NMR titration experiments and a multiple sequence alignment (MSA) with the RBDs 1 and 3 from dmStaufen. A partial assignment allowed for identification of residues with chemical shift perturbations upon RNA titration, pointing at their location within or close to the binding interface. The MSA (Figure 33) reveals that these residues nicely map to the end of helix α_1, loop 2 and the beginning of helix α_2, which are the regions that mediate RNA-binding in a canonical dsRBD. For mutation, conserved dsRBD residues close or within these regions were chosen, namely the conserved RNA-binding residues glutamate in helix α_1 (E15), histidine in loop 2 (H36), lysines from the KKxxK motif (K59 and K60) and furthermore the phenylalanine in β_2 (F40), which is known to indirectly assist RNA-binding by keeping RNA-binding residues in proper orientation (for details, see section 1.3.4). Thus, the RBD1 mutants E15A, H36A, F40A, K59A, K60A and K59A K60A were cloned, expressed

and purified in the RBD1-2 context. As reported before, mutation of these residues in RBD3 from *D. melanogaster* to alanines abolished RNA-binding completely (Ramos et al., 2000) (Figure 33 B).

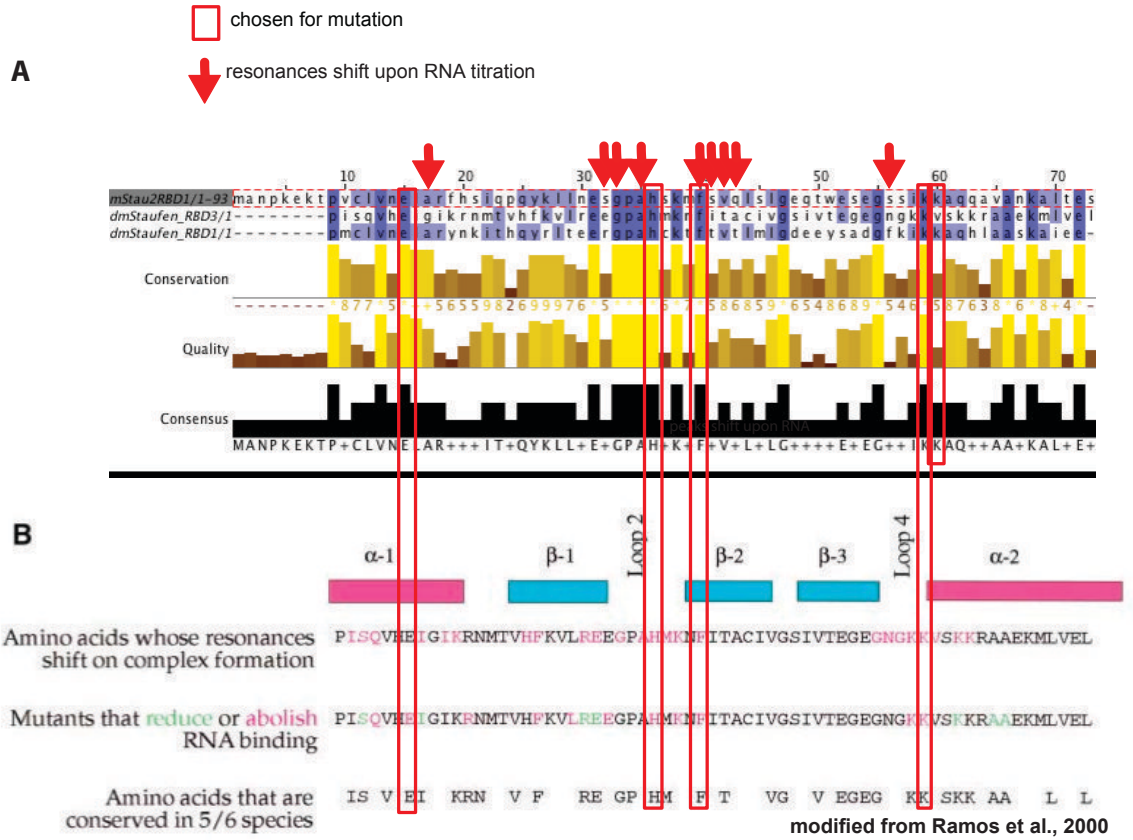

Figure 33: Sequence analysis used for mutant design of RBD1. A) Multiple sequence alignment of mStau2 RBD1 to dmStau RBD1 and dmStau RBD3. Assigned residues with chemical shift perturbations upon RNA titrations are marked. **B)** Designed mutations map to regions previously identified to be involved in RNA binding in dmStau RBD3 (Ramos et al., 2000).

For RBD2, information on the corresponding residues of shifting resonances was not available due to the lack of amino-acid assignments. Thus, mutations were chosen based on an MSA (Figure 34). Because RBD2 is significantly less conserved than RBD1 and presumably contains an inserted extension of loop 2 (based on secondary structure predictions and homology models, see Figure S 1 and Figure S 2, appendix), sequences of 12 species were aligned to ensure correct alignment and identification of conserved residues. Conserved positively charged or aromatic residues were chosen because these residues are likely to interact with RNA by electrostatic interactions with the phosphodiester backbone or base-stacking interactions, respectively. Again, the conserved glutamate residue in helix α_1 was mutated (E99). The RBD2 mutants E99A, K106A, F157A and H169A were cloned, expressed and purified in RBD1-2

context. Furthermore, a mutant in which the extended loop was deleted was cloned (Δ119-135). This mutant, however, could not be purified, most likely due to misfolding.

Correct folding of all other mutant proteins was verified by circular dichroism (CD) spectroscopy to exclude any effects on RNA-binding caused by protein misfolding (see Figure S 3, appendix).

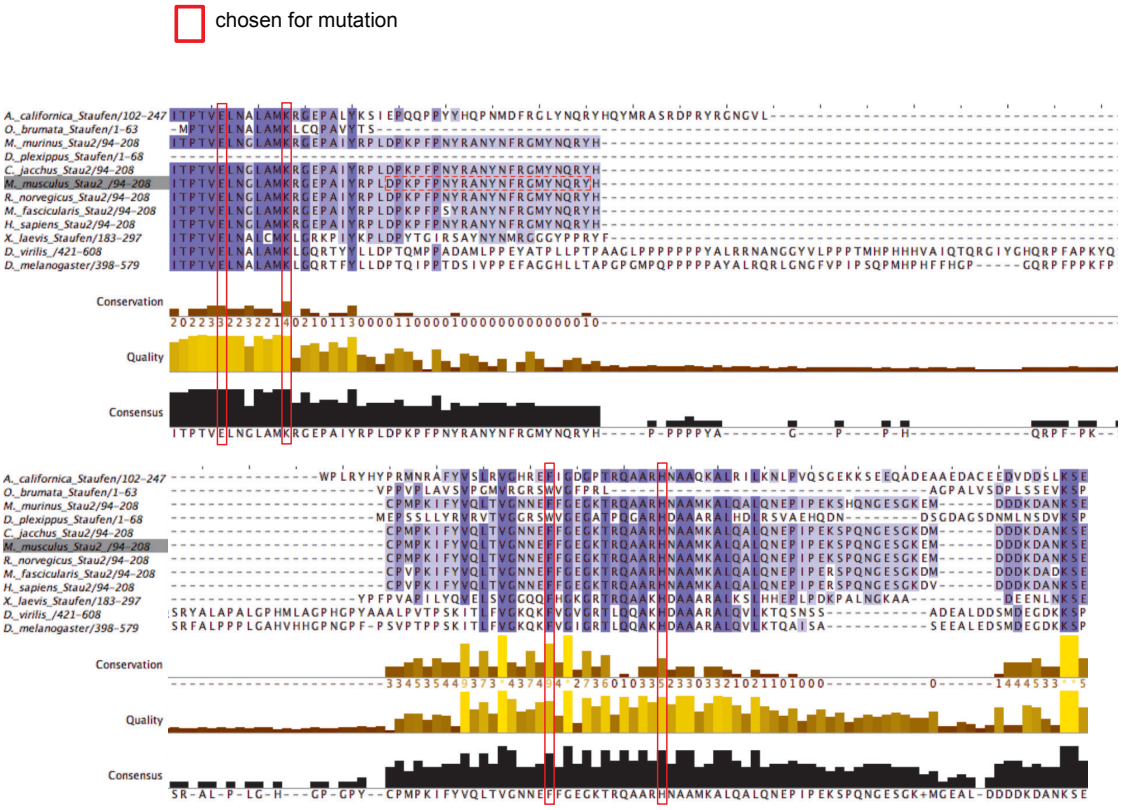

Figure 34: Sequence analysis used for mutant design of RBD2. Multiple sequence alignment of mStau2 RBD2 to Stau proteins from 11 different species. Residues chosen for mutation are marked.

3.6.5.2 Mutations of RBD1 in context of the tandem-domain resembles RBD2-activity

All designed mutants were tested for RNA-binding activity by SPR. When mutations in RBD1 in the tandem-domain RBD1-2 were tested for binding to dsSRS2+5, the single mutations H36A, F40A, K59A, and K60A as well as the double mutation K59A K60A showed binding very similar to the RBD2 domain alone (Figure 35 B to F, compare to Figure 32). Binding kinetics are fast and the steady-state binding curves can be well described by Hill-fits with Hill coefficients n ≈ 1, indicating non-cooperative binding. The observed K_Ds of

RBD1-2 H36A and K59A (Figure 35 B and C) are similar to that of RBD2. RBD1-2 F40A, K60A and K59A K60A bind with lower affinity than RBD2 with K_Ds above the tested concentration range, which could thus not be determined. These results indicate that binding-activity of RBD1 was abolished by these mutations.

Steady-state binding of RBD1-2 E15A to dsSRS2+5 did not resemble the two-state binding previously observed for the wt RBD1-2 (see Figure 30) but still showed a K_D of 132 ± 31 nM (Figure 35 A). Since this value is much better than the individual RBD2, this indicates that RNA-binding activity of RBD1 was possibly compromised but not completely abolished by this mutation.

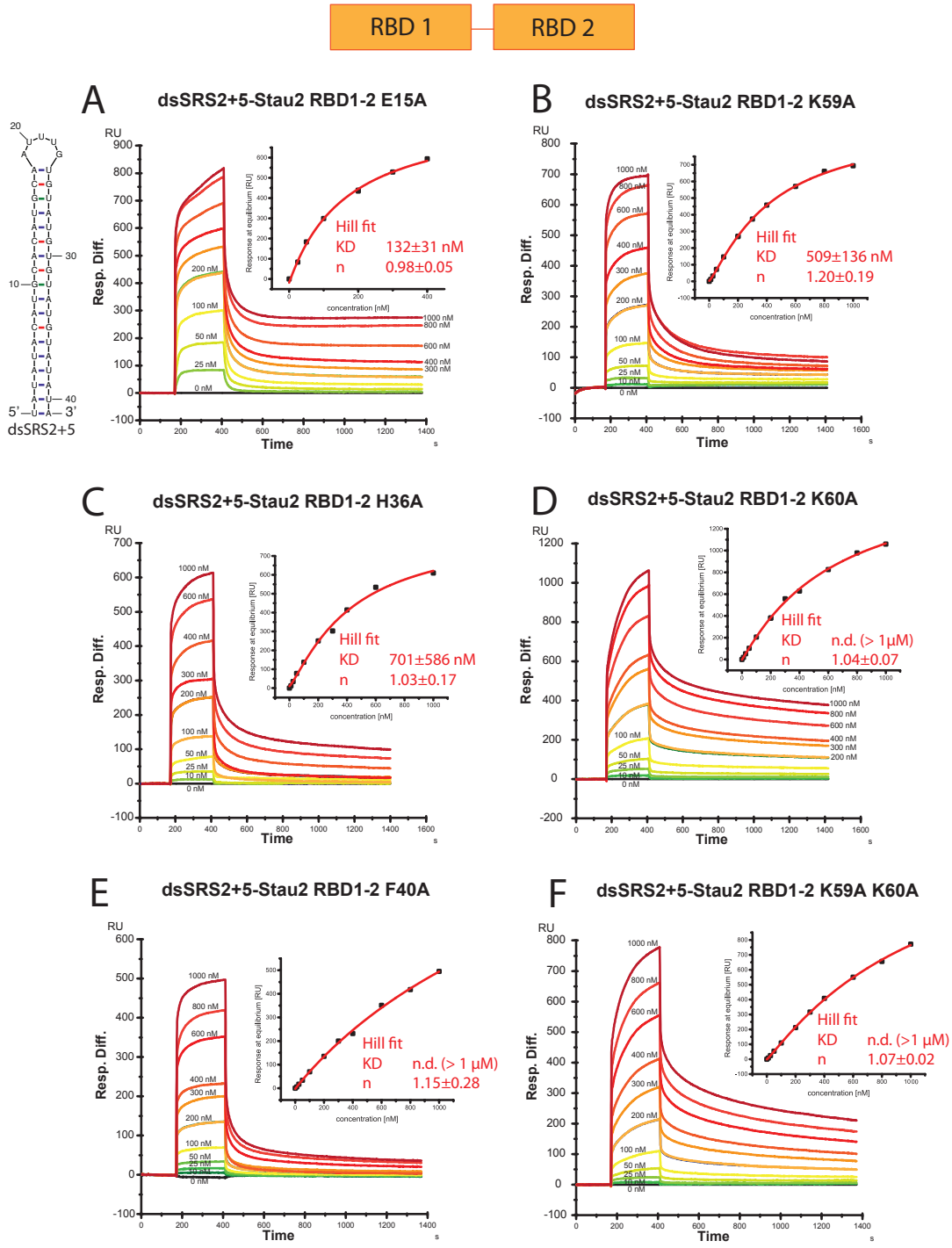

Figure 35: SPR sensorgrams and steady-state binding curves of Stau2 RBD1 mutants (in context of the tandem-domain RBD1-2 binding to dsSRS2+5 RNA. Mutants Stau2 RBD1-2 **A)** E15A, **B)** K59A, **C)** H36A, **D)** K60A, **E)** F40A and **F)** K59A K60A bind SRS2+5 transiently with fast kinetics. The steady-state binding curves are described by Hill-fits with Hill coefficients n ≈ 1, indicating non-cooperative binding.

When the RBD1 mutations in context of the RBD1-2 fragment were tested for binding to SRS3, the mutations H36A, F40A, K59A and K59A K60A behaved again

very similar to their binding to dsSRS2+5, confirming that RNA-binding activity of RBD1 is abolished by these mutations. The observed K_Ds of RBD1-2 H36A and K59A (Figure 36 B and C) are similar to that of RBD2 alone. RBD1-2 F40A and K59A K60A bind with lower affinity and K_Ds outside the tested concentration range. RBD1-2 E15A binds to SRS3 RNA similar to the wt protein, showing two-site binding with K_D1=15±11 nM and K_D2=405±260 nM (Figure 36 A), indicating that RNA-binding activity of RBD1 is not corrupted by this mutation. Also RBD1-2 K60A bound SRS3 RNA, unlike dsSRS2+5 RNA, similar as wt protein (Figure 36 D). This mutation possibly has a less drastic effect that can be compensated for by the longer RNA.

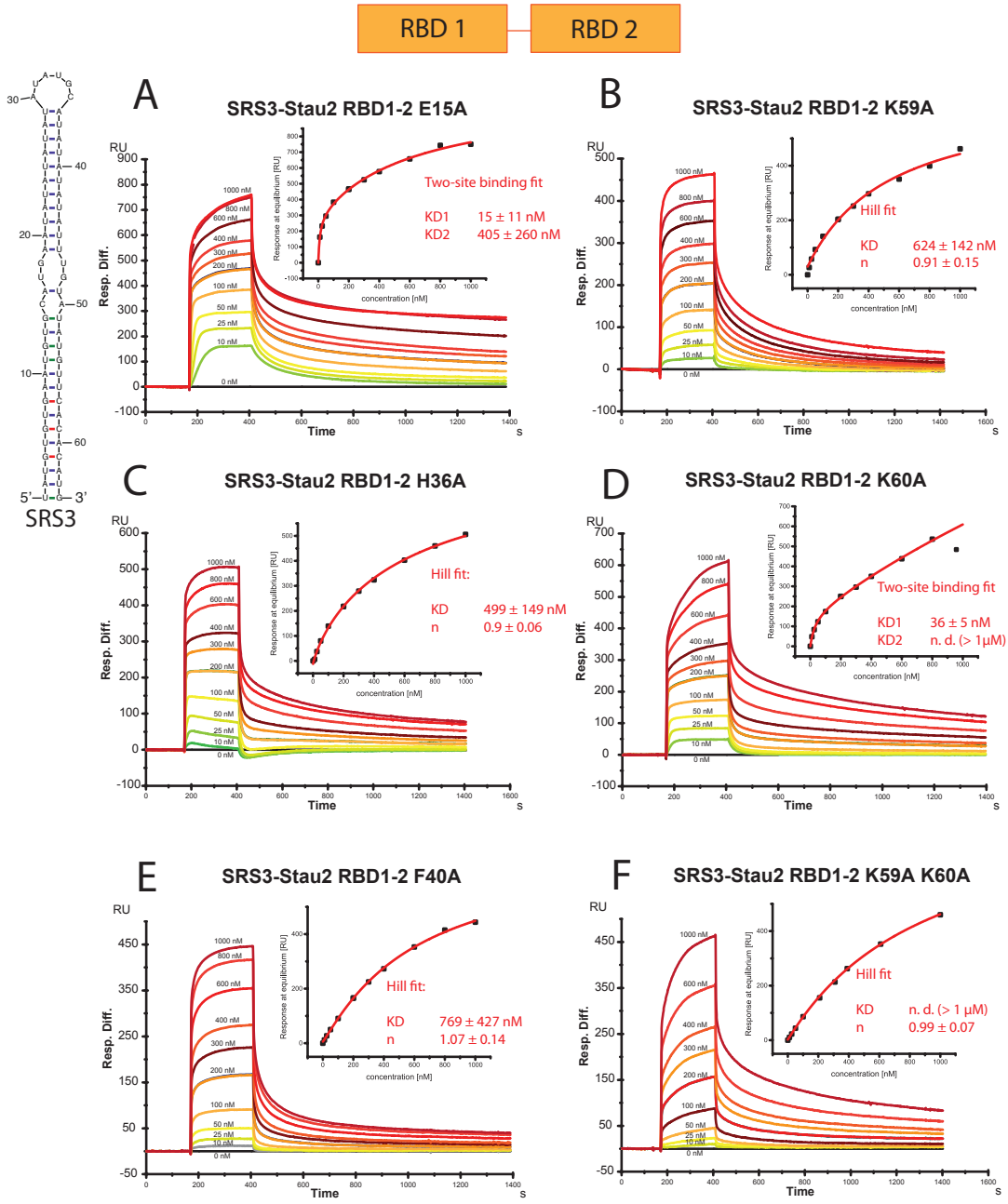

Figure 36: SPR sensorgrams and steady-state binding curves of Stau2 RBD1 mutants (in context of the tandem-domain RBD1-2) binding to SRS3 RNA. Mutants Stau2 RBD1-2 **B)** K59A, **C)** H36A, **E)** F40A and **F)** K59A K60A bind SRS2+5 transiently with fast kinetics. The steady-state binding curves are described by Hill-fits with Hill coefficients n ≈ 1, indicating non-cooperative binding. Mutants Stau2 RBD1-2 **A)** E15A and **D)** K60A bind similar to Stau2 RBD1-2 wt (compare Figure 31).

3.6.5.3 Mutations in RBD2 decrease RNA-binding of Stau2 RBD1-2

Next, binding of Stau2 RBD1-2 constructs harboring mutations in RBD2 were tested for binding to dsSRS2+5 RNA by SPR. All tested mutants showed strongly decreased binding to dsSRS2+5 and could no longer be fitted as a two-site binding event. Whereas Stau2 RBD1-2 E99A and F157A bound dsSRS2+5 with

steady-state K_Ds of 635±308 nM and 497±238 nM, respectively (Figure 37 A and C), binding of K106A and H169A was decreased so much that steady-state could not be reached and no binding curve could be obtained (Figure 37 B and D). Interestingly, RBD1-2 F157A showed clearly altered binding kinetics as compared to the wt protein. Both on- and off-rate are apparently decreased, pointing at a changed binding mechanism.

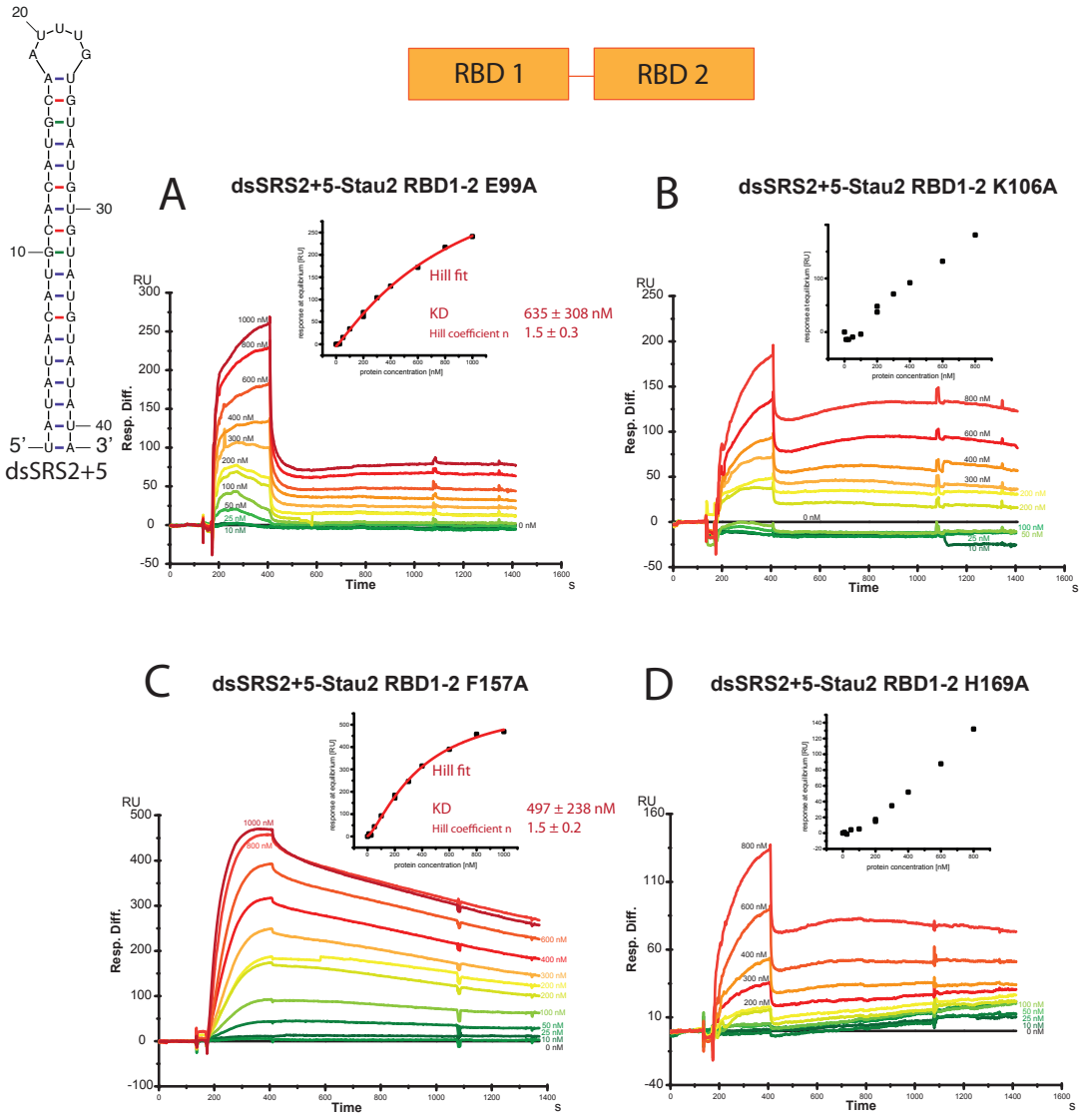

Figure 37: SPR sensorgrams of Stau2 RBD2 mutants (in context of the tandem-domain RBD1-2) binding to dsSRS2+5 RNA. Stau2 RBD1-2 **A)** E99A, **B)** K106A, **C)** F157A, **D)** H169A show decreased binding to dsSRS2+5 RNA. as compared to wt (compare Figure 30). For RBD1-2 E99A (A) and F157A (C), steady-state binding curves are shown. For RBD1-2 K106A (B) and H169A (D), steady-state could not be reached. Plots of maximum response against concentration are shown instead.

RBD2 mutations were also tested for binding to SRS3 RNA. Unlike dsSRS2+5, Stau2 RBD1-2 E99A and K106A bound SRS3 with similar properties as the wt protein (Figure 38 A and C), indicating that the effects of these mutations were rather weak and could be compensated for by the longer RNA. Binding of RBD1-2 H169A, however, was still strongly decreased so that the anticipated K_D was outside the tested concentration range and could not be determined (Figure 38 D). Binding of RBD1-2 F157A showed again altered kinetics and its affinity was decreased so much that the K_D could not be determined (Figure 38 C), thus confirming the results obtained for dsSRS2+5.

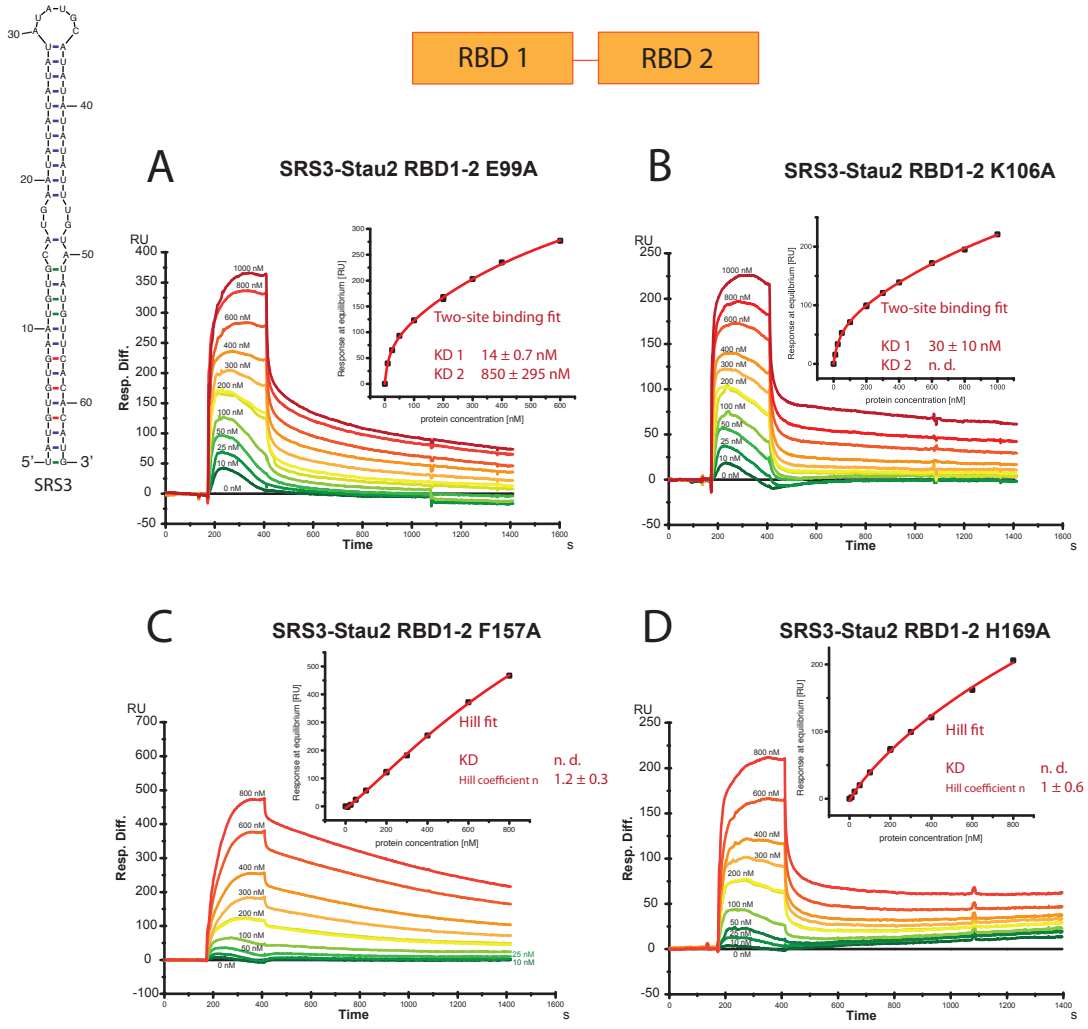

Figure 38: SPR sensorgrams and steady-state binding curves of Stau2 RBD2 mutants (in context of the tandem-domain RBD1-2) binding to SRS3 RNA. Stau2 RBD1-2 **A)** E99A, and **B)** K106A bind similar to Stau2 RBD1-2 wt. Stau2 RBD1-2 **C)** F157A and **D)** H169A show decreased binding to dsSRS2+5 RNA as compared to wt (compare Figure 31).

3.6.5.4 RBD1-2 double-mutants show strongly decreased RNA-binding activity

Based on the SPR results for the single point mutations in RBD1 and RBD2, double-mutants were designed in which the activities of both domains should be compromised. In RBD1, the mutation F40A was chosen because it had a strong effect with both tested RNAs, its resonance shifted upon RNA titration in the ^{1}H, ^{15}N-HSQC and it is conserved in dmStau. In RBD2, the mutations F157A and H169A were chosen. F157A showed altered binding kinetics and H169A had the strongest impaired RNA-binding of all tested RBD2 mutations. Both residues are conserved in dmStau. Again, correct folding of double-mutant proteins was verified by CD spectroscopy and thus any effects by protein misfolding excluded (see Figure S 3, appendix).

When the double-mutants Stau2 RBD1-2 F40A F157A and F40A H169A were tested by SPR, both showed poor binding to both dsSRS2+5 and SRS3 RNA. As shown in Figure 39, total response units upon binding were strongly decreased and steady states could not be reached even during analyte injection of 240 seconds. The effect seems to be even stronger for F40A H169A than for F40A F157A. These results confirmed that the tested double mutations indeed strongly compromised RNA-binding activity of Stau2 RBD1-2.

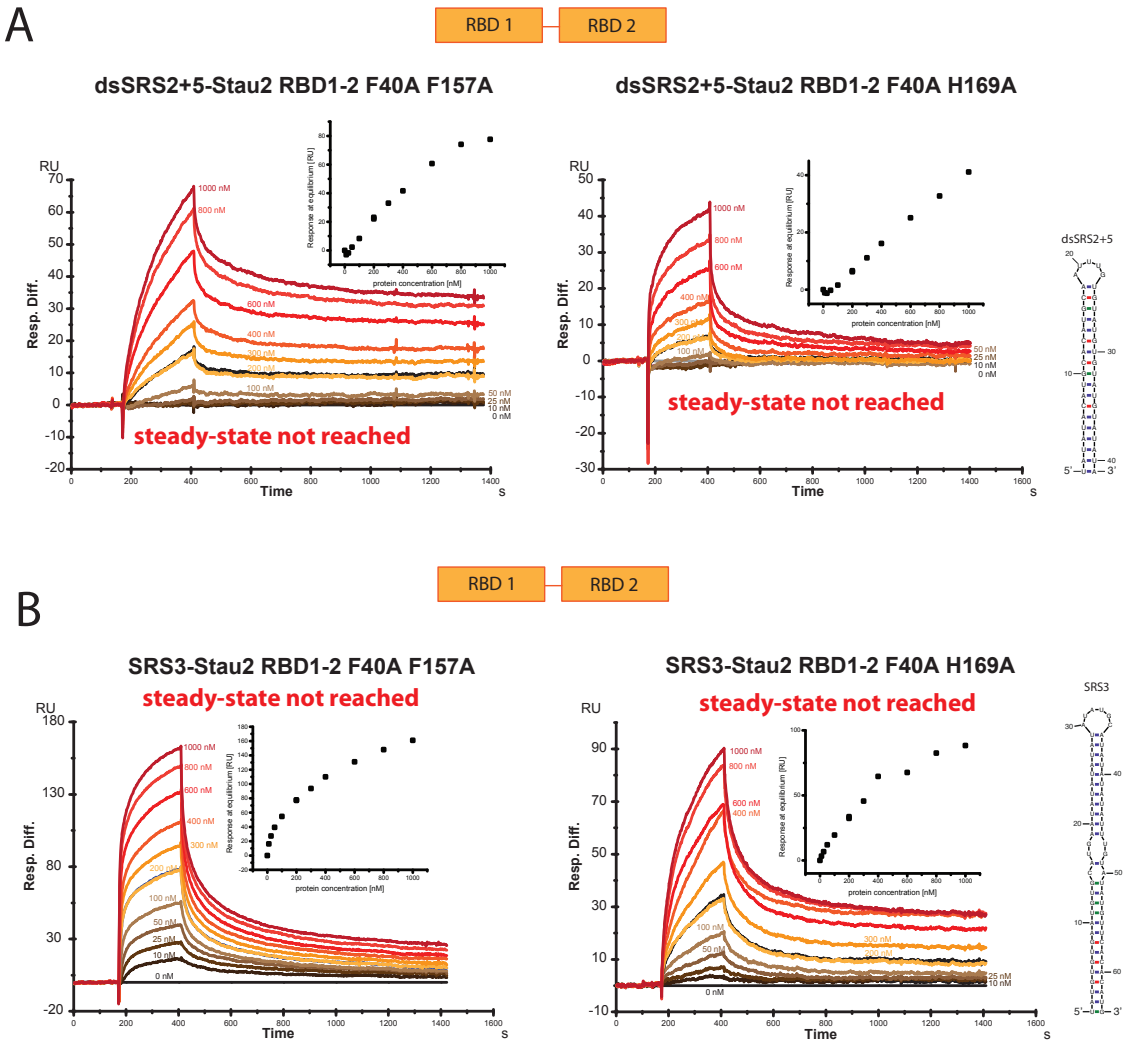

Figure 39: SPR sensorgrams and plots of maximum response against protein concentration of Stau2 RBD1-2 double-mutants binding to SRS RNA. Binding to **A)** dsSRS2+5 and **B)** SRS3 is strongly decreased as compared to Stau2 RBD1-2 wt (compare Figures 30 and 31) so that steady states could not be reached.

The results of the SPR experiments with Stau2 RBD1-2 mutant proteins are summarized in Table 18 and Table 19.

Table 18: Stau2 RBD1-2 mutant-binding to dsSRS2+5 RNA

Stau2 RBD1-2 protein	binding	kinetics	K_D1 [nM]	K_D2 [nM]	Hill coefficient
wt	two-site	transient	130 ± 30	n.d. (>1000)	-
C11S C140S	two-site	transient	27 ± 21	551 ± 261	-
E15A	Hill	transient	-	132 ± 31	1 ± 0.1
H36A	Hill	transient	-	701 ± 386	1 ± 0.2
F40A	Hill	transient	-	n.d. (>1000)	1.2 ± 0.1
K59A	Hill	transient	-	509 ± 136	1.2 ± 0.2
K60A	Hill	transient	-	n.d. (>1000)	1 ± 0.1
K59A K60A	Hill	transient	-	n.d. (>1000)	1 ± 0.02
E99A	Hill	transient	-	635 ± 308	1.5 ± 0.3
K106A	no fit	transient	-	n.d. (>1000)	-
F157A	Hill	stable	-	497 ± 238	1.5 ± 0.2
H169A	no fit	transient	-	n.d. (>1000)	-
F40A F157A	no fit	stable	-	-	-
F40A H169A	no fit	transient	-	-	-

Table 19: Stau2 RBD1-2 mutant-binding to SRS3 RNA

Stau2 RBD1-2 protein	binding	kinetics	K_D1 [nM]	K_D2 [nM]	Hill coefficient
wt	two-site	transient	25 ± 8	n.d. (>1000)	-
C11S C140S	two-site	transient	7 ± 3	555 ± 301	-
E15A	two-site	transient	15 ± 11	406 ± 359	-
H36A	Hill	transient	-	499 ± 149	0.9 ± 0.06
F40A	Hill	transient	-	769 ± 427	1 ± 0.1
K59A	Hill	transient	-	624 ± 142	0.9 ± 0.2
K60A	two-site	transient	36 ± 5	n.d. (>1000)	-
K59A K60A	Hill	transient	-	n.d. (>1000)	1 ± 0.1
E99A	two-site	transient	14 ± 0.7	850 ± 295	-
K106A	two-site	transient	30 ± 10	n.d. (>1000)	-
F157A	Hill	stable	-	n.d. (>1000)	1.2 ± 0.2
H169A	Hill	transient	-	n.d. (>1000)	1 ± 0.6
F40A F157A	no fit	transient	-	-	-
F40A H169A	no fit	transient	-	-	-

3.6.5.5 Mutation of Stau2 RBDs 1 and 2 in the context of RBD1-4 resembles binding by RBD3-4 alone

To confirm that Stau2 RBD1-2 contribute to RNA-binding of the full-length protein, SPR experiments with Stau2 RBD1-4 harboring the identified RBD1 and RBD2 double-mutations were performed. RBD1-4 F40A F157A bound both RNAs weaker than wt RBD1-4 so that steady state could not be reached during analyte

injection (Figure 40). This is consistent with the previous observation that the mutant F157A in context of the tandem-domain RBD1-2 has altered RNA-binding kinetics but binding is not completely abolished. Additionally, kinetic fits to the binding curves obtained at 1000 nM protein were performed. The best description of the data was obtained using a bivalent analyte model for these fits. The bivalent analyte fit shows that for RBD1-4 F40A F157A, the on-rate ka_1 is in the same order of magnitude as for the wt protein with both RNAs dsSRS2+5 and SRS3. The off-rate kd_1 is ~10-fold increased for binding to SRS3 but not to dsSRS2+5 (Figure 40 B and Figure 41 B).

In contrast to wt RBD1-4, Stau2 RBD1-4 F40A H169A bound both dsSRS2+5 and SRS3 RNAs with fast binding kinetics resembling the transient binding by RBD3-4. Also, the steady-state binding curve is well described by a two-site binding fit with K_Ds resembling those of RBD3-4. A bivalent analyte fit to the binding curve at 1000 nM shows that the rate-constants ka_1 and kd_1 are both ~10-fold increased for F40A F169A as compared to the wt protein (Figure 40 C and Figure 41 C). Taken together, this indicates that in RBD1-4 F40A H169A RNA-binding is mediated solely by RBD3-4.

The Stau2 mutant F40A H169A is thus well-suited for *in vivo* studies to test the function of the domains RBD1-2.

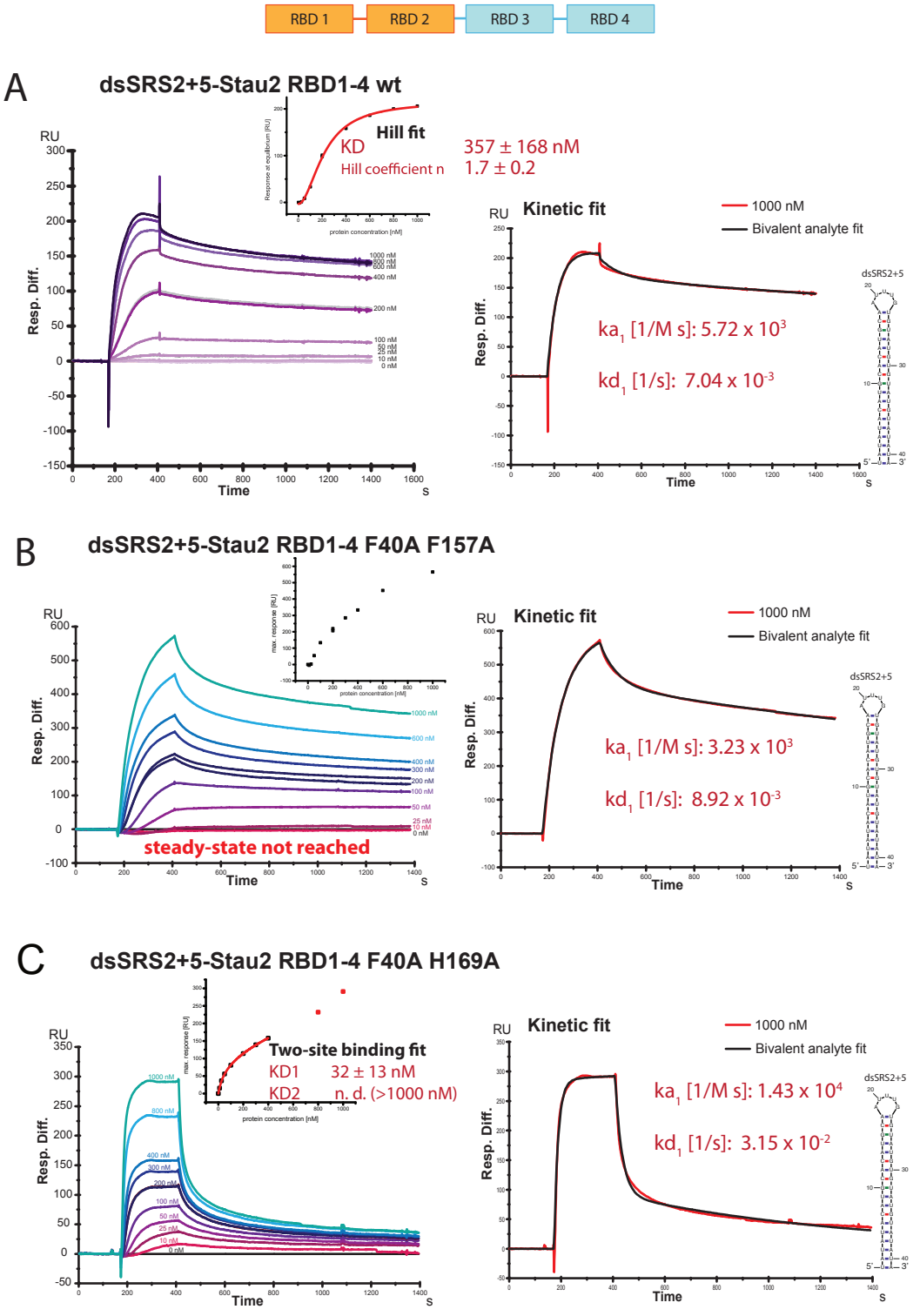

Figure 40: SPR results for Stau2 RBD1-4 wt and double-mutants binding to dsSRS2+5. Sensorgrams with steady-state binding curves (left) and exemplary kinetic fits (bivalent analyte fit) at 1000 nM protein concentration (right) are shown. A) Stau2 RBD1-4 wt. **B)** Stau2 RBD1-4 F40A F157A; plots of maximum response against protein concentration are shown instead of steady-state binding curve because steady-state was not reached. The kinetic fit shows that on- and off-rates (ka_1 and kd_1, respectively) are in the same order of magnitude as for the wt protein. **C)** Stau2 RBD1-4 F40A H169A. The kinetic fit shows that both ka_1 and kd_1 are ~10-fold increased as compared to wt.

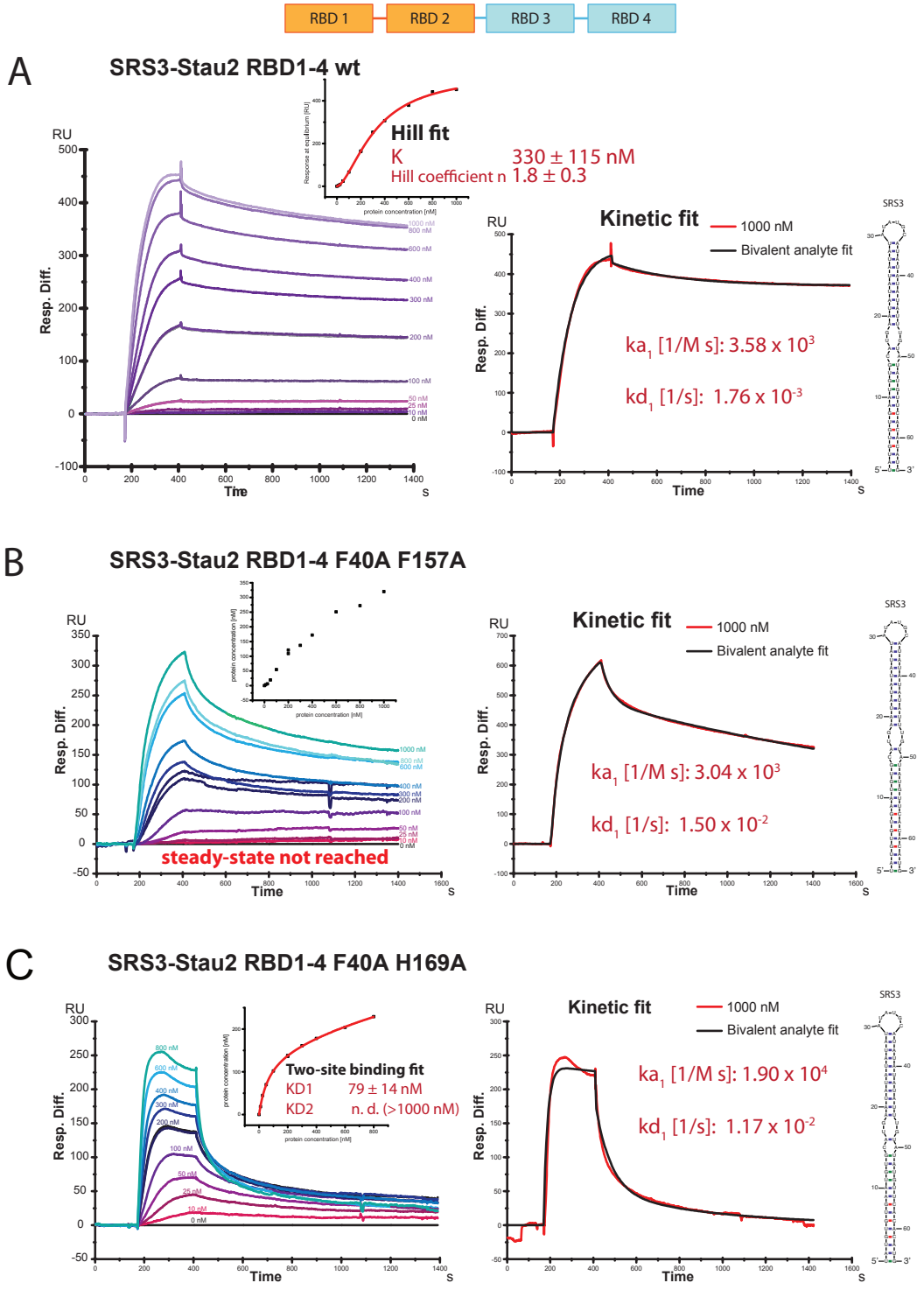

Figure 41: SPR results for Stau2 RBD1-4 wt and double-mutants binding to SRS3. Sensorgrams with steady-state binding curves (left) and exemplary kinetic fits (bivalent analyte fit) at 1000 nM protein concentration (right) are shown. A) Stau2 RBD1-4 wt. **B)** Stau2 RBD1-4 F40A F157A; plots of maximum response against protein concentration are shown instead of steady-state binding curve because steady-state was not reached. The kinetic fit shows that the on-rate ka_1 is in the same order of magnitude as for the wt protein, whereas the off-rate kd_1 is ~10-fold increased. **C)** Stau2 RBD1-4 F40A H169A. The kinetic fit shows that both ka_1 and kd_1 are ~10-fold increased as compared to wt.

The results of the SPR experiments with Stau2 RBD1-4 mutant proteins are summarized in Table 20 and Table 21.

Table 20: Stau2 RBD1-4 mutant-binding to dsSRS2+5 RNA

Stau2 RBD1-4 protein	binding	kinetics	K_D1 [nM]	K_D2 [nM]	Hill coefficient
RBD1-4	Hill	stable	-	330 ± 148	1.6 ± 0.2
F40A F157A	no fit	stable	-	n.d.	-
F40A H169A	two-site	transient	32 ± 13	n.d. (>1000)	-

Table 21: Stau2 RBD1-4 mutant-binding to SRS3 RNA

Stau2 RBD1-4 protein	binding	kinetics	K_D1 [nM]	K_D2 [nM]	Hill coefficient
RBD1-4	Hill	stable	-	287 ± 127	1.7 ± 0.4
F40A F157A	no fit	stable	-	n.d.	-
F40A H169A	two-site	transient	79 ± 14	n.d. (>1000)	-

3.6.6 Stochiometry and oligomeric state of the Stau2 RBD1-2-RNA complex

3.6.6.1 Static light scattering (SLS) reveals several possible stoichiometries of Stau2 RBD1-2-RNA complexes

The performed SPR and crystallization experiments indicated binding of multiple Stau2 domains to one RNA molecule and a previous study reported Stau2 to dimerize *in vivo* (Park et al., 2013). Thus, SLS was measured as described in section 2.10.10 to assess the stoichiometry of the Stau2 RBD1-2-RNA complex in solution. For this, Stau2 RBD1-2 was first mixed with SRS2 RNA at a 1:1 ratio and a total concentration of 4.25 mg/mL and separated on a 10/300 Superdex200 Increase GL column prior to SLS measurement. Several runs with the same sample were performed, which yielded different results each time. While in the first run, the complex dissociated completely and eluted in two peaks with molecular weights corresponding to Stau2 RBD1-2 (23 kDa) and SRS2 (10 kDa), respectively, a second run identified a peak with a MW of 36 kDa, close to the theoretical 33 kDa of a 1:1 Stau2 RBD1-2-SRS2 complex. In a third run, an additional peak with MW of 53 kDa, possibly resembling a 2:1 complex (theoretical MW= 56 kDa). Taken together, this indicates that the complex stoichiometry changes over time, possible due to oligomerization. In all runs, a peak at ~10-12 kDa, probably corresponding to free SRS2 RNA, was detected. An

exemplary experiment, in which several complex species were detected, is shown in Figure 42.

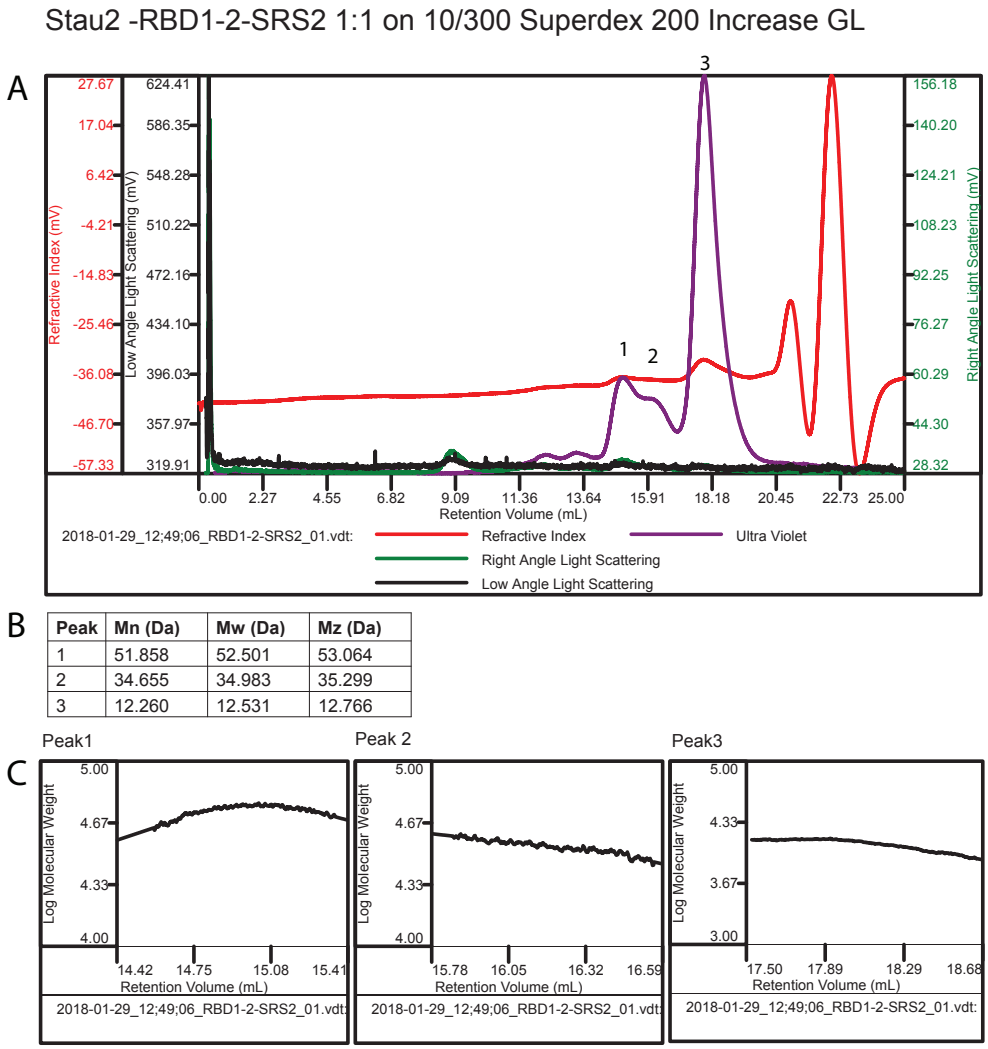

Peak	Mn (Da)	Mw (Da)	Mz (Da)
1	51.858	52.501	53.064
2	34.655	34.983	35.299
3	12.260	12.531	12.766

Figure 42: SLS measurements of Stau2 RBD1-2-SRS2 complex mixed 1:1 at 4.25 mg/mL after SEC on 10/300 Superdex200 Increase GL. A) SEC chromatogram monitored by UV, refractive index (RI), right angle light scattering (RALS) and low angle light scattering (LALS). **B)** Calculated MWs for peaks 1, 2 and 3. Distribution is described by Mw = weight average (average molecular weight), Mn = number average (weights low molecular weights), Mz = z-average (weights high molecular weights). **C)** Plotted MW distribution over the peaks 1, 2 and 3. The sample elutes in three peaks with average MWs of 53 kDa, 35 kDa and 13 kDa, corresponding to a 2:1 protein-RNA complex ($MW_{theoretical}$ = 56 kDa), a 1:1 complex ($MW_{theoretical}$ = 33 kDa) and free SRS2 RNA ($MW_{theoretical}$ = 10 kDa), respectively. The strong RI peak at the end of the run corresponds to DTT from the buffer.

Similar results were obtained when Stau2 RBD1-2 was mixed with SRS2+5/GAAAinsert RNA. Since longer RNA was bound with higher affinity, using a longer RNA was expected to prevent complex dissociation. From crystallization experiments, a 3:1 ratio was suspected of Stau2 RD1-2 with this RNA. In several runs on 5/150 Superdex Increase 200 GL, peaks with MWs

corresponding to 1:1 (~40 kDa), 2:1 (~63 kDa) and 3:1 (~86 kDa) ratios of Stau2 RBD1-2 to RNA were observed as well as free protein and RNA (theoretical MW = 17 kDa) depending on the exact mixing ratio and different high molecular weight species ranging from 116 to 677 kDa, indicating the presence of unspecific oligomers. An exemplary experiment is shown in Figure 43. Taken together, these experiments with Stau2 RBD1-2-RNA complexes indicated that several stochiometries are possible in solution depending on the availability of protein and RNA and that the complexes can form oligomers in a time-dependent manner.

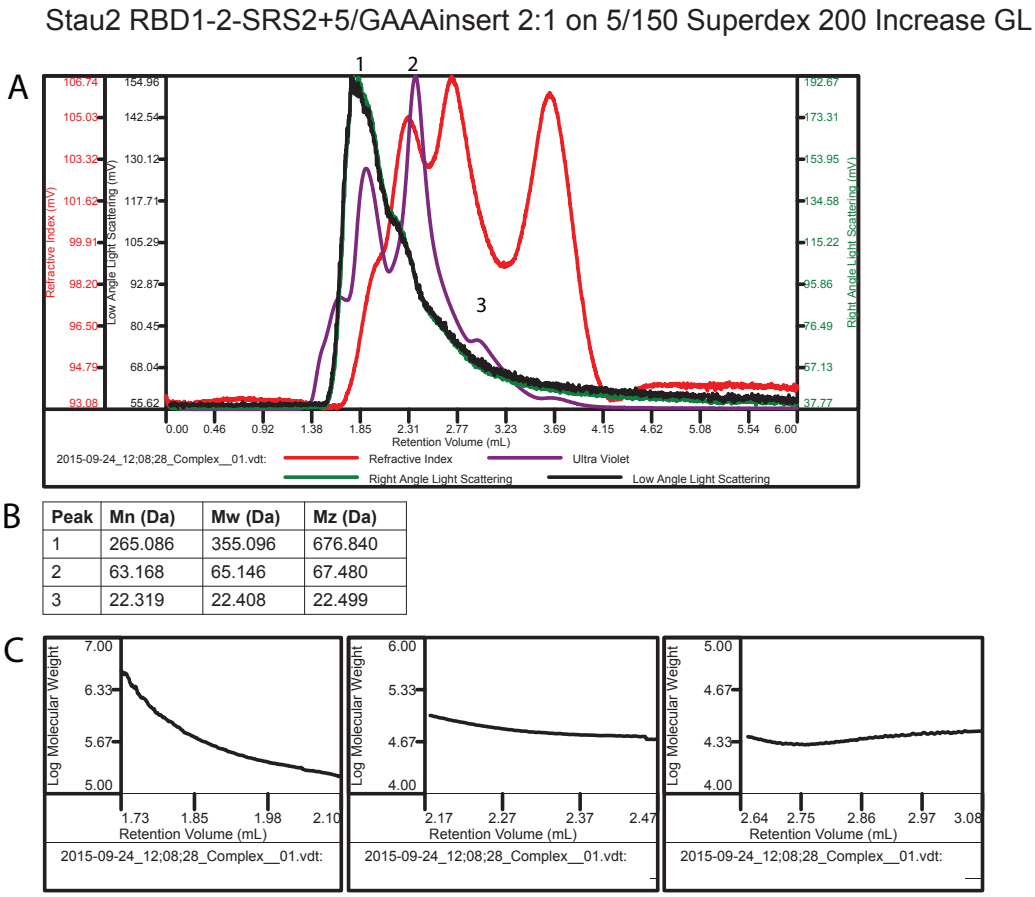

Peak	Mn (Da)	Mw (Da)	Mz (Da)
1	265.086	355.096	676.840
2	63.168	65.146	67.480
3	22.319	22.408	22.499

Figure 43: SLS measurements of Stau2 RBD1-2-SRS2+5/GAAA insert complex mixed 2:1 at 3.3 mg/mL after SEC on 5/150 Superdex200 Increase GL. A) SEC chromatogram monitored by UV, refractive index (RI), right angle light scattering (RALS) and low angle light scattering (LALS). **B)** Calculated MWs for peaks 1, 2 and 3. Distribution is described by Mw = weight average (average molecular weight), Mn = number average (weights low molecular weights), Mz = z-average (weights high molecular weights). **C)** Plotted MW distribution over the peaks 1, 2 and 3. The sample elutes in three peaks with average MWs of 355 kDa, 65 kDa and 22 kDa, corresponding to non-specific higher order oligomers (high poldispersity as shown by Mn and Mz), a 2:1 complex ($MW_{theoretical}$ = 63 kDa) and free Stau2 RBD1-2 protein ($MW_{theoretical}$ = 23 kDa), respectively.

Free, HisSUMO-tagged full-length Stau2 eluted from a 10/300 Superdex200 Increase GL column in two peaks with MWs of 76 and 72 kDa, indicating a monomer (theoretical MW = 75 kDa) accompanied by the slightly smaller degradation product regularly observed during protein purification (Figure 44). A dimeric species was not observed, neither oligomerization of the protein. However, a time-course experiment was not performed with full-length Stau2 and thus time-dependent oligomerization cannot be ruled out.

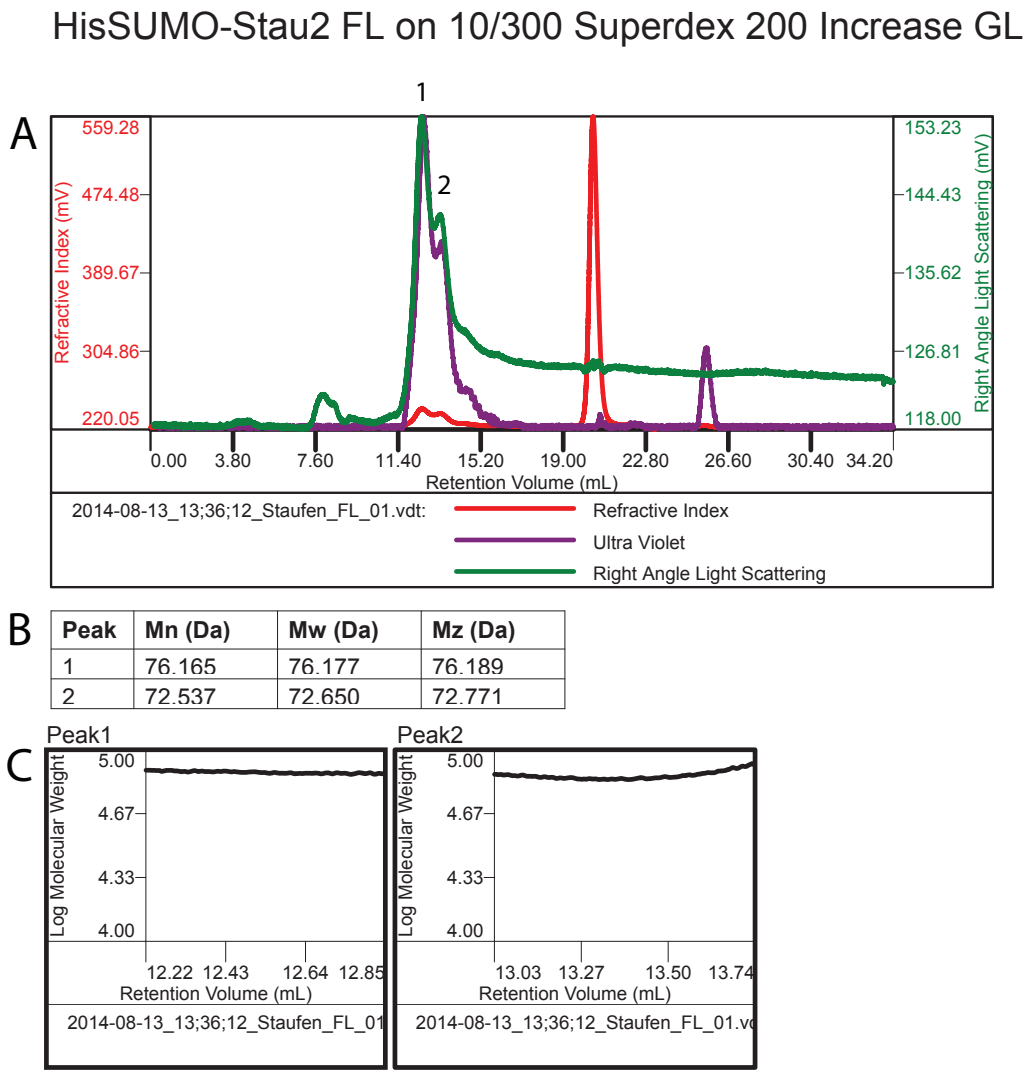

Figure 44: SLS measurements of HisSUMO-Stau2 FL after SEC on 10/300 Superdex200 Increase GL. A) SEC chromatogram monitored by UV, refractive index (RI) and right angle light scattering (RALS). **B)** Calculated MWs for peaks 1 and 2. Distribution is described by Mw = weight average (average molecular weight), Mn = number average (weights low molecular weights), Mz = z-average (weights high molecular weights). **C)** Plotted MW distribution over the peaks 1 and 2. The protein elutes in two peaks with molecular weights of 76 kDa and 72 kDa, corresponding to a monomer. The theoretical molecular weight of HisSUMO-tagged Stau2 FL is 75 kDa. The protein co-purified with a slightly smaller degradation product corresponding to peak 2.

3.6.6.2 Stau2 RBD1-2 oligomerizes over time

To monitor whether Stau2 RBD1-2-RNA complexes indeed oligomerize over time (as indicated by the results of the SLS measurements), a Stau2 RBD1-2-SRS2+5/GAAAinsert RNA complex's particle size distribution in solution was monitored over time by dynamic light scattering (DLS) measurements as described in section 2.10.11. For this purpose, freshly SEC-purified Stau2 RBD1-2 was mixed with SRS2+5/GAAAinsert RNA at a 3:1 ratio and final concentration of 1 mg/mL and DLS measured at several time points. Immediately after mixing (t=0), 96 % of the total particle mass populated the main peak with a radius r= 3.235 nm and quite high polydispersity of 59.1 %. However, already after 1 h, particle radius and polydispersity had increased to r=5.276 nm and 64.8 %, respectively. 93.4 % of total mass populated this peak. After 2 h, this fraction had decreased to 61.3 % with r=6.930 and 65.8 % polydispersity. After incubation for 1 day at RT, the main peak with r=15.274 constituted only 56.2 % of total mass. Data are shown in Figure 45. In summary, particle radius and polydispersity increased over time whereas an increasing fraction of the particle mass populated large species, probably large oligomers and aggregates. Taken together, this indicates that the Stau2-RNA complex forms unspecific, large oligomers over time.

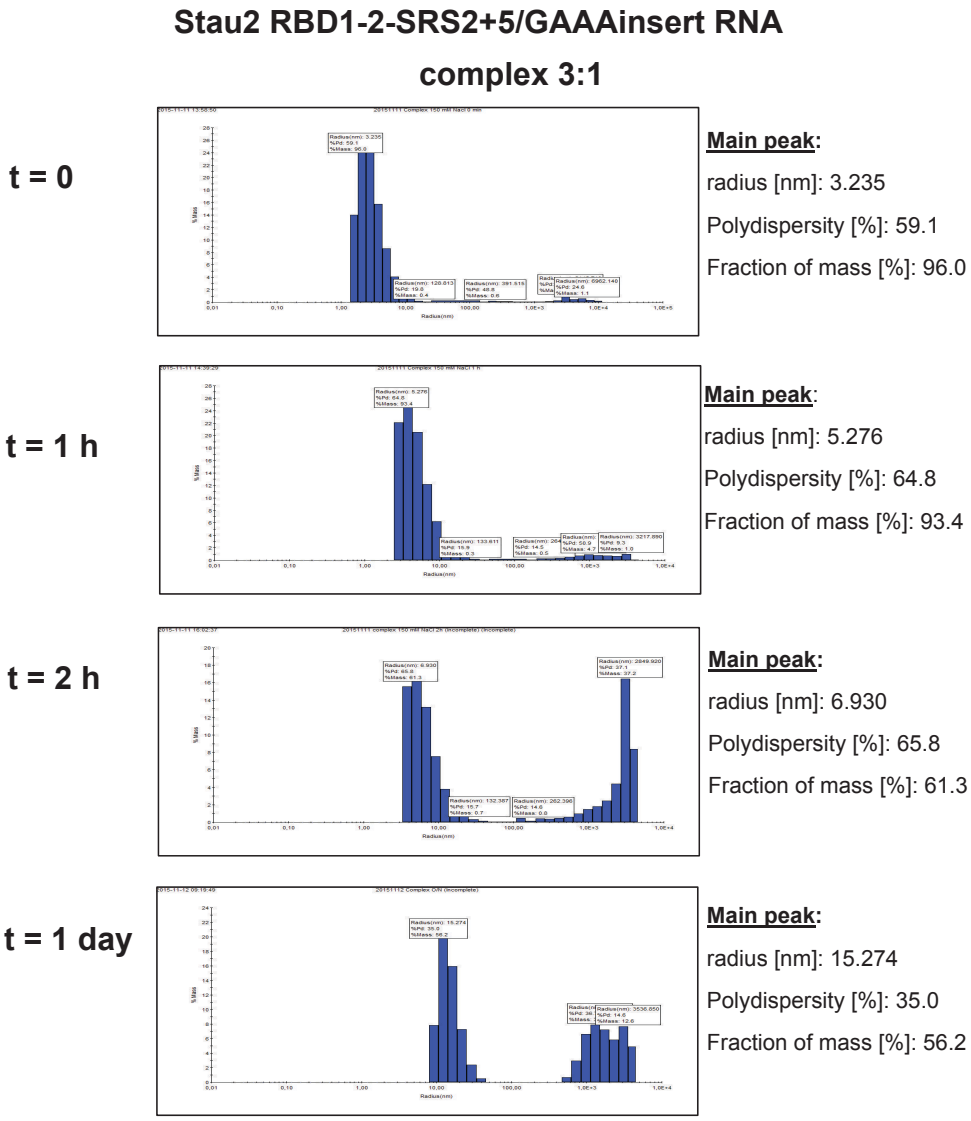

Figure 45: DLS measurements with Stau2 RBD1-2-SRS2+5GAAAinsert complex. Time course measurements were performed as indicated. At each time point t, a measurement with 10 acquisitions (5 s each) was performed. While radius and polydispersity of the main peak increase over time, the fraction of mass in the main peak decreases and moves into larger particles.

To test whether this oligomerization can be prevented by optimization of the buffer conditions, Stau2 RBD1-2 alone at 1 mg/mL was monitored over time by DLS in 150 mM, 250 mM and 350 mM NaCl. At t=0, about 99.9–100 % of the protein populated the main peaks with polydispersities of 26-29 % in all tested salt concentrations. Whereas there were no significant changes after 1 h in 250 mM or 350 mM NaCl, the main particle peak in 150 mM NaCl had already decreased to 89 % with 65.3 % polydispersity. After 2 h, particle size distribution was multimodal not only in 150 mM NaCl but also in 250 mM NaCl.

In 350 mM NaCl, the polydispersity of the main peak, which still consisted of 100 % particle mass, had increased to 41.2 %. After o/n incubation at RT, also the 350 mM NaCl sample had become multimodal, indicating that high salt can slow down the oligomerization of Stau2 RBD1-2 but not prevent it. Data are shown Figure 46.

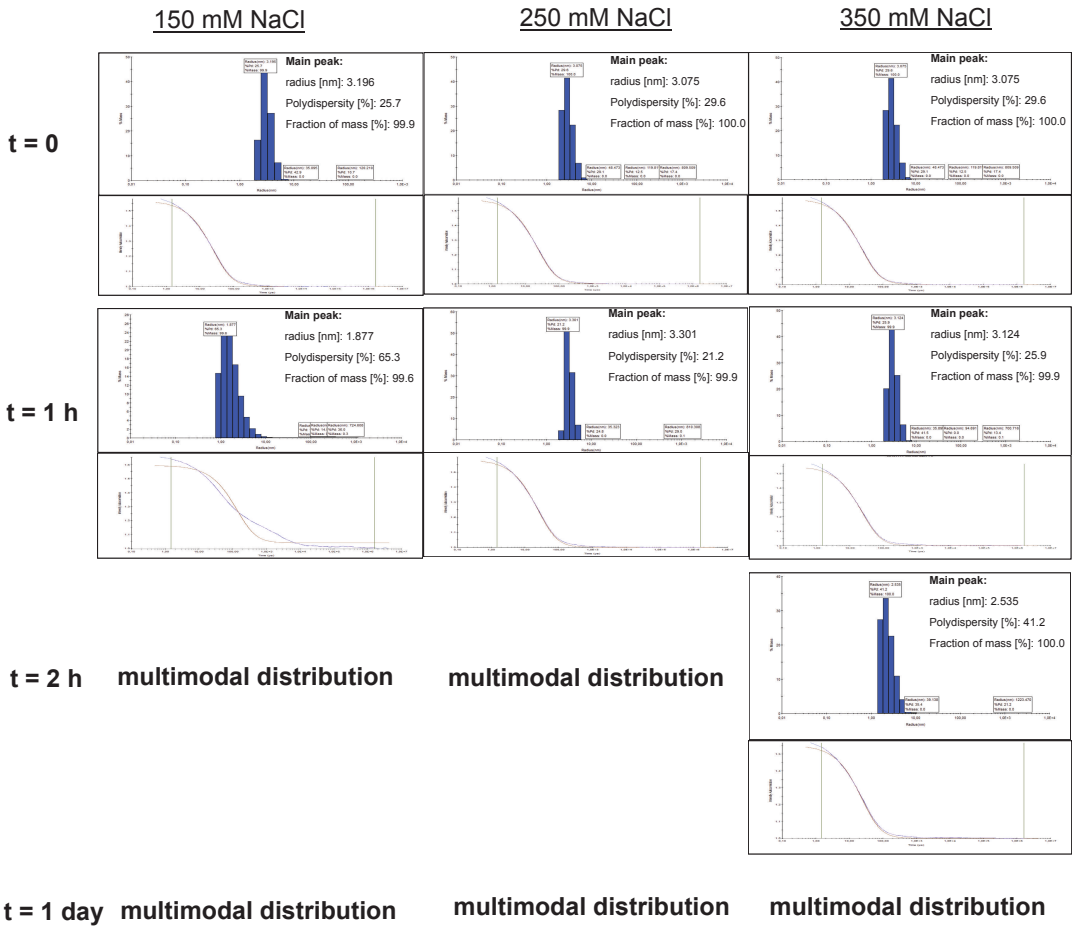

Figure 46: DLS measurements with Stau2 RBD1-2. Time course measurements were performed in buffers with different salt concentrations as indicated. At each time point t, a measurement with 10 acquisitions (5 s each) was performed. With 150 mM and 250 mM NaCl, the sample shows multimodal particle size distribution after 2h. With 350 mM this is observed after 1 day.

3.7 Stau2 functions as an RNA chaperone

After observing that Stau2 binds unspecifically to all dsRNAs *in vitro*, it was tested whether Stau2 has a general function related to RNA double-strand formation or RNA-folding. For this purpose, TAR(+)/TAR(-) annealing assays (Guichard et al., 2011) were performed. In these assays, double-strand formation of a radio-labeled 56 nt-long TAR(-) strand DNA with an unlabeled 56 nt-long TAR(+) strand DNA is monitored upon protein titration. The controls did not

contain any protein. In the positive control, annealing was forced by heating to 72 °C followed by snap-cooling on ice. ssDNA and dsDNA were resolved by native PAGE. As shown in Figure 47, both Stau2 tandem-domains RBD3-4 and RBD1-2 enhanced double-strand formation of TAR DNA in a protein concentration-dependent manner. With RBD3-4, all DNA was annealed at 1000 nM protein concentration. The effect of RBD1-2 is approximately 4-fold stronger as all DNA is annealed already at 250 nM protein.

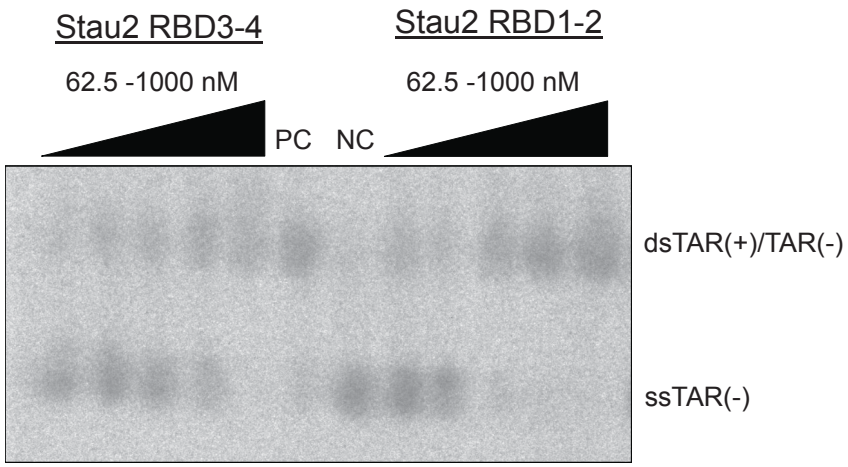

Figure 47: TAR(+)/TAR(-) annealing assay with Stau2 tandem-domains. Radio-labeled TAR(-) was incubated with TAR(+) and incubated at 37 °C with the indicated concentrations of protein. ssDNA and dsDNA were resolved by 8 % native PAGE. Positive control and negative control are shown in lanes 6 and 7, respectively. Both Stau2 tandem-domains RBD3-4 (lanes 1-5) and RBD1-2 (lanes 8-12) facilitate strand annealing with increasing concentrations. 250 nM Stau2 RBD1-2 were sufficient for complete annealing whereas 1000 nM Stau2 RBD3-4 were required for comparable annealing activity.

Next, it was tested whether RNA-binding mutations in RBD1-2 have an effect on its ability to anneal DNA double-strands. The double-mutants F40A F157A and F40A H169A were compared to wt Stau2 RBD1-2. Whereas F40A F157A showed slightly improved annealing activity over wt protein, the activity of F40A H169A was clearly decreased with only partially annealed DNA at 500-1000 nM concentration (Figure 48). These observations are consistent with the effects of these mutants on RNA-binding described above (see section 3.6.5.4). Whereas in F40A F157A, RNA binding is kinetically stabilized, binding is strongly decreased in F40A H169A, possibly explaining the effects on nucleic acid annealing.

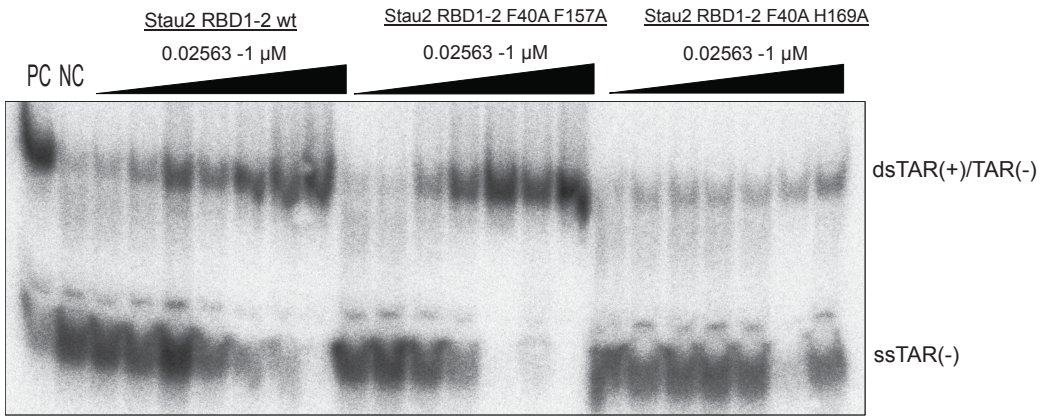

Figure 48: TAR(+)/TAR(-) annealing assay with Stau2 RBD1-2 wt and mutants. Radio-labeled TAR(-) was incubated with TAR(+) and incubated at 37 °C with the indicated concentrations of protein. ssDNA and dsDNA were resolved by 8 % native PAGE. Positive control and negative control are shown in lanes 1 and 2, respectively. Stau2 RBD1-2 wt (lanes 3-8), F40A F157A (lanes 9-15) and F40A H169A (lanes 16-22) facilitate strand annealing with increasing concentrations. The effect is about 2-fold increased over wt protein for RBD1-2 F40A F157A and >4-fold decreased for F40A H169A.

3.7.1 Cloning of Stau2 RBD1-2 double-mutants for functional *in vivo* studies

As described above, it could be shown by mutational analysis that the tandem-domain Stau2 RBD1-2 contributes to the RNA-binding activity of Stau2 (see section 3.6.5.5). Next, it should be tested whether this contribution is important for Stau2 protein function *in vivo*. For this, full-length Stau2 wt, F40A F157A and F40A H169A were cloned as rsEGFP2 fusions in *D. melanogaster* transgenesis vectors to be injected into the pole plasm of early stage embryos and integration into germ-line cells. Genomic integration should allow for Stau2 expression in dmStau-deficient *Drosophila* oocytes and detection of protein localization by super-resolution microscopy. Two sets of vectors were cloned, in which expression was under the control of either an inducible UASp promotor or a constitutive Hsp83p promotor. The vectors harbored an attB integration site for B/P type integration into a defined attP landing site in the *Drosophila* genome. With these vectors, it should be possible to test whether Stau2 can rescue *osk* localization in dmStau null mutant oocytes and whether this rescue is compromised by RBD1-2 mutation (see chapter 1.1 for details on *osk* localization).

Furthermore, dmStau harboring the described analogous mutations (dmStau F343A F533A and F343A H545A) were cloned in the same vectors to test for functional conservation to Stau2. For details on the cloning procedure, see section 2.8.4.

In vivo experiments are performed by Imre Gaspar (group of Anne Ephrussi, Developmental Biology Unit, European Molecular Biology Laboratory) and currently on-going.

4 Discussion

4.1 Characterization of the interaction between Stau2 and *Rgs4*

Despite the importance of the brain-specific Stau2 (Heraud-Farlow and Kiebler, 2014), its molecular action is little understood and how its specificity is achieved remains to be elucidated. Various *in vivo* experiments identified specific sets of target RNAs (Furic et al., 2008, Kusek et al., 2012, Heraud-Farlow et al., 2013). However, it is not understood how these targets are recognized. In this work, novel insights into RNA-binding by Stau2 were obtained, in particular with regards to the interplay of its dsRNA-binding domains. This allows the proposal of a model of structure-specific RNA recognition by Stau2.

4.1.1 Assessment of Stau2-binding to *Rgs4* 3'UTR and to predicted SRS RNAs

In vivo studies had previously identified *Rgs4* as a target of regulation by Stau2 in neurons and two potential SRSs had been predicted in its 3'UTR (Heraud-Farlow et al., 2013).

The here presented work clearly confirmed that Stau2 can directly bind *Rgs4* 3'UTR as well as the proposed SRSs. However, this interaction appeared unspecific and not exclusive *in vitro* because *Rgs4* 3'UTR sequences in which the SRSs were deleted were bound without significant changes in affinity. Furthermore unrelated stem-loop RNAs of comparable length were bound equally well compared to the isolated SRSs. Sequence-unspecific binding by dsRBD-containing proteins was reported before (see section 1.3.4), thus sequence-specificity was not expected. The crystal structure of SRS2 furthermore showed that the predicted SRSs do not adopt any distinguishing structures but form simple A-form stem-loops. This argues against structure-specific recognition of SRSs by Stau2 RBDs but rather points at promiscuous binding of all dsRNA. Furthermore, elongation of the SRS2 stem improved binding by Stau2 and deletion of the SRS2 loop region did not impair binding by Stau2, consistent with recognition of simple A-form dsRNA.

From these results and from published data it cannot be clearly determined whether the predicted SRSs are indeed the physiological Stau2-binding sites of *Rgs4*. Possibly, a co-factor assists specific SRS recognition *in vivo*. Also, it is

possible that *Rgs4* 3'UTR sequences produced by *in vitro* transcription are not properly folded, for instance due to the lack of RNA chaperones or other RBPs that might bind co-transcriptionally to RNA in the nucleus, and thus do not comprise correctly folded SRSs. Furthermore, it is not clear whether *Rgs4* 3'UTR indeed adopts the predicted, SRS-containing fold *in vivo*. Secondary structures predictions for such long RNAs are inherently unreliable, thus it is possible that *Rgs4* 3'UTR does not even contain the predicted SRSs *in vivo*. The predicted SRSs have rather short stems and are therefore thermodynamically not very stable. To assess whether the predicted SRSs in the *Rgs4* 3'UTR indeed form in cells, experimental probing of its secondary structure should be performed, e.g. by Selective 2′-hydroxyl acylation analyzed by primer extension (SHAPE) (Wilkinson et al., 2006, Merino et al., 2005). To account for the possibility of wrong fold predictions, a longer, presumably more stable stem-loop from the *Rgs4* 3'UTR, termed SRS3, which was stably predicted by several available fold prediction tools, was additionally tested in this work. This SRS3, although not a perfect stem-loop with two bulges, indeed bound to Stau2 with higher affinity than the shorter SRSs. This result is in line with the observation that elongation of the stem of SRS2 improves its binding to Stau2.

Unexpectedly, not only the known active RBDs 3 and 4 were found to bind RNA. A protein fragment comprising RBDs 1 and 2 bound RNA similarly well as RBD3-4. Yet, a protein fragment containing RBD2 in addition to RBD3-4 (i.e. RBD2-4) just did not improve its RNA-binding in EMSAs. Further analysis of the RNA-binding activity of RBDs 1 and 2 by EMSA, SPR and NMR revealed that although both individual domains have RNA-binding activity, RBD1 binds much weaker and with different dynamics than RBD2 and the activity of the individual domains does not resemble the activity of the tandem-domain. This shows that the two domains act in tandem to achieve their full functionality. EMSAs showed that also RBD3 alone binds much weaker than RBD4, indicating a similar mechanism for RBD3-4. Furthermore, only when both tandem-domains or, in other words, all four RBDs 1-4 were present, stable complex formation was observed by SPR, pointing at an important role for RBD1-2 in stabilizing the RNA recognition. Furthermore, the overall saturation of RNA binding occurred at a

lower protein concentration (K_D=330 nM for SRS3) than for the tandem domains (K_{D2} > 1 µM for SRS3) (Figure 31).

Different Stau2 isoforms were reported to have different subcellular localization. Whereas Stau2^{62} locates in ribosome-free particles, Stau2^{59} and Stau2^{52} associate with ribosomes (Duchaine et al., 2002). Furthermore, nuclear shuttling of the longest Stau2 isoform Stau2^{62}, which is the only isoform containing RBD1-2, is mediated by a different mechanism than for the other isoforms, which contain a nuclear export signal due to alternative splicing of the N-terminus (Kiebler et al., 2005). RBD1-2 could thus play a role in mediating different functions of the different Stau2 isoforms.

4.1.2 Stau2 tandem-domains act together for full functionality

A previous report had named RBDs 3 and 4 as mainly, if not solely, active with regards to RNA-binding (Duchaine et al., 2002). In this work, it was demonstrated that the Stau2 RBDs 1 and 2 also possess RNA-binding activity very similar to the RBDs 3 and 4. Furthermore, it was demonstrated that the two RBDs 1 and 2 work together as a tandem-domain to achieve their full functionality. The sum of these data suggest a model in which RBD2 binds dsRNA promiscuously with moderate affinity. Binding occurs initially at a random position but is followed by sliding of the protein along the stem, not mediating sequence-specific contacts to the RNA. Through this sliding, RBD2 positions RBD1 close to the dsRNA. When a suitable dsRNA structure is reached, RBD1 also binds, thereby strongly increasing the affinity of the tandem-domain to dsRNA. This model is illustrated in Figure 49 A. Furthermore, only when the two tandem-domains RBD1-2 and RBD3-4 act together, the protein forms a stable complex with RNA. As for RBDs 1 and 2, RBD3-4 proposedly also act as a tandem-domain in which RBD4 performs the first promiscuous binding with moderate affinity. While sliding on dsRNA, RBD2 and RBD4 position RBD1 and RBD3, respectively, on target dsRNA. When a suitable structure is reached the respective domains also bind the dsRNA, thereby increasing affinity. Only when suitable dsRNA binding sites for both tandem-domains are in appropriate spatial proximity, for instance two stem-loops located in appropriate distance or a sufficiently long stretch of dsRNA, all four RBDs can be bound and form a stable complex with the RNA target (Figure 49 B).

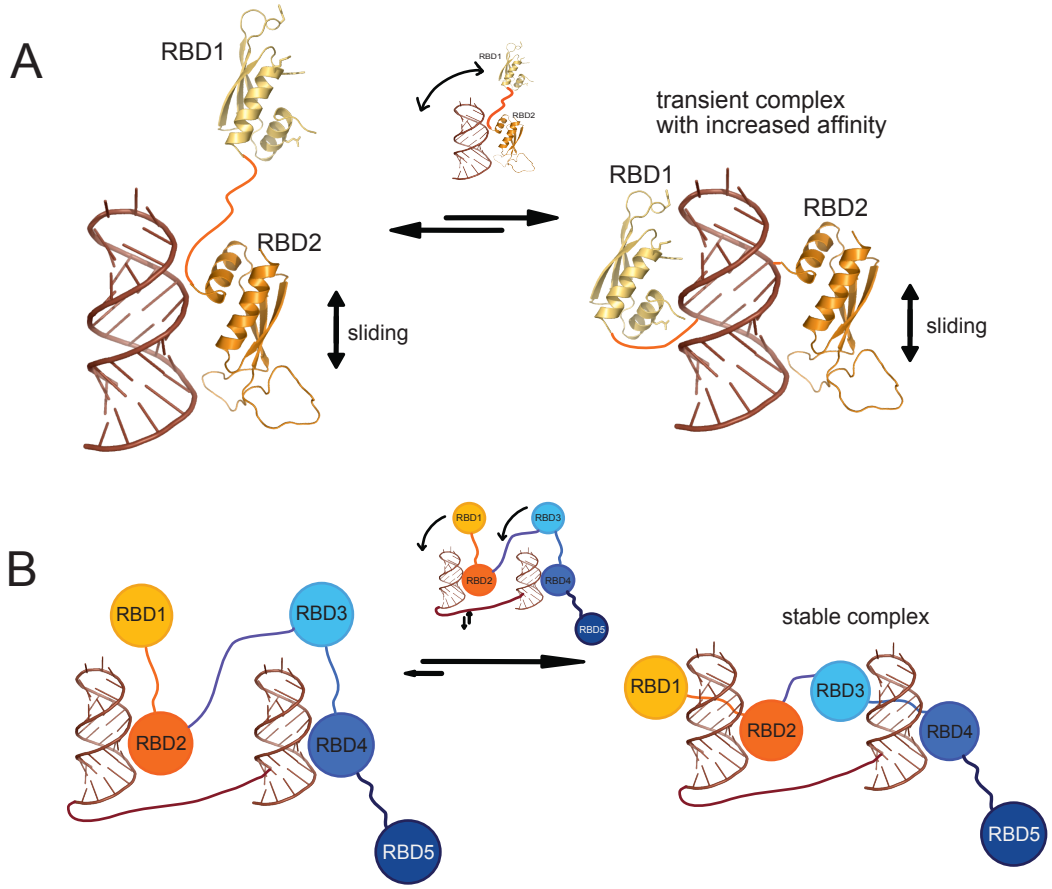

Figure 49: Model of the molecular recognition of dsRNA by Stau2. A) dsRNA recognition by the tandem-domain Stau2 RBD1-2. RBD2 binds dsRNA promiscuously with moderate affinity and slides along the stem. Through this sliding, RBD2 positions RBD1 close to the dsRNA. When a suitable dsRNA structure is reached, RBD1 also binds, thereby strongly increasing the affinity of the tandem-domain to dsRNA. B) Next to the tandem-domain RBD1-2, RBD3-4 act also as a tandem-domain in which RBD4 does the first promiscuous binding with moderate affinity. When RBD2 and RBD4 position RBD1 and RBD3, respectively, close to a suitable dsRNA, the respective domains also bind the dsRNA, thereby increasing affinity. Only when suitable dsRNA binding sites for both tandem-domains are in sufficient spatial proximity (for instance two stem-loops connected by a short ss sequence or a sufficiently long ds stretch), all four RBDs can be bound and form a stable complex with the RNA target.

This feature might be of great importance for stable binding of RNAs during transport over longer distances. The presented model also offers an idea on how the intrinsically unspecific Stau2 may recognize biological targets, which presumably offer dsRNA binding sites in the correct spatial arrangement, and is in line with previous reports on the activities of tandem-dsRBDs. A binding mode that involves sliding was described already for the two canonical dsRBDs of *Drosophila* Loqs-PD, which is a member of the siRNA silencing pathway. In Loqs-PD the RBDs show highly dynamic binding that involves sliding along RNA stems, which may allow searching and scanning of dsRNA for short siRNA helices (Tants

et al., 2017). Similar activity was reported for the human homolog of Loqs-PD, TAR RNA binding protein (TRBP) (Koh et al., 2013). Examples in which two dsRBDs act together as a tandem-domain to achieve their full function have also been described before, for example for the dsRBDs 1 and 2 from the serine/threonine kinase PKR. PKR RBD2 alone has only weak RNA binding activity and does not stimulate gene expression or localize PKR, but strongly enhances these functions of RBD1 (Tian and Mathews, 2001).

While these examples showed the importance of studying the interplay between the multiple dsRBDs that are often contained in RBPs, not many studies are available on this aspect to date. Yet, many examples of other common types of nucleic acid binding domains acting together have been reported. A recent example is the function of the KH3 and KH4 domains from ZBP-1. KH3 and KH4 bind RNA with different dynamics in a weakly coupled reaction. The individual domains interact rather weakly with RNA (~1 μM) and coupling of KH3 and KH4 binding improves binding by 1 to 2 orders of magnitude. Whereas KH4 alone associates and dissociates quickly from zipcode RNA, the affinity of KH3-KH4 is increased due to a lower dissociation rate (Nicastro et al., 2017), meaning the complex is stabilized. Such multiple weak interactions are thought to respond more readily to regulation than a single high-affinity interaction (Mackereth and Sattler, 2012, Lunde et al., 2007).

The presented work on Stau2 further highlights the necessity to study the cooperation of dsRBDs to understand their molecular functions.

4.1.3 Crystallization and structure determination of the Stau2 RBD1-2-RNA complex

In this work, evidence was collected that the Stau2 domains RBD1-2 constitute non-canonical dsRNA-binding domains with a rather high content of unstructured sequences that are nevertheless required for the protein's function. Solving the tandem-domains structure could thus reveal interesting functional insights in the molecular mechanisms by which these domains recognize and bind RNA and contribute to overall RNA-binding by Stau2. Even though well-diffracting crystals of a Stau2 RBD1-2-RNA complex could be obtained in this work, due to perfect pseudomerohedral twinning it was not possible to solve the complex's crystal structure. Pseudomerohedral twinning masks the true

symmetry of the crystal lattice, making it appear to be of higher crystal symmetry than it really is. This made it impossible to determine the crystals' true space groups, especially because it could not be determined whether the crystals were merihedrally twinned, meaning they possessed only two twin-domains, or contained even more twin domains. Neither molecular replacement nor programs used for heavy atom phasing can account for this kind of twinning. Furthermore, only rather poor phasing models were available for molecular replacement trials. Both RNA- or dsRBD-models constitute only a small part of the complete solution which were in all MR trials arranged along the c-axis in a pseudo-continuous order. Contrary to MR programs, refinement programs can account for twinning, however, twin refinement produces a strong model bias which masked errors in the poor, partial models obtained in MR trials and made their improvement impossible. Taken together, the combination of pseudomerohedral twinning and poor phasing models made a solution of the RBD1-2-RNA complex structure impossible. Efforts to optimize the crystals in order to abolish twinning failed, too. This makes it unlikely that the structure will be solved by X-ray crystallography. However, other methods of structural biology could be used. Because the complex readily crystallizes, its structure could possibly be solved by microelectron diffraction (microED), a relatively new cryo electron microscopy (cryoEM) method in which microcrystals diffract low-energy electron beams under cryogenic conditions in an electron microscope (Shi et al., 2016, Rodriguez and Gonen, 2016). Because electrons interact much stronger with matter than X-rays, nano- or microcrystals can be used in this method. It was shown that the method works also on crystals which had been fragmented by mechanic forces, for example by sonication or pipetting, and that such crystal fragments produce higher quality diffraction than the original macrocrystals (de la Cruz et al., 2017). This can be explained by the mosaic model of the imperfect crystals typically produced by biological materials, in which a crystal is composed of small but well-ordered mosaic blocks that are misaligned with each other. Breaking such crystals down to their well-ordered building blocks abolished all pathologies that arise from this misalignment or mosaicity. This feature of microED is also suited to resolve twinning issues, making it a promising approach for the Stau2 RBD1-2-RNA complex crystals.

Alternatively, structure determination by NMR could be attempted. The tandem-domain RBD1-2 as well as the single-domain constructs identified in this work are well-expressed and can readily be isotope-labeled and purified, allowing for the production of highly concentrated, high quality NMR samples. Though resonance assignments were so far complicated by the large fraction of unstructured sequences in the proteins, the ease of sample production enables further experiments to allow for assignment and subsequent determination of distance restraints towards structure calculations. NMR experiments could furthermore give insight into the roles of the unstructured regions of the protein, which probably contribute to the proteins functions, for instance the extended loop 2 in RBD2. Such loop 2 extensions have been described to mediate protein-protein interactions before (see section 1.3.4)

4.1.4 Mutational analysis of Stau2 RBD1-2 RNA-binding

Because structure determination of the Stau2 RBD1-2-RNA complex was so far not successful, a mutational analysis was performed to obtain information on how these two RBDs recognize RNA. For RBD1, mutational analysis verified that conserved, canonical dsRBD residues are used for RNA recognition. RNA-binding by this domain was strongly impaired in the mutants H36A, F40A and K59A K60A. This is consistent with a previous report about mutational analysis in dmStau RBD3, in which corresponding mutations also abolished RNA-binding (Ramos et al., 2000). These residues are key players in RNA recognition by a dsRBD (see section 1.3.4 and Figure 3). H36 corresponds to the conserved histidine in the GPxH motif in region 2, which forms hydrogen bonds with the 2'OH groups in the minor groove of A-form RNA. F40 is a highly conserved residue at the beginning of β_2 which assists RNA-binding by optimally orienting positively charged residues (Masliah et al., 2013). K59 and K60 belong to the KKxxK motif in region 3, which probes the major groove. The mutant E15A corresponds to the conserved glutamate of region 1 at the end of α_1 (see Figure 3) but had in the case of SRS3 RNA, unexpectedly, little effect on RNA-binding. A possible explanation is that in the context of the RBD1-2 tandem, RBD1 is positioned in close proximity to RNA by RBD2, thus facilitating RNA-binding and concomitantly reducing the importance of region 1. To test this hypothesis, mutants could be tested in context of the individual domain RBD1 by NMR

titration experiments. In the individual RBD1, a stronger effect of the E15A mutation would then be expected. Mutants in the poorly conserved RBD2 are more difficult to explain because the known motifs of regions 2 and 3 are absent from the sequence and the large unstructured content of the domain makes structure prediction unreliable. The mutant E99A, which decreased RNA-binding of RBD1-2 is likely to correspond to region 1. The mutants K106A and H169A, which had an even stronger negative effect on RNA-binding, cannot easily be mapped to canonical dsRBD motifs, yet are conserved in Stau RBD2 of many species. As indicated by sequence conservation and secondary structure prediction (Figure S 1, appendix), H169 probably lies in the middle of α_2, putting the mutant F157A, which showed altered RNA-binding kinetics, in β_3. A better understanding of how these residues contribute to supposedly non-canonical RNA recognition demands for structural approaches as discussed above (section 4.1.3).

4.1.5 A possible RNA-chaperone function of Stau2

This work provides evidence that the Stau2 tandem-domains RBD3-4 as well as RBD1-2 catalyze double-strand formation of nucleic acids. This activity seems slightly stronger for RBD1-2 and changes in mutants with altered RNA-binding. Stau2[62], the only isoform comprising the complete RBD1-2 tandem, is a nuclear shuttling protein. It is thus possible that it acts as an RNA chaperone already in the nucleus and later stabilizes proper folding of the mRNA during transport to ensure recognition by certain RBPs and protection from others. The exact function of Stau2 in transport mRNPs is unknown and its promiscuous binding to dsRNA makes it tempting to speculate that Stau2 acts as a stabilizer of RNA structure. However, testing this hypothesis requires further studies. Since the presented chaperone assays were performed with standard DNA oligonucleotides, the primary follow-up experiment should thus be a verification with RNA sequences.

4.1.6 Oligomerization of Stau2-RNA complexes

In this work, oligomerization of Stau2 RBD1-2-RNA complexes over time was observed at several instances and hampered several experimental approaches. For instance small angle X-ray scattering measurements, which could yield information about the shape and stoichiometry of the complex in solution, is

extremely sensitive to high molecular weight species. Even though SLS measurements of full length Stau2 protein revealed a monomeric state of the protein in solution, SLS experiments with Stau2 RBD1-2 in complex with RNA as well as time-course DLS measurements with this complex or RBD1-2 alone provided evidence that unspecific oligomerization can occur over time. It is not clear whether this effect is an artifact of recombinant, truncated protein production or high concentrations, or whether it is a functional feature of Stau2. Homodimerization and heterodimerization with Stau1 was already suggested for Stau2, yet based solely on cell-based assays (Park et al., 2013). It can thus not be excluded that Stau2 does not actually dimerize but oligomerizes and that this contributes to the protein's function. Multimerization of RBPs can contribute to the formation of RNA granules. For instance self-aggregation of either TIA proteins or G3BP was reported to promote assembly of stress granules (Anderson and Kedersha, 2006). Proteins containing so-called intrinsically disordered regions (IDRs) or low-complexity domains recently caught attention for their role in reversible aggregation of RNPs into granules through protein-protein interactions and their ability to induce liquid-liquid phase separation through protein-protein as well as protein-RNA interactions. This is thought to be an organisational principle for subcellular structures like RNA granules (Kato et al., 2012) (Hentze et al., 2018).

A role of Stau2, which has no such IDRs, in such processes, however, is not known and requires further experimental analysis.

4.1.7 Functional relevance of the RBD1-2 RNA binding activity

To assess the functional relevance of the RNA-binding function of Stau2 RBDs 1-2, *in vivo* studies with RNA-binding deficient RBD1-2 are required. A suitable, well-known and readily amenable model system for such studies is the *Drosophila* oocyte, in which Staufen is critically required for posterior localization of *osk* mRNA and thus embryonic patterning (see section 1.1) (St Johnston et al., 1991, Ephrussi et al., 1991). In *staufen null* mutants, *osk* localizes to the anterior pole and the embryo cannot form abdominal patterns. This phenotype can be rescued by exogenous dmStau expression.

The longest isoform of Stau2, which was used in this study, is the closest mammalian homolog of dmStau, sharing the domain architecture with five RBDs.

In case RBDs 1-2 critically contribute to dmStau function *in vivo*, a loss of function due to RNA-binding mutations in RBD1-2 should result in *osk* localization defects. This can be tested by rescue experiments in oocytes of *staufen null* mutant flies by expressing wt and RBD1-2 mutant dmStau. Furthermore, it can be tested whether wt mStau2 can rescue *osk* localization in this setting and a possible rescue could be compared to Stau2 RBD1-2 mutants. This would not only yield information about the functional importance of RBD1-2 but also about the conservation of dmStau and mammalian Stau2.
In this work, suitable RBD1-2 mutants were identified experimentally by SPR in mStau2 and transferred by multiple sequence alignment into dmStau. *Drosophila* transgenesis vectors for the described experiments have been generated (see section 3.7.1) and collaborative *in vivo* experiments are on-going.

4.2 Trimeric interaction between Stau2, Pum2 and *Rgs4*

A fundamental problem in understanding the molecular function of Stau2-containing mRNPs is the complexity of not only their mRNA but also their protein content. Defining the characteristics of Stau2 protein-protein interactions in Stau2-containing mRNPs is thus likely to significantly improve our understanding of their function. Pum2 has been implicated in similar processes as Stau2 (see section 1.5), making it a possible interaction partner for Stau2 in mRNPs. In this work, a possible direct or indirect interaction of the two RBPs in a trimeric complex with *Rgs4* RNA was investigated.

4.2.1 Pum2 binds *Rgs4* 3'UTR via a non-canonical mechanism

The presence of two Pum2 PRE consensus motifs in *Rgs4* 3'UTR indicated binding of Pum2 to this RNA. In this work, binding of Pum2 to *Rgs4* 3'UTR could clearly be verified by EMSAs. Yet, binding of Pum2 occurred not just to wt *Rgs4* RNA but also to mutants, in which the cognate Pum2 consensus sequences were altered, resulting in almost unchanged affinities and pointing at a noncanonical recognition mode. Pum2 also bound SRS3 RNA, in which only 7 nt of the Pum2 PRE consensus sequence are present whereas the A at position 8 is replaced by G, indicating that this position is not required for binding. Other PUF proteins can also bind imperfect consensus sequences, for instance by flipping out bases that cannot be accommodated (Gupta et al., 2008), arguing for the idea that

sequence requirements for Pum HD binding are more relaxed than previously anticipated. Additionally, this incomplete Pum2 consensus in SRS3 is buried largely in an RNA double-strand. Pum canonically recognizes ssRNA, raising the question if dsRNA is unfolded upon Pum2 binding or whether Pum2 can bind dsRNA. Non-canonical PUF proteins like Puf-A contain additional Puf repeats and are known to bind unspecifically to dsRNA sequence. This raises the question whether Pum2 also contains yet unknown non-canonical Puf repeats. Initial crystals of the Pum2 HD-SRS3 complex were obtained in this work, pointing at the possibility to elucidate how Pum2 binds SRS3 by crystal structure determination. Changes of the RNA secondary structure upon binding could also be monitored by NMR spectroscopy.

If Pum2 binding does not strictly require all 8 nt interactions, mutants in which Pum2 consensus sequences are altered but not fully deleted might not be drastic enough to abolish binding, offering an explanation for the observed binding to mutated RNA sequences. Furthermore, binding occurred not just via the conserved Pum2 HD, but most likely also by the N-terminal or possibly the short C-terminal unstructured part of Pum2, indicating that regions outside the Pum2 HD also possess RNA-binding activity. This observation is consistent with a recent publication that identified additional RNA-binding peptides in the N-terminal part of Pum2 by a new method called RBDmap (Castello et al., 2016).

The N-terminal part of the protein is predicted to be unstructured, yet several non-canonical Puf repeats have been identified by structural methods that were not predictable based on amino acid sequence (Qiu et al., 2014, Zhang et al., 2016). Furthermore, RNA-binding by disordered proteins has recently been acknowledged as a wide spread phenomenon (Hentze et al., 2018), for example IDRs do not just aggregate RNPs into RNA granules but also actively bind RNA.

Structural characterization of Pum2 regions outside the Pum2 HD could clarify whether the protein is indeed largely unstructured. An easy first step could be determination of its secondary structure content by CD spectrometry. Also, even though the protein is too big for many NMR experiments, a $^{1}H,^{15}N$-HSQC fingerprint should reveal whether the N-terminal part of the protein has any folded parts. In case any folds are found, the corresponding protein fragments could by identified by limited proteolysis followed by mass spectrometry. In case

the unstructured nature of the Pum2 N-terminus is confirmed, a peptide tiling array could identify RNA-interacting regions of the protein.

4.2.2 No evidence of trimeric Stau2-Pum2-*Rgs4* complex formation

An array of biochemical and biophysical methods was used in this work to identify a possible direct protein-protein interaction between Stau2 and Pum2 and their trimeric complex with *Rgs4* 3'UTR, including *in vitro* pull-down assays, ITC, SPR, EMSAs, UV-crosslinking and co-expression experiments. None of these experiments detected either an interaction between Stau2 and Pum2, nor a trimeric complex with *Rgs4*. These results indicate that the functional interaction of the two proteins in several biological processes is neither mediated by a direct, physical interaction between them, nor by simultaneous binding in close proximity on their target RNAs. Possibly, the close proximity of potential binding sites in *Rgs4* rather indicates competitive binding of either of the two proteins. A common function in certain biological processes mediated by temporally or spatially alternating binding of either Stau2 or Pum2 is conceivable. Alternatively, an adaptor protein that remains to be identified could mediate their interaction *in vivo*. It is furthermore possible that the interaction of the two proteins requires posttranslational modifications (PTMs). Because the experiments were performed with recombinant proteins purified from High-5 insect cells or *E. coli*, the possibility that an interaction between the two proteins was not observed because of the lack of correct PTMs cannot be ruled out.

The idea that Pum2 could be the third binding partner in a trimeric complex that mediates the biological specificity of the intrinsically unspecific Stau2 could not be confirmed in this work. However, by immunoprecipitation experiments, a set of 65 proteins was identified in Stau2 mRNPs, 36 of which were not shared with Barentz mRNPs (Fritzsche et al., 2013), leaving a large number of potential candidates for this role to be investigated.

5 Acknowledgements

During the time I worked on this project, I not only learned a whole lot scientifically and methodologically but also had a great time and lots of fun in and outside the lab, helping me to stay excited about science and motivated to push on my project at all times. For this, I want to thank all the people involved.

First of all, I want to thank Dierk Niessing for giving me the chance to work in his lab and on this project and for not giving up on it. Thanks for constant support, availability for discussions and advice and being a quite likeable boss.

Equally important, I want to thank all members of the Niessing group. You were great company during my time here, always offering scientific or mental support and providing a great atmosphere in the lab. Thanks to Annika, Franzi and Rob for a lot of scientific help and teaching and great synchrotron trips. Thanks to Vera and Simi for running and managing the lab. Special thanks also go to Lena, Elena and most of all Jana for many great lunch break runs and running events that aided a lot to my mental sanity.

Furthermore, I want to thank my collaboration partners who helped me to pursue this project and delivered many helpful and exciting results. Thanks to Jan-Niklas Tants, Johannes Günther and Michael Sattler for their help with NMR experiments. Thanks to Imre Gaspar and Anne Ephrussi for helping out with the on-going functional *in vivo* studies.

I would also like to thank the members of my Thesis Advisory Committee, Dierk Niessing, Michael Kiebler, Gregor Witte and Dietmar Martin. Additional thanks go to Michael Kiebler for initiating this project with us.

Even though this was years ago, I would like to thank Hans Kiefer for waking my interest in X-ray crystallography that drove me to do my doctoral work in a structural biology institute.

Last but not least, I want to thank my family who supported me at all times during my education, especially my parents and my grandmother. Thanks also to Daniel, for support, listening and patience.

6 Appendix

6.1 List of abbreviations

aa	amino acid
AMPA	α-amino-3-hydroxy-5-methyl-4-isoxazolepropionic acid
ARE	AU-rich element
ARF1	ADP ribosylation factor 1
BR	binding region
CaMKII	Ca^{2+}/calmodulin kinase II
CD	circular dichroism
CPEB	Cytoplasmic polyadenylation element binding protein
cryoEM	cryo electron microscopy
DDX1	DEAD-box helicase 1
DEPC	diethylpyrocarbonate
DLS	dynamic light scattering
dmStau	*Drosophila melanogaster* Staufen
dsRBD	double-stranded RNA binding domain
EJC	Exon junction complex
EMSA	Electrophoretic mobility shift assay
FMRP	Fragile X Mental Retardation Protein
FW	forward
GABA	γ-butyric acid
GDP	Guanosine-5'-diphosphate
GIRK	G-protein coupled inwardly rectifying potassium channel
GPCR	G-protein coupled receptor
GTP	Guanosine-5'-triphosphate
HD	homology domain
IMAC	immobilized metal-chelate affinity chromatography
IP	Immunoprecipitation
ITC	Isothermal titration calorimetry
KH	hnRNP K homology domain
LALS	low angle light scattering
LB	Luria Bertani
LE	localization element
lncRNA	long non-coding RNA
LTD	long-term depression
LTP	long-term potentiation
MAD	multiple-wavelength anomalous diffraction
MAP2	microtubule-associated protein 2
mGluR	metabotropic glutamate receptor
microED	microelectron diffraction
mRNP	messenger ribonucleoprotein
MSA	multiple sequence alignmnent
MW	molecular weight
NMD	nonsense-mediated decay
NMDA	*N*-Methyl-D-aspartate

NMR	Nuclear Magnetic Resonance
nt	nucleotide
osk	oskar
PABC1	polyadenylate binding protein 1
PAGE	polyacrylamide gel electrophoresis
PCR	polymerase chain reaction
PD	Parkinson's disease
PRE	Pumilio response element
PUF	Pumilio and FBF
Pum	Pumilio
Pum HD	Pumilio homology domain
RALS	right angle light scattering
RBD	double-stranded RNA binding domain
RBP	RNA-binding protein
Rgs4	Regulator of G-protein signaling 4
RI	refractive index
RNAi	RNA interference
RRM	RNA recognition motif
RT	room temperature
RV	reverse
SA	streptavidin
SBS	Stau1-binding site
SDS	sodium dodecyl sulfate
SEC	size exclusion chromatography
SeMet	selenomethionine
SHAPE	Selective 2′-hydroxyl acylation analyzed by primer extension
SLS	static light scattering
SMD	Staufen-mediated decay
SOLE	spliced oskar localization element
SPR	Surface Plasmon Resonance
SRS	Staufen-recognized structure
SSM	Staufen swapping motif
Stau	Staufen
TBD	tubulin-binding domain
TINCR	terminal differentiation-induced ncRNA
UPF1	up-frameshift protein1
UTR	untranslated region
wt	wild-type
ZBP1	zipcode binding protein 1

6.2 List of Figures

Figure 1: The sushi belt model. Adapted from (Doyle and Kiebler, 2011).. 14
Figure 2: Mammalian Stau proteins. 20
Figure 3: The double-stranded RNA-binding domain. 22
Figure 4: Crystal structures of Puf RNA-binding domains. 28
Figure 5: Predicted secondary structure of the *Rgs4* BR. 30
Figure 6: Result of Stau2 protein purifications. 77
Figure 7: Result of Stau2 RBD1-2 protein purifications 78
Figure 8: Result of Pum2 protein purifications. 85
Figure 9: EMSAs with recombinant Stau2 and *Rgs4* 3'UTR sequences. 87
Figure 10: EMSAs with recombinant Stau2 RBD3-4. 89
Figure 11: EMSAs with A) individual Stau2 RBDs 3 and 4 and *Rgs4* SRS2 RNA or B) extended RBD3-4 constructs comprising either an additional N-terminal or C-terminal RBD. 90
Figure 12: EMSAs with Stau2 tandem-domains RBD3-4 and RBD1-2 with SRS2 RNA. 91
Figure 13: EMSAs with Stau2 tandem-domains RBD3-4 and RBD1-2 and modified SRS2 RNAs. 92
Figure 14: EMSAs with Stau2 tandem-domains and shortened SRS2 RNAs. 93
Figure 15: EMSAs with recombinant Pum2 proteins and *in vitro* transcribed Rgs4 BR. 95
Figure 16: EMSAs with Pum2 protein constructs and *Rgs4* BR RNA. 96
Figure 17: EMSA with Pum2 FL and *Rgs4* SRS3 RNA. 97
Figure 18: EMSAs with Stau2 RBD3-4, Pum2 HD and *Rgs4* BR. 98
Figure 19: Control experiments with minRNA. A) Scheme and PAGE quality control of minRNA. 99
Figure 20: UV-crosslinking experiment with HisMBP-Pum2 FL and HisSUMO-Stau2 FL. 100
Figure 21: *In vitro* pull-down assay with recombinant Stau2 and Pum2. 101
Figure 22: SPR sensorgrams of a kinetic analysis of Stau2 FL and Pum2 FL binding. 102
Figure 23: Crystal structure of the isolated *Rgs4* SRS2 RNA stem-loop. 105
Figure 24: Stau2 RBD1-2-RNA complex crystal optimization. 109
Figure 25: Crystallization of Pum2 HD in complex with SRS3 RNA. 110
Figure 26: EMSAs with the individual domains RBD1 and 2. 112
Figure 27: Overlay of the ^{1}H,^{15}N-HSQC spectra of the tandem-domain RBD1-2 and the individual RBDs 1 and 2. 114
Figure 28: NMR titration experiments of Stau2 RBD1-2 with dsSRS2+5 RNA. 115
Figure 29: NMR titration experiments of Stau2 RBD1 (A and B) and RBD2 (C and D) with dsSRS2+5 RNA. 116
Figure 30: SPR sensorgrams (left) and steady-state binding curves (right) of Stau2 protein binding to SRS2+5 RNA. 118
Figure 31: SPR sensorgrams (left) and steady-state binding curves (right) of Stau2 protein binding to SRS3 RNA. 119
Figure 32: SPR sensorgrams and steady-state binding curves (for RBD2) of Stau2 RBD1 and Stau2 RBD2 binding to A) dsSRS2+5 or B) SRS3. 121
Figure 33: Sequence analysis used for mutant design of RBD1. 123

Figure 34: Sequence analysis used for mutant design of RBD2.....124
Figure 35: SPR sensorgrams and steady-state binding curves of Stau2 RBD1 mutants (in context of the tandem-domain RBD1-2 binding to dsSRS2+5 RNA.....126
Figure 36: SPR sensorgrams and steady-state binding curves of Stau2 RBD1 mutants (in context of the tandem-domain RBD1-2) binding to SRS3 RNA. 128
Figure 37: SPR sensorgrams of Stau2 RBD2 mutants (in context of the tandem-domain RBD1-2) binding to dsSRS2+5 RNA. 129
Figure 38: SPR sensorgrams and steady-state binding curves of Stau2 RBD2 mutants (in context of the tandem-domain RBD1-2) binding to SRS3 RNA. 130
Figure 39: SPR sensorgrams and plots of maximum response against protein concentration of Stau2 RBD1-2 double-mutants binding to SRS RNA.....132
Figure 40: SPR results for Stau2 RBD1-2 wt and double-mutants binding to dsSRS2+5 135
Figure 41: SPR results for Stau2 RBD1-2 wt and double-mutants binding to SRS3 136
Figure 42: SLS measurements of Stau2 RBD1-2-SRS2 complex mixed 1:1 at 4.25 mg/mL after SEC on 10/300 Superdex200 Increase GL.....138
Figure 43: SLS measurements of Stau2 RBD1-2-SRS2+5/GAAA insert complex mixed 2:1 at 3.3 mg/mL after SEC on 5/150 Superdex200 Increase GL. 139
Figure 44: SLS measurements of HisSUMO-Stau2 FL after SEC on 10/300 Superdex200 Increase GL.....140
Figure 45: DLS measurements with Stau2 RBD1-2-SRS2+5GAAAinsert complex. 142
Figure 46: DLS measurements with Stau2 RBD1-2. 143
Figure 47: TAR(+)/TAR(-) annealing assay with Stau2 tandem-domains.....144
Figure 48: TAR(+)/TAR(-) annealing assay with Stau2 RBD1-2 wt and mutants. 145
Figure 49: Model of the molecular recognition of dsRNA by Stau2. 150

List of Tables

Table 1: Media 35
Table 2: Supplements 37
Table 3: Antibiotics 37
Table 4: General buffers and solutions 38
Table 5: Enzymes (additional to molecular biology enzymes) 39
Table 6: Bacteria 39
Table 7: Insect cells 39
Table 8: Plasmids 40
Table 9: Cloning primers 46
Table 10: Mutagenesis primers 48
Table 11: Template primers for RNA *in vitro* transcription 49
Table 12: DNA oligos for anneling assays 51
Table 13: RNA sequences 52
Table 14: Results of Stau2 protein purifications 79
Table 15: Data collection and refinement statistics 104
Table 16: Stau2-binding to dsSRS2+5 RNA 122
Table 17: Stau2-binding to SRS3 RNA 122
Table 18: Stau2 RBD1-2 mutant-binding to dsSRS2+5 RNA 133
Table 19: Stau2 RBD1-2 mutant-binding to SRS3 RNA 133
Table 20: Stau2 RBD1-4 mutant-binding to dsSRS2+5 RNA 137
Table 21: Stau2 RBD1-4 mutant-binding to SRS3 RNA 137

6.3 Supplementary figures

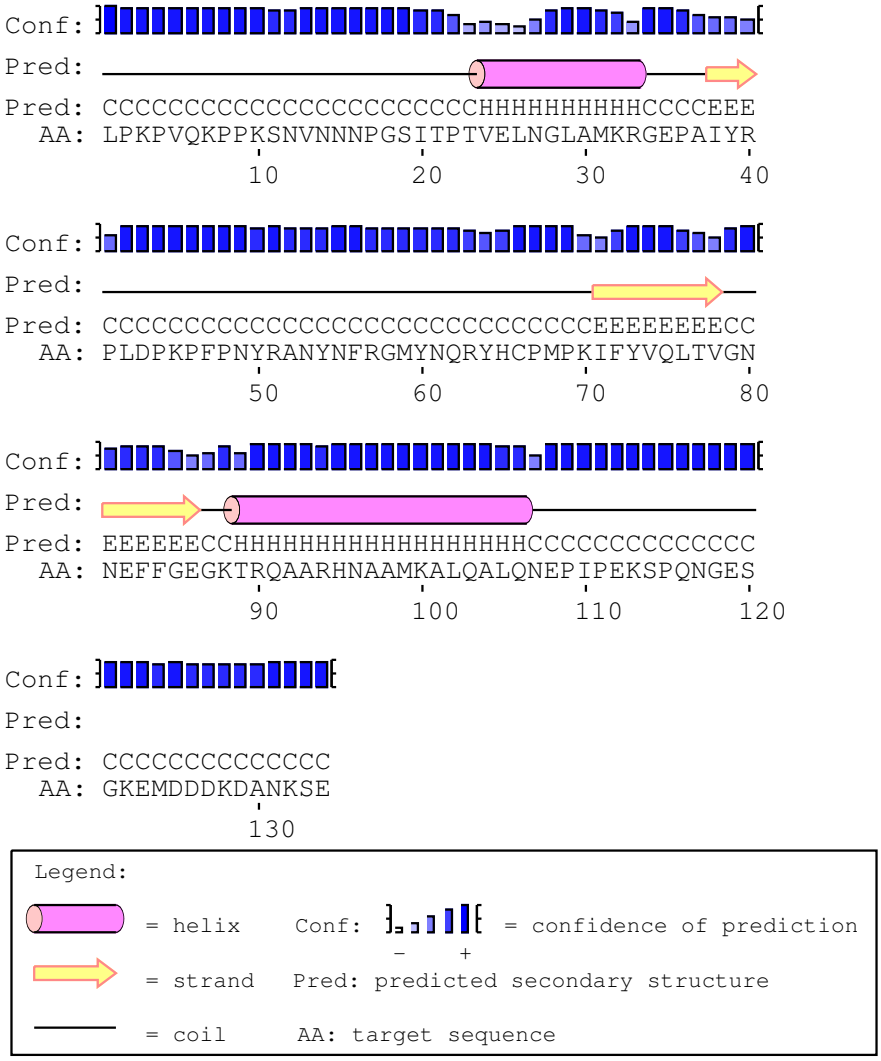

Figure S 1: Result of secondary structure prediction for Stau2 RBD2 (linker-RBD2) with PsiPred. An extended loop 2 is predicted.

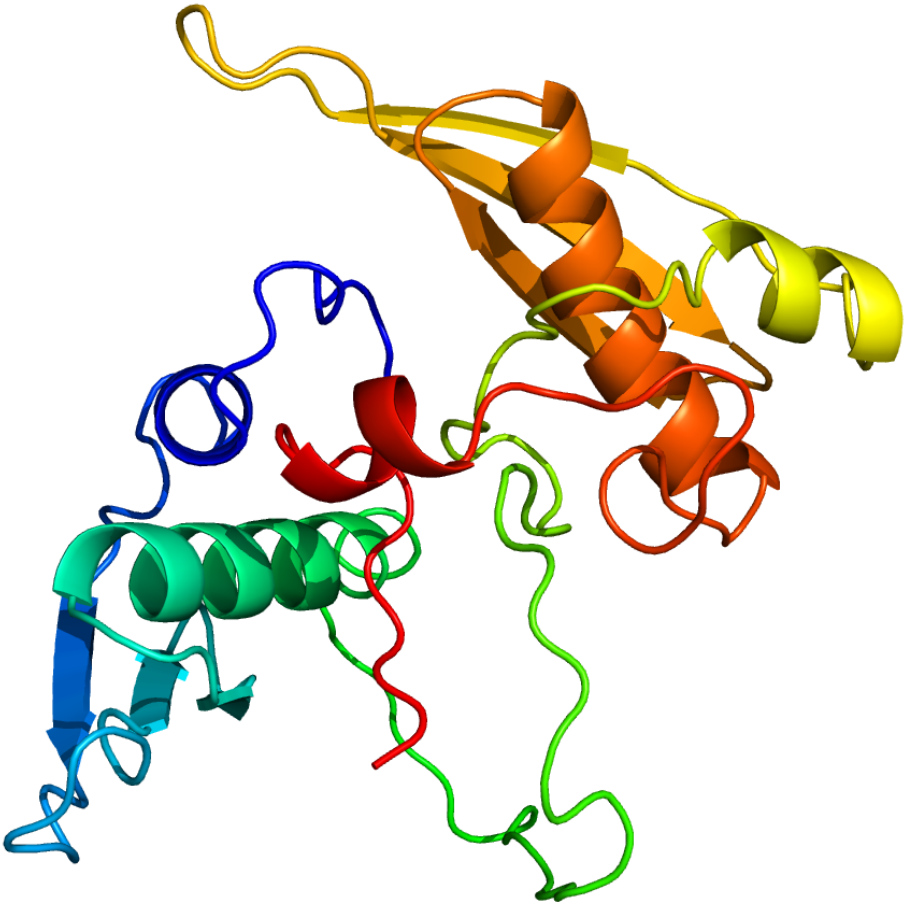

Figure S 2: Homology model of Stau2 RBD1-2 obtained from the Phyre2 webserver (Kelley et al., 2015). RBD1 is shown in blue to green, RBD2 in yellow to red.

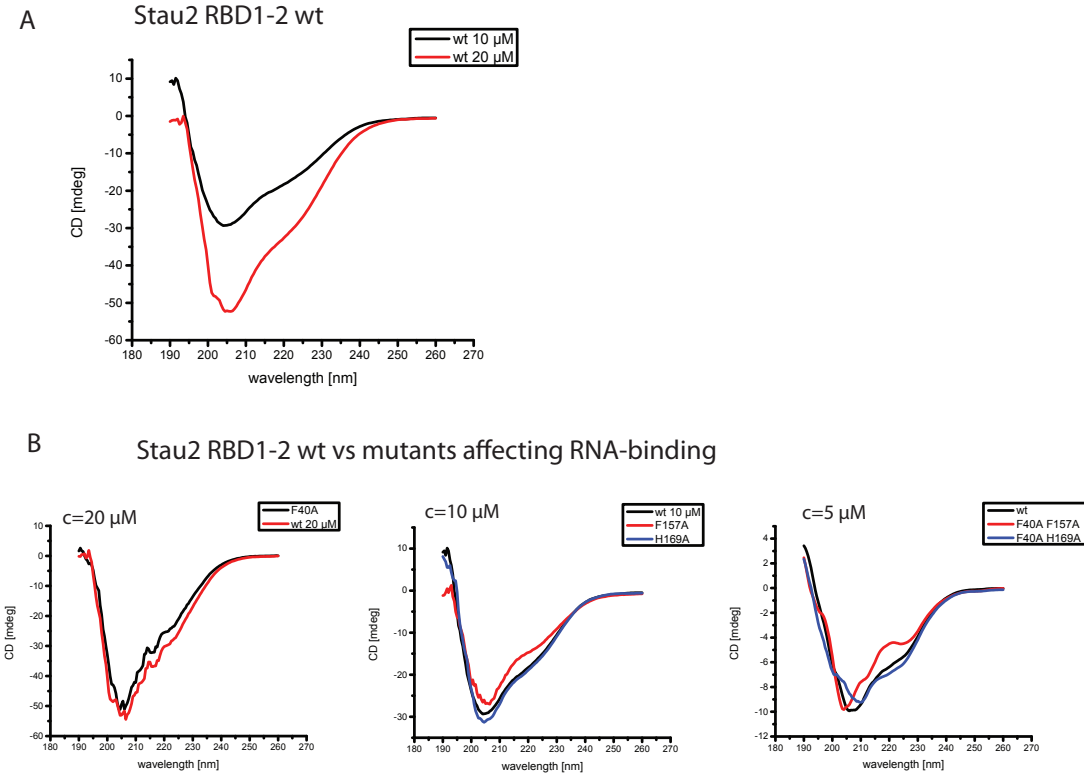

Figure S 3: Circular dichroism spectra of A) Stau2 RBD1-2 wt at different concentrations and B) RNA-binding mutants of RBD1-2 compared to wt. Measurements were performed at the indicated concentrations in buffer containing <50 mM NaCl. All curves show the same shapes, meaning all proteins adopt the same fold.

7 References

ANDERSON, P. & KEDERSHA, N. 2006. RNA granules. *J Cell Biol,* 172**,** 803-8.

ARNOLD, K., BORDOLI, L., KOPP, J. & SCHWEDE, T. 2006. The SWISS-MODEL workspace: a web-based environment for protein structure homology modelling. *Bioinformatics,* 22**,** 195-201.

ASHRAFI, A., GARCIA, P., KOLLMUS, H., SCHUGHART, K., DEL SOL, A., BUTTINI, M. & GLAAB, E. 2017. Absence of regulator of G-protein signaling 4 does not protect against dopamine neuron dysfunction and injury in the mouse 6-hydroxydopamine lesion model of Parkinson's disease. *Neurobiol Aging,* 58**,** 30-33.

BAGNI, C. & OOSTRA, B. A. 2013. Fragile X syndrome: From protein function to therapy. *Am J Med Genet A,* 161A**,** 2809-21.

BARBEAU, A. 1962. The pathogenesis of Parkinson's disease: a new hypothesis. *Can Med Assoc J,* 87**,** 802-7.

BARRAUD, P., EMMERTH, S., SHIMADA, Y., HOTZ, H. R., ALLAIN, F. H. & BUHLER, M. 2011. An extended dsRBD with a novel zinc-binding motif mediates nuclear retention of fission yeast Dicer. *EMBO J,* 30**,** 4223-35.

BASHIRULLAH, A., COOPERSTOCK, R. L. & LIPSHITZ, H. D. 1998. RNA localization in development. *Annu Rev Biochem,* 67**,** 335-94.

BASTOCK, R. & ST JOHNSTON, D. 2008. Drosophila oogenesis. *Curr Biol,* 18**,** R1082-7.

BERGER, S. M., FERNANDEZ-LAMO, I., SCHONIG, K., FERNANDEZ MOYA, S. M., EHSES, J., SCHIEWECK, R., CLEMENTI, S., ENKEL, T., GROTHE, S., VON BOHLEN UND HALBACH, O., SEGURA, I., DELGADO-GARCIA, J. M., GRUART, A., KIEBLER, M. A. & BARTSCH, D. 2017. Forebrain-specific, conditional silencing of Staufen2 alters synaptic plasticity, learning, and memory in rats. *Genome Biol,* 18**,** 222.

BIASINI, M., BIENERT, S., WATERHOUSE, A., ARNOLD, K., STUDER, G., SCHMIDT, T., KIEFER, F., GALLO CASSARINO, T., BERTONI, M., BORDOLI, L. & SCHWEDE, T. 2014. SWISS-MODEL: modelling protein tertiary and quaternary structure using evolutionary information. *Nucleic Acids Res,* 42**,** W252-8.

BOHL, F., KRUSE, C., FRANK, A., FERRING, D. & JANSEN, R. P. 2000. She2p, a novel RNA-binding protein tethers ASH1 mRNA to the Myo4p myosin motor via She3p. *EMBO J,* 19**,** 5514-24.

BUCHAN, D. W., MINNECI, F., NUGENT, T. C., BRYSON, K. & JONES, D. T. 2013. Scalable web services for the PSIPRED Protein Analysis Workbench. *Nucleic Acids Res,* 41**,** W349-57.

BUXBAUM, A. R., YOON, Y. J., SINGER, R. H. & PARK, H. Y. 2015. Single-molecule insights into mRNA dynamics in neurons. *Trends Cell Biol,* 25**,** 468-75.

CAO, Q., PADMANABHAN, K. & RICHTER, J. D. 2010. Pumilio 2 controls translation by competing with eIF4E for 7-methyl guanosine cap recognition. *RNA,* 16**,** 221-7.

CASTELLO, A., FISCHER, B., FRESE, C. K., HOROS, R., ALLEAUME, A. M., FOEHR, S., CURK, T., KRIJGSVELD, J. & HENTZE, M. W. 2016. Comprehensive Identification of RNA-Binding Domains in Human Cells. *Mol Cell,* 63**,** 696-710.

CHA, B. J., KOPPETSCH, B. S. & THEURKAUF, W. E. 2001. In vivo analysis of Drosophila bicoid mRNA localization reveals a novel microtubule-dependent axis specification pathway. *Cell,* 106**,** 35-46.

CHARTRAND, P., MENG, X. H., HUTTELMAIER, S., DONATO, D. & SINGER, R. H. 2002. Asymmetric sorting of ash1p in yeast results from inhibition of translation by localization elements in the mRNA. *Mol Cell,* 10**,** 1319-30.

CHEKULAEVA, M., HENTZE, M. W. & EPHRUSSI, A. 2006. Bruno acts as a dual repressor of oskar translation, promoting mRNA oligomerization and formation of silencing particles. *Cell,* 124**,** 521-33.

COONROD, L. A., LOHMAN, J. R. & BERGLUND, J. A. 2012. Utilizing the GAAA tetraloop/receptor to facilitate crystal packing and determination of the structure of a CUG RNA helix. *Biochemistry,* 51**,** 8330-7.

DE LA CRUZ, M. J., HATTNE, J., SHI, D., SEIDLER, P., RODRIGUEZ, J., REYES, F. E., SAWAYA, M. R., CASCIO, D., WEISS, S. C., KIM, S. K., HINCK, C. S., HINCK, A. P., CALERO, G., EISENBERG, D. & GONEN, T. 2017. Atomic-resolution structures from fragmented protein crystals with the cryoEM method MicroED. *Nat Methods,* 14**,** 399-402.

DEININGER, P. 2011. Alu elements: know the SINEs. *Genome Biol,* 12**,** 236.

DENG, Y., SINGER, R. H. & GU, W. 2008. Translation of ASH1 mRNA is repressed by Puf6p-Fun12p/eIF5B interaction and released by CK2 phosphorylation. *Genes Dev,* 22**,** 1037-50.

DICTENBERG, J. B., SWANGER, S. A., ANTAR, L. N., SINGER, R. H. & BASSELL, G. J. 2008. A direct role for FMRP in activity-dependent dendritic mRNA transport links filopodial-spine morphogenesis to fragile X syndrome. *Dev Cell,* 14**,** 926-39.

DIENSTBIER, M., BOEHL, F., LI, X. & BULLOCK, S. L. 2009. Egalitarian is a selective RNA-binding protein linking mRNA localization signals to the dynein motor. *Genes Dev,* 23**,** 1546-58.

DING, J., GUZMAN, J. N., TKATCH, T., CHEN, S., GOLDBERG, J. A., EBERT, P. J., LEVITT, P., WILSON, C. J., HAMM, H. E. & SURMEIER, D. J. 2006. RGS4-dependent attenuation of M4 autoreceptor function in striatal cholinergic interneurons following dopamine depletion. *Nat Neurosci,* 9**,** 832-42.

DOYLE, M. & KIEBLER, M. A. 2011. Mechanisms of dendritic mRNA transport and its role in synaptic tagging. *EMBO J,* 30**,** 3540-52.

DUBNAU, J., CHIANG, A. S., GRADY, L., BARDITCH, J., GOSSWEILER, S., MCNEIL, J., SMITH, P., BULDOC, F., SCOTT, R., CERTA, U., BROGER, C. & TULLY, T. 2003. The staufen/pumilio pathway is involved in Drosophila long-term memory. *Curr Biol,* 13**,** 286-96.

DUCHAINE, T. F., HEMRAJ, I., FURIC, L., DEITINGHOFF, A., KIEBLER, M. A. & DESGROSEILLERS, L. 2002. Staufen2 isoforms localize to the somatodendritic domain of neurons and interact with different organelles. *J Cell Sci,* 115**,** 3285-95.

DUGRE-BRISSON, S., ELVIRA, G., BOULAY, K., CHATEL-CHAIX, L., MOULAND, A. J. & DESGROSEILLERS, L. 2005. Interaction of Staufen1 with the 5' end of

mRNA facilitates translation of these RNAs. *Nucleic Acids Res,* 33**,** 4797-812.

EDELMANN, F. T., NIEDNER, A. & NIESSING, D. 2015. ASH1 mRNP-core factors form stable complexes in absence of cargo RNA at physiological conditions. *RNA Biol,* 12**,** 233-7.

EPHRUSSI, A., DICKINSON, L. K. & LEHMANN, R. 1991. Oskar organizes the germ plasm and directs localization of the posterior determinant nanos. *Cell,* 66**,** 37-50.

FERRE-D'AMARE, A. R., ZHOU, K. & DOUDNA, J. A. 1998. A general module for RNA crystallization. *J Mol Biol,* 279**,** 621-31.

FIORE, R., KHUDAYBERDIEV, S., CHRISTENSEN, M., SIEGEL, G., FLAVELL, S. W., KIM, T. K., GREENBERG, M. E. & SCHRATT, G. 2009. Mef2-mediated transcription of the miR379-410 cluster regulates activity-dependent dendritogenesis by fine-tuning Pumilio2 protein levels. *EMBO J,* 28**,** 697-710.

FOLLWACZNY, P., SCHIEWECK, R., RIEDEMANN, T., DEMLEITNER, A., STRAUB, T., KLEMM, A. H., BILBAN, M., SUTOR, B., POPPER, B. & KIEBLER, M. A. 2017. Pumilio2-deficient mice show a predisposition for epilepsy. *Dis Model Mech,* 10**,** 1333-1342.

FRITZSCHE, R., KARRA, D., BENNETT, K. L., ANG, F. Y., HERAUD-FARLOW, J. E., TOLINO, M., DOYLE, M., BAUER, K. E., THOMAS, S., PLANYAVSKY, M., ARN, E., BAKOSOVA, A., JUNGWIRTH, K., HORMANN, A., PALFI, Z., SANDHOLZER, J., SCHWARZ, M., MACCHI, P., COLINGE, J., SUPERTI-FURGA, G. & KIEBLER, M. A. 2013. Interactome of two diverse RNA granules links mRNA localization to translational repression in neurons. *Cell Rep,* 5**,** 1749-62.

FURIC, L., MAHER-LAPORTE, M. & DESGROSEILLERS, L. 2008. A genome-wide approach identifies distinct but overlapping subsets of cellular mRNAs associated with Staufen1- and Staufen2-containing ribonucleoprotein complexes. *RNA,* 14**,** 324-35.

GALGANO, A., FORRER, M., JASKIEWICZ, L., KANITZ, A., ZAVOLAN, M. & GERBER, A. P. 2008. Comparative analysis of mRNA targets for human PUF-family proteins suggests extensive interaction with the miRNA regulatory system. *PLoS One,* 3**,** e3164.

GASTEIGER, E., GATTIKER, A., HOOGLAND, C., IVANYI, I., APPEL, R. D. & BAIROCH, A. 2003. ExPASy: The proteomics server for in-depth protein knowledge and analysis. *Nucleic Acids Res,* 31**,** 3784-8.

GERBER, A. P., HERSCHLAG, D. & BROWN, P. O. 2004. Extensive association of functionally and cytotopically related mRNAs with Puf family RNA-binding proteins in yeast. *PLoS Biol,* 2**,** E79.

GERBER, K. J., SQUIRES, K. E. & HEPLER, J. R. 2016. Roles for Regulator of G Protein Signaling Proteins in Synaptic Signaling and Plasticity. *Mol Pharmacol,* 89**,** 273-86.

GHOSH, S., MARCHAND, V., GASPAR, I. & EPHRUSSI, A. 2012. Control of RNP motility and localization by a splicing-dependent structure in oskar mRNA. *Nat Struct Mol Biol,* 19**,** 441-9.

GLEGHORN, M. L., GONG, C., KIELKOPF, C. L. & MAQUAT, L. E. 2013. Staufen1 dimerizes through a conserved motif and a degenerate dsRNA-binding domain to promote mRNA decay. *Nat Struct Mol Biol,* 20**,** 515-24.

GLEGHORN, M. L. & MAQUAT, L. E. 2014. 'Black sheep' that don't leave the double-stranded RNA-binding domain fold. *Trends Biochem Sci,* 39**,** 328-40.

GOETZE, B., TUEBING, F., XIE, Y., DOROSTKAR, M. M., THOMAS, S., PEHL, U., BOEHM, S., MACCHI, P. & KIEBLER, M. A. 2006. The brain-specific double-stranded RNA-binding protein Staufen2 is required for dendritic spine morphogenesis. *J Cell Biol,* 172**,** 221-31.

GOLDSTROHM, A. C., HOOK, B. A., SEAY, D. J. & WICKENS, M. 2006. PUF proteins bind Pop2p to regulate messenger RNAs. *Nat Struct Mol Biol,* 13**,** 533-9.

GOLDSTROHM, A. C., SEAY, D. J., HOOK, B. A. & WICKENS, M. 2007. PUF protein-mediated deadenylation is catalyzed by Ccr4p. *J Biol Chem,* 282**,** 109-14.

GONG, C. & MAQUAT, L. E. 2011. lncRNAs transactivate STAU1-mediated mRNA decay by duplexing with 3' UTRs via Alu elements. *Nature,* 470**,** 284-8.

GU, W., DENG, Y., ZENKLUSEN, D. & SINGER, R. H. 2004. A new yeast PUF family protein, Puf6p, represses ASH1 mRNA translation and is required for its localization. *Genes Dev,* 18**,** 1452-65.

GUEX, N. & PEITSCH, M. C. 1997. SWISS-MODEL and the Swiss-PdbViewer: an environment for comparative protein modeling. *Electrophoresis,* 18**,** 2714-23.

GUICHARD, C., IVANYI-NAGY, R., SHARMA, K. K., GABUS, C., MARC, D., MELY, Y. & DARLIX, J. L. 2011. Analysis of nucleic acid chaperoning by the prion protein and its inhibition by oligonucleotides. *Nucleic Acids Res,* 39**,** 8544-58.

GUPTA, P. & LI, Y. R. 2018. Upf proteins: highly conserved factors involved in nonsense mRNA mediated decay. *Mol Biol Rep,* 45**,** 39-55.

GUPTA, Y. K., NAIR, D. T., WHARTON, R. P. & AGGARWAL, A. K. 2008. Structures of human Pumilio with noncognate RNAs reveal molecular mechanisms for binding promiscuity. *Structure,* 16**,** 549-57.

HACHET, O. & EPHRUSSI, A. 2004. Splicing of oskar RNA in the nucleus is coupled to its cytoplasmic localization. *Nature,* 428**,** 959-63.

HENTZE, M. W., CASTELLO, A., SCHWARZL, T. & PREISS, T. 2018. A brave new world of RNA-binding proteins. *Nat Rev Mol Cell Biol*.

HERAUD-FARLOW, J. E. & KIEBLER, M. A. 2014. The multifunctional Staufen proteins: conserved roles from neurogenesis to synaptic plasticity. *Trends Neurosci*.

HERAUD-FARLOW, J. E., SHARANGDHAR, T., LI, X., PFEIFER, P., TAUBER, S., OROZCO, D., HORMANN, A., THOMAS, S., BAKOSOVA, A., FARLOW, A. R., EDBAUER, D., LIPSHITZ, H. D., MORRIS, Q. D., BILBAN, M., DOYLE, M. & KIEBLER, M. A. 2013. Staufen2 Regulates Neuronal Target RNAs. *Cell Rep,* 5**,** 1511-8.

HEYM, R. G., ZIMMERMANN, D., EDELMANN, F. T., ISRAEL, L., OKTEN, Z., KOVAR, D. R. & NIESSING, D. 2013. In vitro reconstitution of an mRNA-transport complex reveals mechanisms of assembly and motor activation. *J Cell Biol,* 203**,** 971-84.

HO, S. N., HUNT, H. D., HORTON, R. M., PULLEN, J. K. & PEASE, L. R. 1989. Site-directed mutagenesis by overlap extension using the polymerase chain reaction. *Gene,* 77**,** 51-9.

HOLLINGER, S. & HEPLER, J. R. 2002. Cellular regulation of RGS proteins: modulators and integrators of G protein signaling. *Pharmacol Rev,* 54**,** 527-59.

HOLT, C. E. & SCHUMAN, E. M. 2013. The central dogma decentralized: new perspectives on RNA function and local translation in neurons. *Neuron,* 80**,** 648-57.

HOOK, B. A., GOLDSTROHM, A. C., SEAY, D. J. & WICKENS, M. 2007. Two yeast PUF proteins negatively regulate a single mRNA. *J Biol Chem,* 282**,** 15430-8.

HUANG, Y., JI, L., HUANG, Q., VASSYLYEV, D. G., CHEN, X. & MA, J. B. 2009. Structural insights into mechanisms of the small RNA methyltransferase HEN1. *Nature,* 461**,** 823-7.

HUTTELMAIER, S., ZENKLUSEN, D., LEDERER, M., DICTENBERG, J., LORENZ, M., MENG, X., BASSELL, G. J., CONDEELIS, J. & SINGER, R. H. 2005. Spatial regulation of beta-actin translation by Src-dependent phosphorylation of ZBP1. *Nature,* 438**,** 512-5.

INOUE, H., NOJIMA, H. & OKAYAMA, H. 1990. High efficiency transformation of Escherichia coli with plasmids. *Gene,* 96**,** 23-8.

IWAKAWA, H. O. & TOMARI, Y. 2015. The Functions of MicroRNAs: mRNA Decay and Translational Repression. *Trends Cell Biol,* 25**,** 651-65.

JAMBOR, H., BRUNEL, C. & EPHRUSSI, A. 2011. Dimerization of oskar 3' UTRs promotes hitchhiking for RNA localization in the Drosophila oocyte. *RNA,* 17**,** 2049-57.

JAMBOR, H., MUELLER, S., BULLOCK, S. L. & EPHRUSSI, A. 2014. A stem-loop structure directs oskar mRNA to microtubule minus ends. *RNA,* 20**,** 429-39.

JAMBOR, H., SURENDRANATH, V., KALINKA, A. T., MEJSTRIK, P., SAALFELD, S. & TOMANCAK, P. 2015. Systematic imaging reveals features and changing localization of mRNAs in Drosophila development. *Elife,* 4.

JANSEN, R. P. & NIESSING, D. 2012. Assembly of mRNA-protein complexes for directional mRNA transport in eukaryotes--an overview. *Curr Protein Pept Sci,* 13**,** 284-93.

JARAMILLO, A. M., WEIL, T. T., GOODHOUSE, J., GAVIS, E. R. & SCHUPBACH, T. 2008. The dynamics of fluorescently labeled endogenous gurken mRNA in Drosophila. *J Cell Sci,* 121**,** 887-94.

JONES, D. T. 1999. Protein secondary structure prediction based on position-specific scoring matrices. *J Mol Biol,* 292**,** 195-202.

KANAI, Y., DOHMAE, N. & HIROKAWA, N. 2004. Kinesin transports RNA: isolation and characterization of an RNA-transporting granule. *Neuron,* 43**,** 513-25.

KATO, M., HAN, T. W., XIE, S., SHI, K., DU, X., WU, L. C., MIRZAEI, H., GOLDSMITH, E. J., LONGGOOD, J., PEI, J., GRISHIN, N. V., FRANTZ, D. E., SCHNEIDER, J. W., CHEN, S., LI, L., SAWAYA, M. R., EISENBERG, D., TYCKO, R. & MCKNIGHT, S. L. 2012. Cell-free formation of RNA granules: low complexity sequence domains form dynamic fibers within hydrogels. *Cell,* 149**,** 753-67.

KATOH, K. & STANDLEY, D. M. 2013. MAFFT multiple sequence alignment software version 7: improvements in performance and usability. *Mol Biol Evol,* 30**,** 772-80.

KAYE, J. A., ROSE, N. C., GOLDSWORTHY, B., GOGA, A. & L'ETOILE, N. D. 2009. A 3'UTR pumilio-binding element directs translational activation in olfactory sensory neurons. *Neuron,* 61**,** 57-70.

KELLEY, L. A., MEZULIS, S., YATES, C. M., WASS, M. N. & STERNBERG, M. J. 2015. The Phyre2 web portal for protein modeling, prediction and analysis. *Nat Protoc,* 10**,** 845-58.

KIEBLER, M. A. & DESGROSEILLERS, L. 2000. Molecular insights into mRNA transport and local translation in the mammalian nervous system. *Neuron,* 25**,** 19-28.

KIEBLER, M. A., HEMRAJ, I., VERKADE, P., KOHRMANN, M., FORTES, P., MARION, R. M., ORTIN, J. & DOTTI, C. G. 1999. The mammalian staufen protein localizes to the somatodendritic domain of cultured hippocampal neurons: implications for its involvement in mRNA transport. *J Neurosci,* 19**,** 288-97.

KIEBLER, M. A., JANSEN, R. P., DAHM, R. & MACCHI, P. 2005. A putative nuclear function for mammalian Staufen. *Trends Biochem Sci,* 30**,** 228-31.

KIEFER, F., ARNOLD, K., KUNZLI, M., BORDOLI, L. & SCHWEDE, T. 2009. The SWISS-MODEL Repository and associated resources. *Nucleic Acids Res,* 37**,** D387-92.

KIM, Y. K., FURIC, L., DESGROSEILLERS, L. & MAQUAT, L. E. 2005. Mammalian Staufen1 recruits Upf1 to specific mRNA 3'UTRs so as to elicit mRNA decay. *Cell,* 120**,** 195-208.

KIM, Y. K., FURIC, L., PARISIEN, M., MAJOR, F., DESGROSEILLERS, L. & MAQUAT, L. E. 2007. Staufen1 regulates diverse classes of mammalian transcripts. *EMBO J,* 26**,** 2670-81.

KIM-HA, J., KERR, K. & MACDONALD, P. M. 1995. Translational regulation of oskar mRNA by bruno, an ovarian RNA-binding protein, is essential. *Cell,* 81**,** 403-12.

KIM-HA, J., SMITH, J. L. & MACDONALD, P. M. 1991. oskar mRNA is localized to the posterior pole of the Drosophila oocyte. *Cell,* 66**,** 23-35.

KNELLER, T. D. G. A. D. G. 2000. SPARKY 3. *University of California, San Francisco*.

KOH, H. R., KIDWELL, M. A., RAGUNATHAN, K., DOUDNA, J. A. & MYONG, S. 2013. ATP-independent diffusion of double-stranded RNA binding proteins. *Proc Natl Acad Sci U S A,* 110**,** 151-6.

KRETZ, M., SIPRASHVILI, Z., CHU, C., WEBSTER, D. E., ZEHNDER, A., QU, K., LEE, C. S., FLOCKHART, R. J., GROFF, A. F., CHOW, J., JOHNSTON, D., KIM, G. E., SPITALE, R. C., FLYNN, R. A., ZHENG, G. X., AIYER, S., RAJ, A., RINN, J. L., CHANG, H. Y. & KHAVARI, P. A. 2013. Control of somatic tissue differentiation by the long non-coding RNA TINCR. *Nature,* 493**,** 231-5.

KUGLER, J. M. & LASKO, P. 2009. Localization, anchoring and translational control of oskar, gurken, bicoid and nanos mRNA during Drosophila oogenesis. *Fly (Austin),* 3**,** 15-28.

KUO, M. W., WANG, S. H., CHANG, J. C., CHANG, C. H., HUANG, L. J., LIN, H. H., YU, A. L., LI, W. H. & YU, J. 2009. A novel puf-A gene predicted from evolutionary analysis is involved in the development of eyes and primordial germ-cells. *PLoS One,* 4**,** e4980.

KUSEK, G., CAMPBELL, M., DOYLE, F., TENENBAUM, S. A., KIEBLER, M. & TEMPLE, S. 2012. Asymmetric segregation of the double-stranded RNA

binding protein Staufen2 during mammalian neural stem cell divisions promotes lineage progression. *Cell Stem Cell,* 11**,** 505-16.
LAEMMLI, U. K. 1970. Cleavage of structural proteins during the assembly of the head of bacteriophage T4. *Nature,* 227**,** 680-5.
LASKO, P. 2012. mRNA localization and translational control in Drosophila oogenesis. *Cold Spring Harb Perspect Biol,* 4.
LAVER, J. D., LI, X., ANCEVICIUS, K., WESTWOOD, J. T., SMIBERT, C. A., MORRIS, Q. D. & LIPSHITZ, H. D. 2013. Genome-wide analysis of Staufen-associated mRNAs identifies secondary structures that confer target specificity. *Nucleic Acids Res,* 41**,** 9438-60.
LEBEAU, G., MAHER-LAPORTE, M., TOPOLNIK, L., LAURENT, C. E., SOSSIN, W., DESGROSEILLERS, L. & LACAILLE, J. C. 2008. Staufen1 regulation of protein synthesis-dependent long-term potentiation and synaptic function in hippocampal pyramidal cells. *Mol Cell Biol,* 28**,** 2896-907.
LEBEAU, G., MILLER, L. C., TARTAS, M., MCADAM, R., LAPLANTE, I., BADEAUX, F., DESGROSEILLERS, L., SOSSIN, W. S. & LACAILLE, J. C. 2011. Staufen 2 regulates mGluR long-term depression and Map1b mRNA distribution in hippocampal neurons. *Learn Mem,* 18**,** 314-26.
LECUYER, E., YOSHIDA, H., PARTHASARATHY, N., ALM, C., BABAK, T., CEROVINA, T., HUGHES, T. R., TOMANCAK, P. & KRAUSE, H. M. 2007. Global analysis of mRNA localization reveals a prominent role in organizing cellular architecture and function. *Cell,* 131**,** 174-87.
LEE, D., OHN, T., CHIANG, Y. C., QUIGLEY, G., YAO, G., LIU, Y. & DENIS, C. L. 2010. PUF3 acceleration of deadenylation in vivo can operate independently of CCR4 activity, possibly involving effects on the PAB1-mRNP structure. *J Mol Biol,* 399**,** 562-75.
LEHMANN, R. & NUSSLEIN-VOLHARD, C. 1987. hunchback, a gene required for segmentation of an anterior and posterior region of the Drosophila embryo. *Dev Biol,* 119**,** 402-17.
LERNER, T. N. & KREITZER, A. C. 2012. RGS4 is required for dopaminergic control of striatal LTD and susceptibility to parkinsonian motor deficits. *Neuron,* 73**,** 347-59.
LI, W., COWLEY, A., ULUDAG, M., GUR, T., MCWILLIAM, H., SQUIZZATO, S., PARK, Y. M., BUSO, N. & LOPEZ, R. 2015. The EMBL-EBI bioinformatics web and programmatic tools framework. *Nucleic Acids Res,* 43**,** W580-4.
LIN, A. C. & HOLT, C. E. 2007. Local translation and directional steering in axons. *EMBO J,* 26**,** 3729-36.
LONG, R. M., GU, W., LORIMER, E., SINGER, R. H. & CHARTRAND, P. 2000. She2p is a novel RNA-binding protein that recruits the Myo4p-She3p complex to ASH1 mRNA. *EMBO J,* 19**,** 6592-601.
LUNDE, B. M., MOORE, C. & VARANI, G. 2007. RNA-binding proteins: modular design for efficient function. *Nat Rev Mol Cell Biol,* 8**,** 479-90.
LUR, G. & HIGLEY, M. J. 2015. Glutamate Receptor Modulation Is Restricted to Synaptic Microdomains. *Cell Rep,* 12**,** 326-34.
MACCHI, P., BROWNAWELL, A. M., GRUNEWALD, B., DESGROSEILLERS, L., MACARA, I. G. & KIEBLER, M. A. 2004. The brain-specific double-stranded RNA-binding protein Staufen2: nucleolar accumulation and isoform-specific exportin-5-dependent export. *J Biol Chem,* 279**,** 31440-4.

MACDOUGALL, N., CLARK, A., MACDOUGALL, E. & DAVIS, I. 2003. Drosophila gurken (TGFalpha) mRNA localizes as particles that move within the oocyte in two dynein-dependent steps. *Dev Cell,* 4**,** 307-19.

MACKERETH, C. D. & SATTLER, M. 2012. Dynamics in multi-domain protein recognition of RNA. *Curr Opin Struct Biol,* 22**,** 287-96.

MAHER-LAPORTE, M., BERTHIAUME, F., MOREAU, M., JULIEN, L. A., LAPOINTE, G., MOUREZ, M. & DESGROSEILLERS, L. 2010. Molecular composition of staufen2-containing ribonucleoproteins in embryonic rat brain. *PLoS One,* 5**,** e11350.

MARCHAND, V., GASPAR, I. & EPHRUSSI, A. 2012. An intracellular transmission control protocol: assembly and transport of ribonucleoprotein complexes. *Curr Opin Cell Biol,* 24**,** 202-10.

MASLIAH, G., BARRAUD, P. & ALLAIN, F. H. 2013. RNA recognition by double-stranded RNA binding domains: a matter of shape and sequence. *Cell Mol Life Sci,* 70**,** 1875-95.

MCWILLIAM, H., LI, W., ULUDAG, M., SQUIZZATO, S., PARK, Y. M., BUSO, N., COWLEY, A. P. & LOPEZ, R. 2013. Analysis Tool Web Services from the EMBL-EBI. *Nucleic Acids Res,* 41**,** W597-600.

MEE, C. J., PYM, E. C., MOFFAT, K. G. & BAINES, R. A. 2004. Regulation of neuronal excitability through pumilio-dependent control of a sodium channel gene. *J Neurosci,* 24**,** 8695-703.

MENON, K. P., ANDREWS, S., MURTHY, M., GAVIS, E. R. & ZINN, K. 2009. The translational repressors Nanos and Pumilio have divergent effects on presynaptic terminal growth and postsynaptic glutamate receptor subunit composition. *J Neurosci,* 29**,** 5558-72.

MENON, K. P., SANYAL, S., HABARA, Y., SANCHEZ, R., WHARTON, R. P., RAMASWAMI, M. & ZINN, K. 2004. The translational repressor Pumilio regulates presynaptic morphology and controls postsynaptic accumulation of translation factor eIF-4E. *Neuron,* 44**,** 663-76.

MERINO, E. J., WILKINSON, K. A., COUGHLAN, J. L. & WEEKS, K. M. 2005. RNA structure analysis at single nucleotide resolution by selective 2'-hydroxyl acylation and primer extension (SHAPE). *J Am Chem Soc,* 127**,** 4223-31.

MICKLEM, D. R., ADAMS, J., GRUNERT, S. & ST JOHNSTON, D. 2000. Distinct roles of two conserved Staufen domains in oskar mRNA localization and translation. *EMBO J,* 19**,** 1366-77.

MIKI, T., KAMIKAWA, Y., KURONO, S., KANEKO, Y., KATAHIRA, J. & YONEDA, Y. 2011. Cell type-dependent gene regulation by Staufen2 in conjunction with Upf1. *BMC Mol Biol,* 12**,** 48.

MIKI, T., TAKANO, K. & YONEDA, Y. 2005. The role of mammalian Staufen on mRNA traffic: a view from its nucleocytoplasmic shuttling function. *Cell Struct Funct,* 30**,** 51-6.

MILLER, M. A. & OLIVAS, W. M. 2011. Roles of Puf proteins in mRNA degradation and translation. *Wiley Interdiscip Rev RNA,* 2**,** 471-92.

MONSHAUSEN, M., GEHRING, N. H. & KOSIK, K. S. 2004. The mammalian RNA-binding protein Staufen2 links nuclear and cytoplasmic RNA processing pathways in neurons. *Neuromolecular Med,* 6**,** 127-44.

MOORE, M. J. 2005. From birth to death: the complex lives of eukaryotic mRNAs. *Science,* 309**,** 1514-8.

MORRIS, A. R., MUKHERJEE, N. & KEENE, J. D. 2008. Ribonomic analysis of human Pum1 reveals cis-trans conservation across species despite evolution of diverse mRNA target sets. *Mol Cell Biol,* 28**,** 4093-103.

MUDDASHETTY, R. S., NALAVADI, V. C., GROSS, C., YAO, X., XING, L., LAUR, O., WARREN, S. T. & BASSELL, G. J. 2011. Reversible inhibition of PSD-95 mRNA translation by miR-125a, FMRP phosphorylation, and mGluR signaling. *Mol Cell,* 42**,** 673-88.

MURARO, N. I., WESTON, A. J., GERBER, A. P., LUSCHNIG, S., MOFFAT, K. G. & BAINES, R. A. 2008. Pumilio binds para mRNA and requires Nanos and Brat to regulate sodium current in Drosophila motoneurons. *J Neurosci,* 28**,** 2099-109.

MURPHY, F. L. & CECH, T. R. 1994. GAAA tetraloop and conserved bulge stabilize tertiary structure of a group I intron domain. *J Mol Biol,* 236**,** 49-63.

NAKAMURA, A., SATO, K. & HANYU-NAKAMURA, K. 2004. Drosophila cup is an eIF4E binding protein that associates with Bruno and regulates oskar mRNA translation in oogenesis. *Dev Cell,* 6**,** 69-78.

NANDURI, S., CARPICK, B. W., YANG, Y., WILLIAMS, B. R. & QIN, J. 1998. Structure of the double-stranded RNA-binding domain of the protein kinase PKR reveals the molecular basis of its dsRNA-mediated activation. *EMBO J,* 17**,** 5458-65.

NASIF, S., CONTU, L. & MUHLEMANN, O. 2018. Beyond quality control: The role of nonsense-mediated mRNA decay (NMD) in regulating gene expression. *Semin Cell Dev Biol,* 75**,** 78-87.

NAVARRO, C., PUTHALAKATH, H., ADAMS, J. M., STRASSER, A. & LEHMANN, R. 2004. Egalitarian binds dynein light chain to establish oocyte polarity and maintain oocyte fate. *Nat Cell Biol,* 6**,** 427-35.

NICASTRO, G., CANDEL, A. M., UHL, M., OREGIONI, A., HOLLINGWORTH, D., BACKOFEN, R., MARTIN, S. R. & RAMOS, A. 2017. Mechanism of beta-actin mRNA Recognition by ZBP1. *Cell Rep,* 18**,** 1187-1199.

NIEDNER, A., MULLER, M., MOORTHY, B. T., JANSEN, R. P. & NIESSING, D. 2013. Role of Loc1p in assembly and reorganization of nuclear ASH1 messenger ribonucleoprotein particles in yeast. *Proc Natl Acad Sci U S A,* 110**,** E5049-58.

OLIVIER, C., POIRIER, G., GENDRON, P., BOISGONTIER, A., MAJOR, F. & CHARTRAND, P. 2005. Identification of a conserved RNA motif essential for She2p recognition and mRNA localization to the yeast bud. *Mol Cell Biol,* 25**,** 4752-66.

PADILLA, J. E. & YEATES, T. O. 2003. A statistic for local intensity differences: robustness to anisotropy and pseudo-centering and utility for detecting twinning. *Acta Crystallogr D Biol Crystallogr,* 59**,** 1124-30.

PANJIKAR, S., PARTHASARATHY, V., LAMZIN, V. S., WEISS, M. S. & TUCKER, P. A. 2005. Auto-rickshaw: an automated crystal structure determination platform as an efficient tool for the validation of an X-ray diffraction experiment. *Acta Crystallogr D Biol Crystallogr,* 61**,** 449-57.

PARK, E., GLEGHORN, M. L. & MAQUAT, L. E. 2013. Staufen2 functions in Staufen1-mediated mRNA decay by binding to itself and its paralog and promoting UPF1 helicase but not ATPase activity. *Proc Natl Acad Sci U S A,* 110**,** 405-12.

PARK, E. & MAQUAT, L. E. 2013. Staufen-mediated mRNA decay. *Wiley Interdiscip Rev RNA,* 4**,** 423-35.

PASTUZYN, E. D., DAY, C. E., KEARNS, R. B., KYRKE-SMITH, M., TAIBI, A. V., MCCORMICK, J., YODER, N., BELNAP, D. M., ERLENDSSON, S., MORADO, D. R., BRIGGS, J. A. G., FESCHOTTE, C. & SHEPHERD, J. D. 2018. The Neuronal Gene Arc Encodes a Repurposed Retrotransposon Gag Protein that Mediates Intercellular RNA Transfer. *Cell,* 172**,** 275-288 e18.

PATEL, V. L., MITRA, S., HARRIS, R., BUXBAUM, A. R., LIONNET, T., BRENOWITZ, M., GIRVIN, M., LEVY, M., ALMO, S. C., SINGER, R. H. & CHAO, J. A. 2012. Spatial arrangement of an RNA zipcode identifies mRNAs under post-transcriptional control. *Genes Dev,* 26**,** 43-53.

PIQUE, M., LOPEZ, J. M., FOISSAC, S., GUIGO, R. & MENDEZ, R. 2008. A combinatorial code for CPE-mediated translational control. *Cell,* 132**,** 434-48.

QIU, C., MCCANN, K. L., WINE, R. N., BASERGA, S. J. & HALL, T. M. 2014. A divergent Pumilio repeat protein family for pre-rRNA processing and mRNA localization. *Proc Natl Acad Sci U S A,* 111**,** 18554-9.

QUENAULT, T., LITHGOW, T. & TRAVEN, A. 2011. PUF proteins: repression, activation and mRNA localization. *Trends Cell Biol,* 21**,** 104-12.

RAMOS, A., GRUNERT, S., ADAMS, J., MICKLEM, D. R., PROCTOR, M. R., FREUND, S., BYCROFT, M., ST JOHNSTON, D. & VARANI, G. 2000. RNA recognition by a Staufen double-stranded RNA-binding domain. *EMBO J,* 19**,** 997-1009.

RIECHMANN, V. & EPHRUSSI, A. 2001. Axis formation during Drosophila oogenesis. *Curr Opin Genet Dev,* 11**,** 374-83.

RODRIGUEZ, J. A. & GONEN, T. 2016. High-Resolution Macromolecular Structure Determination by MicroED, a cryo-EM Method. *Methods Enzymol,* 579**,** 369-92.

ROMAN, D. L. & TRAYNOR, J. R. 2011. Regulators of G protein signaling (RGS) proteins as drug targets: modulating G-protein-coupled receptor (GPCR) signal transduction. *J Med Chem,* 54**,** 7433-40.

SAENGER, W. 1984. *Principles of Nucleic Acid Structure,* New York, Springer.

SAINT-GEORGES, Y., GARCIA, M., DELAVEAU, T., JOURDREN, L., LE CROM, S., LEMOINE, S., TANTY, V., DEVAUX, F. & JACQ, C. 2008. Yeast mitochondrial biogenesis: a role for the PUF RNA-binding protein Puf3p in mRNA localization. *PLoS One,* 3**,** e2293.

SANTORO, M. R., BRAY, S. M. & WARREN, S. T. 2012. Molecular mechanisms of fragile X syndrome: a twenty-year perspective. *Annu Rev Pathol,* 7**,** 219-45.

SAUGSTAD, J. A., MARINO, M. J., FOLK, J. A., HEPLER, J. R. & CONN, P. J. 1998. RGS4 inhibits signaling by group I metabotropic glutamate receptors. *J Neurosci,* 18**,** 905-13.

SCHWARZ, E. 2018. A gene-based review of RGS4 as a putative risk gene for psychiatric illness. *Am J Med Genet B Neuropsychiatr Genet,* 177**,** 267-273.

SCHWEERS, B. A., WALTERS, K. J. & STERN, M. 2002. The Drosophila melanogaster translational repressor pumilio regulates neuronal excitability. *Genetics,* 161**,** 1177-85.

SHI, D., NANNENGA, B. L., DE LA CRUZ, M. J., LIU, J., SAWTELLE, S., CALERO, G., REYES, F. E., HATTNE, J. & GONEN, T. 2016. The collection of MicroED data for macromolecular crystallography. *Nat Protoc,* 11**,** 895-904.

SIEVERS, F., WILM, A., DINEEN, D., GIBSON, T. J., KARPLUS, K., LI, W., LOPEZ, R., MCWILLIAM, H., REMMERT, M., SODING, J., THOMPSON, J. D. & HIGGINS, D. G. 2011. Fast, scalable generation of high-quality protein multiple sequence alignments using Clustal Omega. *Mol Syst Biol,* 7**,** 539.

SINGER-KRUGER, B. & JANSEN, R. P. 2014. Here, there, everywhere. mRNA localization in budding yeast. *RNA Biol,* 11**,** 1031-9.

SOHN, S. Y., BAE, W. J., KIM, J. J., YEOM, K. H., KIM, V. N. & CHO, Y. 2007. Crystal structure of human DGCR8 core. *Nat Struct Mol Biol,* 14**,** 847-53.

SONODA, J. & WHARTON, R. P. 1999. Recruitment of Nanos to hunchback mRNA by Pumilio. *Genes Dev,* 13**,** 2704-12.

SPASSOV, D. S. & JURECIC, R. 2003. Mouse Pum1 and Pum2 genes, members of the Pumilio family of RNA-binding proteins, show differential expression in fetal and adult hematopoietic stem cells and progenitors. *Blood Cells Mol Dis,* 30**,** 55-69.

ST JOHNSTON, D., BEUCHLE, D. & NUSSLEIN-VOLHARD, C. 1991. Staufen, a gene required to localize maternal RNAs in the Drosophila egg. *Cell,* 66**,** 51-63.

ST JOHNSTON, D., BROWN, N. H., GALL, J. G. & JANTSCH, M. 1992. A conserved double-stranded RNA-binding domain. *Proc Natl Acad Sci U S A,* 89**,** 10979-83.

STEFL, R., OBERSTRASS, F. C., HOOD, J. L., JOURDAN, M., ZIMMERMANN, M., SKRISOVSKA, L., MARIS, C., PENG, L., HOFR, C., EMESON, R. B. & ALLAIN, F. H. 2010. The solution structure of the ADAR2 dsRBM-RNA complex reveals a sequence-specific readout of the minor groove. *Cell,* 143**,** 225-37.

STEFL, R., XU, M., SKRISOVSKA, L., EMESON, R. B. & ALLAIN, F. H. 2006. Structure and specific RNA binding of ADAR2 double-stranded RNA binding motifs. *Structure,* 14**,** 345-55.

SUH, N., CRITTENDEN, S. L., GOLDSTROHM, A., HOOK, B., THOMPSON, B., WICKENS, M. & KIMBLE, J. 2009. FBF and its dual control of gld-1 expression in the Caenorhabditis elegans germline. *Genetics,* 181**,** 1249-60.

SUTTON, M. A. & SCHUMAN, E. M. 2006. Dendritic protein synthesis, synaptic plasticity, and memory. *Cell,* 127**,** 49-58.

TAKIZAWA, P. A., SIL, A., SWEDLOW, J. R., HERSKOWITZ, I. & VALE, R. D. 1997. Actin-dependent localization of an RNA encoding a cell-fate determinant in yeast. *Nature,* 389**,** 90-3.

TAKIZAWA, P. A. & VALE, R. D. 2000. The myosin motor, Myo4p, binds Ash1 mRNA via the adapter protein, She3p. *Proc Natl Acad Sci U S A,* 97**,** 5273-8.

TANG, S. J., MEULEMANS, D., VAZQUEZ, L., COLACO, N. & SCHUMAN, E. 2001. A role for a rat homolog of staufen in the transport of RNA to neuronal dendrites. *Neuron,* 32**,** 463-75.

TANTS, J. N., FESSER, S., KERN, T., STEHLE, R., GEERLOF, A., WUNDERLICH, C., JUEN, M., HARTLMULLER, C., BOTTCHER, R., KUNZELMANN, S., LANGE, O., KREUTZ, C., FORSTEMANN, K. & SATTLER, M. 2017. Molecular basis for asymmetry sensing of siRNAs by the Drosophila Loqs-PD/Dcr-2 complex in RNA interference. *Nucleic Acids Res,* 45**,** 12536-12550.

TIAN, B. & MATHEWS, M. B. 2001. Functional characterization of and cooperation between the double-stranded RNA-binding motifs of the protein kinase PKR. *J Biol Chem,* 276**,** 9936-44.

TOSAR, L. J., THOMAS, M. G., BAEZ, M. V., IBANEZ, I., CHERNOMORETZ, A. & BOCCACCIO, G. L. 2012. Staufen: from embryo polarity to cellular stress and neurodegeneration. *Front Biosci (Schol Ed),* 4**,** 432-52.

VESSEY, J. P., AMADEI, G., BURNS, S. E., KIEBLER, M. A., KAPLAN, D. R. & MILLER, F. D. 2012. An asymmetrically localized Staufen2-dependent RNA complex regulates maintenance of mammalian neural stem cells. *Cell Stem Cell,* 11**,** 517-28.

VESSEY, J. P., SCHODERBOECK, L., GINGL, E., LUZI, E., RIEFLER, J., DI LEVA, F., KARRA, D., THOMAS, S., KIEBLER, M. A. & MACCHI, P. 2010. Mammalian Pumilio 2 regulates dendrite morphogenesis and synaptic function. *Proc Natl Acad Sci U S A,* 107**,** 3222-7.

VESSEY, J. P., VACCANI, A., XIE, Y., DAHM, R., KARRA, D., KIEBLER, M. A. & MACCHI, P. 2006. Dendritic localization of the translational repressor Pumilio 2 and its contribution to dendritic stress granules. *J Neurosci,* 26**,** 6496-508.

VON RORETZ, C. & GALLOUZI, I. E. 2008. Decoding ARE-mediated decay: is microRNA part of the equation? *J Cell Biol,* 181**,** 189-94.

WANG, M., OGE, L., PEREZ-GARCIA, M. D., HAMAMA, L. & SAKR, S. 2018. The PUF Protein Family: Overview on PUF RNA Targets, Biological Functions, and Post Transcriptional Regulation. *Int J Mol Sci,* 19.

WANG, X., VUKOVIC, L., KOH, H. R., SCHULTEN, K. & MYONG, S. 2015. Dynamic profiling of double-stranded RNA binding proteins. *Nucleic Acids Res,* 43**,** 7566-76.

WANG, X., ZAMORE, P. D. & HALL, T. M. 2001. Crystal structure of a Pumilio homology domain. *Mol Cell,* 7**,** 855-65.

WANG, Y., OPPERMAN, L., WICKENS, M. & HALL, T. M. 2009. Structural basis for specific recognition of multiple mRNA targets by a PUF regulatory protein. *Proc Natl Acad Sci U S A,* 106**,** 20186-91.

WATERHOUSE, A. M., PROCTER, J. B., MARTIN, D. M., CLAMP, M. & BARTON, G. J. 2009. Jalview Version 2--a multiple sequence alignment editor and analysis workbench. *Bioinformatics,* 25**,** 1189-91.

WEIDMANN, C. A. & GOLDSTROHM, A. C. 2012. Drosophila Pumilio protein contains multiple autonomous repression domains that regulate mRNAs independently of Nanos and brain tumor. *Mol Cell Biol,* 32**,** 527-40.

WHARTON, R. P. & AGGARWAL, A. K. 2006. mRNA regulation by Puf domain proteins. *Sci STKE,* 2006**,** pe37.

WICKENS, M., BERNSTEIN, D. S., KIMBLE, J. & PARKER, R. 2002. A PUF family portrait: 3'UTR regulation as a way of life. *Trends Genet,* 18**,** 150-7.

WICKHAM, L., DUCHAINE, T., LUO, M., NABI, I. R. & DESGROSEILLERS, L. 1999. Mammalian staufen is a double-stranded-RNA- and tubulin-binding protein which localizes to the rough endoplasmic reticulum. *Mol Cell Biol,* 19**,** 2220-30.

WILKINSON, K. A., MERINO, E. J. & WEEKS, K. M. 2006. Selective 2'-hydroxyl acylation analyzed by primer extension (SHAPE): quantitative RNA structure analysis at single nucleotide resolution. *Nat Protoc,* 1**,** 1610-6.

WILLARS, G. B. 2006. Mammalian RGS proteins: multifunctional regulators of cellular signalling. *Semin Cell Dev Biol,* 17**,** 363-76.

WINN, M. D., BALLARD, C. C., COWTAN, K. D., DODSON, E. J., EMSLEY, P., EVANS, P. R., KEEGAN, R. M., KRISSINEL, E. B., LESLIE, A. G., MCCOY, A.,

MCNICHOLAS, S. J., MURSHUDOV, G. N., PANNU, N. S., POTTERTON, E. A., POWELL, H. R., READ, R. J., VAGIN, A. & WILSON, K. S. 2011. Overview of the CCP4 suite and current developments. *Acta Crystallogr D Biol Crystallogr,* 67**,** 235-42.

YE, B., PETRITSCH, C., CLARK, I. E., GAVIS, E. R., JAN, L. Y. & JAN, Y. N. 2004. Nanos and Pumilio are essential for dendrite morphogenesis in Drosophila peripheral neurons. *Curr Biol,* 14**,** 314-21.

ZAHR, S. K., YANG, G., KAZAN, H., BORRETT, M. J., YUZWA, S. A., VORONOVA, A., KAPLAN, D. R. & MILLER, F. D. 2018. A Translational Repression Complex in Developing Mammalian Neural Stem Cells that Regulates Neuronal Specification. *Neuron,* 97**,** 520-537 e6.

ZHANG, J., MCCANN, K. L., QIU, C., GONZALEZ, L. E., BASERGA, S. J. & HALL, T. M. 2016. Nop9 is a PUF-like protein that prevents premature cleavage to correctly process pre-18S rRNA. *Nat Commun,* 7**,** 13085.

ZIMYANIN, V. L., BELAYA, K., PECREAUX, J., GILCHRIST, M. J., CLARK, A., DAVIS, I. & ST JOHNSTON, D. 2008. In vivo imaging of oskar mRNA transport reveals the mechanism of posterior localization. *Cell,* 134**,** 843-53.

ZUKER, M. 2003. Mfold web server for nucleic acid folding and hybridization prediction. *Nucleic Acids Res,* 31**,** 3406-15.